12-2020

Hazard Analysis of a Segment of Highway SR-12 through Bryce Canyon National Park, Southern Utah

Tomsen Reed
Utah State University

HAZARD ANALYSIS OF A SEGMENT OF HIGHWAY SR-12 THROUGH BRYCE CANYON NATIONAL PARK, SOUTHERN UTAH

by

Tomsen Reed

A research report submitted in partial fulfillment
of the requirements for the degree

of

MASTER OF SCIENCE

in

Applied Environmental Geoscience

Approved:

Tammy Rittenour, Ph.D.
Major Professor

Kelly Bradbury, Ph.D., P.G.
Committee Member

Joel Pederson, Ph.D.
Committee Member

UTAH STATE UNIVERSITY
Logan, Utah

2020

ABSTRACT

Hazard Analysis of a segment of Highway SR-12 through Bryce Canyon National Park, Southern Utah

by

Tomsen Reed, Master of Science

Utah State University, 2020

Major Professor: Dr. Tammy Rittenour
Department: Geosciences

Over 2.6 million people travel along highway SR-12, a National Scenic Byway, through Bryce Canyon in southern Utah each year. This highway is a major thoroughfare for tourists traveling to Bryce Canyon National Park, Grand Staircase-Escalante National Monument, and other scenic attractions. SR-12 is susceptible to rockfall and landslide hazards where it descends from the Paunsaugunt Plateau into Tropic Canyon, and these hazards have potential consequences of economic loss due to travel delays for tourists and commodities, and possible loss of life. Rockfall could have devastating effects at this location because of the traffic volume, sharp turns, low visibility, and steep drop-offs. A landslide on SR-12 in 2017 prompted emergency repairs that cost over $2.6 million dollars.

SR-12 runs below a cliff band of the relatively weak limestones and mudstones, the Tertiary Claron Formation, that make up the colorful hoodoos and erosional features of Bryce Canyon. The Oligocene- to Miocene-aged Ruby's Inn Thrust Fault has juxtaposed a resistant, cliff-forming Claron layer on a weak, slope-forming layer of the Claron

Formation, creating the potential for rockfall that could impact the roadway and associated travel. The research hypothesis of this project is that the Ruby's Inn Thrust Fault and associated fracturing have weakened the rocks in this cliff band creating a rockfall hazard**.** Research objectives are 1) to characterize cliff-forming lithologies within the study area; 2) to examine the fracture characteristics in cliffs using scanline techniques; 3) to measure the topography and assess physical properties of the toe slope; and 4) to assess rockfall potential and identify contributing factors for hazards posed by this cliff band in between SR-12 milepost markers 15 and 15.7. Field data collected included linear scanlines along the thrust fault and at a control location site, sample collection, contact geologic mapping, and lithologic unit descriptions. Laboratory testing was performed to assess physical characteristics of the rock, soil, and fracture infillings. These data are used for kinematic analyses of the cliff band to assess failure potential. Rockfall analyses were also performed to assess the probability of rocks reaching the roadway after failure.

(213 pages)

PUBLIC ABSTRACT

Hazard Analysis of a segment of Highway SR-12 through Bryce Canyon National Park, Southern Utah

Tomsen Reed

Over 2.6 million people travel along highway SR-12 through Bryce Canyon in southern Utah every year. This highway is a National Scenic Byway, and a major thoroughfare for tourists traveling to Bryce Canyon National Park, Grand Staircase-Escalante National Monument, and other scenic attractions. SR-12 is susceptible to rockfall and landslide hazards where it descends from the Paunsaugunt Plateau into Tropic Canyon. These hazards have potential consequences of economic loss due to travel delays for tourists and commodities, injury to people travelling this popular roadway, and possible loss of life. Rockfall could have devastating effects at this location because of the traffic volume, sharp turns, low visibility, and steep drop-offs. A landslide on SR-12 in 2017 prompted emergency repairs that cost over 2.6 million dollars. This research focuses on the hazards posed to the highway by an approximately 1-mile long cliff band that is positioned above the highway. This research attempts to assess the potential of rocks becoming dislodged from this cliff, and then their subsequent probability of reaching SR-12 after becoming dislodged. This research will provide important information that can be used to make informed decisions about the future of this roadway through Bryce Canyon National Park.

ACKNOWLEDGMENTS

I would like to thank my wife for the encouragement and support she has given me throughout this process of finishing another degree. I know it was a sacrifice for her to take care of our family and their needs while I returned to school, and I really am so grateful for everything she has done for us during this process. I would also like to thank my major professor and advisor, Dr. Tammy Rittenour, she has been extremely encouraging and supportive during this entire process of completing this project. She encouraged me to apply for grants to fund my research, which I probably would not have done without her encouragement, and would not have obtained without her reviews. I would also like to thank Dr. Kelly Bradbury for helping me to develop a unique direction for my project that was applicable for the project and for my future career. Dr. Joel Pederson also provided very constructive comments during his reviews of my project and progress, and I really appreciate his insight and understanding of important issues. Tyler Knudsen from the Utah Geological Survey was also very helpful with resources and even preliminary revised mapping in the project area, which ended up being very useful in understanding the deposits in the area. I am grateful to the Geological Society of America, the Colorado Scientific Society, and the Association of Environmental and Engineering Geologists for their support through student grants and scholarships. Without their financial support, I would not have been able to perform the testing and research that I ended up being able to perform. Lastly, I would like to thank Ryan Cole and Ryan Maw from Gerhart Cole for supporting my desire to obtain additional education, and for the use of the programs like Dips and Rocfall that I would not have had access to otherwise.

CONTENTS

Page

ABSTRACT iii
PUBLIC ABSTRACT v
ACKNOWLEDGMENTS vi
LIST OF TABLES viii
LIST OF FIGURES ix
INTRODUCTION 1
GEOLOGIC SETTING 6
Regional Geologic Setting 6
Study Area 10
Background on Rockfall Processes 14
RESEARCH DESIGN AND METHODOLOGY 15
Site Selection 16
Objective 1 – Characterize lithologies at control and test locations 19
Objective 2 – Characterize fracture networks 22
Objective 3 – Characterize toeslope materials and geometry 26
Objective 4 – Perform rockfall assessment 29
RESULTS AND DISCUSSION 33
Objective 1 – Characterize lithologies at control and test locations 33
Objective 2 – Characterize fracture networks 52
Objective 3 – Characterize toeslope materials and geometry 66
Objective 4 – Rockfall assessment 71
CONCLUSION 81
APPENDIX A 87
APPENDIX B 136
APPENDIX C 151
APPENDIX D 162
APPENDIX E 188
APPENDIX G 213

LIST OF TABLES

Table Page

Table 1 – X-ray diffraction testing results 50
Table 2 – Schmidt hammer rebound R-values from each sample location 51
Table 3 – Stereonet data summary. Where the fracture sets were nearly vertical, two dip direction windows were included in the set 62
Table 4 – Grain-size distribution of toeslope samples 67
Table 5 – Kinematic analysis results for each scanline 71
Table 6 – Rockfall analysis results 73
Table 7 – Combined hazard calculation for each scanline, incorporating rockfall potential from kinematic analysis and probability of propagation from rockfall modeling 75

Table G-1 – Infrared Stimulated Luminescence (IRSL) Age Information 213
Table G-2 – Dose Rate Information 213

LIST OF FIGURES

Figure Page

Figure 1 – Physiographic map of southwestern to southcentral Utah, including the Bryce Canyon study area. Hillshade created from 90 meter DEM (Hanser, 2008)..... 1
Figure 2 – Location map of the project area. 2
Figure 3 - Cliffband above a toeslope leading down to SR-12, view looking east..... 3
Figure 4 - Landslide along SR-12 in 2017 looking west, photo credit UDOT. 4
Figure 5 – Physiographic Provinces of the southwestern United States..... 6
Figure 6 – Regional structure map adjacent to the Paunsaugunt Plateau 7
Figure 7 – Highway SR-12 mile post marker map (UDOT, 2012) 10
Figure 8 – Hillshade and elevation data from 0.5-meter LiDAR data for the Bryce Canyon area, within the project vicinity (AGRC, 2018). 11
Figure 9 – Geologic mapping of Biek et al. (2015) in project vicinity. Kw = Cretaceous Wahweap Formation. Tcp = Tertiary Pink Member of the Claron Formation. Tcw = Tertiary White Member of the Claron Formation. Qap = Quaternary piedmont alluvium. Qac = Quaternary alluvium and colluvium. Qaly = Quaternary stream alluvium. RITF = Ruby's Inn Thrust Fault, several splays..... 12
Figure 10 – Typical outcrop along the RITF, cliffs approximately 20 to 30 meters tall. RITF at the base of the cliff..... 16
Figure 11 - Control outcrop, with generally flat-lying bedding, appears generally unaltered and in-place. Cliff approximately 15 meters tall..... 17
Figure 12 - Scanline location map, overlaid on aerial imagery 18
Figure 13 - Scanline locations, overlaid on the Panguitch 1:62,500 Quad (Biek et al., 2015). Qaly – Young stream alluvium. Qac – Alluvium and colluvium. Qap – Quaternary piedmont alluvium. Tcw – Tertiary White Member of the Claron Formation. Tcp – Tertiary Pink Member of the Claron Formation. Kw – Cretaceous Wahweap Formation. 18
Figure 14 – RITF and differential erosion where the hanging wall forms a cliff and the footwall forms the toeslope..... 19
Figure 15 - Dual carbonate staining results key (Precimat, 2020)..... 21
Figure 16 - A representation of discontinuity data to be collected in the field, from Hudson and Harrison (1997)..... 22
Figure 17 – True versus apparent fracture spacing (USBR, 2001)..... 25
Figure 18 – Scanline profile locations, shown on a slope map of the project vicinity. Slope is in degrees, calculated in ArcMap from the 0.5 meter LiDAR data (Utah AGRC, 2018) 27
Figure 19 – Longitudinal profile graphs of cliff and toeslope at each rockfall analysis location, from LiDAR data (Utah AGRC, 2018). Profiles end at the white line of roadway..... 28

Figure 20 – the three main failure modes associated with rockfall hazards, from Hoek and Bray (1981)..... 31
Figure 21 - Full outcrop where control scanline was performed. Aluminum clipboard (approximately 31 cm long) visible in lower left for scale. Approximate scanline location shown in yellow. View looking southeast. 34
Figure 22 - Dolomite crossed by the control scanline, metric tape measure showing scale (in cm.). Lower part of picture shows a portion of the adjacent marlstone, mostly weathered surfaces visible 34
Figure 23 - Control Scanline thin section – plane polarized light, scale bar of 2.5 mm shown. 35
Figure 24 - Upper portion of outcrop where Scanline 1 was performed (scanline location obscured by the trees, but general location marked in yellow dashes). View looking north, and up at the outcrop from the roadway 36
Figure 25 - Wide view of units visible at Scanline 1. Near the middle of the photo, a zone of abundant cavities visible. 36
Figure 26 – Continuation of Scanline 1, to the end of scanline. 37
Figure 27 - Unit 1A at Scanline 1, rock hammer (33 cm. long) for scale. Weathered surface 38
Figure 28 - Unit 1B found at Scanline 1. Weathered surface, with visible subangular inclusions of yellowish brown sandstone clasts, along with what appear to be pebble lenses. Pencil for scale (full length 15 cm.) 39
Figure 29 - Thin Section of sample 1A – plane polarized light, scale bar of 2.5 mm shown. 40
Figure 30 - Thin section of sample 1B – plane polarized light, scale bar of 2.5 mm shown. 40
Figure 31 – Outcrop view of location of Scanline 2 (marked in yellow, behind the vegetation). Note the large overhang, and small portions of footwall material underneath the overhang, but mostly eroded away. The overhang extends approximately 8 meters out from the back of the wall (scanline location) to the cliff face. View looking north from the roadway. 41
Figure 32 - View of limestone at Scanline 2, metric tape measure for scale (in cm.), rock faces near tape measure are mostly fresh..... 42
Figure 33 - Thin section of unit 2 – plane polarized light, scale bar of 2.5 mm shown. .. 43
Figure 34 – Partial outcrop view of Scanline 3 location. Scanline location marked in yellow. View to the northwest from just below the scanline location. 44
Figure 35 - Dolomite found at Scanline 3, with abundant manganese oxide staining visible on the surface. Tape measure showing scale (in cm.). 44
Figure 36 - Thin section of Unit 3 – plane polarized light, scale bar of 2.5 mm shown. . 45
Figure 37 - Outcrop view of Scanline 4, with scanline marked in yellow. View looking north 46

Figure 38 - Unit 4A, limestone found at Scanline 4, with dissolution cleavage, rock faces are mostly fresh 46
Figure 39 - Thin section of Unit 4A – plane polarized light, scale bar of 2.5 mm shown.47
Figure 40 - Thin section of Unit 4B – plane polarized light, scale bar of 2.5 mm shown.47
Figure 41 - Wider view of Scanline 5 48
Figure 42 - Limestone found at Scanline 5, showing both fresh (lower left) and weathered (upper right) surfaces, tape measure visible for scale (in cm.)..... 49
Figure 43 - Thin section of Unit 5 – plane polarized light, scale bar of 2.5 mm shown. . 49
Figure 44 – Schmidt Hammer R-values measured in the field in the units crossed by each scanline 51
Figure 45 - Histograms for all six scanlines showing number of fractures per scanline where full fracture length was measurable. Length is plotted in 0.2 meter bins. 54
Figure 46 - Histograms for all six scanlines showing number of fractures of certain minimum length per scanline. Minimum length is plotted in 0.2 meter bins. Minimum length recorded where only one termination could be measured (not shown in Figure 45) 55
Figure 47 - Histograms for all six scanlines showing number of fractures of certain maximum aperture per scanline. Maximum aperture is generally divided into 5 millimeter bins. Maximum aperture recorded because of variability in aperture within fractures 57
Figure 48 - Scanline Control outcrop with major, near-vertical fractures marked in blue (upper photo) and unmarked but visible in lower photo..... 58
Figure 49 - Scanline 1 with major fractures marked in green, thrust fault strand marked in red, and a long, prominent fracture marked in purple which is not part of a major set (upper photo), and unmarked but visible (lower photo) 59
Figure 50 – Scanline fracture intensity histogram, including unscreened data (red) and data screened to remove fractures less than 0.5 meters long (blue)..... 60
Figure 51 - Apparent fracture spacing per scanline at each scanline using a box-and-whisker plot. Dots above Scanline 2 and 5 are considered outliers, according to Microsoft Excel. However, it should be noted that the datasets were small, and therefore determination of outliers may not be representative. The “X” symbol indicates the average apparent spacing. The n value is equal to the total number of fractures that were grouped into major joint sets at each scanline.... 61
Figure 52 – Stereonet of major joint set mean planes plotted as dark red lines at Scanline Control, with the scanline orientation plotted as green line..... 63
Figure 53 - Stereonet of major joint set mean planes plotted as dark red lines at Scanline 1, with the RITF plotted as red line and scanline orientation plotted as green line..... 63
Figure 54 - Stereonet of major joint set mean planes as dark red lines at Scanline 2, with the RITF plotted as red line and scanline orientation plotted as green line..... 64

Figure 55 - Stereonet of major joint set mean planes plotted as dark red lines at Scanline 3, with the RITF plotted as red line, and scanline orientation plotted as green line..... 64
Figure 56 - Stereonet of major joint set mean plane plotted as dark red line at Scanline 4, with the RITF plotted as red line, and scanline orientation plotted as green line..... 65
Figure 57 - Stereonet of major joint set mean planes plotted as dark red lines at Scanline 5, with the RITF plotted as red line, and scanline orientation plotted as green line..... 65
Figure 58 – Complete grain-size distribution of toeslope samples based on combination of mechanical sieving and Malvern Mastersizer results. 67
Figure 59 – Grain-size distribution of toeslope matrix material (<2 mm.). Based on partial mechanical sieving and Malvern Mastersizer data. 68
Figure 60 – Surficial geologic mapping within the project area, between SR-12 and the RITF. Photographs and study locations indicated on the map are included in Appendix C. Mapped units are described as follows: Hf/Hd – Historical fill and disturbed ground. Qct – undifferentiated Quaternary colluvial and talus deposits. Tcw – Eocene White Member of the Claron Formation. Tcp – Paleocene to Eocene Pink Member of the Claron Formation. 69
Figure 61 – Photograph of an unconsolidated deposit that has scoured out part of the underling White Member bedrock and replaced it. This photograph was taken from the roadway between Scanlines 1 and 2, looking north. Labeled Photo 2 on the geologic map in Figure 60. 70
Figure 62 - Annotated, diagrammatic view of a kinematic analysis stereonet 72
Figure 63 - Relative rockfall hazard map, with an inset of the control location in upper left hand side of figure 78
Figure 64 – Google Maps imagery of a fan-shaped deposit where boulders from the Scanline 5 cliffband appear to stop, well above the roadway. See Appendix C for test pit log, 19-TP-14. Green on roadway indicates this is an area of low rockfall hazard (Figure 63)..... 79
Figure 65 – LiDAR hillshade in the vicinity of Scanline 5, showing a fan-shaped deposit where boulders from the Scanline 5 cliffband appear to generally stop, well above the roadway. 80

Figure A-1 – Geologic mapping performed in the project area..... 88
Figure A-2 – Unit descriptions and key to map symbols from the geologic mapping in Figure A-1..... 89
Figure A-3 – Photograph of unconsolidated deposit in roadway below Scanlines 1 and 2..... 90
Figure A-4 – Photograph of unconsolidated deposit in roadway below Scanlines 1 and 2..... 91

Figure A-5 – Photograph of unconsolidated deposit in roadway below Scanlines 1 and 2 92
Figure A-6 – Photograph of unconsolidated deposit in roadway below Scanline 2 93
Figure A-7 – Photograph of unconsolidated deposit in roadway below Scanline 2 94
Figure A-8 – Photograph of unconsolidated deposit in roadway below Scanlines 2 and 3 95
Figure A-9 – Photograph of unconsolidated deposit in roadway below Scanlines 2 and 3 96
Figure A-10 – Photograph of unconsolidated deposit in roadway below Scanlines 2 and 3 97
Figure A-11 – Photograph of unconsolidated deposit in roadway below Scanlines 2 and 3 98
Figure A-12 – Photograph of unconsolidated deposit in roadway below Scanlines 2 and 3 99
Figure A-13 – Photograph of unconsolidated deposit in roadway below Scanline 3 100
Figure A-14 – Photograph of unconsolidated deposit in roadway below Scanline 3 101
Figure A-15 – Photograph of unconsolidated deposit in roadway below Scanlines 3 and 4 102
Figure A-16 – Photograph of unconsolidated deposit in roadway below Scanlines 3 and 4 103
Figure A-17 – Photograph of unconsolidated deposit in roadway below Scanlines 3 and 4 104
Figure A-18 – Photograph of unconsolidated deposit in roadway below Scanline 4 105
Figure A-19 – Photograph of unconsolidated deposit in roadway below Scanline 4 106
Figure A-20 – Photograph of unconsolidated deposit in roadway below Scanline 5 107
Figure A-21 - Marlstone described near the control scanline. Rock hammer (33 cm. long) for scale, mostly weathered surface 108
Figure A-22 - Conglomerate overlying marlstone near control scanline. Pencil (15 cm. long) for scale 109
Figure A-23 - Altered unit near Scanline 1, pencil (15 cm. long) for scale. Pencil pointing to a possible fault zone, with what appear to be clasts of Pink Member of the Claron Formation mixed in with the yellowish brown sandy matrix. 110
Figure A-24 – Test pit log of 19-TP-11 from Gerhart Cole, (2019) 113
Figure A-25 - Photograph of 19-TP-11 from Gerhart Cole, (2019) 114
Figure A-26 – Test pit log of 19-TP-12 from Gerhart Cole, (2019) 115
Figure A-27 - Photograph of 19-TP-12 from Gerhart Cole, (2019) 116
Figure A-28 – Test pit log of 19-TP-13 from Gerhart Cole, (2019) 117
Figure A-29 - Photograph of 19-TP-13 from Gerhart Cole, (2019) 118
Figure A-30 – Test pit log of 19-TP-14 from Gerhart Cole, (2019) 119
Figure A-31 - Photograph of 19-TP-14 from Gerhart Cole, (2019) 120

Figure A-32 - Test hole log of 19-TH-06 from Gerhart Cole, (2019). 121
Figure A-33 – Test hole log of 19-TH-07 from Gerhart Cole, (2019). 122
Figure A-34 - Test hole log of 19-TH-08 from Gerhart Cole, (2019) 123
Figure A-35 - Test hole log of 19-TH-10 from Gerhart Cole, (2019) 124
Figure A-36 - Test hole log of 19-TH-10 (cont'd.) from Gerhart Cole, (2019) 125
Figure A-37 - Test hole log of 19-TH-10 (cont'd) from Gerhart Cole, (2019) 126
Figure A-38 - Test hole log of 19-TH-10 (cont'd) from Gerhart Cole, (2019) 127
Figure A-39 - Test hole log of 19-TH-10 (cont'd) from Gerhart Cole, (2019) 128
Figure A-40 – Rock core photographs from 19-TH-10, from Gerhart Cole, (2019)..... 129
Figure A-41 – Rock core photographs from 19-TH-10, from Gerhart Cole, (2019)..... 130
Figure A-42 – Rock core photographs from 19-TH-10, from Gerhart Cole, (2019)..... 131
Figure A-43 – Rock core photographs from 19-TH-10, from Gerhart Cole, (2019)..... 132
Figure A-44 – Legend to Soil Descriptions, from Gerhart Cole (2019)..... 133
Figure A-45 – Legend to Soil and Rock Descriptions, from Gerhart Cole (2019)..... 134
Figure A-46 – Legend to Soil and Rock Descriptions (cont'd.), from Gerhart Cole (2019)..... 135

Figure B-1 – Scanline Locations..... 137
Figure B-2 – Scanline and sample locations for the control scanline..... 138
Figure B-3 – Scanline and sample locations for Scanline 1 139
Figure B-4 – Scanline and sample locations for Scanline 2 140
Figure B-5 – Scanline and sample locations for Scanline 3 141
Figure B-6 – Scanline and sample locations for Scanline 4 142
Figure B-7 – Scanline and sample locations for Scanline 5 143
Figure B-8 – Raw scanline data from control scanline..... 144
Figure B-9 – Raw scanline data from Scanline 1 145
Figure B-10 – Raw scanline data from Scanline 2 146
Figure B-11 – Raw scanline data from Scanline 3 147
Figure B-12 – Raw scanline data from Scanline 4 148
Figure B-13 – Raw scanline data from Scanline 5 149
Figure B-14 – Raw scanline data from Scanline 5 (cont'd.)..... 150

Figure C-1 – Historical rockfall information, from Gary Spencer, UDOT Region 4 Maintenance. See Figure C-2 – UDOT Mile post marker locations with respect to the project alignment for map of mile post markers 152
Figure C-2 – UDOT Mile post marker locations with respect to the project alignment 153
Figure C-3 – Photo of boulder found during field studies, indicating both the size of potential rockfall blocks and the potential for blocks with dissolution cleavage to still release in a larger mass 154
Figure C-4 – Large boulders partially embedded in the slope near Scanline 4 155
Figure C-5 – Very large boulder partially embedded in slope..... 156

Figure C-6 – Large boulder sitting on top of slope..... 157
Figure C-7 – Large boulder at roadway level between Scanlines 2 and 3, new as of Spring 2020, appears to have been pushed off the road or shoulder..... 158
Figure C-8 – Additional photograph of the new boulder shown in Figure C-7 – Large boulder at roadway level between Scanlines 2 and 3, new as of Spring 2020, appears to have been pushed off the road or shoulder 159
Figure C-9 – Photograph of boulder below highway level..... 160
Figure C-10 – Photograph of boulders sitting just above the roadway cut, between Scanlines 4 and 5 161
Figure C-11 – Photograph of large (up to 15-meter diameter) blocks that have detached from the main cliff band 162

Figure D-1 – Inputs for the kinematic analysis performed at the control scanline..... 164
Figure D-2 – Planar sliding kinematic analysis at the control scanline..... 165
Figure D-3 – Direct toppling kinematic analysis at the control scanline..... 166
Figure D-4 – Wedge sliding kinematic analysis at the control scanline..... 167
Figure D-5 – Inputs for the kinematic analysis performed at Scanline 1 168
Figure D-6 – Planar sliding kinematic analysis at Scanline 1 169
Figure D-7 – Direct toppling kinematic analysis at Scanline 1 170
Figure D-8 – Wedge sliding kinematic analysis at Scanline 1 171
Figure D-9 – Inputs for the kinematic analysis performed at Scanline 2 172
Figure D-10 – Planar sliding kinematic analysis at Scanline 2 173
Figure D-11 – Direct toppling kinematic analysis at Scanline 2 174
Figure D-12 – Wedge sliding kinematic analysis at Scanline 2 175
Figure D-13 – Inputs for the kinematic analysis performed at Scanline 3 176
Figure D-14 – Planar sliding kinematic analysis at Scanline 3 177
Figure D-15 – Direct toppling kinematic analysis at Scanline 3 178
Figure D-16 – Wedge sliding kinematic analysis at Scanline 3 179
Figure D-17 – Inputs for the kinematic analysis performed at Scanline 4 180
Figure D-18 – Planar sliding kinematic analysis at Scanline 4 181
Figure D-19 – Direct toppling kinematic analysis at Scanline 4 182
Figure D-20 – Wedge sliding kinematic analysis at Scanline 4 183
Figure D-21 – Inputs for the kinematic analysis performed at Scanline 5 184
Figure D-22 – Planar sliding kinematic analysis at Scanline 5 185
Figure D-23 – Direct toppling kinematic analysis at Scanline 5 186
Figure D-24 – Wedge sliding kinematic analysis at Scanline 5 187

Figure E-1 – Rockfall modeling inputs..... 188
Figure E-2 – Rockfall model setup for the control scanline..... 189
Figure E-3 – Full rockfall modeling results distribution for the control scanline 190
Figure E-4 – Rockfall modeling results crossing the white line for the control scanline 191

Figure E-5 – Rockfall model setup for Scanline 1 192
Figure E-6 – Full rockfall modeling results distribution for Scanline 1 193
Figure E-7 – Rockfall modeling results crossing the white line for Scanline 1 194
Figure E-8 – Rockfall model setup for Scanline 2 195
Figure E-9 – Full rockfall modeling results distribution for Scanline 2 196
Figure E-10 – Rockfall modeling results crossing the white line for Scanline 2 197
Figure E-11 – Rockfall model setup for Scanline 3 198
Figure E-12 – Full rockfall modeling results distribution for Scanline 3 199
Figure E-13 – Rockfall modeling results crossing the white line for Scanline 3 200
Figure E-14 – Rockfall model setup for Scanline 4 201
Figure E-15 – Full rockfall modeling results distribution for Scanline 4 202
Figure E-16 – Rockfall modeling results crossing the white line for Scanline 4 203
Figure E-17 – Rockfall model setup for Scanline 5 204
Figure E-18 – Full rockfall modeling results distribution for Scanline 5 205
Figure E-19 – Rockfall modeling results crossing the white line for Scanline 5 206
Figure E-20 – Rockfall model setup for between Scanlines 2 and 3 207
Figure E-21 – Full rockfall modeling results distribution for between Scanlines 2 and 3 208
Figure E-22 – Rockfall modeling results crossing the white line for between Scanlines 2 and 3 209
Figure E-23 – Rockfall model setup for between Scanlines 4 and 5 210
Figure E-24 – Full rockfall modeling results distribution for between Scanlines 4 and 5 211
Figure E-25 – Rockfall modeling results crossing the white line for between Scanlines 4 and 5 212

CHAPTER 1

INTRODUCTION

Highway SR-12 is a heavily used tourist route in southern Utah and is the main paved highway that provides access to Bryce Canyon National Park (Figure 1). SR-12 is susceptible to rockfall and landslides where it descends from the Paunsaugunt Plateau down toward Tropic (Figure 2). SR-12 runs below a cliff band of the Tertiary Claron Formation, which consists of limestones and mudstones that make up the colorful hoodoos and erosional features of Bryce Canyon. The Oligocene to Miocene Ruby's Inn Thrust

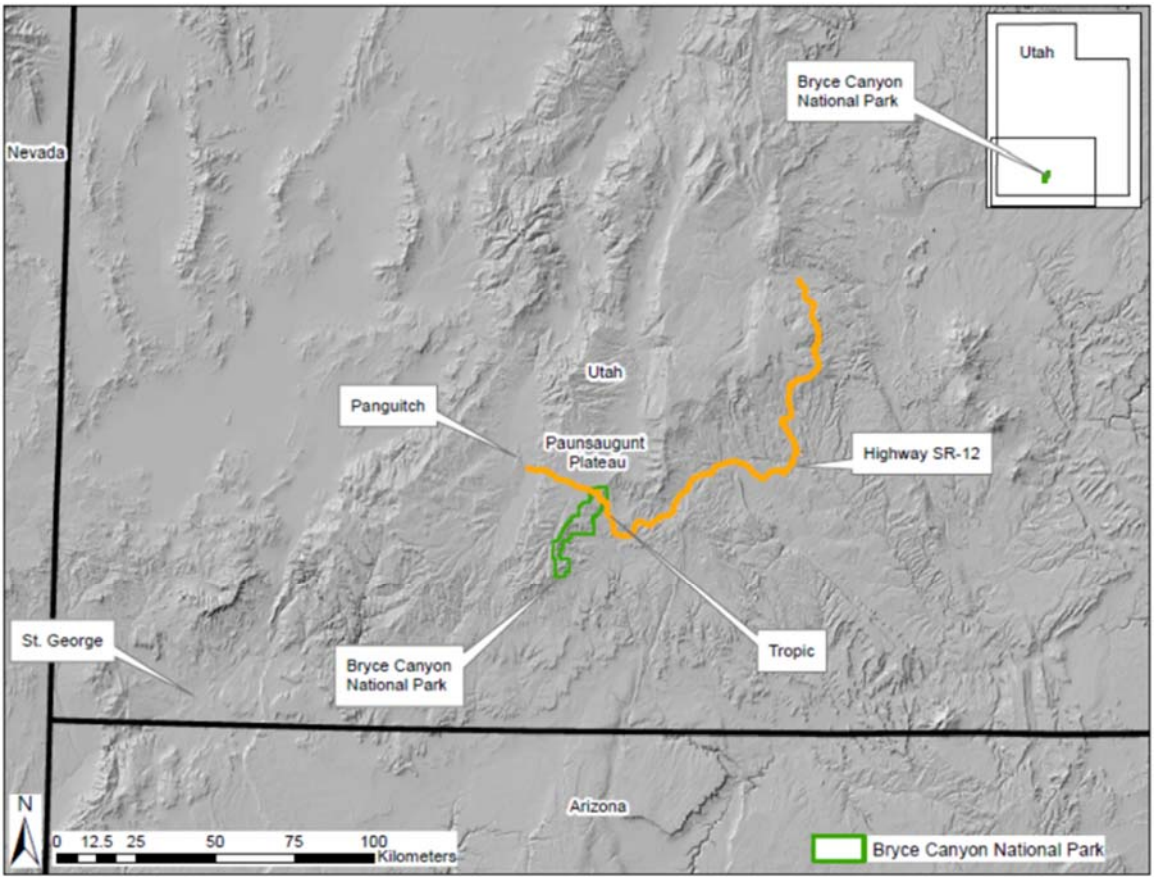

Figure 1 – Physiographic map of southwestern to southcentral Utah, including the Bryce Canyon study area. Hillshade created from 90 meter DEM (Hanser, 2008).

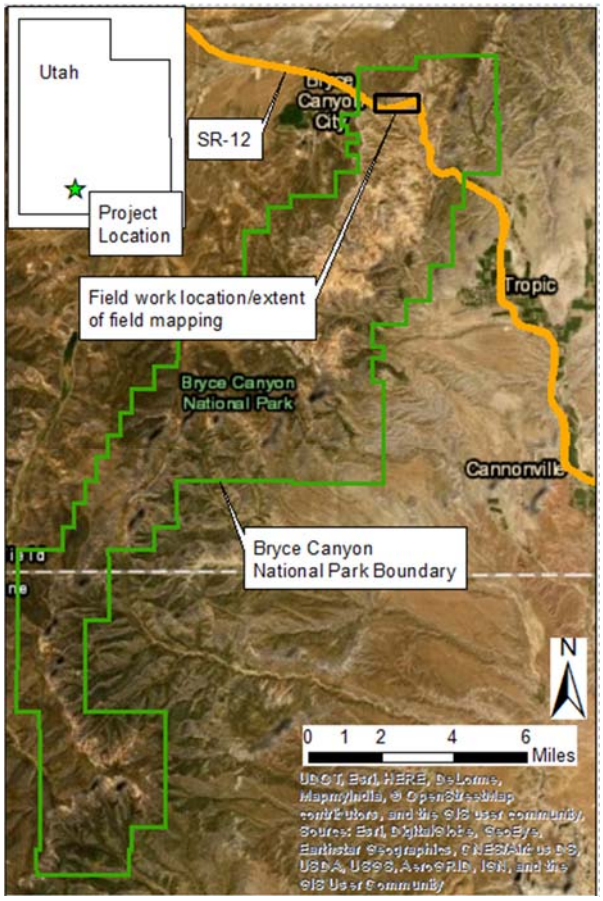

Figure 2 – Location map of the project area.

Fault (RITF) has juxtaposed a sequence of cliff-forming Claron beds on a slope-forming Claron sequence, creating the cliff band above the roadway (Figure 3).

My research hypothesis is that the fracturing associated with the RITF has weakened the rocks in this cliff band, resulting in increased mass-wasting hazards. This research is limited to a study reach where SR-12 drops below the Paunsaugunt Plateau, on the northern end of Bryce Canyon National Park (Figure 2). To test the proposed hypothesis, the research objectives of this study are: 1) to characterize cliff-forming lithologies at control and test locations, to assess similarity; 2) to characterize fracture networks and distribution in cliffs; 3) to measure the topography and assess physical

properties of the toeslope; and 4) to assess rockfall potential and risk to SR-12 within the study area.

Figure 3 - Cliffband above a toeslope leading down to SR-12, view looking east.

Significance and Justification

Over 2.6 million people travel along SR-12 through Bryce Canyon every year (Densmore, 2019). It is a National Scenic Byway, and a major thoroughfare for tourists traveling to Bryce Canyon National Park, Grand Staircase-Escalante National Monument, and other scenic attractions. The rockfall and landslide hazards to this highway have potential consequences of economic loss due to travel delays for tourists and commodities.

More directly, rockfalls could have devastating impacts because of the sharp turns, low visibility, and steep drop-offs in the study area. A landslide occurred in the study reach in 2017 (Figure 4) and emergency repairs cost over $2.6 million dollars (UDOT, 2019).

Figure 4 - Landslide along SR-12 in 2017 looking west, photo credit UDOT.

Outcomes of this study aim to aid public knowledge of potential hazards and could prevent economic loss or tragedy. Improved hazard assessment will help the National Park Service and the Utah Department of Transportation (UDOT) make informed decisions regarding alternative travel and evacuation routes. This project has particular societal significance at this time because UDOT is currently working on highway improvements within the study area.

More broadly, rockfall is a common process, and this research could provide an example for assessment of rockfall hazards beyond Bryce Canyon. Rockfall hazard maps have been created in surrounding areas of southern Utah like Zion National Park (Lund et

al., 2010), and one is currently being developed for the Bryce Canyon area (Knudsen, 2020). However, these maps are generally created using aerial photography and geospatial data with limited resources for site visits, but certain aspects of rockfall hazard that need to be assessed in the field. This research attempts to demonstrate the importance of field-based rockfall assessments.

CHAPTER 2

GEOLOGIC SETTING

Regional Geologic Setting

The project is located on the eastern portion of the Paunsaugunt Plateau in the transition zone between the Basin and Range and the Colorado Plateau (Figure 5). The Basin and Range is a region characterized by generally north-south trending mountain ranges separated by similarly trending valleys. The Colorado Plateau is a region characterized by generally flat-lying to gently dipping sedimentary rocks. The Paunsaugunt Plateau is geomorphically more similar to the Colorado Plateau, although north-trending, down-to-the-west normal faults cut the plateau.

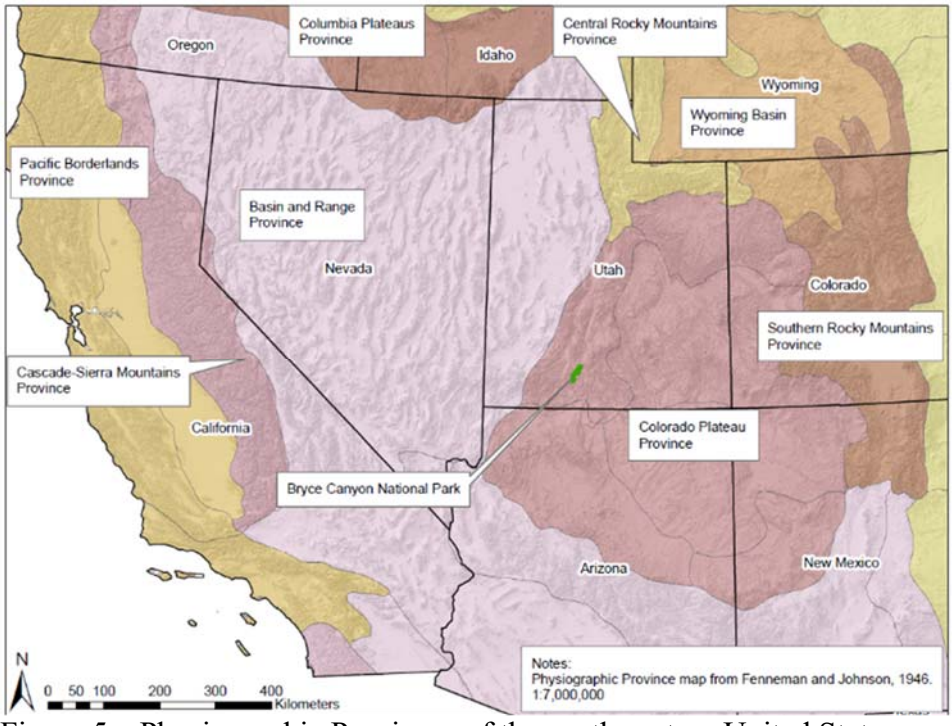

Figure 5 – Physiographic Provinces of the southwestern United States

Structure

Part of the structure of the Paunsaugunt Plateau is the result of thrust faulting and recumbent folding associated with generally southeast-directed compressional tectonics during the Sevier Orogeny (Baer, et.al., 1982). Additional south-directed thrust faulting, the Ruby's Inn Thrust Fault, occurred during the Oligocene to Miocene, oblique to the Sevier Orogenic belt (Figure 6). This later thrust faulting is thought to be associated with the gravitational collapse of the Tertiary-aged Marysvale Volcanic Field (Biek et al., 2015). Neither the Ruby's Inn Thrust Fault nor the faulting associated with the Sevier Orogenic Belt are considered active faults (UGS, 2020)

The plateau is bounded on the east by the Paunsaugunt Normal Fault Zone, and on the west by the Sevier Normal Fault Zone, which are both related to Basin and Range

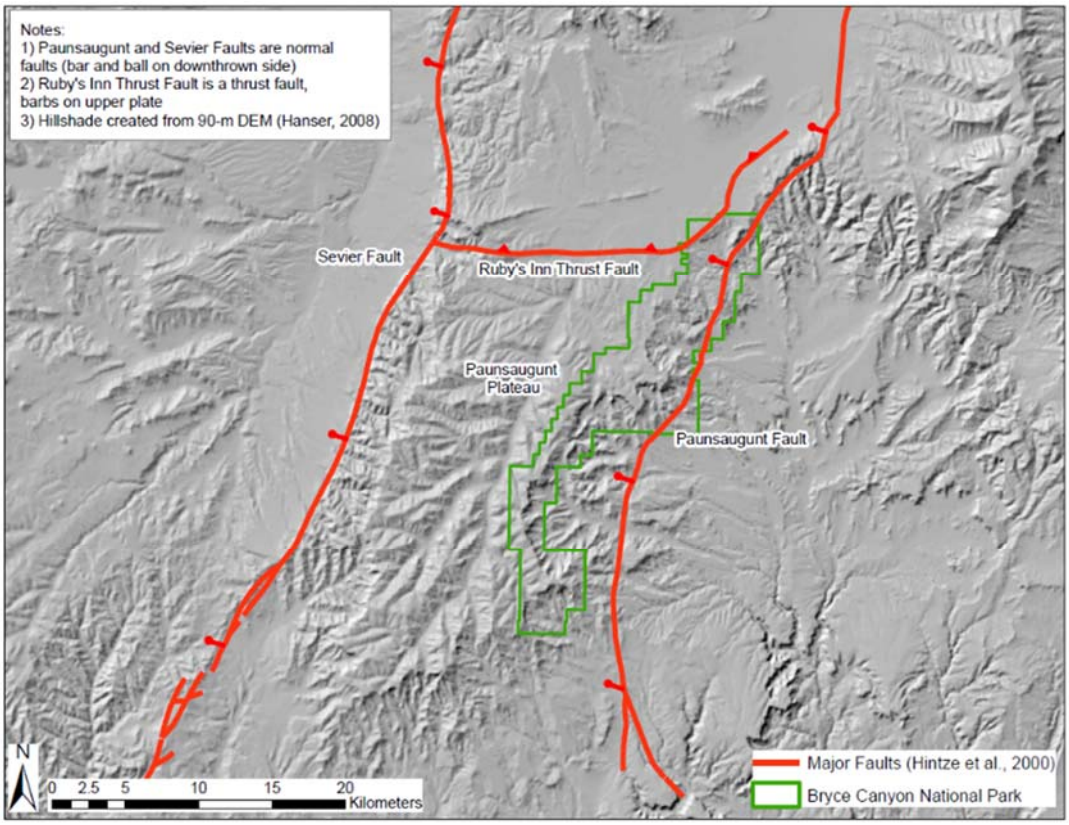

Figure 6 – Regional structure map adjacent to the Paunsaugunt Plateau

extension. The Paunsaugunt Fault Zone is the easternmost fault in the transition between the Basin and Range and the Colorado Plateau. The Paunsaugunt Fault Zone is not included in the UGS Quaternary Fault and Fold Database (UGS, 2020), but additional sources have indicated that it may have been active during the Quaternary (Black and Hecker, 1999). The Sevier Fault Zone is considered to be active, with the most recent surface-fault-rupture occurring less than 130,000 years ago (UGS, 2020).

Stratigraphy

The exposed stratigraphy of the Paunsaugunt Plateau consists of Cretaceous fluvial and coastal deltaic deposits that are overlain by Tertiary lacustrine and fluvial deposits, and then later Tertiary volcanics. More specifically, the exposed stratigraphy in the project area is mapped as Paleocene to Eocene Claron Formation.

The Paleocene to Eocene Claron Formation consists of alternating limestones, mudstones, calcareous sandstones and occasional pebble conglomerate. It includes two main units – the lower Pink Member and the upper White Member (Taylor, 1993). The Claron Basin was one of a series of large basins bounded by the Sevier Orogenic Belt on the west and Laramide uplifts on the east (VanDeVelde and Bowen, 2014). The Pink Member of the Claron Formation is mapped as underlying the entire study area. It consists of alternating beds of varicolored and commonly mottled, pale reddish-orange, reddish-brown, moderate-orange pink, dark-yellowish-orange, and grayish-pink, sandy and micritic limestone, calcite-cemented sandstone, calcareous mudstone, and minor pebbly conglomerate. The limestone is poorly bedded, microcrystalline, generally sandy, and is locally argillaceous. The sandstone is thick-bedded, fine- to coarse-grained, calcareous,

and locally cross-bedded. The mudstone is generally moderate reddish orange, silty, calcareous, contains calcareous nodules. The pebbly conglomerate forms lenticular beds typically 5 to 15 feet (2–5 m) thick containing rounded quartzite, limestone, and chert pebbles, cobbles, and, locally, small boulders. The Pink Member is proposed to have been deposited in fluvial, floodplain, and lacustrine environments (Biek et al., 2015). The upper White Member is more consistently lacustrine than the lower Pink Member, and it contains several thick sequences (up to 180 meters thick) of limestone, but it also contains fluvial mudstones and sandstones (Biek et al., 2015).

Geomorphology

Late Cenozoic base-level fall has led to the erosion of the greater Paria drainage, including the exposure of the Ruby's Inn Thrust Fault (RITF) adjacent to highway SR-12. The Oligocene to Miocene RITF has placed a cliff-forming carbonate sequence above a slope-forming sequence (Lundin, 1989), which has led to the development of a cliff band and a toeslope above the road. Weathering occurs through a combination of physical weathering from freeze-thaw cycles, as well as chemical weathering along preexisting fractures and bedding. Material is removed from the cliff and surrounding areas by ephemeral streams, rockfall, landslides, slopewash, creep, and other mass movement processes. Recent calculations of catchment-averaged erosion rates in the area are on the order of 400 mm/kyr or 0.4 mm/yr, based on Beryllium-10 cosmogenic inventory of sediments in local streams (Riley et al., 2019). This relatively high catchment erosion rate should be considered a minimum in comparison to specific erosion rates along cliffs due to steeper slopes (Forte et al., 2016).

Study Area

The project area along highway SR-12 is in the northeastern portion of Bryce Canyon National Park, between SR-12 mile post markers 15 and 15.7 (Figure 7). The focus is on the area between the roadway and the cliffband between these mile post markers. The highway drops from the top of the Paunsaugunt Plateau into Tropic Canyon at a grade of 3 to 6 degrees (5 to 10 percent), dropping from 2310 to 2190 meters in elevation. Under the current configuration (as of August, 2020), the asphalt shoulders along the roadway are on average 3 feet wide, with the roadway ditch width varying from 10 to up to 40 feet wide and generally between 10 to 20 feet. Roadway construction cut slopes adjacent to the existing roadway range from 40 to 55 degrees.

The surrounding topography within the immediate project vicinity ranges from approximately 2105 to 2370 meters in elevation (Figure 8). Natural slopes between the roadway and the cliff band range from 20 to 35 degrees. The cliffband ranges from 30 to

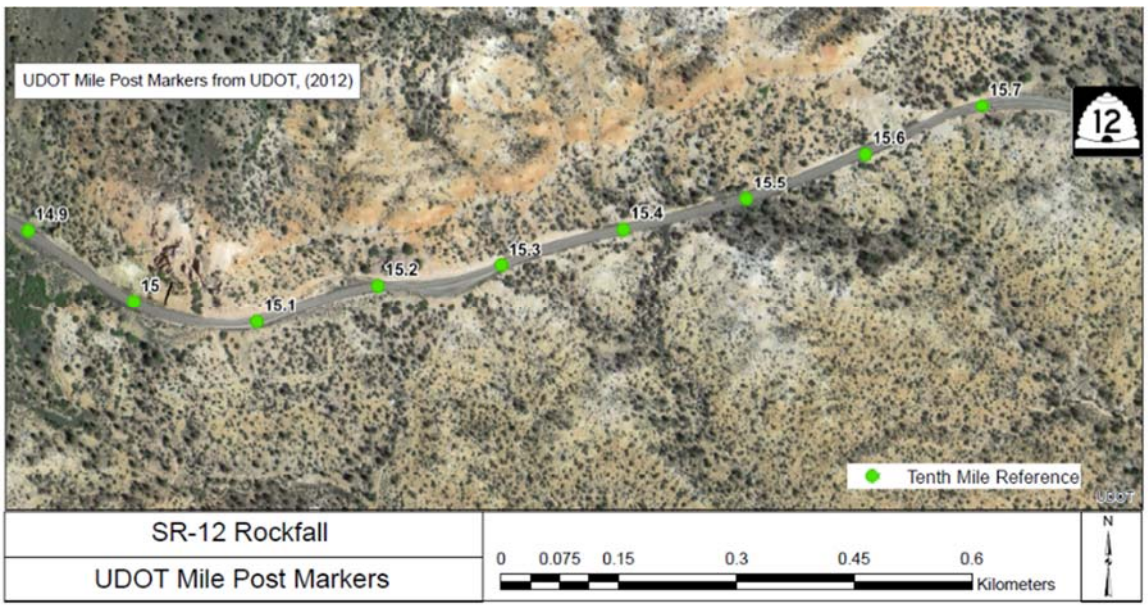

Figure 7 – Highway SR-12 mile post marker map (UDOT, 2012)

over 100 meters north of the roadway and is situated from 50 to 70 meters in elevation above it. Ephemeral drainages incise the cliffband and the underlying toeslope in several locations (Figure 8).

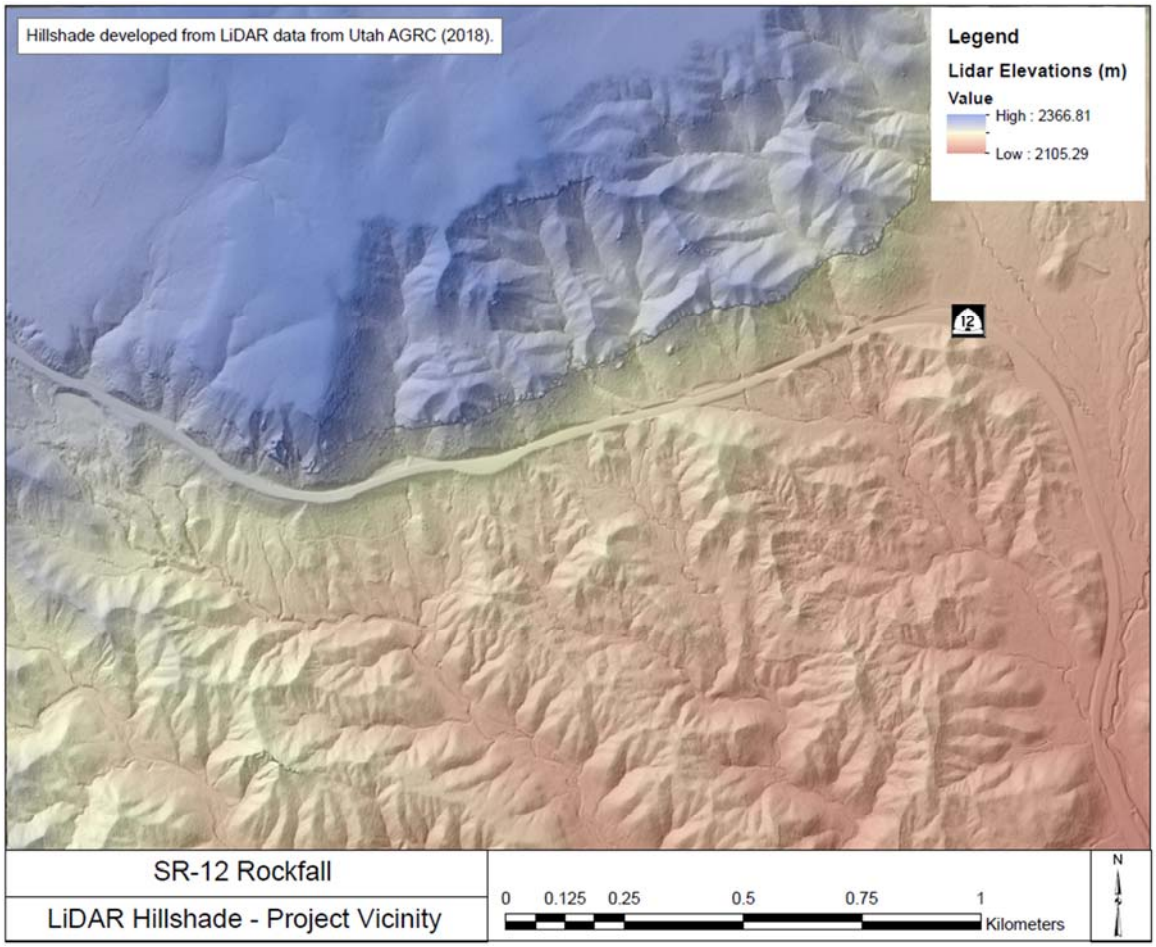

Figure 8 – Hillshade and elevation data from 0.5-meter LiDAR data for the Bryce Canyon area, within the project vicinity (AGRC, 2018).

The main lithologic unit that is mapped in the project area is the Tertiary Pink Member of the Claron Formation (Tcp; Biek et al., 2015, Bowers, 1991, Figure 9), which is described above in the Stratigraphy section. Additional units including as the Cretaceous Wahweap Formation (Kw), Quaternary piedmont alluvium (Qap) and Quaternary alluvium and colluvium (Qac) were mapped near the project area, but not within the study area.

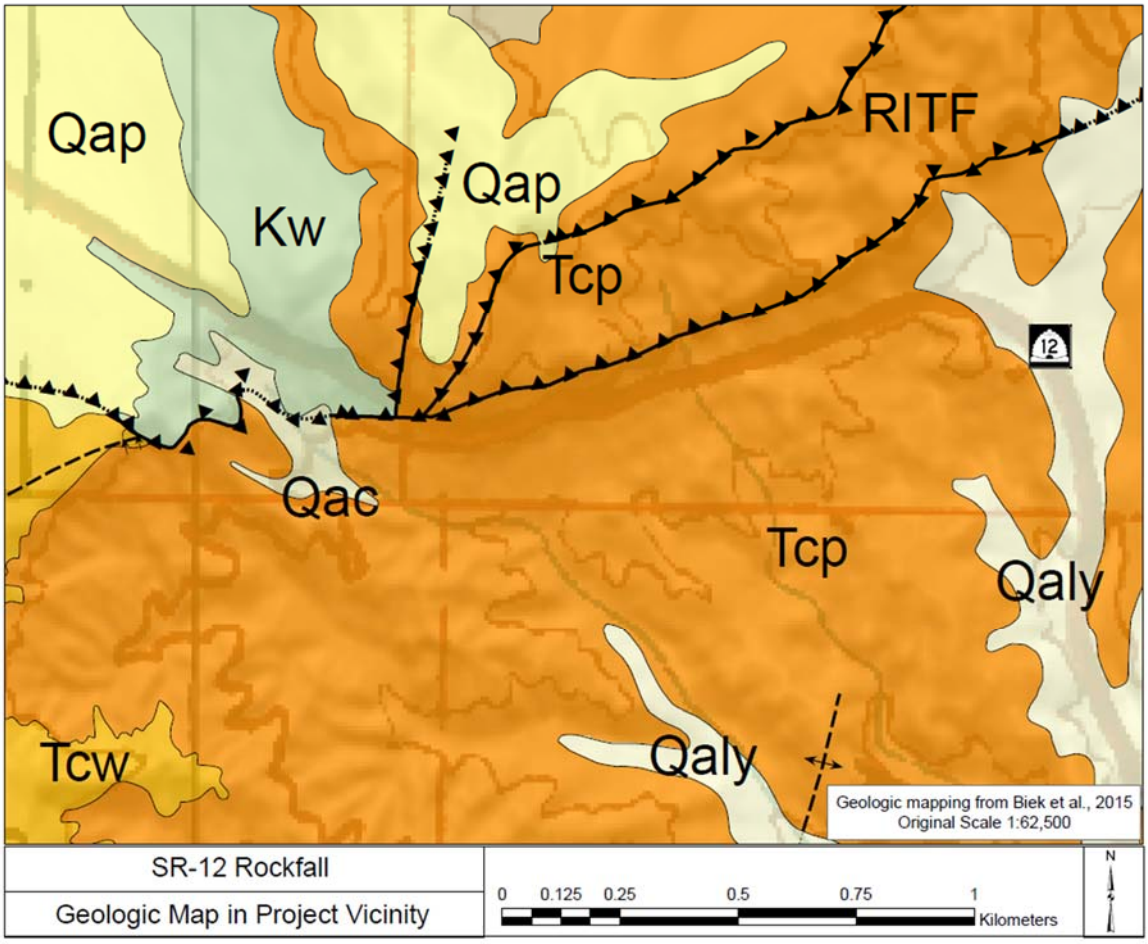

Figure 9 – Geologic mapping of Biek et al. (2015) in project vicinity. Kw = Cretaceous Wahweap Formation. Tcp = Tertiary Pink Member of the Claron Formation. Tcw = Tertiary White Member of the Claron Formation. Qap = Quaternary piedmont alluvium. Qac = Quaternary alluvium and colluvium. Qaly = Quaternary stream alluvium. RITF = Ruby's Inn Thrust Fault, several splays

Although the currently published mapping indicates the presence of Pink Member in the hanging wall and footwall of the RITF north of SR-12, unpublished mapping performed by Knudsen (2020) identifies the White Member of the Claron Formation in the footwall of the RITF in this location. This interpretation was supported by field observations and observations made using aerial imagery during this research (Appendix A).

The geomorphology of the project area is in large part controlled by the Ruby's Inn Thrust Fault. The RITF has been studied in detail (Lundin, 1989, Davis and Pollock, 2010,

Biek et al., 2015), but remains enigmatic in some ways because of a lack of reliable timing constraints for the faulting and its unusual spatial orientation. In a region where a majority of thrust faulting occurred as part of either the Sevier or Laramide Orogenies, which were characterized by northeast-southwest trending thrust faults, the RITF trends generally east-west. The RITF also displaces strata of the Brian Head Formation (37 to 33 Ma), west of the study area, that postdate the Sevier and Laramide Orogenies.

The RITF is at least 40 kilometers long and appears to have accommodated between 500 and 1000 meters of south-directed offset in the project area (Lundin, 1989). The main fault strand has an approximate dip angle between 25 to 35 degrees, and dips to the north (Biek et al., 2015). Based on well logs, the fault appears to sole into Jurassic evaporites (Lundin, 1989). East of SR-12, the fault splits into two strands, an upper and a lower strand. The lower strand is the one closest to SR-12, and the one that this research is concerned with.

Deformation in the footwall consists largely of conjugate fracturing, overturned and vertical bedding, and folding. The fault surface is characterized by a thin zone of reddish-brown gouge, and striation of materials on the underside of the hanging wall rocks. Rocks in the hanging wall, especially marlstones and carbonates, display a pattern of closely spaced fractures. This fracture pattern has been interpreted by others as pressure solution cleavage, which occurred in response to the compression and horizontal shortening during thrusting (Lundin, 1989).

Because of the overall geometry of the RITF, its proximity to the Oligocene-to-Miocene Marysvale volcanic field, it has been interpreted that the RITF formed as a result of gravitational collapse and spreading during a late phase of the formation of the volcanic

field, during the late Oligocene to early Miocene (Biek et al., 2015).

Background on Rockfall Processes

Rockfall is a mass-wasting process that consists of slope failure and rapid downslope movement of blocks and rock masses (Cruden and Varnes, 1993). Rockfall is generally caused by one of two conditions: the coincidence of joints, bedding planes, and other discontinuities with a slope or rock face, or differential erosion and oversteepening of a slope or rock face (Pierson, 1992). Initiation of movement is often caused by freeze-thaw cycles, shrinking and swelling of clay minerals, increases in pore pressure, root wedging, seismic ground shaking. Following slope failure, blocks or masses fall, bounce, or roll, depending on the toeslope configuration and cliff height (Cruden and Varnes, 1993). Free fall often occurs where toeslope angles are greater than 76 degrees; bouncing on slopes between 45 and 76 degrees; and rolling on slopes shallower than 45 degrees (Cruden and Varnes, 1993). Transport distance is controlled by the geometry, frictional characteristics, and restitutive properties of the toeslope.

The magnitude of a rockfall hazard is generally characterized by run-out length and size and frequency of rockfall events. Small fractures contribute to the hazard by contributing to differential erosion, but small blocks resultant from small fractures do not contribute directly to risk at the roadway. This is because smaller rocks generally either cannot gather enough momentum to reach the roadway, or do not cause significant damage to property or human life if they do reach the roadway. The risk associated with rockfall events is related to the potential of the rockfall hazard to reach infrastructure and cause damage or loss of life.

CHAPTER 3

RESEARCH DESIGN AND METHODOLOGY

The main hypothesis to be tested by this research is that the additional fracturing associated with the RITF has weakened the Claron Formation rocks above SR-12, creating an enhanced rockfall hazard and increasing rockfall risk to SR-12. This research has been designed to specifically test the effects of fracturing caused by the RITF, and to control the topographic effect of the cliffband, which has potential to create a rockfall risk without the presence of a fault. That is, it is possible that the fracturing caused by the RITF has little to no measurable effect on rockfall hazard, and that rockfall hazard simply exists at this location due to the presence of a cliff.

To test the fault-fracture enhancement hypothesis of this research, four major objectives were identified. The first objective was to characterize lithologies among the control and test locations, to demonstrate that the Claron units are analogous. Significantly different lithologies, rock strengths, and bedding thickness can induce different fracture intensities in response to the same stress. The second objective was to characterize the fracture networks and distribution at a control location, away from the RITF, and at several locations adjacent to the RITF. The third objective was to measure the geometry of the toeslope and assess the physical properties its material, to aid in the assessment of the probability of rockfall reaching the roadway after falling from the cliffband. The final objective was to compile results in a rockfall-potential assessment at the control and test locations.

Site Selection

To accomplish the research objectives, five test sites near the RITF (Figure 10) and a control site away from the RITF (Figure 11) were selected for collection of

Figure 10 – Typical outcrop along the RITF, cliffs approximately 20 to 30 meters tall. RITF at the base of the cliff

fracture data using scanline techniques similar to those discussed in Watkins et al. (2015). The control location, is approximately 500 meters south of the RITF (Figure 12 and Figure 13).

Test scanlines 1 through 5 were selected based on equal spacing from the westernmost and easternmost locations on the RITF that could affect SR-12 with rockfall.

Figure 11 - Control outcrop, with generally flat-lying bedding, appears generally unaltered and in-place. Cliff approximately 15 meters tall

Scanline locations were also influenced by the need to study at least one location that would be in the footwall and hanging wall of the RITF, with Scanline 1 being the only one in the footwall. The majority of hangingwall scanlines is justified because the hanging wall it forms the more prominent parts of the cliffband and the large blocks that could reach SR-12 (Figure 14). This indicates that the hanging wall rocks are less likely to fracture and erode into smaller fragments, and more likely to come down as large blocks that could reach SR-12. The orientations of the scanlines were varied (Figure 12) to reduce sampling bias in a linear scanline method against fractures that trend parallel to the scanline.

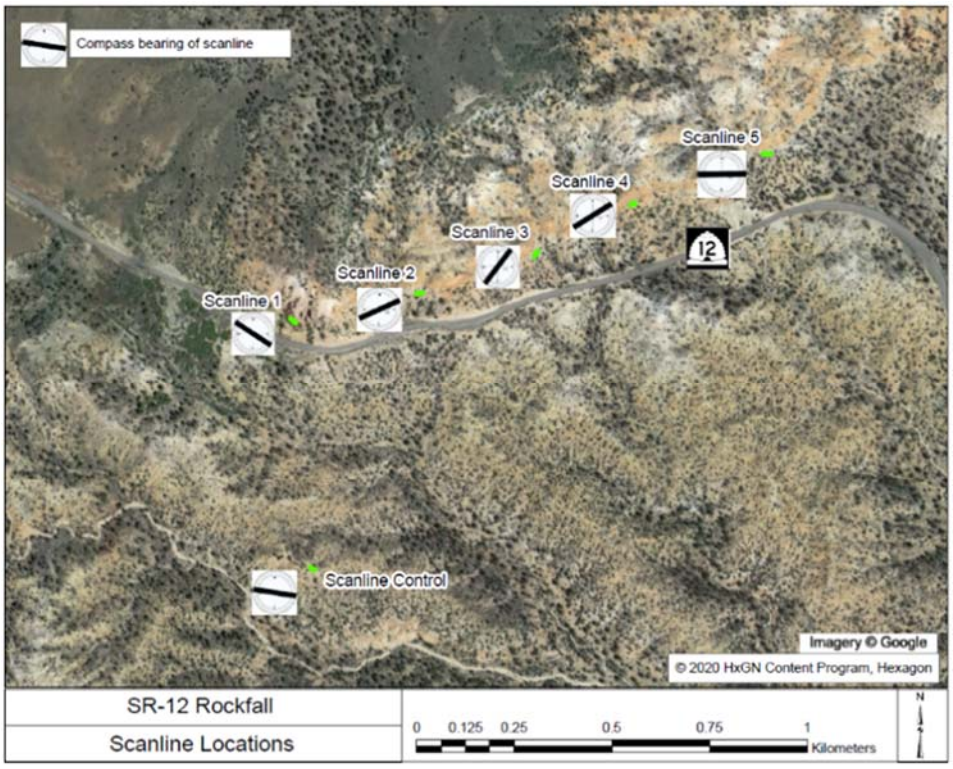

Figure 12 - Scanline location map, overlaid on aerial imagery

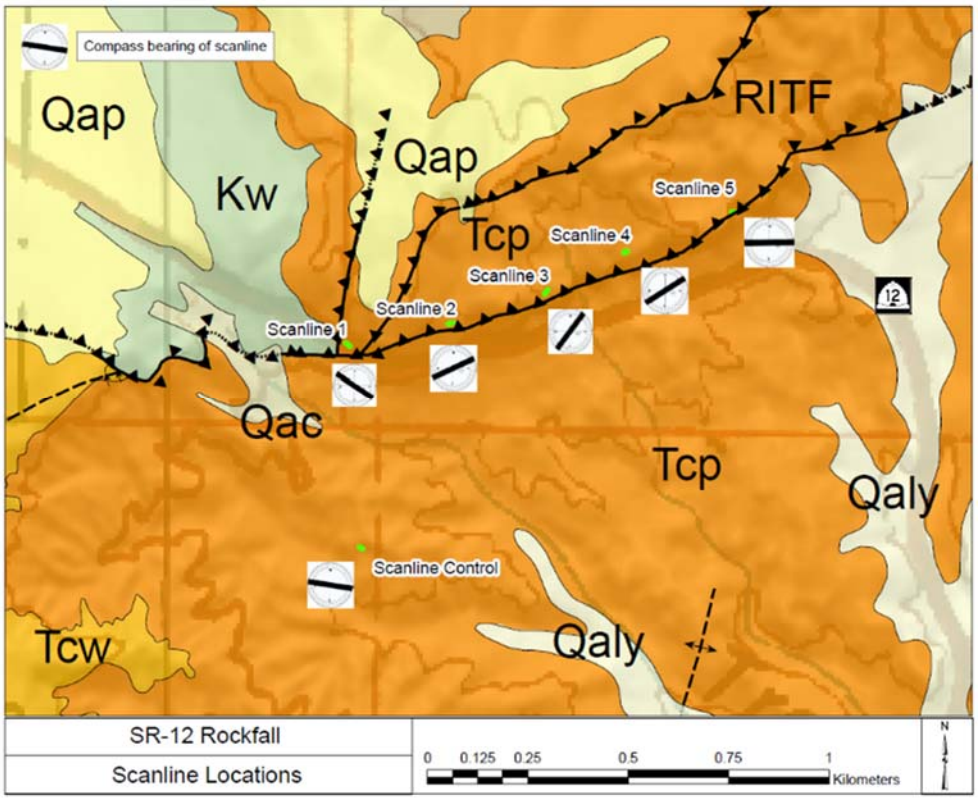

Figure 13 - Scanline locations, overlaid on the Panguitch 1:62,500 Quad (Biek et al., 2015). Qaly – Young stream alluvium. Qac – Alluvium and colluvium. Qap – Quaternary piedmont alluvium. Tcw – Tertiary White Member of the Claron Formation. Tcp – Tertiary Pink Member of the Claron Formation. Kw – Cretaceous Wahweap Formation.

Figure 14 – RITF and differential erosion where the hanging wall forms a cliff and the footwall forms the toeslope

Objective 1 – Characterize lithologies at control and test locations

To characterize lithology, four techniques were used: field descriptions, field measurements of rock hardness, and collection of representative hand samples to examine by thin-section petrography and X-ray diffraction (XRD).

Outcrop lithology was described similar to method recommendations found in the Engineering Geology Field Manual (USBR, 2001). Descriptions were generally limited to units that were intersected by the scanlines. Most scanlines only traversed across one lithology, except for scanlines 1 and 4, which crossed two distinct lithologies. Due to lithologic variability, two samples each were collected from these scanlines, while only

one sample was collected from the other scanlines.

Rock hardness was assessed in the field using a Schmidt Hammer. The Schmidt Hammer is a device that measures the elastic rebound of a calibrated impact on a surface, and records an "R-value" for each impact. This R-value can be correlated with uniaxial compressive strength in some cases, and can be an indicator of relative rock strength (Goudie, 2006). The Schmidt Hammer was used at each scanline location, and applied to each lithology along each scanline so that all of the same rocks that were sampled could be compared in terms of relative strength. The Schmidt Hammer was generally used on unprepared but flat and smooth portions of the outcrop, to promote uniformity in the method of testing. Tests were performed perpendicular to the outcrop face, and the hammer was held horizontally in all of the testing except for at scanline 2, where the outcrop is an overhang and the hammer was held almost vertically. Tests were performed in 10 unique locations within each bed, within a 2-meter radius of the sampling locations.

X-ray diffraction testing was performed on sample powders, which were prepared from hand samples ground in a Rocklab R.C. Ring Mill pulverizer using a tungsten carbide head. Powders were compacted into sample holders with a smooth surface for analysis. X-ray diffraction was performed using a Panalytical X'Pert Pro X-ray Diffraction Spectrometer with a Cu anode tube (PW3050/6) under 45 kV tension and 40 mA current operating conditions. The samples were run with a continuous scan step size of 0.02 degrees per second, from 2-75° (2θ).

Thin sections were prepared by Wagner Petrographic in Lehi, Utah after cutting portions of the original hand samples into approximately billet-sized samples (24x46 mm). Thin sections were impregnated with blue epoxy, and then half of each thin section was stained with alizarin red S and potassium ferricyanide to distinguish carbonate minerals (Figure 15, Precimat, 2020). Full thin section pictures were then taken using a

Mineral	Stain Result			Crystal Structure
	Alizarin Red S (ARS)	Potassium Ferricyanide (PF)	ARS & PF	
Calcite	Pink Orange	None	Pink Orange	Hexagonal
Ferroan Calcite	Pink Orange	Blue	Mauve, Purple Blue	
Dolomite	None	None	None	
Ferroan Dolomite	Pale Mauve	Blue Turquoise	Turqoise Green	
Siderite	None	None	None	
Magnesite	None	None	None	
Rhodochrosite	None	Pale Brown	Pale Brown	
Aragonite	Pink Orange	None	Pink Orange	Orthorhombic
Witherite	Red	None	Red	
Cerussite	Mauve	None	Mauve	

Figure 15 - Dual carbonate staining results key (Precimat, 2020).

microscope camera mounted to a Leica Z16 APO microscope using an exposure of 20 ms, contrast of 0.60, illumination intensity of 75, aperture at 100%, and the High Dynamic Range setting enabled, in plane polarized light. The zoom of the microscope was set to 0.57 on 1.51x, and the camera was set to 0.3x, visual 8.6x magnification, and iris set to 100%. Images were spliced using Adobe Photoshop after taking two photographs of each thin section. Zoomed images of the thin sections were taken using a microscope camera mounted to a Leica DM2700P microscope, using the same parameters as were used with the Z16 APO, except that the microscope magnification and illumination changed depending on the sample and the image. Samples were examined and various images were recorded using both cross-polarized light and plane polarized light.

Objective 2 – Characterize fracture networks

Scanlines were set up by establishing a starting point of the scanline, fixing one end of a tape measure to that starting point, and extending the tape for at least 10 meters along the outcrop face. Fracture data were collected from every fracture that intersected the tape measure, and included rock type at the fracture location, fracture type, fracture trace length, thickness, filling, roughness, spacing, orientation, weathering, and qualitative moisture assessment (Figure 16). One exception to collecting all of the fracture data was a very dense cleavage pattern found at Scanline 4 and Scanline 5. The small-fracture cleavage data was collected at Scanline 5, but not collected at Scanline 4. The reason for not collecting this data at Scanline 4 was the high number of these small fractures that were assumed in the field to not contribute directly to the risk of blocks reaching the roadway. As discussed previously, these fractures are important in the differential weathering aspect

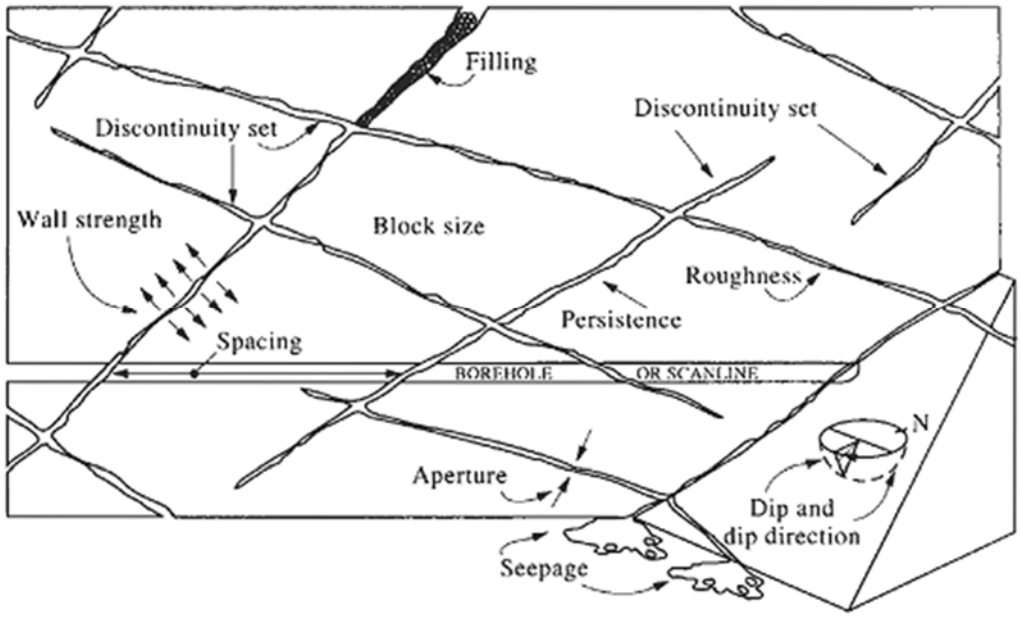

Figure 16 - A representation of discontinuity data to be collected in the field, from Hudson and Harrison (1997)

of creating the rockfall hazard here, but do not create blocks large enough to pose a risk to the highway. The cleavage fracture data from Scanline 5 is included in the raw data sheet, but generally excluded from data analysis, discussed below in the Results and Discussion section. The scanline data collection was performed until at least 30 fractures were analyzed, to collect a statistically significant dataset at each scanline location. All scanlines were at least 10 meters long. Photographs, GPS locations, and representative samples of the fracture filling (if present) were collected at scanline locations. However, generally the fractures encountered at the scanline locations either did not contain fracture filling, had very thin veneers of fracture filling, or were rough enough to not have their strength controlled by fracture filling. Only one fracture filling sample was collected, at the control scanline, but no analysis was performed on this sample.

Following the collection of this fracture data, the data were reduced in several ways to assess similarities and differences between the control and test scanlines. Fracture intensity, fracture length, aperture, maximum apparent spacing, and weighted average apparent spacing were compared using histograms.

Fracture intensity was calculated along each scanline and comparisons were made between scanlines Because the scanlines are basically one-dimensional transects, the one-dimensional parameter of fracture intensity was chosen to describe the frequency of fractures occurring along the scanlines. Fracture intensity is measured in number of fractures per unit length, or in this case fractures per meter. It is calculated by simply dividing the total number of fractures crossing a given scanline by the total length of the scanline (Mauldon and Dershowitz, 2000). As this measure is direction-dependent, the orientations of the scanlines have been measured and provided in the raw data sheets

(Appendix B). Fracture intensity was compared in two ways: one data set included all of the data recorded in the field from each scanline, and a second data set screened all fractures that were less than 0.5 meters long. The purpose of screening data less than 0.5 meters was to remove fractures that would not initiate failure of significant blocks or masses, that could have the potential to reach the roadway. As discussed in the Rockfall section, above, small blocks do not generally pose a direct risk to the roadway.

Certain data were screened from the measurable fracture length comparison because some of the fracture length data collected were recorded as minimum fracture lengths, where the measurable fracture length could not be recorded. This occurred in cases where either the fracture continued down and disappeared into the bottom of the outcrop, so no lower termination could be found to measure, or the fracture continued up through the outcrop to the point where it could no longer be traced or seen, and no upper termination could be found to measure. Data from both measurable fracture length and the minimum fracture length are compared in Chapter 4.

Stereonets were created to isolate major joint sets and compare fracture patterns spatially. Additional direct measurements were taken on the surface of the RITF, where exposed near the scanlines, to include it in the stereonets. The fault plane was generally not measured during linear scanline data collection because of the parallel orientations of the fault and the scanlines. It was, however, measured separately because of its prominence as a feature in the area, and because of its obvious contribution to rockfall hazard.

Using the data screened at 0.5 meters, major joint sets were delineated using stereonets. These major joint sets were then used to estimate apparent fracture spacing among the major joint sets at each scanline. Both an average apparent fracture spacing and a maximum apparent fracture spacing were calculated for each scanline, to assess the average and maximum block size that could become dislodge from the cliffs from the discontinuities. The fracture spacings are noted to be apparent because true fracture spacing is measured perpendicular to the joint sets, and these apparent fracture spacings were calculated along the direction of the scanlines. Using an apparent fracture spacing instead of true fracture spacing has potential to increase the calculated fracture spacing, because of how oblique angles distort the measured spacing at the scanline (Figure 17). Weighted

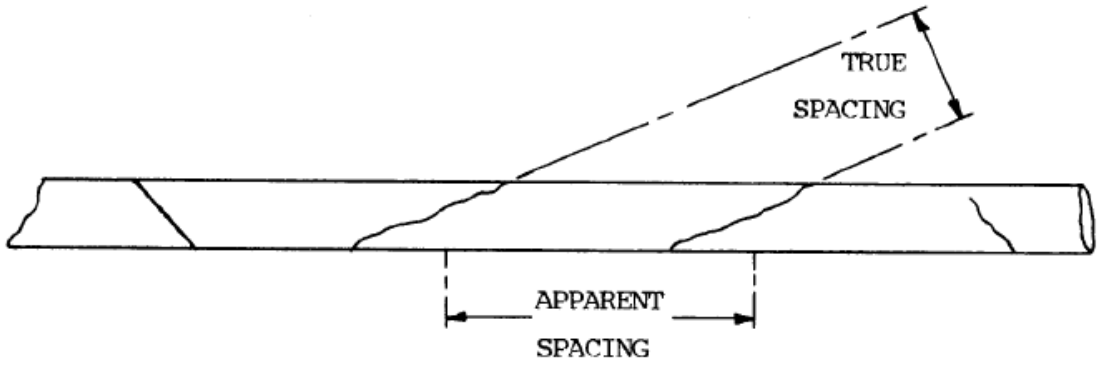

Figure 17 – True versus apparent fracture spacing (USBR, 2001)

average apparent spacing was calculated by using the following weighted average formula:

$$\bar{x} = \frac{\sum_{i=1}^{n} (x_i * w_i)}{\sum_{i=1}^{n} w_i} \qquad \text{Eq. 1}$$

where x_i represents the average spacing per major joint set, and w_i represents the number of joints measured within that major joint set per scanline.

Objective 3 – Characterize toeslope materials and geometry

Geometry of the toeslope was characterized using available lidar data from the Utah Automated Geographic Reference Center (AGRC), which has 0.5-meter pixel resolution (Utah AGRC, 2018. This data was imported into ArcMap 10.8.1, and analyzed by drawing profiles and raster calculation of slope. Slope profiles were drawn using a straight-line method above and below the scanline locations, following the steepest initial slope at the base of the scanline outcrop. Profiles were drawn to the white line of the roadway that was closest to the slope. For the control, a "white line" was arbitrarily placed at the base of the profile for comparison, because there is no roadway below the control scanline. Profiles for each of the scanlines and their locations, along with two additional profiles can be found in Figure 18 and Figure 19. The additional profiles were drawn between scanlines 2 and 3, and 4 and 5.

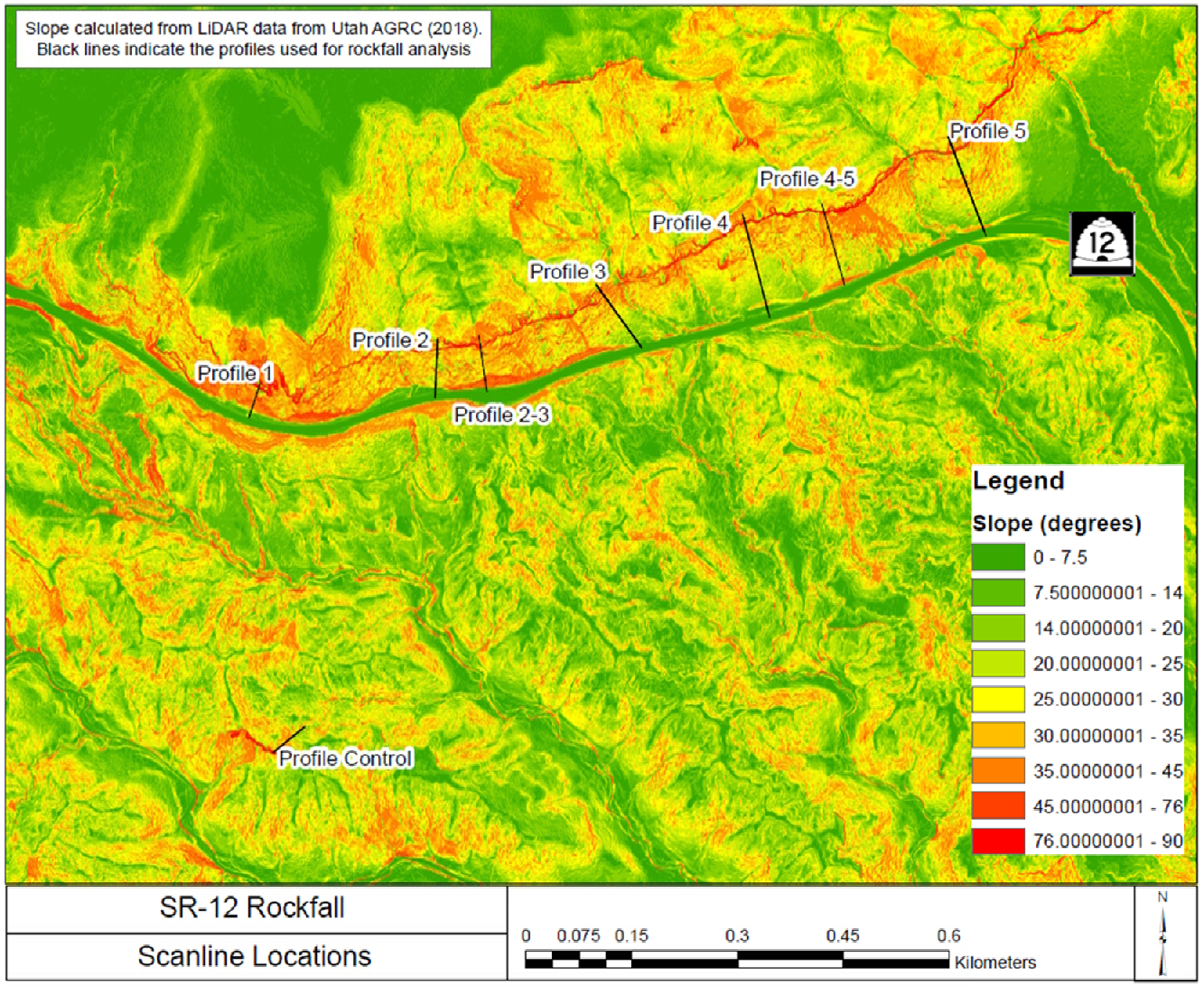

Figure 18 – Scanline profile locations, shown on a slope map of the project vicinity. Slope is in degrees, calculated in ArcMap from the 0.5 meter LiDAR data (Utah AGRC, 2018)

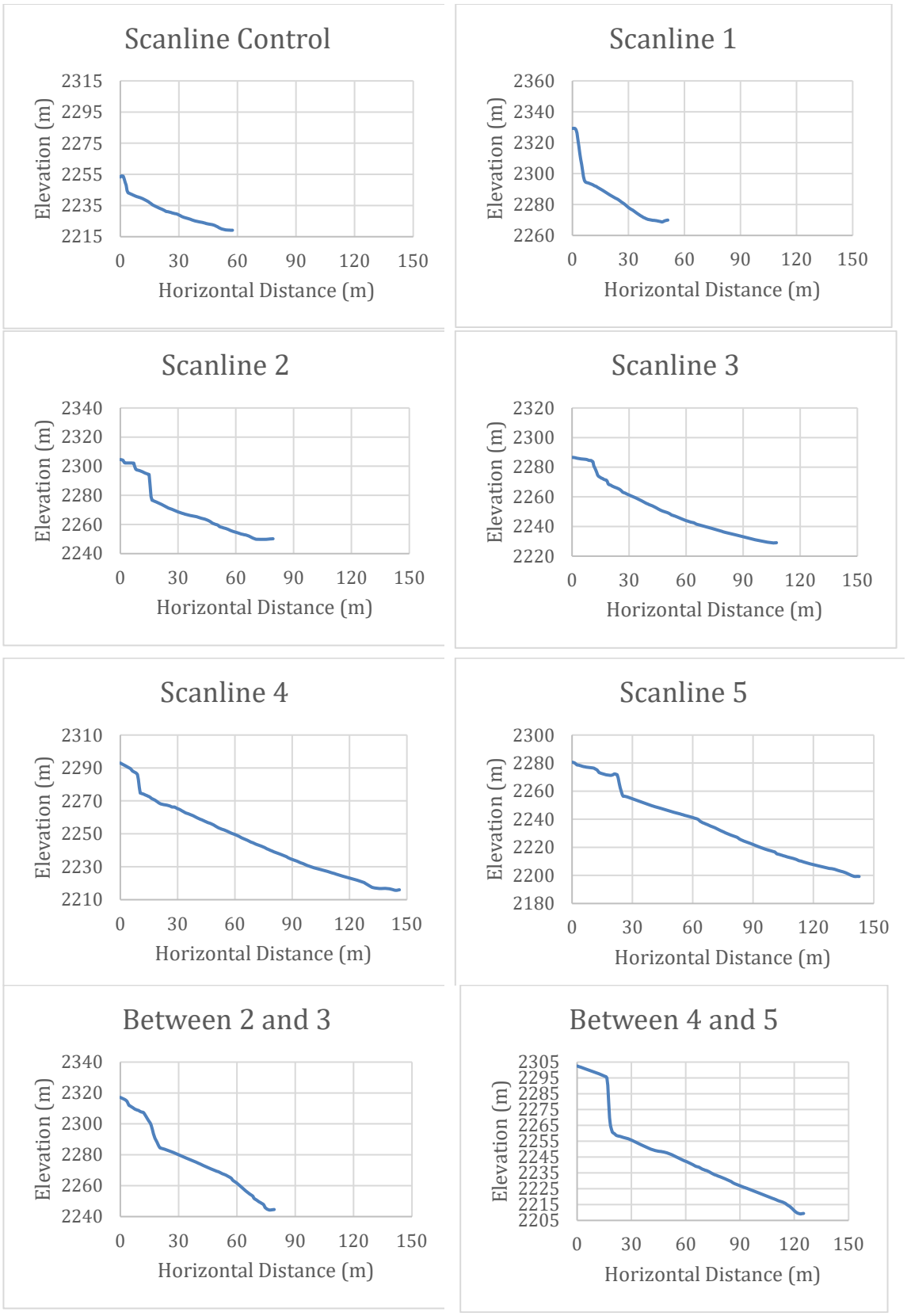

Figure 19 – Longitudinal profile graphs of cliff and toeslope at each rockfall analysis location, from LiDAR data (Utah AGRC, 2018). Profiles end at the white line of roadway

Assessment of physical properties of the toeslope was limited to grain-size analysis of grab samples, from toeslopes directly below the scanline locations. The grain size distribution can be used to assess toeslope friction angle and roughness. Samples were collected below each scanline location, for a total of six samples, by selecting three representative spots within a 2 meter radius, from 5 to 15 meters downslope from the scanline locations. At these three representative spots, a hand trowel was used to gather sample from the slope and place it into a sealable bag. Samples were generally gathered from the upper 6 inches of slope material. Grain-size distribution was measured by sieving and then laser diffraction. Samples were sieved using a 2 millimeter and a 1 millimeter sieve, creating 3 size fractions: greater than 2 millimeters, between 1-2 millimeters, and less than 1 millimeter.

While attempting to characterize the toeslope material in the field, it was observed that many of the toeslopes consisted of unconsolidated deposits, not lithified Pink Member of the Claron Formation as mapped by Biek et al. (2015). This observation was supported by unit descriptions made at roadway cuts along SR-12, as well as observations made in several subsurface explorations performed by Gerhart Cole in the area in 2019 (Gerhart Cole, 2019). Aerial photography and LiDAR data were also used to distinguish contacts between the unconsolidated units and adjacent bedrock. Techniques used while mapping using aerial photography and LiDAR included searching for boulders embedded in slopes, color differentiation, and finding intact bedding.

Objective 4 – Perform rockfall assessment

The data collected in the field, lab, and terrain model were used to develop input parameters

for two models applied at each scanline location: a kinematic analysis model (Hoek and Bray, 1981), and a rockfall model (Jones, Higgins and Andrew, 2000) The purpose of the kinematic analysis is to assess the relative failure potential among the six scanline locations caused by fracture intersections. Failure along fractures cause rockfall, and so the kinematic analysis was used to test the hypothesis that extra fracturing from the RITF has increased rockfall potential near the RITF. Three main failure types have been identified that can occur as a result of the intersection of discontinuity planes (Hoek and Bray, 1981). These failure types include plane failure, wedge failure, and topple failure (Figure 20). The slope angle and orientation, dip and dip direction of discontinuities, and discontinuity interface friction angle are the inputs for the kinematic analysis. These slope angle and orientation inputs were developed using the LiDAR data. Along with inputting a slope orientation, a lateral limit of reasonable slope orientations can be entered. The purpose of the lateral limit is to account for variability in slope orientation. A window of 40 degrees was used for all of the analyses, or in other words the slope could vary up to 20 degrees in either compass direction and still fall within this analysis. Dip and dip direction of discontinuities were taken directly from field scanline measurements. Discontinuity interface friction angle was developed based on joint roughness, thickness, weathering, filling type, and moisture content data collected in the field, using recommended values provided by Barton (1973). The result of the kinematic analyses is a percentage of failure plane intersections that could contribute to each of the three failure modes, providing a relative rockfall potential due to structural features. Kinematic analyses were performed using the software Dips 8.0 (Rocscience, 2020a).

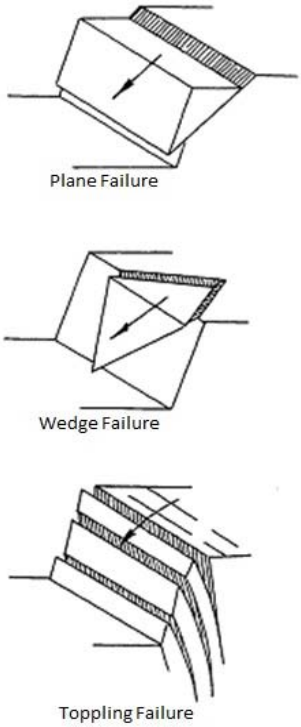

Figure 20 – the three main failure modes associated with rockfall hazards, from Hoek and Bray (1981)

The rockfall transport model was performed at the six scanline locations to assess the probability of rocks reaching the roadway after failure, also known as the probability of propagation (Crosta and Agliardi, 2003, Lambert et al., 2012). The probability of propagation was calculated using a stochastic rockfall simulation program, which calculates the probability of rocks hitting the roadway based on inputs of rock size and mass, initial velocity, material coefficient of restitution, friction angle, and slope configuration. Within the program, the coefficient of restitution and friction angle are varied randomly within a statistical distribution during a number of simulations, to create variable possible trajectories. The coefficient of restitution is the ratio of velocity prior to rockfall impact with the slope and the velocity after impacting the slope, where a

coefficient of restitution of 1 would signify a perfectly elastic impact, with the same velocity before and after impact (Asteriou, Saroglou, and Tsiambaos, 2013). Average rock size was developed at each scanline location by using fracture trace length, density and spacing data from the scanline data collection. Rocks were treated as lump masses, with an assumed uniform density of 2500 kg/m^3, based on a value for carbonates in a similar rockfall study (Dorren and Seijmonsbergen, 2003). A rough sensitivity analysis was performed on the density and size of rocks and changing the density within reasonable values did not significantly change the results of the analysis. Initial velocity of the rocks was set to zero for all of the models, assuming that the blocks coming out of the cliff would have no initial velocity before breaking loose and falling down the slope. Coefficient of restitution for each slope material was selected from a distribution summarized by Rocscience, based on parameters developed by Hoek and others (Rocsience, 2020b). Rockfall analyses were performed using the software Rocfall 8.0 (Rocscience, 2020c). Rocfall 8.0 is a statistical program that can calculate energy, velocity, and bounce heights for a number of possible trajectories sourced from a "seeder", or a location that could produce rockfall. Each rockfall simulation calculated the possible trajectory of a single rockfall 5000 times.

In addition to rockfall analyses, historical data about rockfall was used to assess continuing rockfall risk in the area. Some historical rockfall information was provided in an email by Gary Spencer from UDOT (Spencer, 2019). Also, one large, approximately 1.5-meter diameter boulder was observed at the roadway in the spring of 2020, which had not been there in the fall of 2019. Observations and historical data are in Appendix C.

CHAPTER 4

RESULTS AND DISCUSSION

The results and potential implications of the data and analyses performed according to the methodology discussed in Chapter 3 are discussed in this chapter. The results are organized by the numbered research objectives previously discussed.

Objective 1 – Characterize lithologies at control and test locations

Scanline Control

The control outcrop is approximately 10 to 15 meters high, with 3 units: a lower sequence of alternating yellow, siliceous, calcareous dolomite, and a pink marlstone and an upper interfingering conglomerate/sandstone (Figure 21). The dolomite and marlstone alternate and appear to have been deposited during environmental fluctuations. These units were interpreted to be part of the Pink Member of the Claron Formation, and are described in additional detail in Appendix A.

The scanline was performed all within the dolomite unit, which is described as: Siliceous, calcareous dolomite, light gray to dark yellowish brown, occasionally light pink, moderately hard, massive in terms of sedimentary structures, 70 centimeter bed, relatively planar upper and lower contacts, cavities up to 6 centimeters (Figure 22). In thin section (Figure 27), the sample appears to be composed mainly of carbonate with some quartz grains visible.

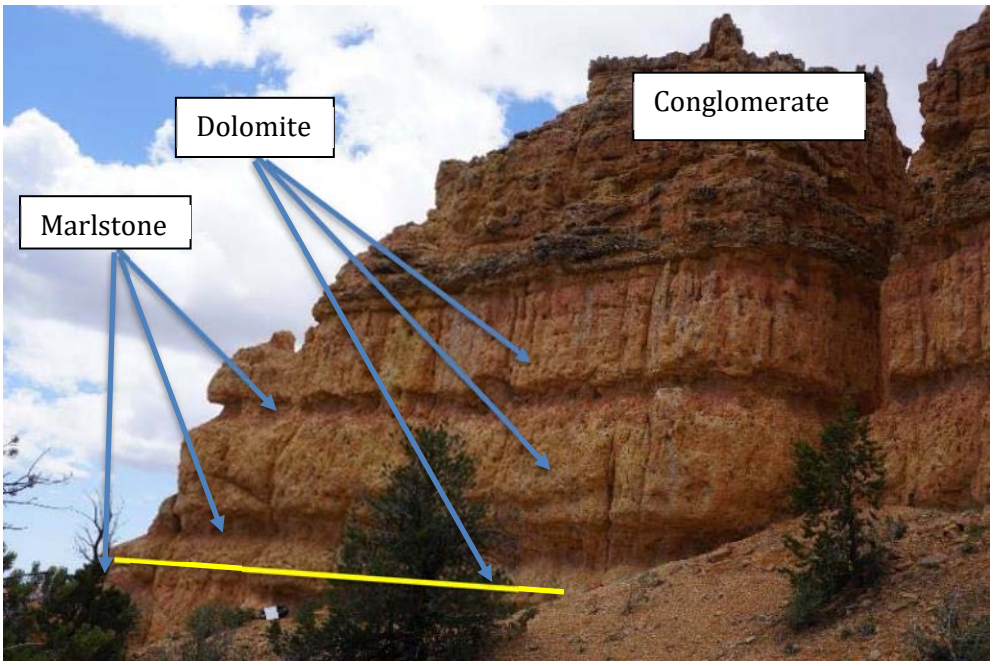

Figure 21 - Full outcrop where control scanline was performed. Aluminum clipboard (approximately 31 cm long) visible in lower left for scale. Approximate scanline location shown in yellow. View looking southeast.

Figure 22 - Dolomite crossed by the control scanline, metric tape measure showing scale (in cm.). Lower part of picture shows a portion of the adjacent marlstone, mostly weathered surfaces visible

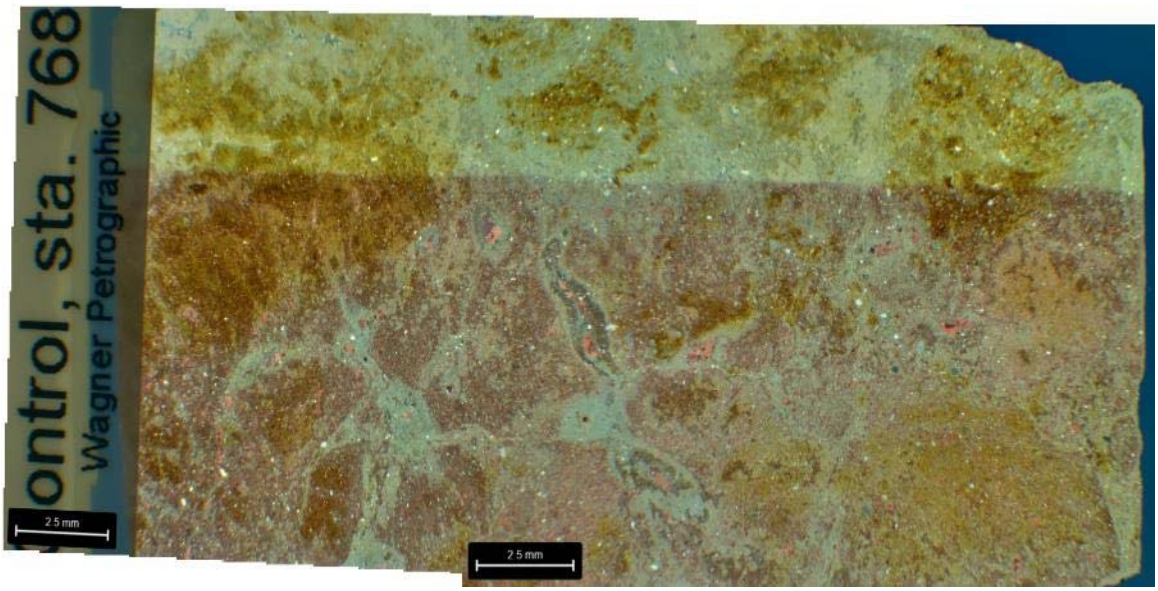

Figure 23 - Control Scanline thin section – plane polarized light, scale bar of 2.5 mm shown.

Scanline 1

Scanline 1 was performed at an outcrop that is approximately 30 to 35 meters high, and contained 3 main units that could be observed from the scanline location, at the base of the cliff: a lower, highly altered unit that was truncated laterally by a fault in the outcrop, a dolomite, and a limestone (Figure 24 and Figure 25). The dolomite overlies the limestone, and continues vertically for several meters above the scanline location. Observations of the upper portions of the cliff could not be made due to access.

Figure 24 - Upper portion of outcrop where Scanline 1 was performed (scanline location obscured by the trees, but general location marked in yellow dashes). View looking north, and up at the outcrop from the roadway

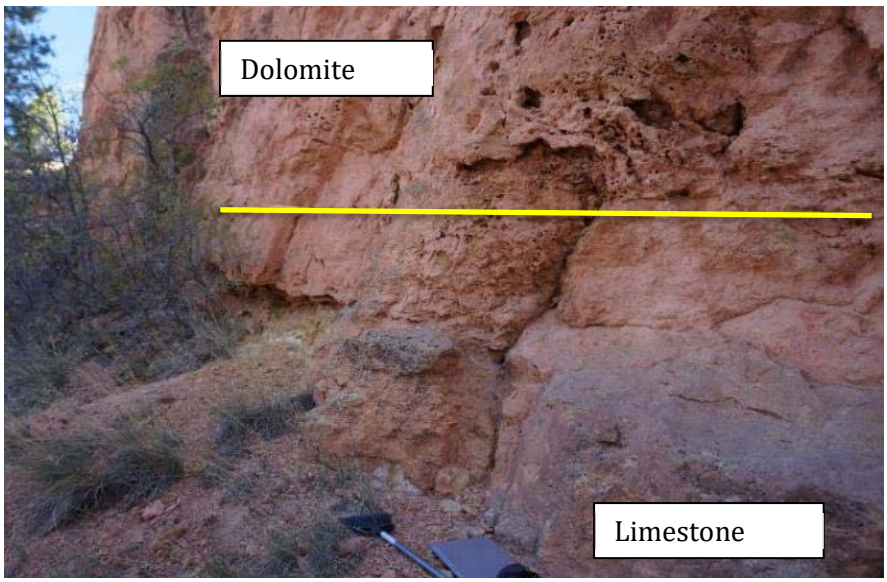

Figure 25 - Wide view of units visible at Scanline 1. Near the middle of the photo, a zone of abundant cavities visible.

Scanline 1 crossed 2 units that were both sampled, units 1A and 1B (Figure 26). Sample 1A was taken from a dolomite, with a few cavities which were in places filled with calcite crystals. Weathered and fresh surfaces were light pinkish orange, moderately hard, and reacted strongly with hydrochloric acid.

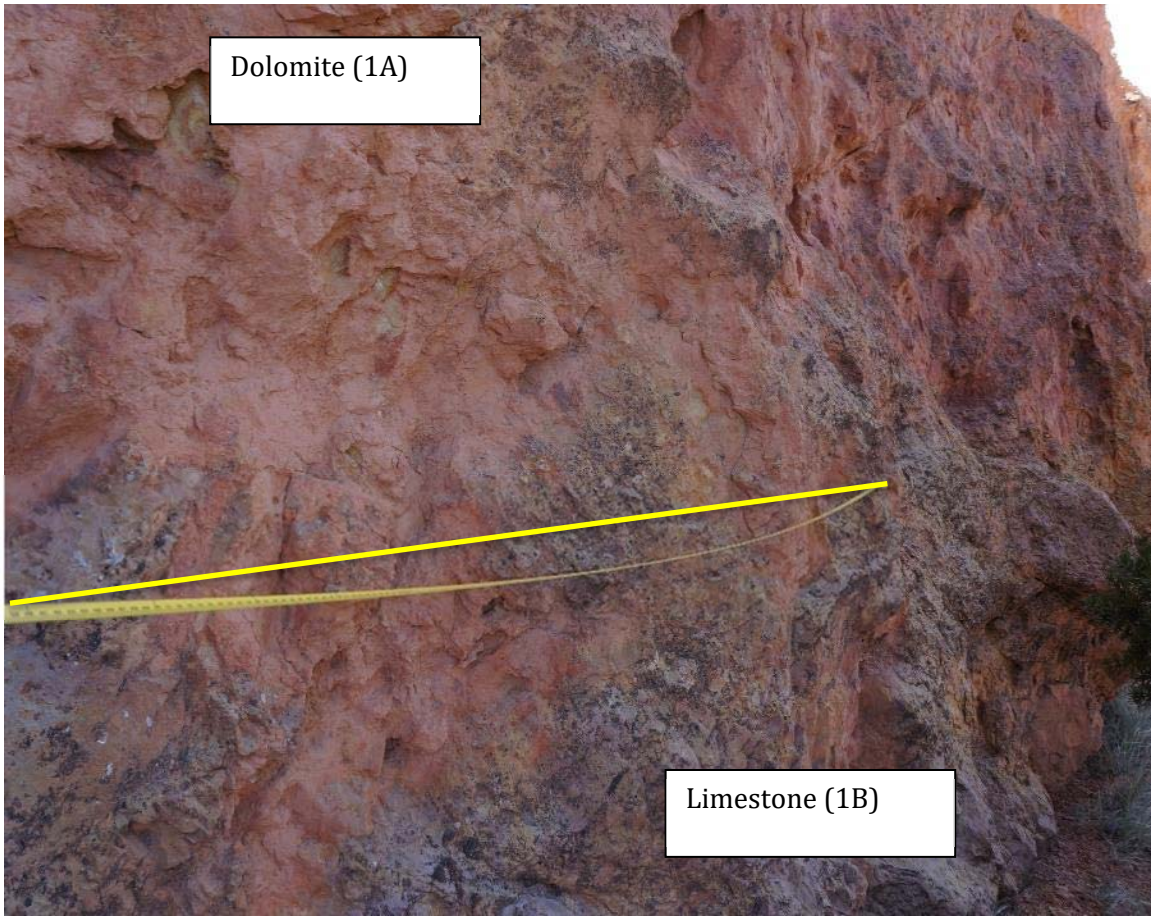

Figure 26 – Continuation of Scanline 1, to the end of scanline.

Figure 27 - Unit 1A at Scanline 1, rock hammer (33 cm. long) for scale. Weathered surface

Sample 1B (Figure 28) was taken from the basal limestone, few pebble lenses and angular clasts of dark yellowish brown sandstone (possibly underlying Wahweap Formation). This limestone weathers to a light purple to light olive green on the surface, but fresh faces are generally pinkish orange. It is massive in terms of sedimentary structures, reacts strongly with hydrochloric acid, and has some cavities at fractures. Contact between 1A and 1B is gradational, and difficult to identify in fresh surfaces, but weathered surfaces are more easily distinguished (Figure 25).

Figure 28 - Unit 1B found at Scanline 1. Weathered surface, with visible subangular inclusions of yellowish brown sandstone clasts, along with what appear to be pebble lenses. Pencil for scale (full length 15 cm.)

In thin section, Sample 1A is identified as a dolomite by the general lack of coloration from the dual carbonate stain, except in locations where cavities had been filled with secondary calcite. There is also a significant amount of small, angular quartz grains, which appear to be detrital quartz within the dolomite (Figure 29).

Sample 1B was affected more by the dual carbonate stain due to the elevated quantity of calcite in the sample. Some of the calcite is secondary, but there is also primary calcite in the sample. Sample 1B also contains abundant angular quartz grains (Figure 30).

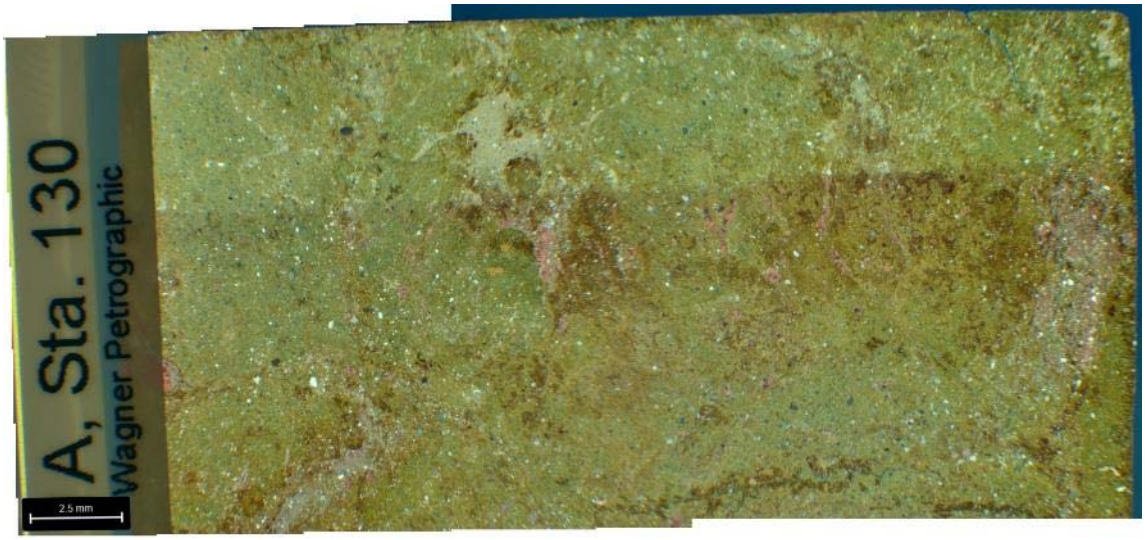

Figure 29 - Thin Section of sample 1A – plane polarized light, scale bar of 2.5 mm shown.

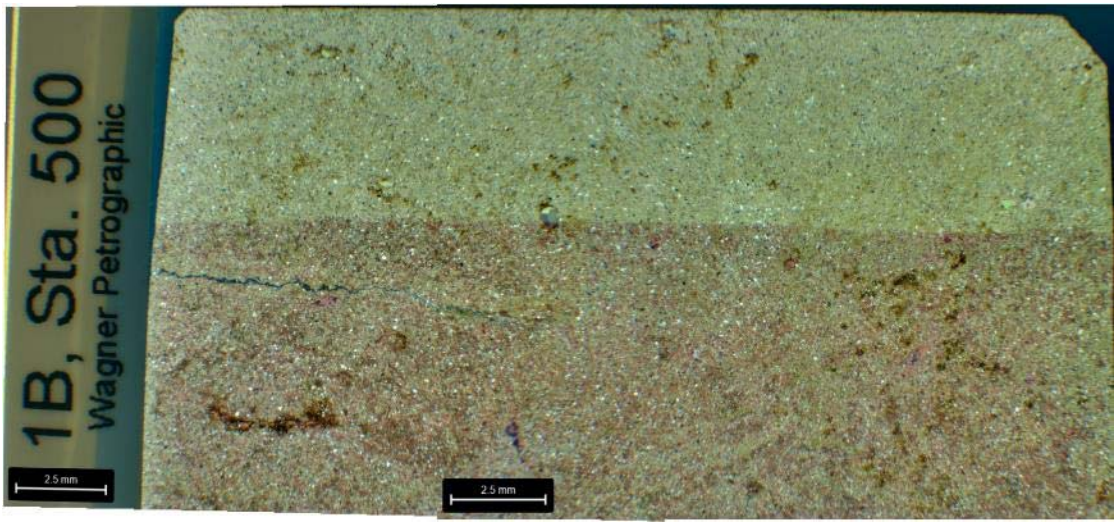

Figure 30 - Thin section of sample 1B – plane polarized light, scale bar of 2.5 mm shown.

Scanline 2

Scanline 2 was performed at an outcrop that is approximately 25 to 30 meters high, and was performed near the fault surface of the RITF. The outcrop contained 2 main units

that could be observed from the scanline location: a footwall unit and a hanging wall unit. The unit in the footwall was interpreted to be weak calcareous mudstone that was not included in the scanline data collection (Appendix A for additional description). The footwall at this location eroded out much more quickly than the overlying hanging wall material, leaving a large overhang above the thrust fault (Figure 31).

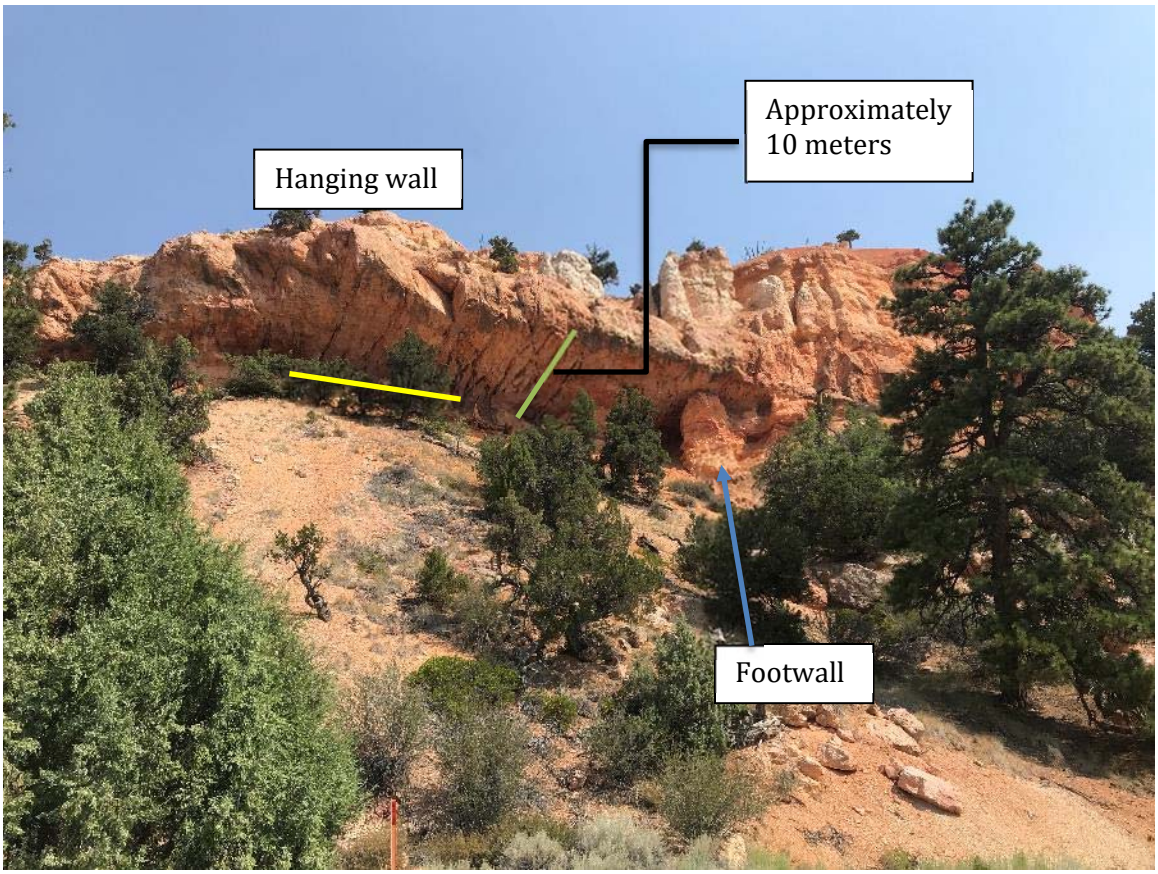

Figure 31 – Outcrop view of location of Scanline 2 (marked in yellow, behind the vegetation). Note the large overhang, and small portions of footwall material underneath the overhang, but mostly eroded away. The overhang extends approximately 8 meters out from the back of the wall (scanline location) to the cliff face. View looking north from the roadway.

Because the footwall had mostly eroded out, Scanline 2 was performed solely in the hanging wall unit. This unit was a limestone (Figure 32), with occasional cavities up to

2 centimeters in diameter, filled with calcite crystals, possibly burrows. The color of the limestone ranges from light pink to orange, with black staining around major fractures. It is massive in terms of bedding, and sedimentary structure, and is very fine-grained, possibly micritic. It reacts strongly to hydrochloric acid.

Figure 32 - View of limestone at Scanline 2, metric tape measure for scale (in cm.), rock faces near tape measure are mostly fresh

In thin section, this unit appears to consist mostly of calcite and possibly ferroan calcite. Much of the sample appears to have been introduced as secondary calcite, in veins and possible burrows, but there does appear to be some primary micrite as well (Figure 33).

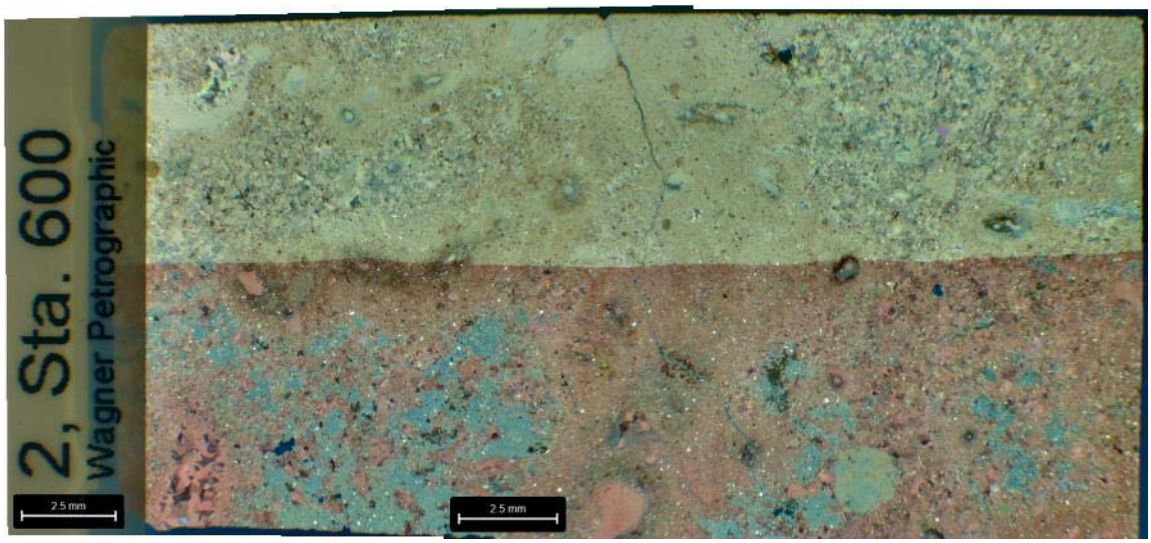

Figure 33 - Thin section of unit 2 – plane polarized light, scale bar of 2.5 mm shown.

Scanline 3

Scanline 3 was performed in an outcrop that was approximately 15 to 20 meters high in total height. The outcrop contained 1 unit that could be observed from the scanline location (Figure 34).

Scanline 3 was performed in a dolomite (Figure 35), with some cavities filled with calcite crystals. The color of the dolomite ranges from light pink to orange, with black staining on a large portion of the outcrop. It is massive in terms of bedding and sedimentary structures, and is very fine-grained, possibly micritic.

In thin section, the sample from Scanline 3 appears to contain a significant amount of calcite, which was not found in the XRD testing. (Figure 36).

Figure 34 – Partial outcrop view of Scanline 3 location. Scanline location marked in yellow. View to the northwest from just below the scanline location.

Figure 35 - Dolomite found at Scanline 3, with abundant manganese oxide staining visible on the surface. Tape measure showing scale (in cm.).

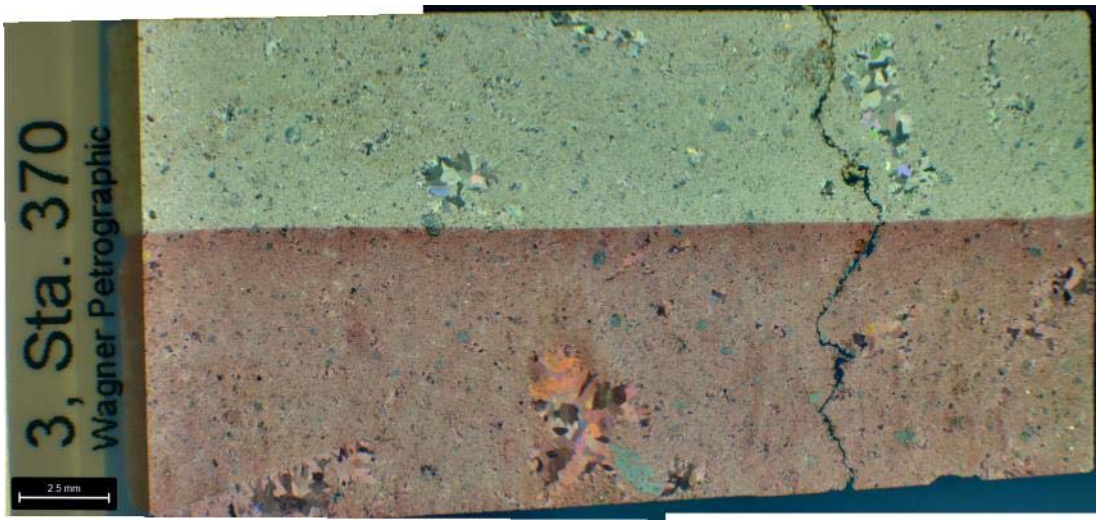

Figure 36 - Thin section of Unit 3 – plane polarized light, scale bar of 2.5 mm shown.

Scanline 4

Scanline 4 was performed in an outcrop that was approximately 15 to 20 meters high in total height. The outcrop contained 2 units that could be observed from the scanline location (Figure 37). The two units were adjacent to each other, the first unit was a pink to orange limestone, and the second was a light tan to white limestone that was found within an erosional alcove within the outcrop.

From the two units that were crossed by Scanline 4, samples were collected from each unit. Units 4A and 4B are described below, and samples from these units were labeled samples 4A and 4B. Sample 4A (Figure 38) was taken from a limestone that contains some subrounded inclusions from 1 to 6 mm, possible burrows. It is light pink to orange to light tan, and weathers to light to dark gray and occasionally yellowish brown. Some joints and cavities in this unit are filled with calcite crystals. It displays numerous small-aperture and short-length fractures at this location, which are interpreted to be dissolution cleavage.

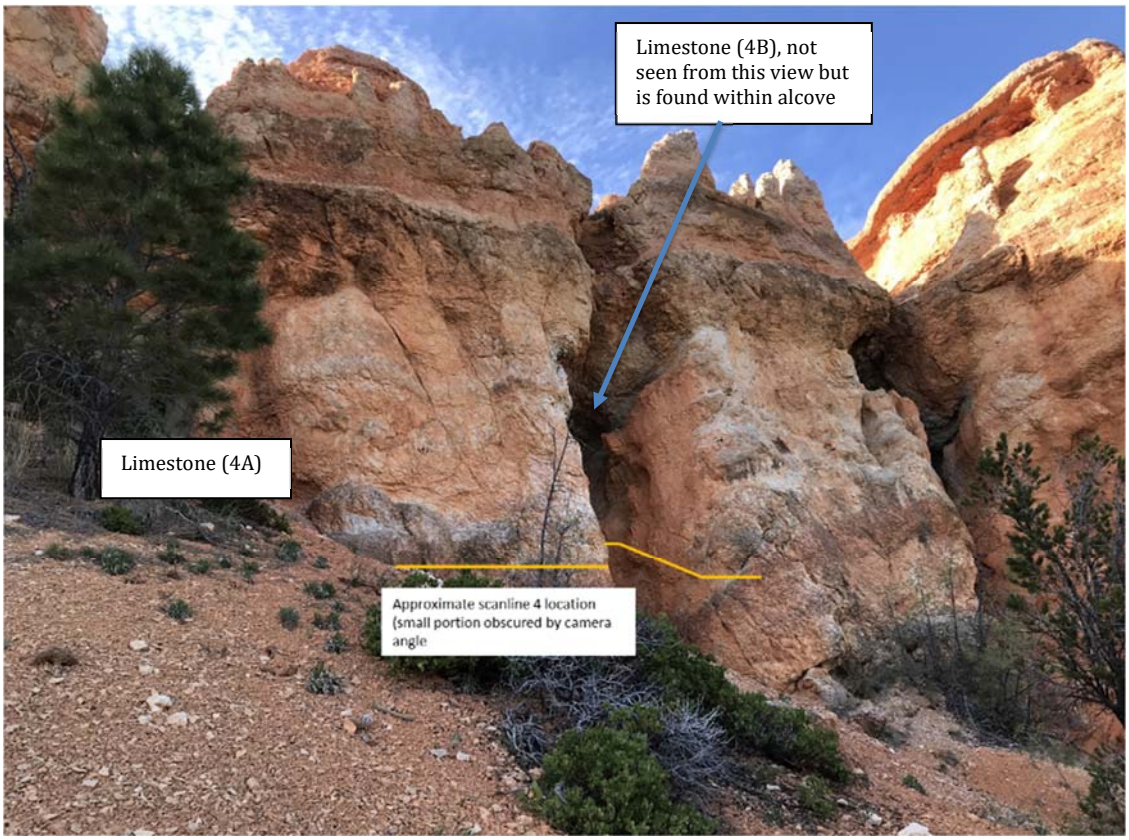

Figure 37 - Outcrop view of Scanline 4, with scanline marked in yellow. View looking north

Figure 38 - Unit 4A, limestone found at Scanline 4, with dissolution cleavage, rock faces are mostly fresh

The description for Sample 4B is nearly identical to unit 4A, except that the color is mostly light tan to white. This unit is only found adjacent to two large fractures outcrop (Figure 37), and is possibly discolored related to fluid flow.

In thin section, units 4A and 4B appear very similar in composition. The thin section for Unit 4A contains more calcite-filled fractures, but both samples contain cavities that were filled with calcite crystals (Figure 39 and Figure 40).

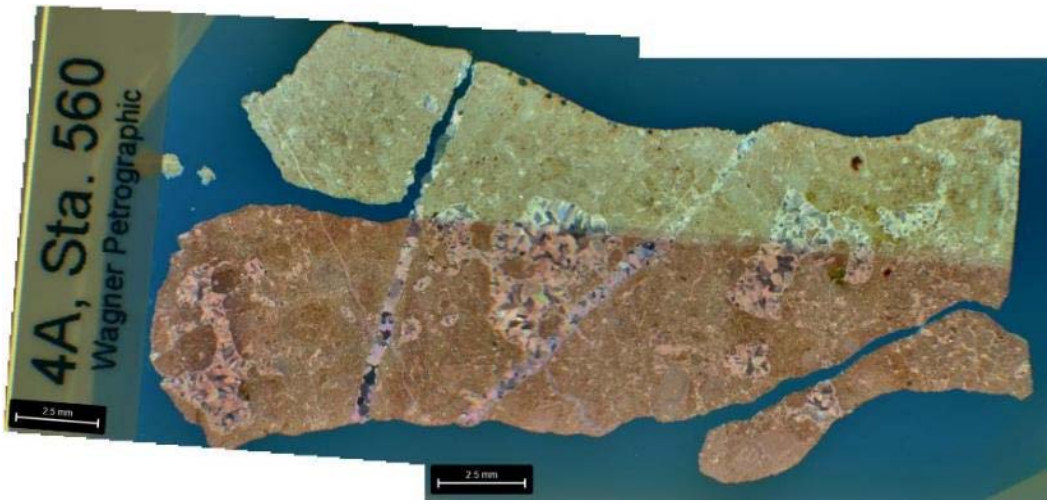

Figure 39 - Thin section of Unit 4A – plane polarized light, scale bar of 2.5 mm shown.

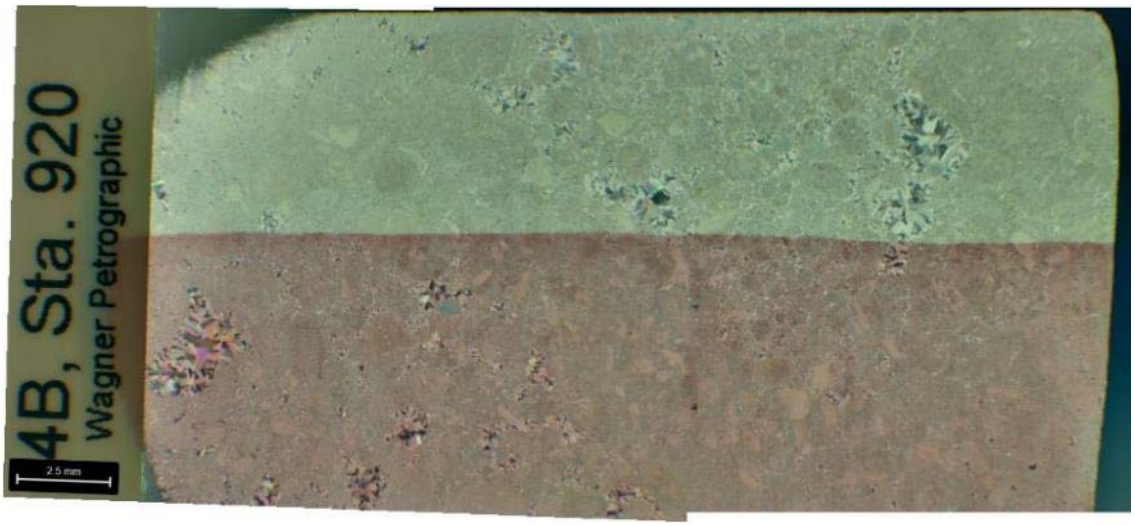

Figure 40 - Thin section of Unit 4B – plane polarized light, scale bar of 2.5 mm shown.

Scanline 5

Scanline 5 was performed in an outcrop that was approximately 15 to 20 meters high. The outcrop contained 1 unit that could be observed from the scanline location (Figure 41). The unit was possibly overlain by different units, but these could not be described due to access.

Figure 41 - Wider view of Scanline 5

Scanline 5 was performed in a limestone that varies in color from light pink to light orange to light yellowish brown, and occasionally light gray on fresh surfaces. The limestone contains some cavities and veins filled with calcite crystals, and fresh faces frequently exhibit irregular, dense cleavage, especially on the western part of the scanline (interpreted to be dissolution cleavage). The limestone is hard, and in some locations weathers to a pitted texture with dark gray to black staining (Figure 41 and Figure 42).

In thin section, the limestone appears to be micritic, with some evidence of secondary calcite formation in cavities (Figure 43).

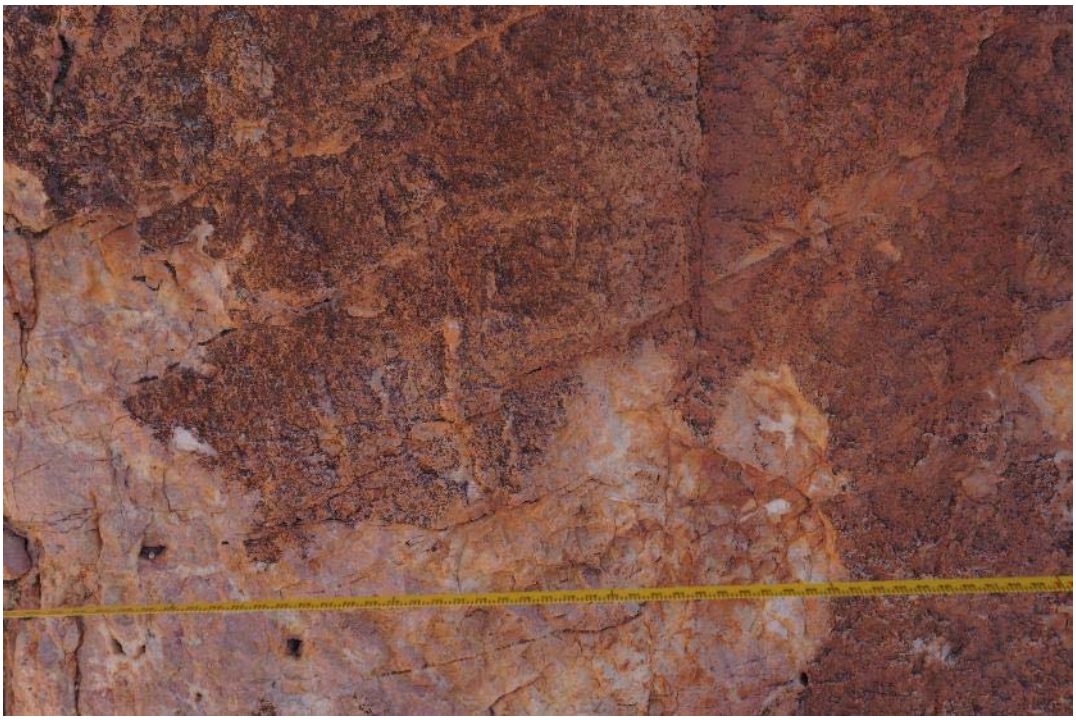

Figure 42 - Limestone found at Scanline 5, showing both fresh (lower left) and weathered (upper right) surfaces, tape measure visible for scale (in cm.)

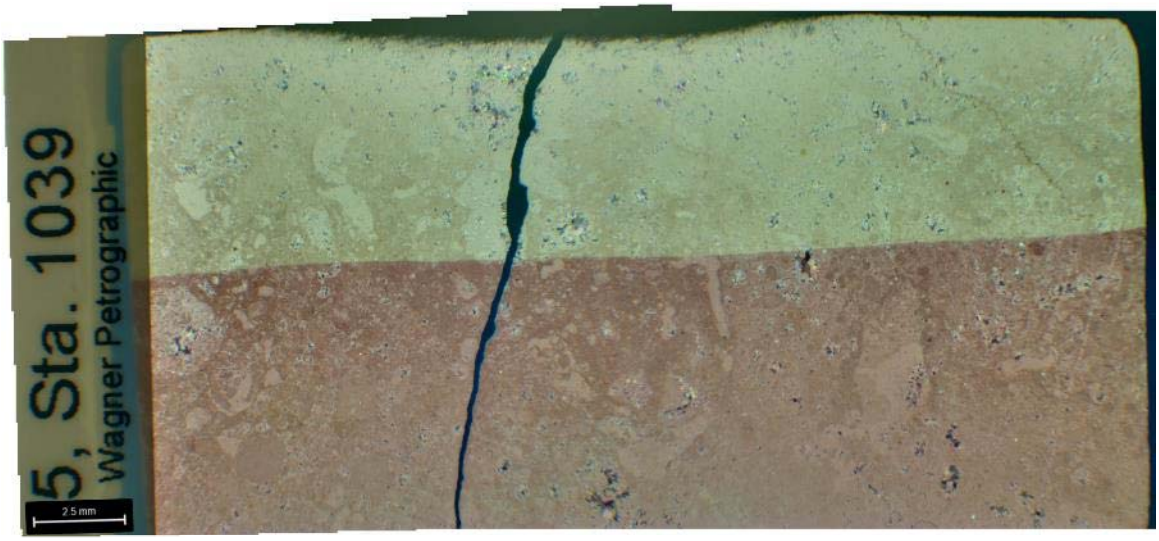

Figure 43 - Thin section of Unit 5 – plane polarized light, scale bar of 2.5 mm shown.

X-Ray Diffraction Testing

A summary of XRD mineral composition results is provided in Table 1.

Table 1 – X-ray diffraction testing results

Sample ID	XRD Mineralogy -- Listed in order of major to minor ± (trace)
Control	Quartz + Dolomite + Calcite
1A	Dolomite + Quartz + Calcite
1B	Calcite + Quartz + Dolomite ± (Ti-Fe-Oxides)
2	Calcite + Dolomite ± (Fe-oxide) ± (Graphite) ± (Quartz)
3	Dolomite ± (Fe-Mn oxides) ± (Graphite) ± (Quartz)
4A	Mg-Calcite + Calcite + Fe-Oxide ± (Graphite)
4B	Calcite + Fe-oxide
5	Mg-Calcite + Fe-Oxide ± (Graphite)
Notes:	1) XRD Mineralogy listed in order of major to minor elements 2) Trace elements are listed in parentheses after ±

Although the XRD data indicates that the major mineral of the control sample is quartz, the combined percentage of calcite and dolomite (both carbonates) was greater than the quantity of quartz in the sample. Based on this data and the thin sections discussed below, all of the samples gathered in the field consist mainly of various carbonates. The control sample also lists the next minor elements both as carbonates.

Relative Rock Strength

Results from Schmidt Hammer testing are summarized in Table 2 and Figure 44. Results from half of the scanline localities indicated rock that was weak (R=35-40) to moderately strong (R=40-50, Goudie, 2006). Scanlines 2, 4, and the control indicate very weak rock (R=10-35). Scanline 4 had abundant fractures not found at the other scanlines.

Table 2 – Schmidt hammer rebound R-values from each sample location

	Schmidt Hammer R-Values per sample location at each scanline							
	Control	**1A**	**1B**	**2**	**3**	**4A**	**4B**	**5**
	26	34	40	30	35	18	20	30
	28	42	44	30	36	18	23	33
	31	42	44	31	37	21	23	34
	33	44	45	32	38	21	24	38
	34	44	46	34	39	26	25	42
	34	44	48	34	40	27	26	42
	34	48	48	38	42	30	28	43
	34	50	50	40	43	34	30	48
Average	32	44	46	34	39	24	25	39

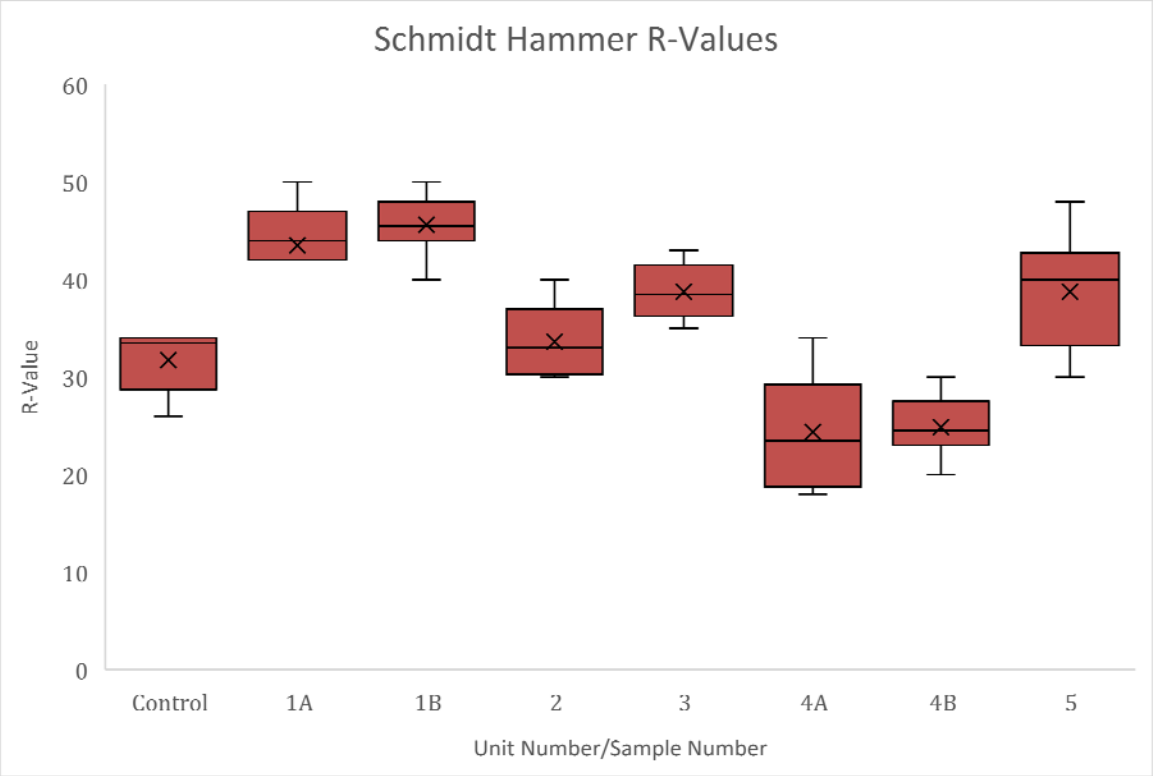

Figure 44 – Schmidt Hammer R-values measured in the field in the units crossed by each scanline

Based on the results of the field descriptions, XRD testing, thin section descriptions, and Schmidt Hammer data, the rocks are similar between the test and control scanlines. All of the materials are some form of carbonate, and generally demonstrate a similar rock strength.

Another parameter that can affect fracture intensity is bed thickness. This is a potential concern for this research, where the test scanlines were all performed in relatively massive, thick beds, while the control scanline was performed in a 70-centimeter thick bed, in an outcrop that displayed a series of similarly-sized beds. However, the major fracture sets of concern penetrate the entire thickness of the outcrop section at the control scanline, alleviating this concern.

Objective 2 – Characterize fracture networks

Raw fracture data along scanlines are found in Appendix B. It should be noted that, although quantitative uncertainties were not calculated for the data, there are inherent uncertainties involved in the collection of this sort of data.

Fracture length is compared between test and control scanlines to assess whether or not the RITF has increased the average or maximum length of fractures at these locations (Figure 45). Both a minimum fracture length, with all of the data from each scanline, and a measurable fracture length, which screened certain data, were compared from each scanline. Results show that, in general, the control scanline and Scanline 1 have a similar distribution of small and large fractures. Scanlines 2 and 3 display slightly higher numbers of fractures greater than 2 meters long, and fewer smaller fractures. Scanlines 4 and 5 contain close to twice as many fractures longer than 2 meters than the control scanline. The

minimum fracture length and actual fracture length display similar trends (Figure 45 and Figure 46). The differences between the control scanline and scanlines 1, 2, and 3 do not appear to be significantly different, which seems to refute the original hypothesis, but the difference between the control scanline and scanlines 4 and 5 seems to support the hypothesis. The similarity between the control scanline and scanline 1 appears to be justified, as they are both in the footwall of the fault. Although the control location is distant from the fault, evidence of footwall compression and shear has been documented as far as 29 kilometers south of the RITF (May et al., 2012). Based on estimates of southward movement of the RITF (Biek et al., 2015), it is possible that the fault extended to the control location prior to erosion, although the fault surface would have been significantly higher in elevation than the control outcrop.

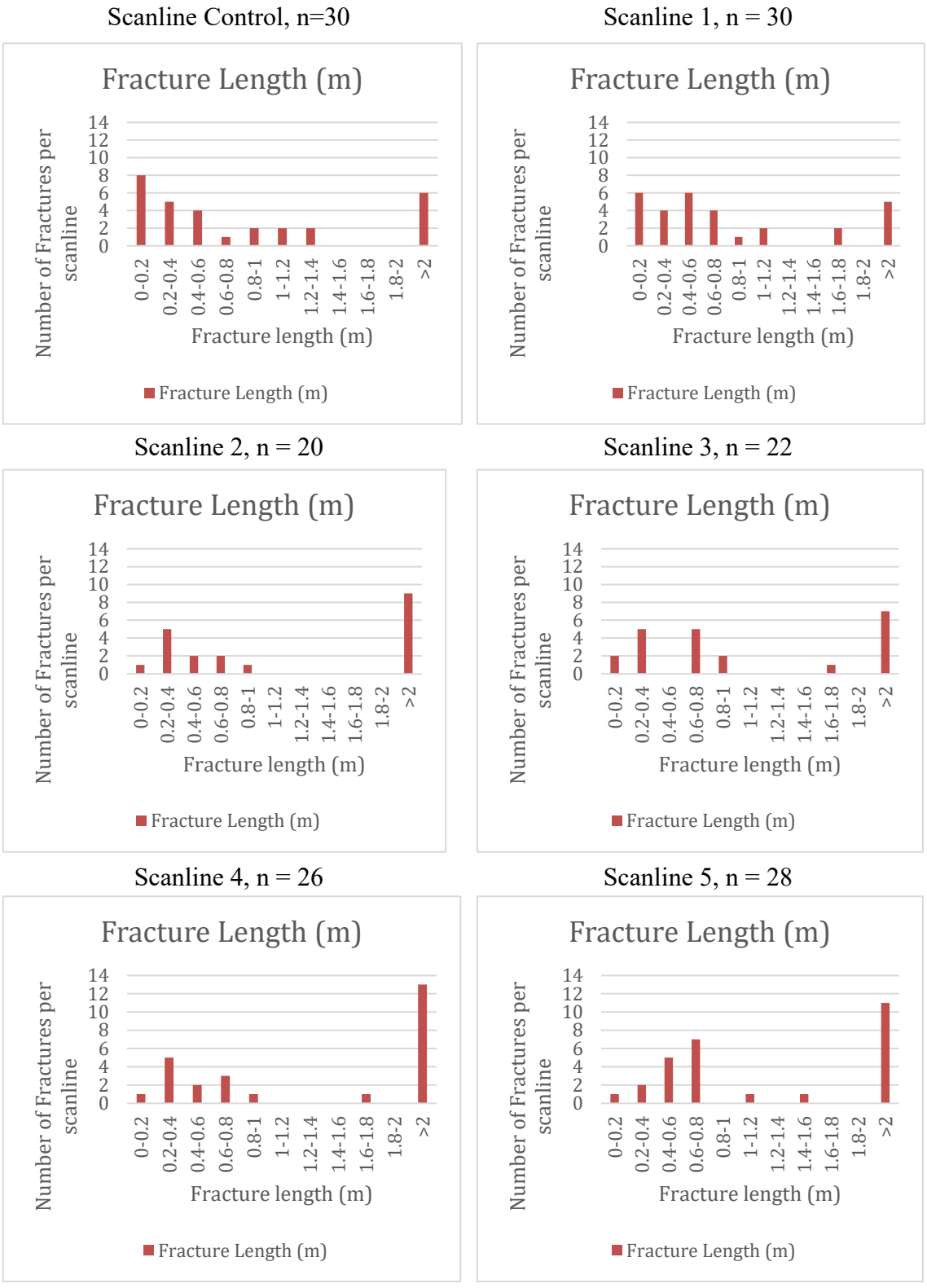

Figure 45 - Histograms for all six scanlines showing number of fractures per scanline where full fracture length was measurable. Length is plotted in 0.2 meter bins.

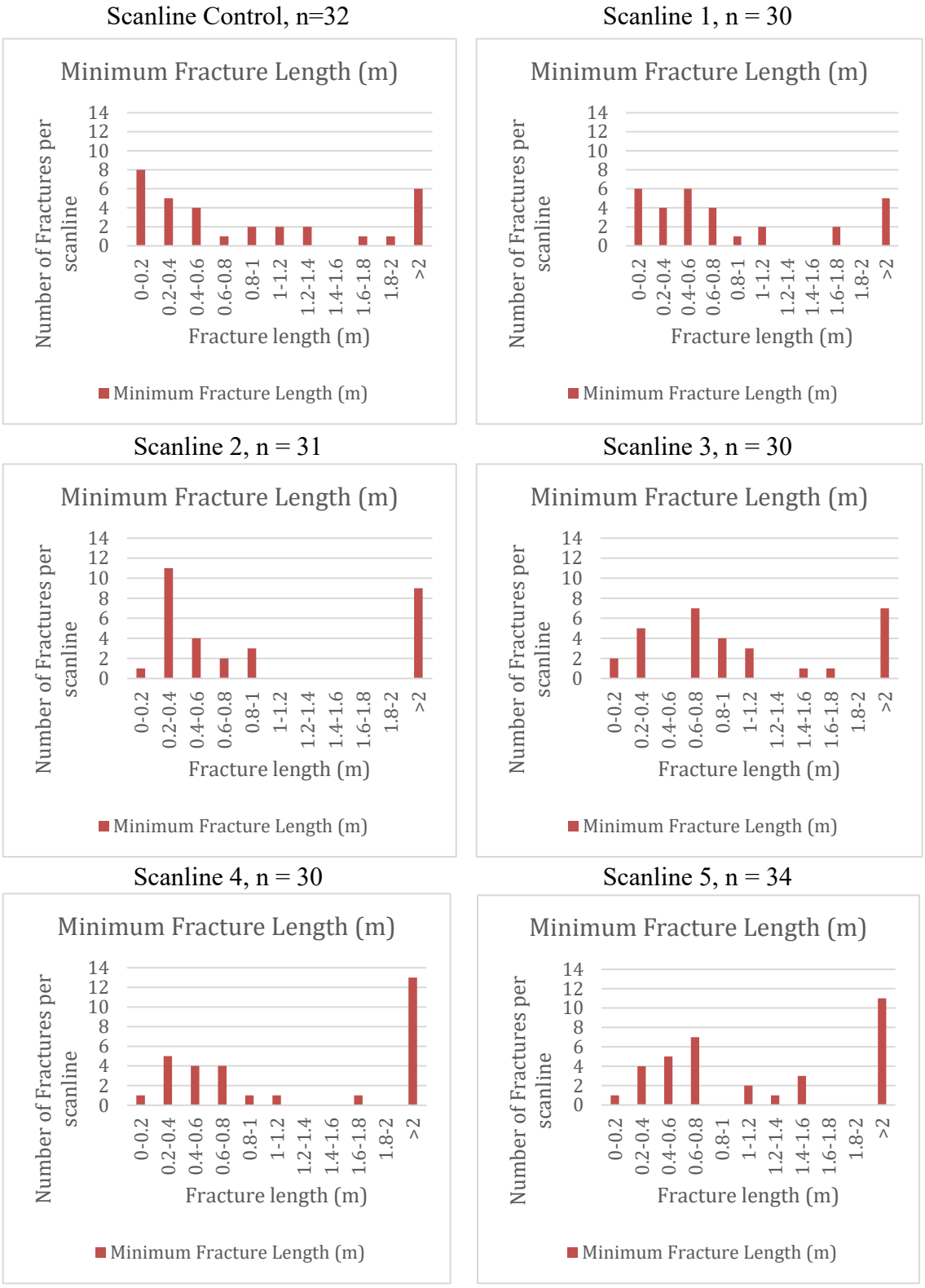

Figure 46 - Histograms for all six scanlines showing number of fractures of certain minimum length per scanline. Minimum length is plotted in 0.2 meter bins. Minimum length recorded where only one termination could be measured (not shown in Figure 45)

Maximum fracture aperture was also used to compare the fracture networks. Fractures that intersected the scanlines generally had a range of fracture aperture, and vary widely along the fracture at times. Because of this, the maximum fracture aperture was chosen for comparison. The original hypothesis of this research was that the fractures would be generally wider at the RITF, indicating increased fracturing during the thrusting. Based on the data, however, it appears that the opposite is true. There is a higher number of large-aperture fractures at the control scanline than any of the test scanlines (Figure 50). However, the difference is slight, and as there are only four fractures wider than 20 millimeters at the control site in comparison to zero to two at the test scanlines. All four of the widest fractures in the control scanline are nearly vertical, dipping at angles between 85 to 90 degrees. The control scanline was performed on an isolated cliffband, and it is possible that the additional wide fractures were created from slight lateral movements caused by stress release following erosion of this intact block (Figure 48). Wide aperture stress release joints may not be as common in the test scanlines because of existing confining stress that the extensive cliff face provides (Figure 49). Both the screened and unscreened data are plotted below (Figure 50). Unscreened data appears to demonstrate a higher fracture intensity at the control scanline, indicating a higher degree of fracturing at the control, which is in direct opposition to the hypothesis of this research. However, once the fractures have been screened at 0.5 meters, the fracture intensity is generally very similar, in the range of 1.5 to 2.1 fractures per meter among all of the scanlines. The tighter interval between unscreened and screened fracture intensity among the test scanlines indicates that, although there may be fewer overall fractures at the test scanlines, the fractures are in general more continuous at the test scanlines.

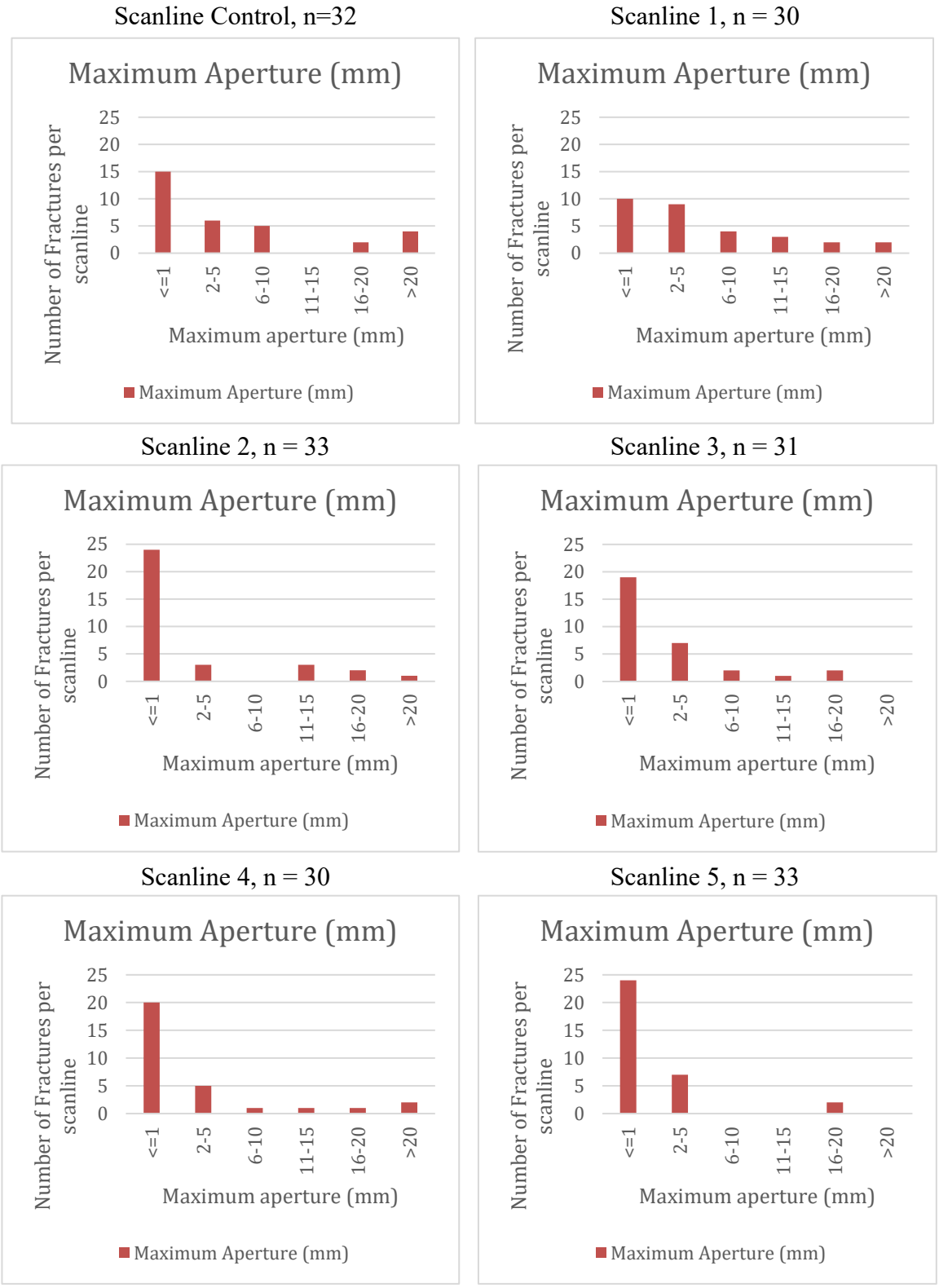

Figure 47 - Histograms for all six scanlines showing number of fractures of certain maximum aperture per scanline. Maximum aperture is generally divided into 5 millimeter bins. Maximum aperture recorded because of variability in aperture within fractures

Figure 48 - Scanline Control outcrop with major, near-vertical fractures marked in blue (upper photo) and unmarked but visible in lower photo

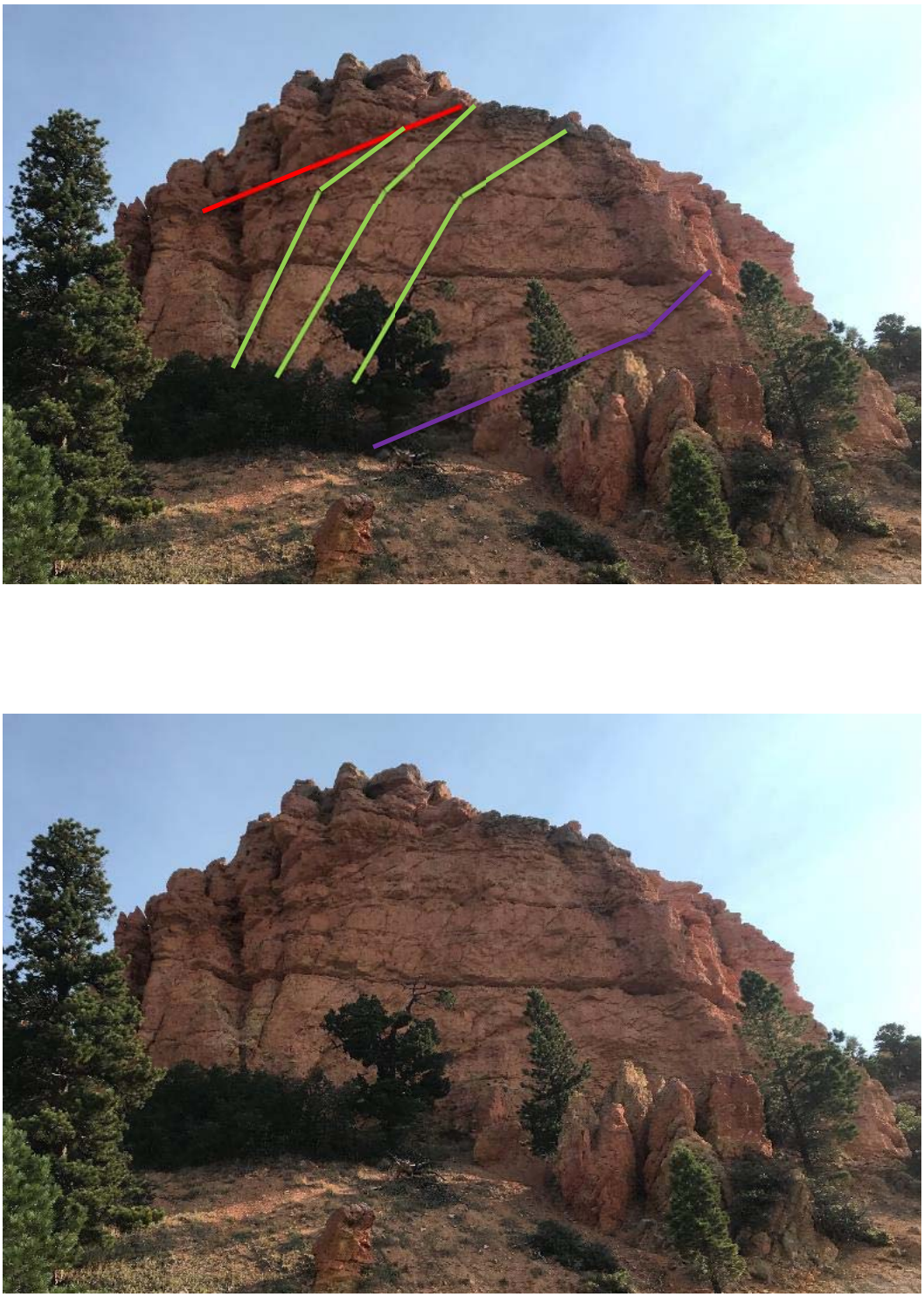

Figure 49 - Scanline 1 with major fractures marked in green, thrust fault strand marked in red, and a long, prominent fracture marked in purple which is not part of a major set (upper photo), and unmarked but visible (lower photo)

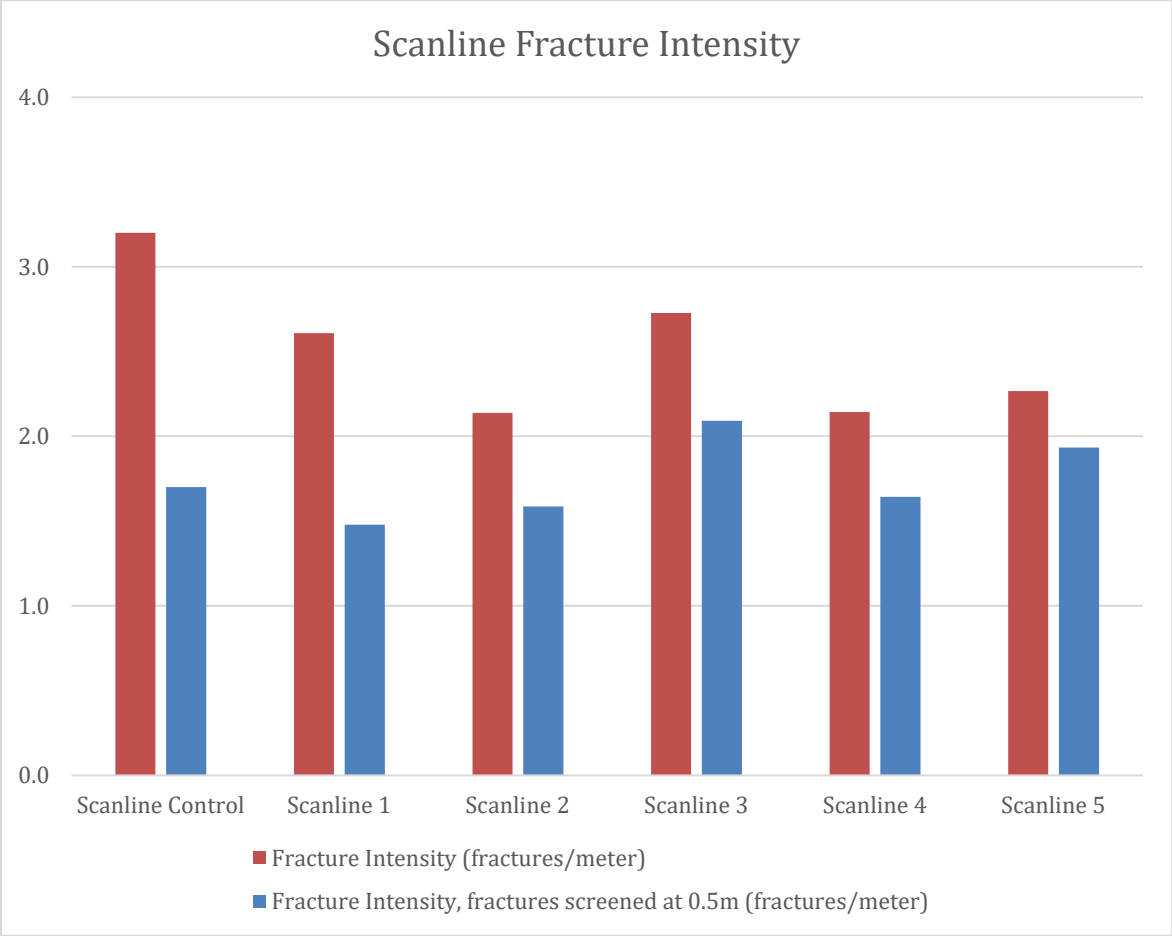

Figure 50 – Scanline fracture intensity histogram, including unscreened data (red) and data screened to remove fractures less than 0.5 meters long (blue)

Average apparent fracture spacing does not seem to vary significantly from the control scanline to the test scanlines (Figure 51). Scanlines 2 and 5 have the largest spacing, between 225 to 250 centimeters, while Scanline 3 has the smallest spacing, at approximately 150 centimeters. Scanlines Control, 1 and 4 have similar spacing, just below 200 centimeters. There does not appear to be any evidence related to fracture spacing that indicates that the control site is less fractured, or fractured significantly differently than the test sites. Maximum apparent fracture spacing appears to display a similar lack of trend.

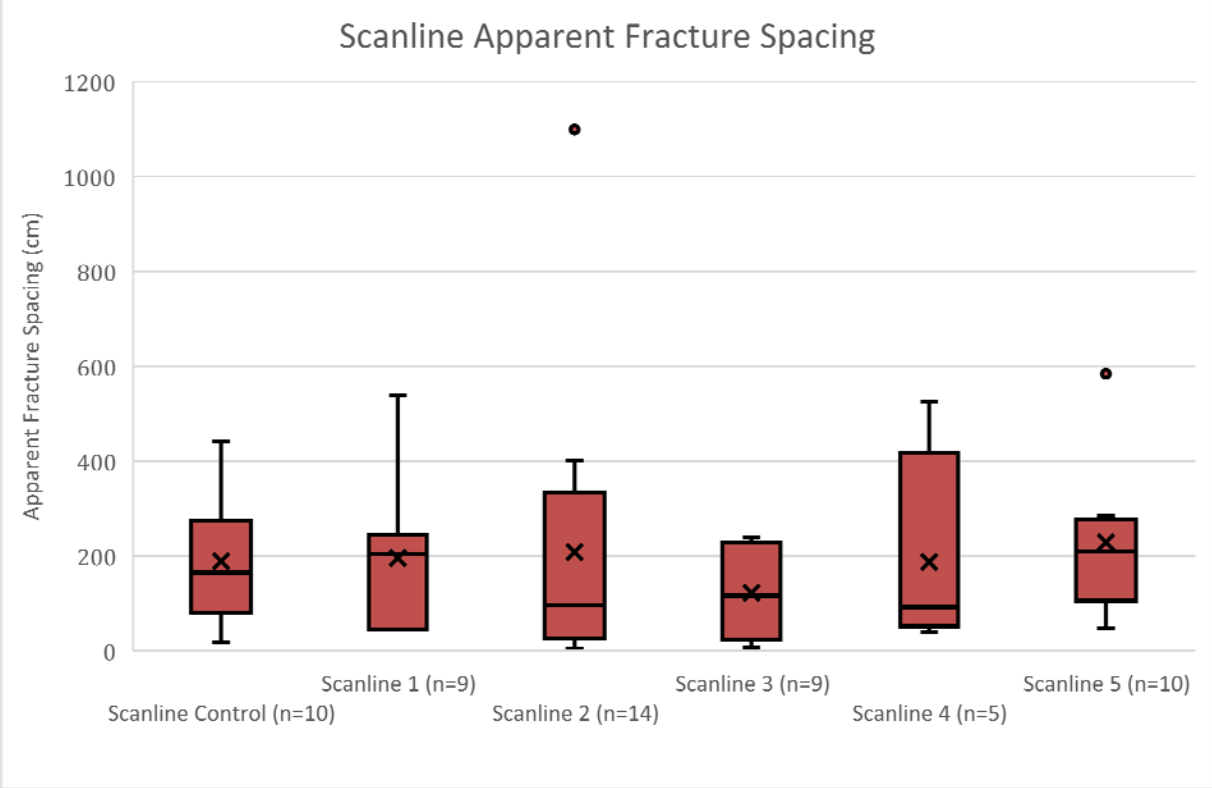

Figure 51 - Apparent fracture spacing per scanline at each scanline using a box-and-whisker plot. Dots above Scanline 2 and 5 are considered outliers, according to Microsoft Excel. However, it should be noted that the datasets were small, and therefore determination of outliers may not be representative. The "X" symbol indicates the average apparent spacing. The n value is equal to the total number of fractures that were grouped into major joint sets at each scanline.

Fracture set orientations were also considered, to understand if the orientations would display any patterns or trends between control and test scanlines. Scanline orientation and the orientation of the RITF in the vicinity of the scanlines were plotted on the stereonets, to compare with the orientations of major joint sets (Table 3 and Figure 52 through Figure 57). The discontinuities plotted on the stereonets only include fractures longer than 0.5 meters. Polar, equal angle, lower hemisphere stereonets were used for comparison Major joint sets were generally selected in 15-degree azimuth windows where

3 or more discontinuities clustered. In some cases, a wider azimuth window was used to include additional points. In the stereonets, the control scanline appears to indicate a very different fracture pattern than the test scanlines. All five of the test scanlines record at least one major joint set that trends due north or to the northwest, while all three of the major joint sets found in the control scanline trend to the northeast. Although the test scanlines appeared to be somewhat different than the control scanline in the previously discussed metrics, fracture orientation appears to be significantly different when comparing the control scanline to the test scanlines.

Table 3 – Stereonet data summary. Where the fracture sets were nearly vertical, two dip direction windows were included in the set

Scanline	Set Number	Dip range (degrees)	Dip Direction Range(s) (degrees)		Average Spacing (cm)	n
Control	Set 1	80-90	320-335	140-155	143	4
	Set 2	80-90	270-285	90-105	177	3
	Set 3	80-90	290-300	110-120	269	3
1	Set 1	70-80	240-250	---	160	3
	Set 2	45-65	270-295	---	210	6
2	Set 1	70-90	260-275	80-95	126	11
	Set 2	50-60	0-15	---	621	3
3	Set 1	70-90	40-50	220-230	137	4
	Set 2	75-90	265-285	85-105	158	3
4	Set 1	80-90	230-255	50-75	187	5
5	Set 1	65-85	245-260	---	141	5
	Set 2	75-90	165-180	345-360	316	5

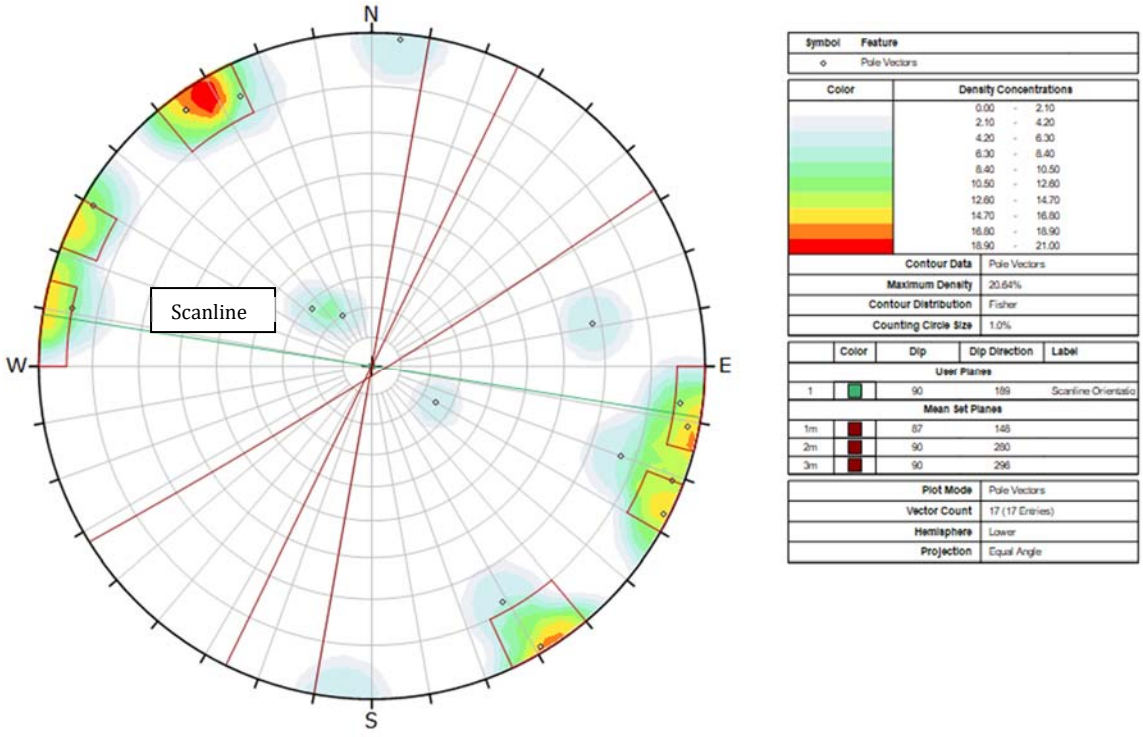

Figure 52 – Stereonet of major joint set mean planes plotted as dark red lines at Scanline Control, with the scanline orientation plotted as green line

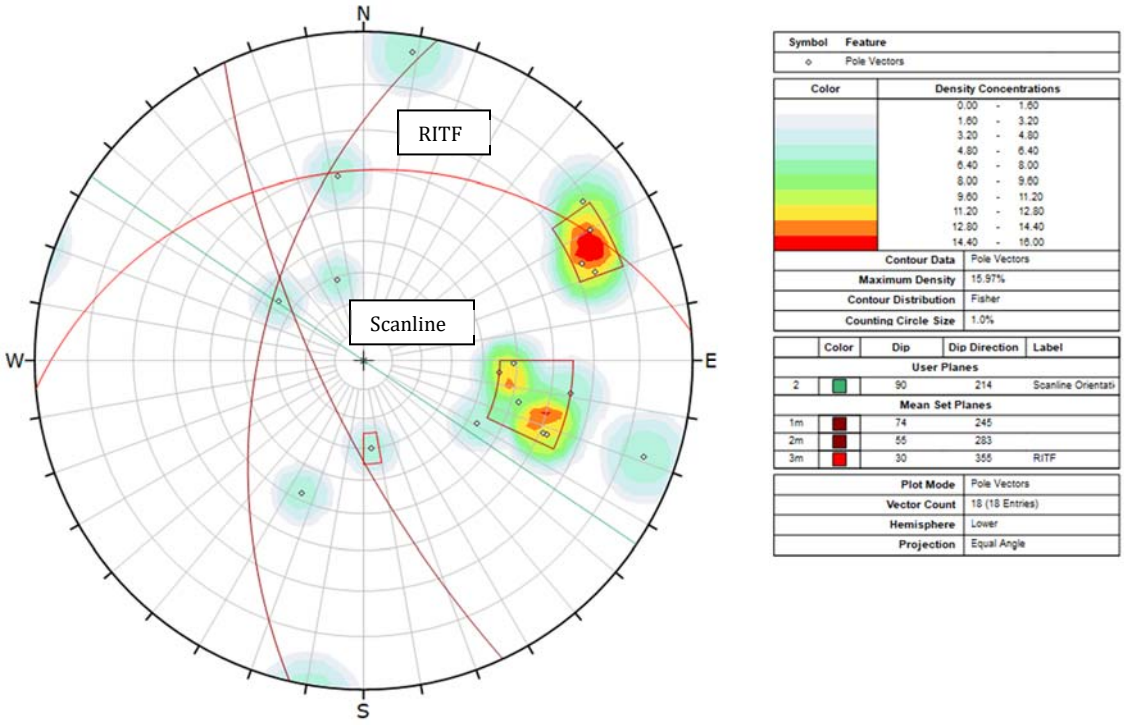

Figure 53 - Stereonet of major joint set mean planes plotted as dark red lines at Scanline 1, with the RITF plotted as red line and scanline orientation plotted as green line

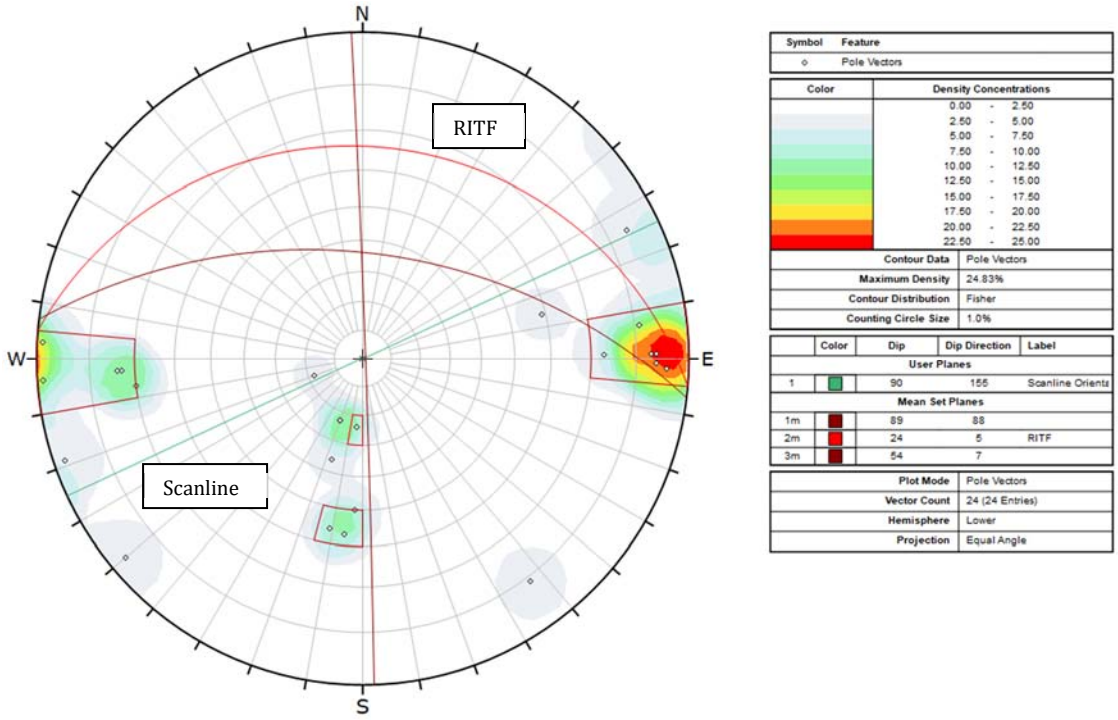

Figure 54 - Stereonet of major joint set mean planes as dark red lines at Scanline 2, with the RITF plotted as red line and scanline orientation plotted as green line

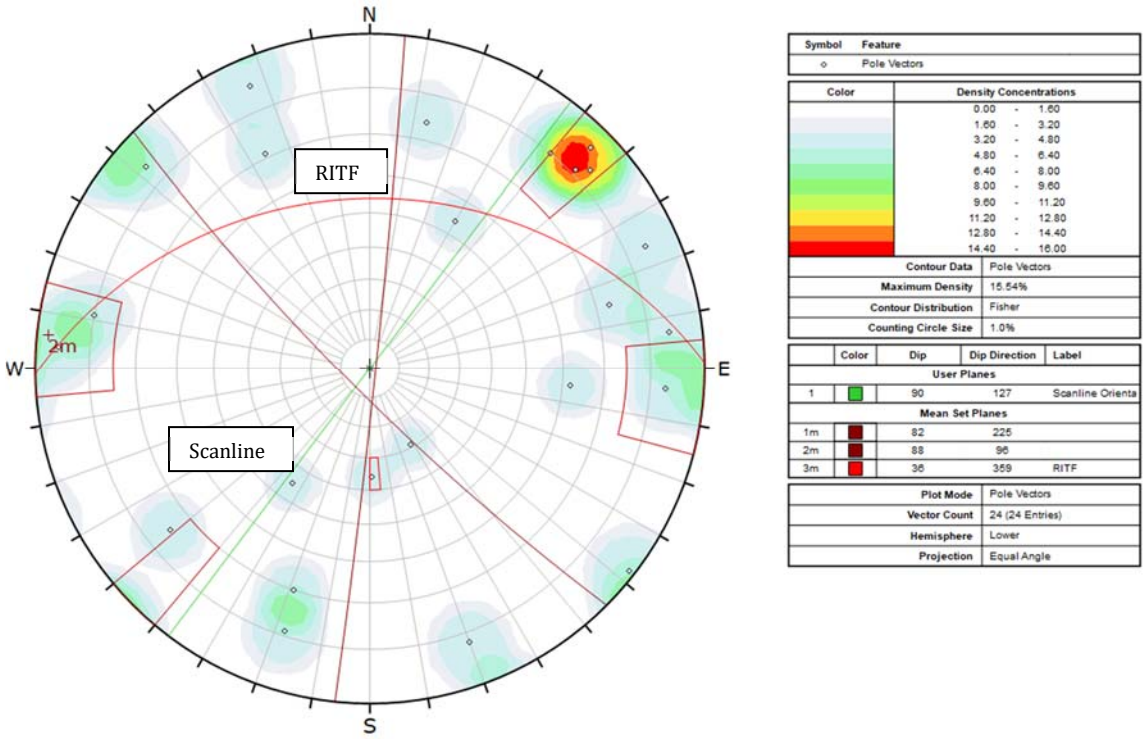

Figure 55 - Stereonet of major joint set mean planes plotted as dark red lines at Scanline 3, with the RITF plotted as red line, and scanline orientation plotted as green line

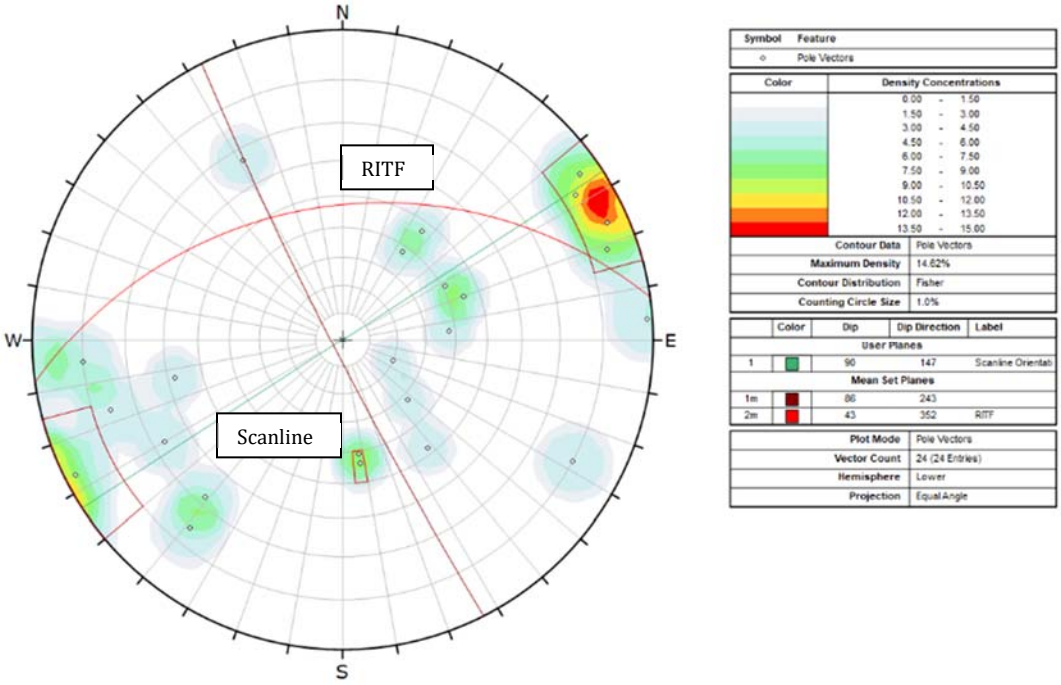

Figure 56 - Stereonet of major joint set mean plane plotted as dark red line at Scanline 4, with the RITF plotted as red line, and scanline orientation plotted as green line

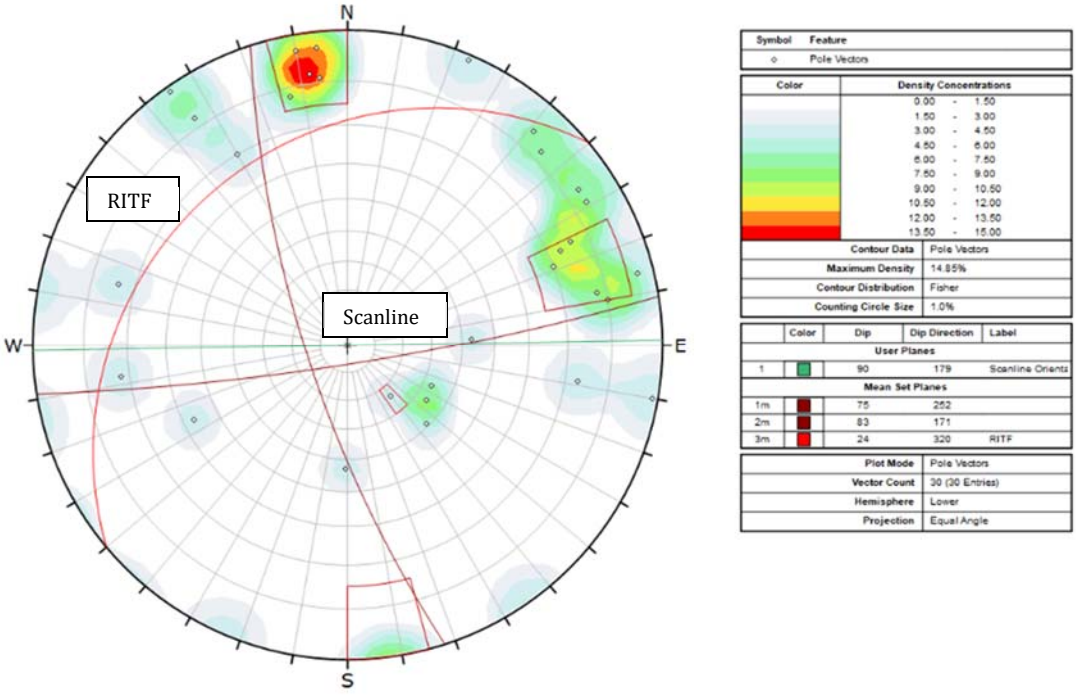

Figure 57 - Stereonet of major joint set mean planes plotted as dark red lines at Scanline 5, with the RITF plotted as red line, and scanline orientation plotted as green line

Fracture strength is often controlled by fracture fillings, moisture, openness, and asperities. To assess the strength of fractures, it was originally planned to sample representative fracture filling at each scanline location. However, during field studies, fractures were generally devoid of or had very thin fillings at the test scanlines, and a majority of the fractures were thin and had enough asperity to overcome the effects of fracture filling. Fracture filling was not sampled in the field, but was described in scanline fractures (Appendix B).

Objective 3 – Characterize toeslope materials and geometry

Grain size testing performed on the toeslope material indicated more gravel, sand and silt, and low clay contents. Figure 58 summarizes the overall grain size distribution, and Figure 59 summarizes the distribution of sand and fine material. In general, the material appears to be consistently a muddy gravel or a muddy sandy gravel. The matrix material is either a sandy silt or a silty sand and comprises anywhere from 34 to 64 percent of the material sampled. Major size fractions of gravel, sand, silt, and clay are summarized in Table 4. Clay comprised less than five percent in all of the samples tested. Originally, testing was going to include Atterberg Limits, to assess whether the slope matrix material would behave like a clay or a silt, but as a result of the low clay contents this testing was abandoned. It is assumed that the matrix material will behave more like silt. XRD testing of the parent rock also did not measure significant amounts of clay minerals.

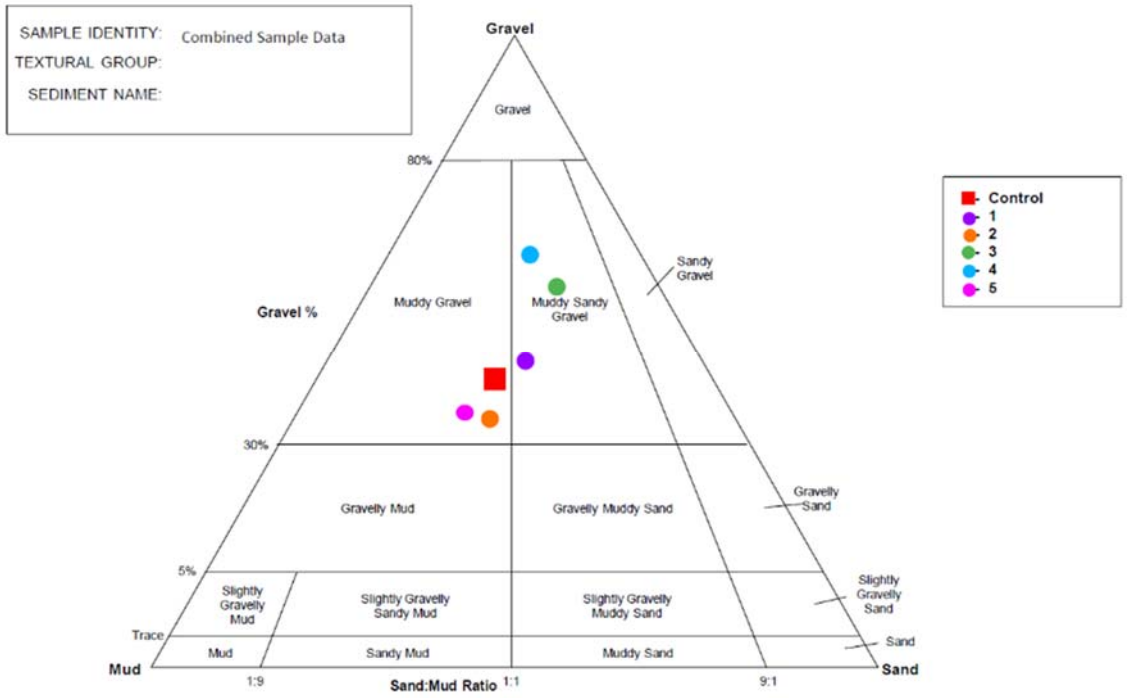

Figure 58 – Complete grain-size distribution of toeslope samples based on combination of mechanical sieving and Malvern Mastersizer results.

Table 4 – Grain-size distribution of toeslope samples

Sample	Percent Gravel	Percent Sand	Percent Silt	Percent Clay
Control	44.0%	23.4%	28.1%	4.5%
Sample 1	46.9%	27.1%	23.2%	2.8%
Sample 2	36.6%	26.2%	33.0%	4.2%
Sample 3	60.5%	25.5%	12.5%	1.5%
Sample 4	66.0%	17.9%	13.1%	3.0%
Sample 5	37.6%	21.4%	36.2%	4.8%
Notes:	1) Gravel is defined here as material that is greater than 2 mm. in diameter 2) Sand is defined here as material that is between 2 mm. and 0.063 mm. 3) Silt is defined here as material between 0.063 mm. and 0.002 mm. 4) Clay is defined here as material finer than 0.002 mm.			

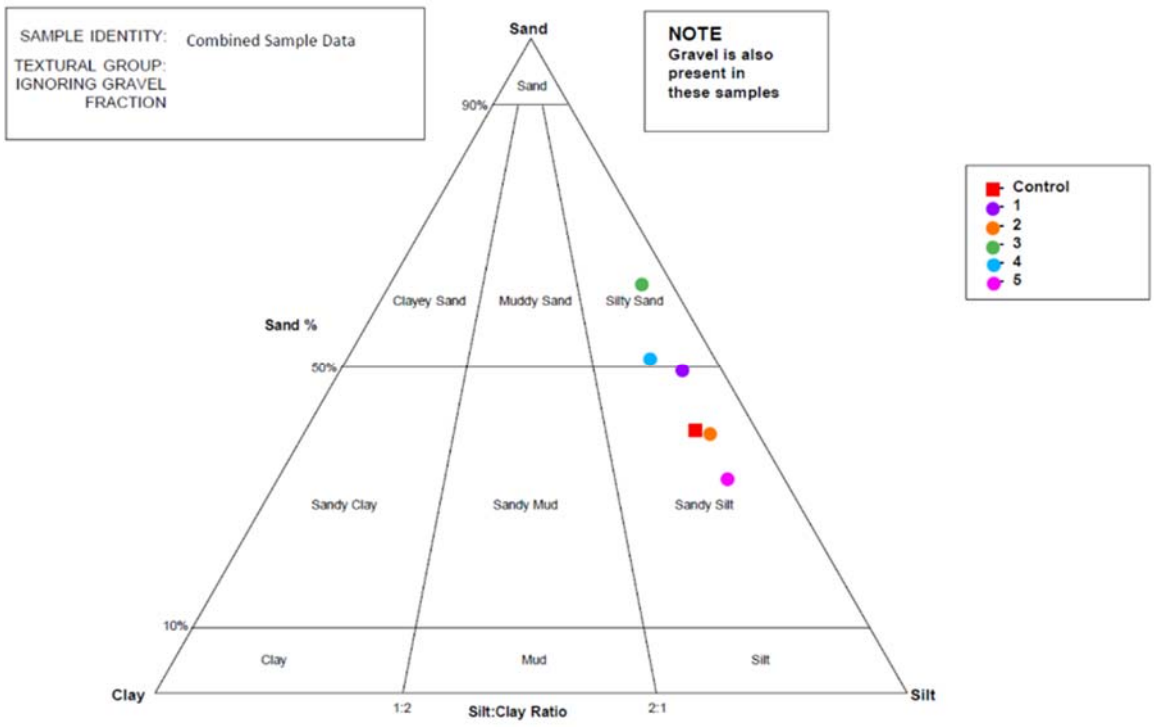

Figure 59 – Grain-size distribution of toeslope matrix material (<2 mm.). Based on partial mechanical sieving and Malvern Mastersizer data.

Given the low clay content, but high silt and fine sand content, friction angles have been assumed to be 30 degrees for all of the toeslopes, for the purpose of this study. Although the classifications differed among the six locations, they were all classified as either muddy gravel or muddy sandy gravel, with a silty sand to sandy silt matrix. It has been assumed for this study that the materials are similar enough to produce similar friction angles, and similar resistance to rockfall propagation downslope.

After making the observation that most of the toeslopes below the RITF were made up of unconsolidated material, a surficial map was created to display this information (Figure 60). The mapping scale is 1:6,000, and covers only the area north of SR-12 to just above the RITF. The mapping does not include new structural mapping, because the observations made during this research generally agree with the location of the RITF as

mapped by Biek et al. (2015). This surficial mapping influenced the development of input parameters for the rockfall model, discussed below in the section for Objective 4. Although the deposits themselves were not considered as potential sources of rockfall in the rockfall assessment, rockfall could occur from these deposits as the unconsolidated sediments erode, exposing the large boulders that are frequently found in these deposits along SR-12.

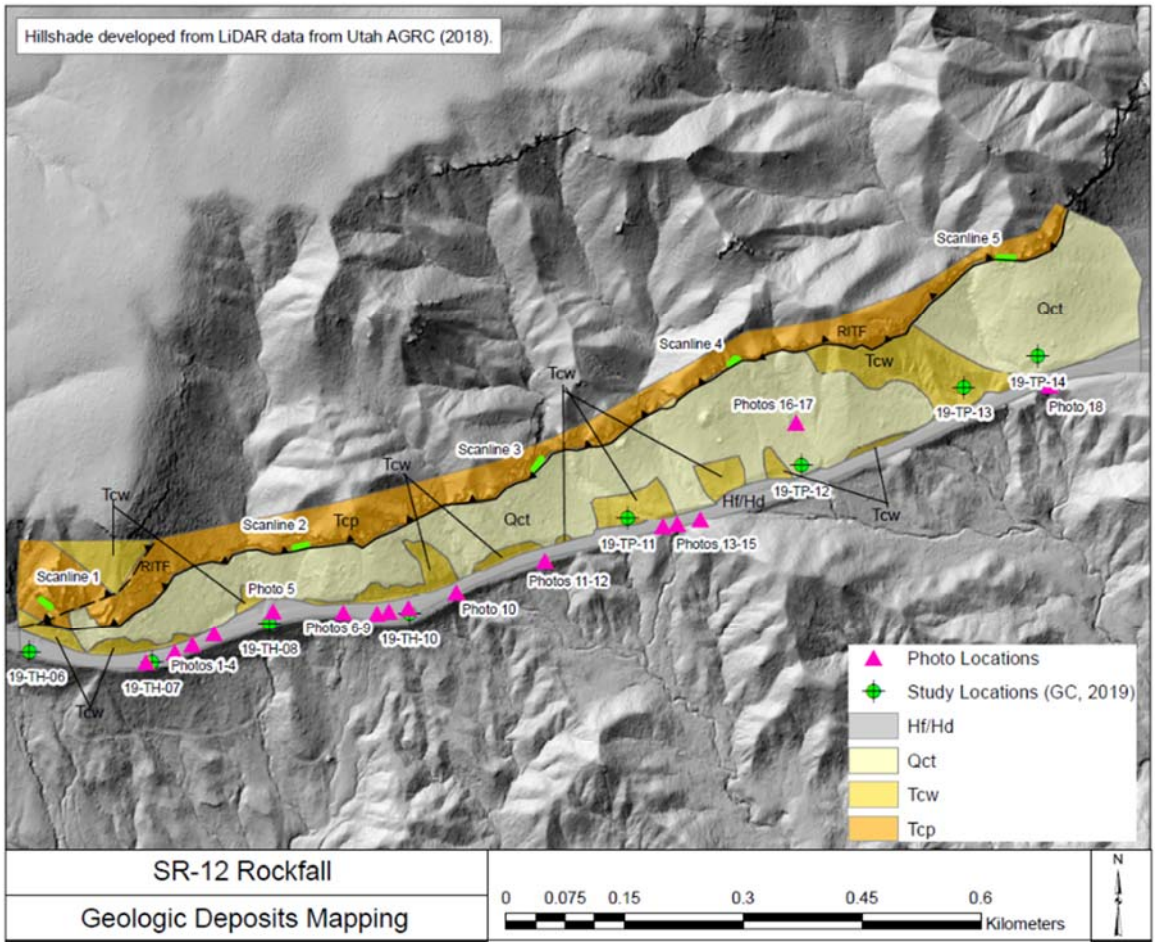

Figure 60 – Surficial geologic mapping within the project area, between SR-12 and the RITF. Photographs and study locations indicated on the map are included in Appendix C. Mapped units are described as follows: Hf/Hd – Historical fill and disturbed ground. Qct – undifferentiated Quaternary colluvial and talus deposits. Tcw – Eocene White Member of the Claron Formation. Tcp – Paleocene to Eocene Pink Member of the Claron Formation.

The undifferentiated colluvial and talus deposits are described as poorly sorted silt- to boulder-sized material; generally matrix supported, but some locations include clast-supported talus deposits (19-TP-13 in Appendix A). These deposits generally contain no evidence of imbrication or bedding. Boulders are angular to subrounded, the contact with underlying Claron Formation is undulating; matrix is a light orange silt with sand and some clay. At times, this deposit is found draped over underlying Claron Formation, but there are road cuts along SR-12 where the unit appears incised into the underlying bedrock. Locally it is less coarse, as in 19-TP-14 below Scanline 5 (Appendix A). The toeslope processes are interpreted to be mainly rockfall, slopewash and creep.

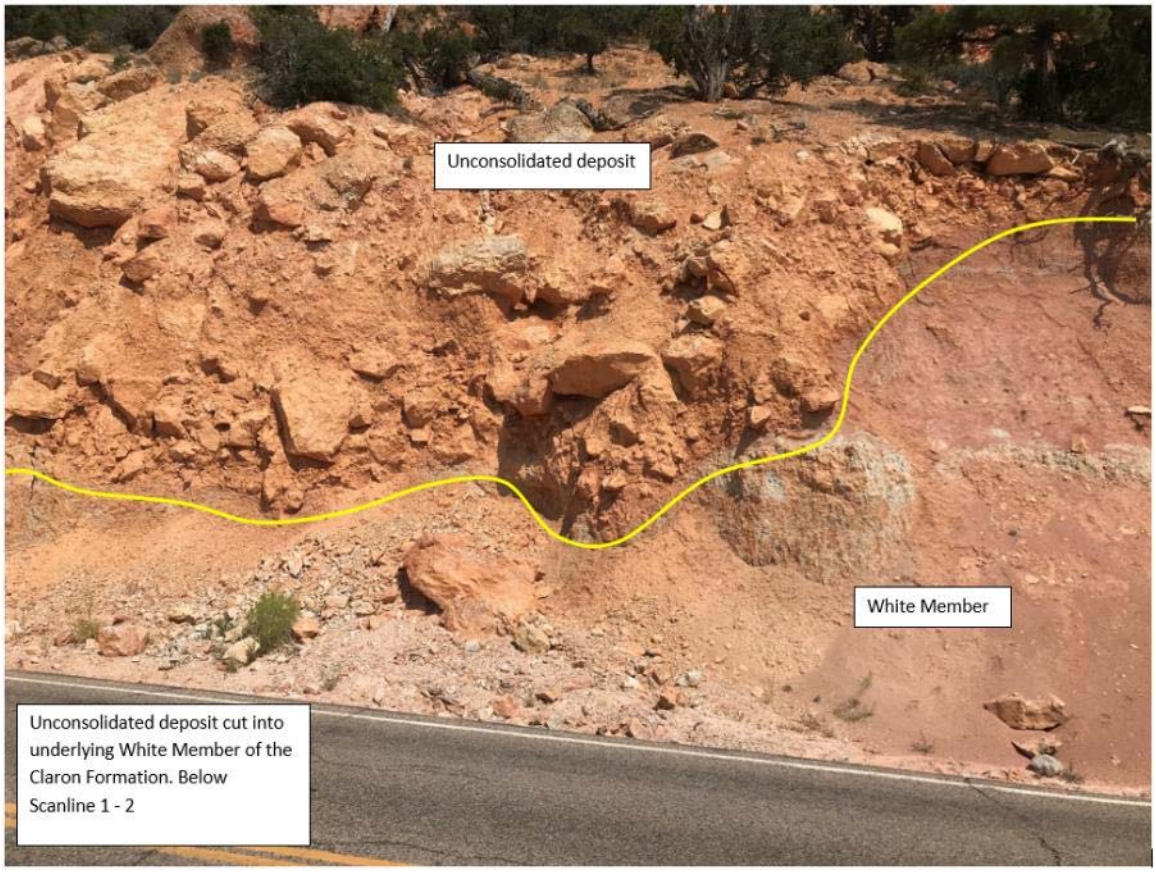

Figure 61 – Photograph of an unconsolidated deposit that has scoured out part of the underling White Member bedrock and replaced it. This photograph was taken from the roadway between Scanlines 1 and 2, looking north. Labeled Photo 2 on the geologic map in Figure 60.

Objective 4 – Rockfall assessment

Kinematic analysis was performed on cliff profiles taken from all six of the scanline locations. The percentage of fracture intersections that fall within the failure windows for each kinematic mode are summarized in Table 5, and the full kinematic analysis results are provided in Appendix D.

Table 5 – Kinematic analysis results for each scanline

	Percent of Intersections per Failure Mode (%)			
Scanline Number	Planar Sliding	Wedge Sliding	Direct Toppling	Combined Wedge and Toppling
Control	0	5.9	16.3	22.2%
1	5.6	21.6	2.0	23.5%
2	0	6.6	28	34.6%
3	0	21.7	17.4	39.1%
4	4.2	13.4	27.5	41.0%
5	3.3	24.6	11.7	36.3%

These are percentages of fracture intersections that fall within windows of orientations that could produce each failure mode. Each orientation window is a combination of slope angle and orientation, lateral limits (to account for variability in slope angle and orientation), and rock mass friction angle. If the pole of intersection plots within the orientation window, it is termed a "critical intersection" (Figure 62), the ratio of critical intersections to total intersections are the percentages in Table 5. Generally between 20 to 40 percent of intersections are conducive to failure of the rock. Additional factors influence whether a rockfall occurs or not at the critical intersections, including fracture length and driving forces. If fractures intersect but have short lengths, it is less likely to cause rockfall. In addition, if no driving process beyond gravity (i.e. freeze-thaw action, or wetting of

expansive clays) acts on the intersections, it may remain stable and not cause rockfall.

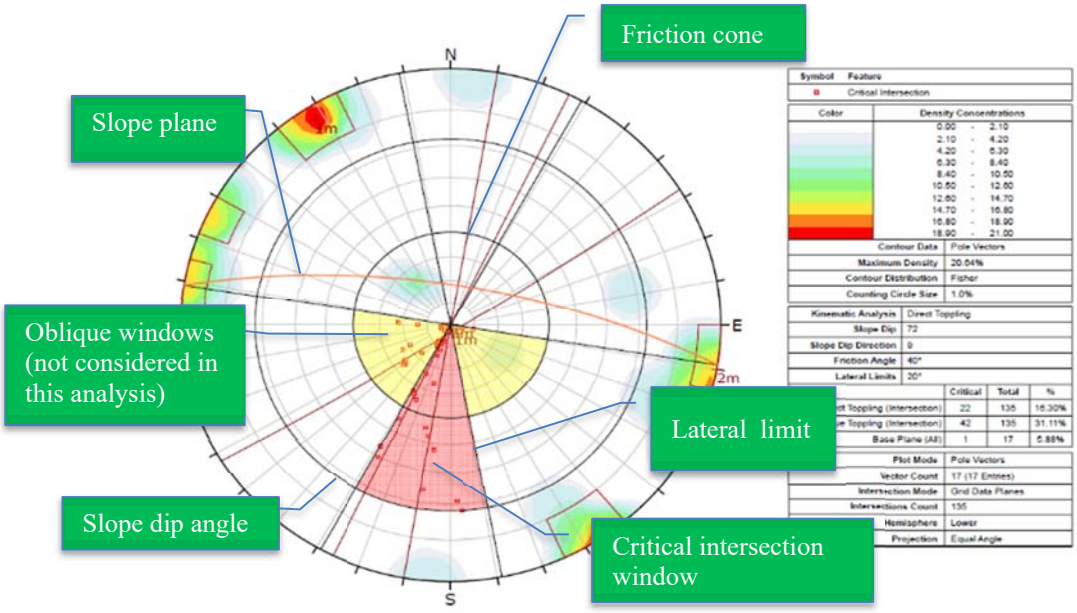

Figure 62 - Annotated, diagrammatic view of a kinematic analysis stereonet

The test scanlines all have a higher percentage of fractures that have potential to fail compared to the control scanline. All of the scanlines indicated a relatively low potential for planar sliding, which is to be expected at the test scanlines, given the orientation of the thrust fault and bedding with respect to the cliff face. Based on the combined percentages for failure modes shown in Table 5, the kinematic analysis generally confirms the hypothesis that fracturing caused by the RITF has created a higher rockfall hazard at the cliffband above SR-12 compared to a control site. The combined percentages of Wedge Sliding and Direct Toppling, which can be directly compared in terms of total fracture intersections, are around 22 to 23 percent for the control location and Scanline 1, which was in the footwall of the thrust. The remaining scanlines resulted in combined percentages between 34 to 41 percent, which is greater than 1.5 times the percentage of intersections found in the control location and Scanline 1.

Rockfall transport modeling was performed at the six scanline locations, to assess relative rockfall risk to the roadway. To be able to compare rockfall risks among the scanline locations, the UDOT rockfall retention criteria was used, which specifies that 95% of rocks should be retained at the outside edge of the travel lane closest to the slope (UDOT, 2017), or in other words 5 percent of falling rocks can cross the white line. The outside edge of the travel lane, also known as the white line, was selected as a reference point for all of the analyses, and a percentage of rocks crossing that reference point for each analysis is provided in Table 6.

Table 6 – Rockfall analysis results

Scanline Number	Number of simulated rocks	Number of rocks crossing white line	Percentage of rocks Crossing White Line
Control	5000	435	8.7%
1	5000	2232	44.6%
2	5000	628	12.6%
3	5000	55	1.1%
4	5000	15	0.3%
5	5000	10	0.2%
Additional Analyses			
Between 2 and 3	5000	1451	29.0%
Between 4 and 5	5000	263	5.3%
Notes:	1) White line is synonymous with the edge of roadway 2) This rockfall analysis used a simulation of 5000 rocks, and then assess the probability of each crossing the white line based on a series of randomized trajectories. 3) Percentage of rocks crossing the white line is reported to a tenth of a percent , but not accurate to this level, as uncertainties exist in input parameters, etc.		

Based on the results of the modeling, it appears that the toeslope length below Scanlines 3, 4, 5 all reduce the probability of propagation to almost zero, with respect to

the white line of the roadway. Although the rock mass varied slightly among scanlines, this does not appear to have changed the probability of propagation significantly. Scanlines 1, 2, and Control all demonstrated probabilities of propagation that exceed the UDOT 95% retention criteria (UDOT, 2017), based on the parameters used in these analyses. Two additional profiles, between Scanlines 2 and 3, and between Scanlines 4 and 5 were created to assess the rockfall risk in locations with existing roadway cuts that create a steep dropoff at the toe of the slope, just above the roadway. These two modeled profiles also indicated the possibility of exceeding the UDOT criteria. Printouts of the rockfall analyses and assumed parameters can be found in Appendix E.

Following the kinematic and rockfall transport analyses, a map was created for the study area, with a focus on rockfall hazard associated with the cliff band of the Claron Formation above SR-12, including zoning of potential rockfall hazard. The combined rockfall hazard at each scanline locations was calculated using the equation:

$$H(E,x) = \lambda_{\mathrm{f}} \times P_{\mathrm{p}}(E,x) \qquad \text{Eq. 2}$$

from Jaboyedoff et al., (2005), where H(E,x) is the rockfall hazard for a given kinetic energy, E, at a given point, x, λf is the rock failure mean probability or frequency, and Pp(E,x) is the probability of propagation for a given kinetic energy, E, at a given point, x. Although the kinematic analysis does not produce a direct probability or frequency of failure, it can give a relative idea of the rock failure potential at each scanline location. Kinematic analysis results and rockfall transport model percentages were multiplied at each scanline to create a more representative hazard potential for each scanline location (Table 7). These hazard calculations were then used to delineate zones of different hazard levels

in the study area for the hazard map, similar to methods in Swiss national building codes summarized in Jaboyedoff et al., (2005). The results of this combined hazard calculation indicates increased rockfall hazards to the roadway below Scanlines 1 and 2, and between 2 and 3.

Table 7 – Combined hazard calculation for each scanline, incorporating rockfall potential from kinematic analysis and probability of propagation from rockfall modeling

Scanline Number	Combined Wedge and Toppling	Percentage of rocks Crossing White Line	Combined Hazard
Control	22.2%	8.7%	1.9%
1	23.5%	44.6%	10.5%
2	34.6%	12.6%	4.4%
3	39.1%	1.1%	0.4%
4	41.0%	0.3%	0.1%
5	36.3%	0.2%	0.1%
Additional Analyses			
Between 2 and 3	36.8%	29.0%	10.7%
Between 4 and 5	38.6%	5.3%	2.0%
Notes:	1) Kinematic indicators for between scanlines 2 and 3, and between 4 and 5 were calculated using an average of the results of the two adjacent scanlines		

Based on the kinematic analyses and fracture spacing data it is kinematically possible for any of the slopes along the RITF to release large blocks that could reach the roadway, given favorable slope conditions. This indicates that the most important factor in rockfall risk to the roadway is the distance from the cliff to the road. The failure potential was similar among the test locations, but the distance from the cliff band to the roadway changed significantly between scanlines, and the combined hazard responded to these changes. Because of the nature of the data collected and the calculations performed, the

hazard map is a qualitative map, indicating roadway sections with Low, Moderate, or High risk of potentially damaging rockfall (Figure 63).

Low hazard was classified as locations that generated less than 2 percent the combined hazard calculated and summarized in Table 7. Moderate hazard was classified as locations that generated 2 to 5 percent in the combined hazard, and high hazard was classified as locations that generated greater than 5 percent in the combined hazard (Table 7).

Certain locations, like below Scanline 2, may actually have a higher risk just because of the potential block size that could come out of the cliff at that location. Figure 51 indicates that, based on the maximum spacing found between major joints, a block as large as 10 meters in diameter could come out of the cliff at Scanline 2, although this spacing was considered to be an outlier. A block this size could have catastrophic consequences if it were able to propagate to the roadway, which seems possible based on the rockfall analyses performed at this location. If an energy/recurrence-interval-based hazard assessment had been performed at this location, the results of the hazard map may have come out differently.

Although the accuracy or validity of a hazard map is difficult to fully confirm, several indicators were observed in the field and in aerial imagery and LiDAR data that support the results of this hazard mapping. One of the main indicators was a large boulder that was encountered between Scanlines 2 and 3 in the spring of 2020, that was not at the roadway level in the fall of 2019 (Figure 63). This approximately 1.5 meter boulder (Appendix A for photo) had evidently reached the roadway level, most likely from a freeze-thaw cycle in the winter or early spring of 2020. This boulder was found in a location that

was mapped as having a high potential rockfall hazard in Figure 63. Another location where the hazard mapping is supported by external evidence is at Scanline 5. Using aerial imagery and LiDAR, it was observed that large rocks appear to gather near the toe of a small, fan-shaped deposit below the Scanline 5 cliffband (Figure 64). The bottom of this fan is approximately halfway up the slope, over 30 meters above the roadway level. A test pit performed near the bottom of this slope also indicated a lack of large materials reaching the bottom of the slope (Gerhart Cole, 2019).

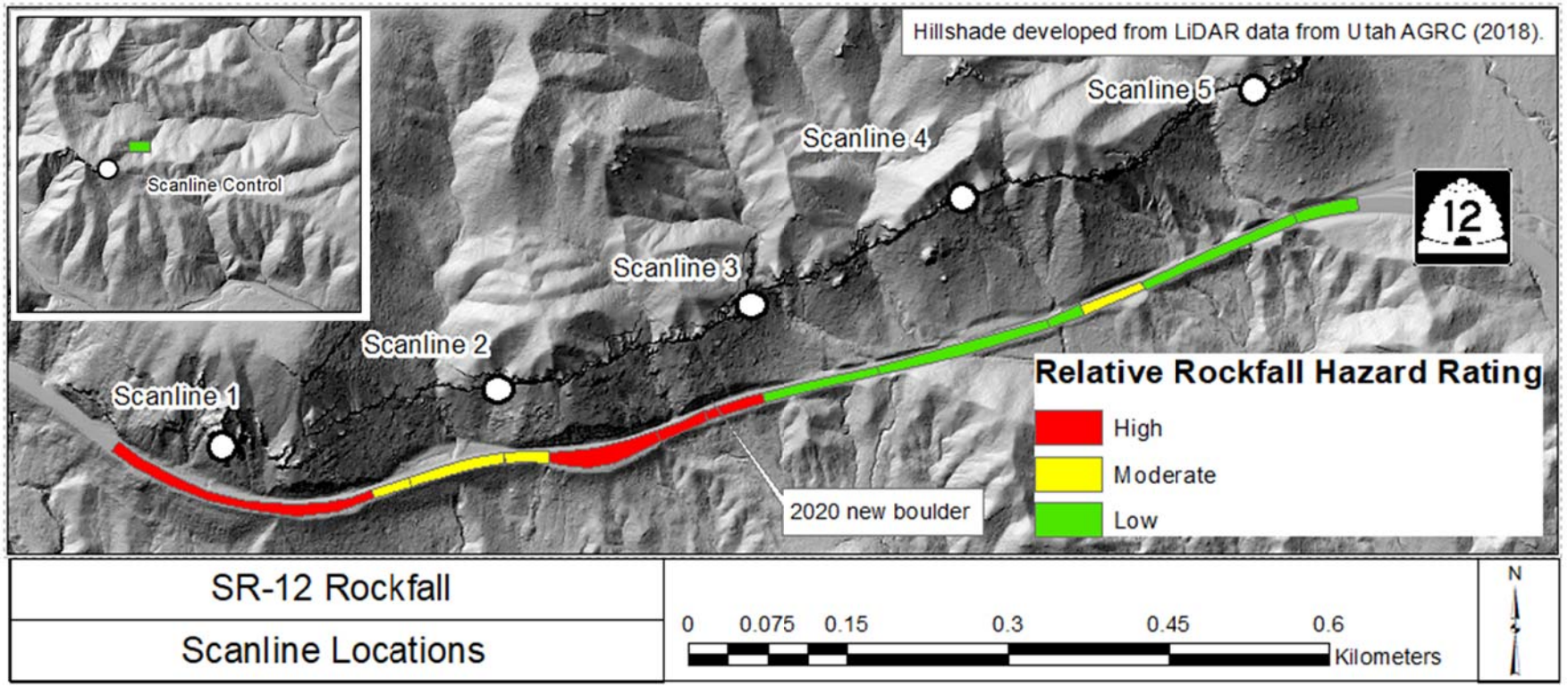

Figure 63 - Relative rockfall hazard map, with an inset of the control location in upper left hand side of figure

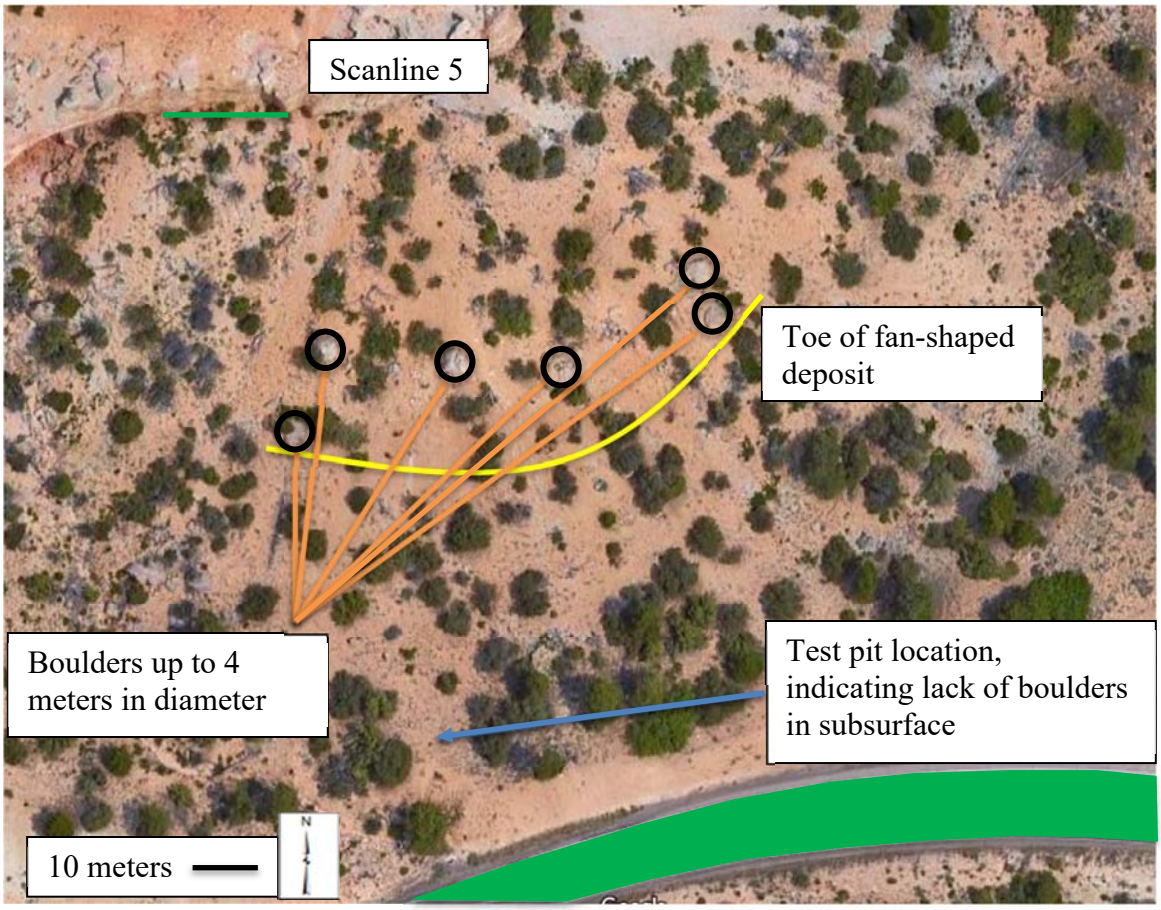

Figure 64 – Google Maps imagery of a fan-shaped deposit where boulders from the Scanline 5 cliffband appear to stop, well above the roadway. See Appendix C for test pit log, 19-TP-14. Green on roadway indicates this is an area of low rockfall hazard (Figure 63)

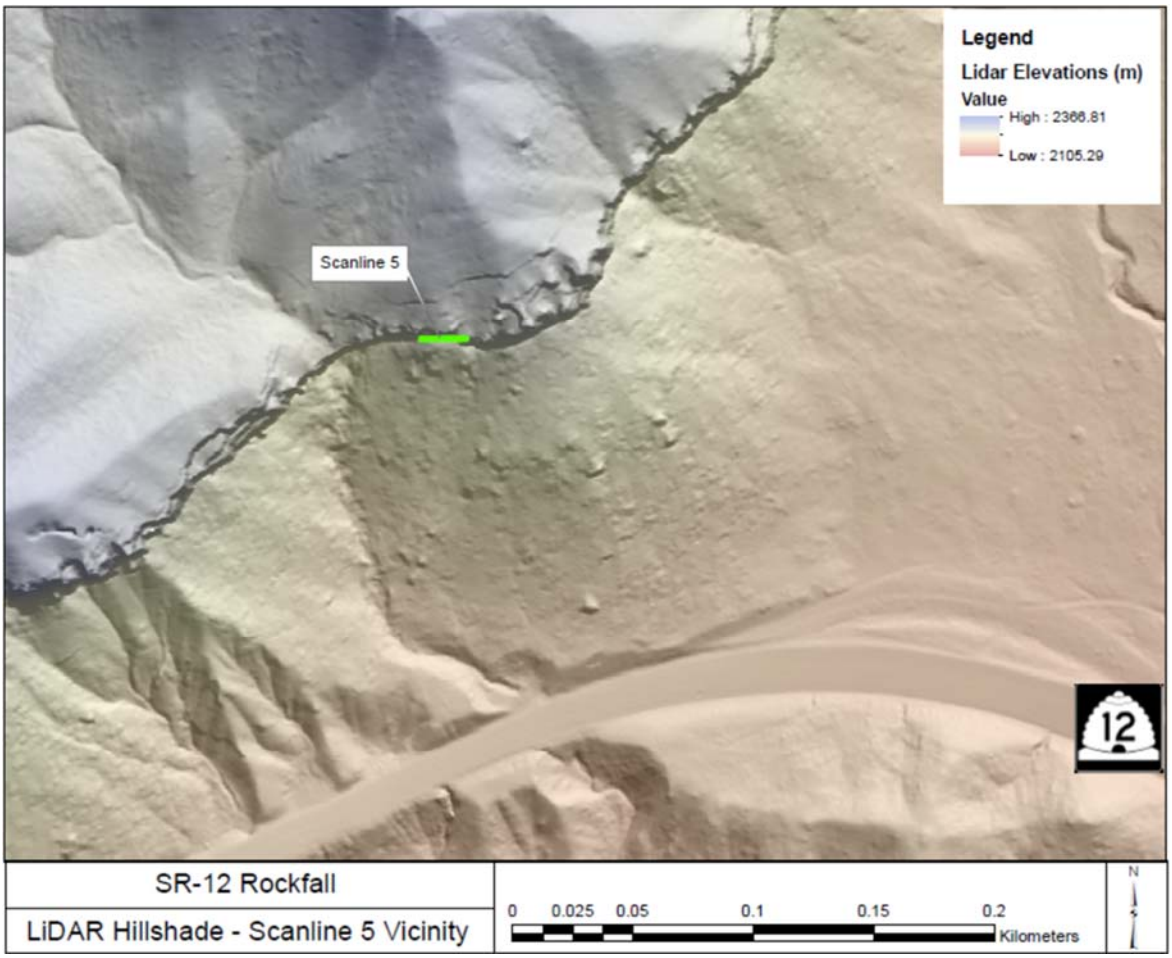

Figure 65 – LiDAR hillshade in the vicinity of Scanline 5, showing a fan-shaped deposit where boulders from the Scanline 5 cliffband appear to generally stop, well above the roadway.

CHAPTER 5

CONCLUSION

This research focused on collecting data about structural rock fractures in a cliffband above highway SR-12 to assess their contribution to rockfall hazards to the roadway. Scanline data collection was employed, along with hand sampling and laboratory testing of outcrop rocks and toeslope materials. Geologic mapping, especially of unconsolidated deposits, which were not previously mapped in this project area, was performed to aid in the assessment of rockfall hazard to the highway. As a result of this research, it appears that there are locations along SR-12 with moderate to high rockfall hazards. However, it appears that as the highway extends to the east, the hazards generally decrease due to the topography and material properties of the toeslopes below the cliff band.

Future work could include refining the unconsolidated deposits map, to better understand the interaction of creep and slopewash processes with rockfall and other mass-wasting processes in this region. The types and concentrations of mass-wasting deposits found along and below the roadway suggest that there are significant implications for hazards to the roadway beyond those discussed in this research. Additionally, the boulders found on the toeslope and below the roadway could be more thoroughly catalogued. This data could potentially be used to develop a rock failure frequency, which could be used with the rockfall analyses performed here to calculate a more meaningful hazard, using Equation 2 found in Chapter 4, above (Jaboyedoff et al., 2005). More work could also be done to better understand the structural relationships where the Ruby's Inn Thrust Fault

crosses SR-12, and where several strands appear to connect and combine. Lastly, future work in the area could include a more detailed stratigraphic assessment of the Pink Member of the Claron Formation, with tighter age constraints. It has been difficult in the past to constrain the age of the Pink Member, but perhaps with newer dating techniques, the age could be constrained better.

References

Asteriou, P., Saroglou, H., and Tsiambaos, G., 2013. Rockfall: Scaling factors for the Coefficient of Restitution. Rock Mechanics for Resources, Energy, and Environment, September 2013, pp. 195-200.

Barton, N. R. (1973). "Review of a New Shear Strength Criterion for Rock Joints." Engineering Geology, Elsevier, v.7, 1973, pp 287-333.

Biek, R.F., Rowley, P.D., Anderson, J.J., Maldonado, F., Moore, D.W., Hacker, D.B., Eaton, J.G., Hereford, R., Sable, E.G., Filkorn, H.F., and Matyjasik, B., 2015. Geologic Map of the Panguitch 30' x 60' Quadrangle, Garfield, Iron, and Kane Counties, Utah. 1:62,500. Map 270 DM, Utah Geological Survey.

Black, B.D., and Hecker, S., compilers, 1999, Fault number 2504, Paunsaugunt fault, in Quaternary fault and fold database of the United States: Accessed on 08/28/2020 from https://earthquakes.usgs.gov/hazards/qfaults

Blott, S.J., 2020. GRADISTAT version 9.1, A Grain Size Distribution and Statistics Package for the Analysis of Unconsolidated Sediments by Sieving or Laser Granulometer. Accessed May 31, 2020 from http://www.kpal.co.uk/gradistat.html

Bowers, W.E., 1991. Geologic Map of Bryce Canyon national Park and Vicinity, Southwestern Utah. United States Geological Survey Miscellaneous Investigations Series Map I-2108. Scale 1:24,000.

Crosta, G.B., and Agliardi, F., 2003. A methodology for physically based rockfall hazard assessment. Natural Hazards and Earth System Science, Copernicus Publications on behalf of the European Geosciences Union, 2003, 3: pp. 407-422.

Cruden, D.M., and Varnes, D.J., 1993. Landslides: Investigation and Mitigation – Chapter 3: Landslide Types and Processes. Transportation Research Board, National Academy of Sciences. Published July 15, 1993.

Davis, G.H., and Pollock, G.L., 2010. Geology of Bryce Canyon National Park, from Geology of Utah's Parks and Monuments, 2003 Utah Geological Association Publication 28 (2nd Edition), D.A. Sprinkel, T.C. Chidsey, and P.B. Anderson, editors.

Dorren, L., and Seijmonsbergen, A.C., 2003. Comparison of three GIS-based models for predicting rockfall runout zones at a regional scale. Geomorphology. 56: pp. 49-64.

Densmore, P., 2019. 2018 Another Record Year for Visitation at Bryce Canyon National Park. National Parks Service [NPS] News Release, March 14, 2019, accessed on January 28, 2020 at https://www.nps.gov/brca/learn/news/2018-another-record-year-for-visitation-at-bryce-canyon-national-park.htm

Fenneman, N.M., and Johnson, D.W., 1946. Physiographic Divisions of the Conterminous U.S. 1:7,000,000. Accessed on October 3, 2020 from https://water.usgs.gov/GIS/metadata/usgswrd/XML/physio.xml

Forte, A.M., Yanites, B.J., and Whipple, K.X, 2016. Complexities of landscape evolution during incision through layered stratigraphy with contrasts in rock strength: Earth Surface Processes and Landforms, v. 41, pp. 1736–1757.

Gerhart Cole, 2019. Geotechnical Design Report, SR-12 Emergency Slope Stabiliziation, Phase 2; Garfield County, Utah; Project No. F-0012(43)15; Pin 15632. March 2, 2020.

Goudie, A.S., 2006. The Schmidt Hammer in geomorphological research. Progress in Physical Geography 30, 6 (2006), pp. 703-718.

Hanser, S., 2008. Elevation in the Western United States (90 meter DEM). USGS-FRESC, Snake River Field Station.

Hintze, L.F., Willis, G.C., Laes, D.Y.M., Sprinkel, D.A., and Brown, K.D., 2000. Digital Geologic Map of Utah. 1:500,000. Map 179 DM. Utah Geological Survey. Accessed on October 3, 2020 from https://ugspub.nr.utah.gov/publications/geologicmaps/M-179DM.pdf

Hoek, E., and Bray, J.W., 1981. Rock Slope Engineering: The Institute of Mining and Metallurgy, London, England, 358 p.

Hudson, J.A., and Harrison, J.P., 1997. Engineering rock mechanics: an introduction to the principles. Elsevier Science Ltd., Oxford, England, 444 p.

Jaboyedoff, M., Dudt, J. P., Labiouse, V., 2005. An attempt to refine rockfall hazard zoning based on the kinetic energy, frequency and fragmentation degree. Natural Hazards and Earth System Science, Copernicus Publications on behalf of the European Geosciences Union, 2005, 5 (5), pp.621-632.

Jones, C.L., Higgins, J.D., and Andrew, R.D., 2000. Colorado Rockfall Simulation Program Version 4.0 (For Windows). Colorado Department of Transportation. March 2000.

Knudsen, T.R., 2020. Personal communication via telephone and email on January 8, 2020, including GIS files of preliminary geologic mapping in the Bryce Canyon area.

Lambert, C., Thoeni, K., Giacomini, A., Casagrande, D., and Sloan, S., 2012. Rockfall Hazard Analysis From Discrete Fracture Network Modelling with Finite Persistence Discontinuities. Rock Mechanics and Rock Engineering, Volume 45, Issue 5, pp. 871-884.

Lund, W.R., Knudsen, T.R., and Sharrow, D.L., 2010. Geologic Hazards of the Zion National Park Geologic-Hazard Study Area, Washington and Kane Counties, Utah. 1:24,000. Special Study 133, Utah Geological Survey.

Lundin, E.R., 1989. Thrusting of the Claron Formation, the Bryce Canyon region, Utah. Geological Society of America Bulletin, v. 101, p. 1038-1050, August 1989

Mauldon, M., and Dershowitz, W., 2000. A Multi-Dimensional System of Fracture Abundance Measures. Summit 2000 presentation, Geological Society of America Annual Meeting, Reno, Nevada, November 2000

Malvern Panalytical, 2020. Mastersizer 3000 brochure. Accessed on May 30, 2020 from https://www.malvernpanalytical.com/en/products/product-range/mastersizer-range

May, S.B., Leavitt, R.E., and MacLean, J.S., 2012. Extent and mechanism of footwall shear adjacent to the Ruby's Inn Thrust Fault, Southern Utah. The Compass: Earth Science Journal of Sigma gamma Epsilon, v. 84(1), 2012. pp. 30-41.

Pierson, L.A., 1992. Rockfall Hazard Rating System. Transportation Research Record 1343. P. 6-13.

Precimat, 2020. Thin Sections, Additional Thin Section Options – Carbonate Staining. After "Carbonate Identification and Genesis as revealed by Staining, Dickson, J.A.D., Journal of Sedimentary Petrology, Vol. 36, No. 22, pp. 491-505, June 1966". Accessed on May 30 from http://www.precimat.com/services/petrographic-manufacturing/thin-sections/

Riley, K.E., Rittenour, T.M., Pederson, J.L., and Belmont, P., 2019, Erosion rates and patterns in a transient landscape, Grand Staircase, southern Utah, USA: Geology, v. 47, p. 811–814, https:// doi .org /10 .1130 /G45993.1

Rocscience, 2020a. Dips version 8.004. Build date June 19, 2020. Toronto, Ontario, Canada.

Rocscience, 2020b. Rocscience Coefficient of Restitution Table. Accessed on September 7, 2020 from https://www.rocscience.com/help/rocfall/baggage/rn_rt_table.htm

Rocscience, 2020c. Rocfall version 8.008. Build date May 6, 2020. Toronto, Ontario, Canada.

Taylor, W.J., 1993. Stratigraphic and Lithologic analysis of the Claron Formation in southwestern Utah. Miscellaneous publication 93-1, Utah Geological Survey.

United States Geological Survey [USGS], 2020. The National Map Download, version 1.0., Elevation Source Data (3DEP) – Lidar, IfSAR. Accessed online on September 5, 2020 from https://viewer.nationalmap.gov/basic/#productSearch

United States Bureau of Reclamation [USBR], 2001, Engineering Geology Field Manual, Second Edition, Volume 1: Technical Service Center, Bureau of Reclamation, U.S. Department of the Interior, accessed online on May 15, 2020 from http://www.ov/pmts/geology/geoman.html

Utah Automated Geographic Reference Center [AGRC], 2018. 2018 Southern Utah LiDAR Elevation Data, 2.2.4. Tile 12SVG0070, Bryce Canyon National Park.

Utah Department of Transportation [UDOT], 2012. UDOT Mile Posts Map. Updated September 15, 2020. Accessed on September 17, 2020 from https://www.arcgis.com/home/item.html?id=6e2fdb123fed426cb839195f1b37e9f5

Utah Department of Transportation [UDOT], 2017. UDOT Geotechnical Manual of Instruction, September 2017.

Utah Department of Transportation [UDOT], 2019. UDOT Region 4 Projects Page, Garfield County, PIN 15584, SR-12 Slope Stabilization in Bryce Canyon National Park. Accessed on January 28, 2020 from https://www.udot.utah.gov/projectpages/f?p=250:2008:::NO::P2008_EPM_PROJ_XREF_NO,P2008_EPM_MASTER_PROJ_XREF_NO,P2008_PROJECT_TYPE_IND_FLAG:12955,0,0

Utah Department of Transportation [UDOT], 2020. Plans of Proposed State Road Federal Aid Project F-0012(43)15, PIN 15632, SR-12; Connecting Passing Lanes, MP 14.6-15.86; Passing Lane; Garfield County; Length 1.250 miles. Comment Resolution set, dated February 10, 2020.

Utah Geological Survey [UGS], (2020). Utah Quaternary Fault and Fold Map, UGS website, https://geology.utah.gov/apps/qfaults/index.html, accessed 08/28/2020.

VanDeVelde, J.H., and Bowen, G.J., 2014. Isotope hydrology of early Paleogene Lake Flagstaff, Central Utah: Implications for Cordilleran evolution. American Journal of Science, Vol. 314, December, 2014, P. 1436–1461, DOI 10.2475/10.2014.02

Watkins, H., Bond, C.E., Healy, D., and Butler, R.W.H., 2015. Appraisal of fracture sampling methods and a new workflow to characterize heterogeneous fracture networks at outcrop. Journal of Structural Geology, 72 (2015) 67-82.

APPENDIX A

Appendix A presents the geologic mapping performed in the field and using aerial photography for the study area, along with including photographs and subsurface information collected by a consulting firm (Gerhart Cole, 2019). “White Member” in the photograph captions refers to the White Member of the Claron Formation.

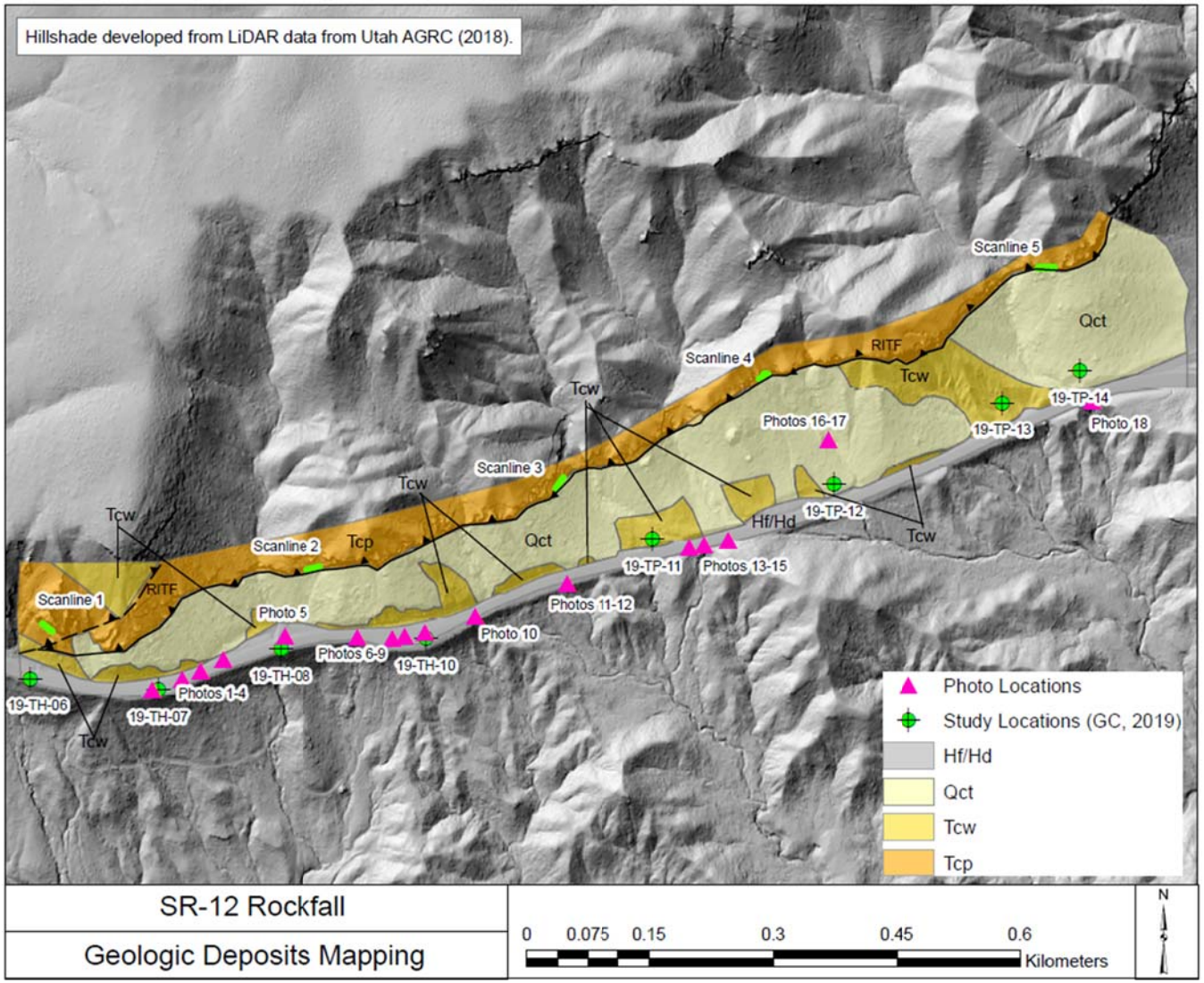

Figure A-1 – Geologic mapping performed in the project area

Geologic Map Unit Descriptions

Hf/Hd – Fill and disturbed land (historical) – Undifferentiated human fill and disturbance related to the construction of SR-12 through the mapped area.

Qct – Undifferentiated colluvial and talus deposits (Quaternary) – Poorly sorted silt- to boulder-sized material; generally matrix supported, but some locations include clast supported talus deposits (see 19-TP-13). Generally no evidence of imbrication, boulders are angular to subrounded, pinhole structure is frequently found in matrix, undulating contact with underlying White Member of the Claron Formation; matrix is silt with sand and some clay, light orange. At times, this deposit is found draped over underlying White Member or Pink Member, but there are several locations in road cuts along SR-12 where the unit appears incised into the underlying bedrock.

Tcw – White Member of the Claron Formation (Eocene) – In the study area, the White Member generally consists of Interbedded light tan to pale olive brown limestone and olive brown to tan mudstone, with occasional layers with pink to red staining. Thickly to very thickly bedded, fresh to moderately weathered, moderately hard to soft. Limestone beds often form ledges while mudstones form slopes. Generally previously mapped by Biek et al. (2015) as Pink member, but Knudsen (2020) mapped these units as White Member, which seems more likely.

Tcp – Pink Member of the Claron Formation (Paleocene to Eocene) – In the study area, the Pink Member generally consists of varicolored, thickly bedded limestone, dolomite, and marlstone, ranging from light orange to light pink to yellowish brown. Often stained with manganese oxide and calcium carbonate, frequently vuggy and vugs frequently filled with calcite crystals. In some locations displays dissolution cleavage (Lundin, 1989). Generally micritic. Frequent bioturbation in the form of burrows.

Ruby's Inn Thrust Fault, dashed where approximate, teeth on upper plate

Figure A-2 – Unit descriptions and key to map symbols from the geologic mapping in Figure A-1

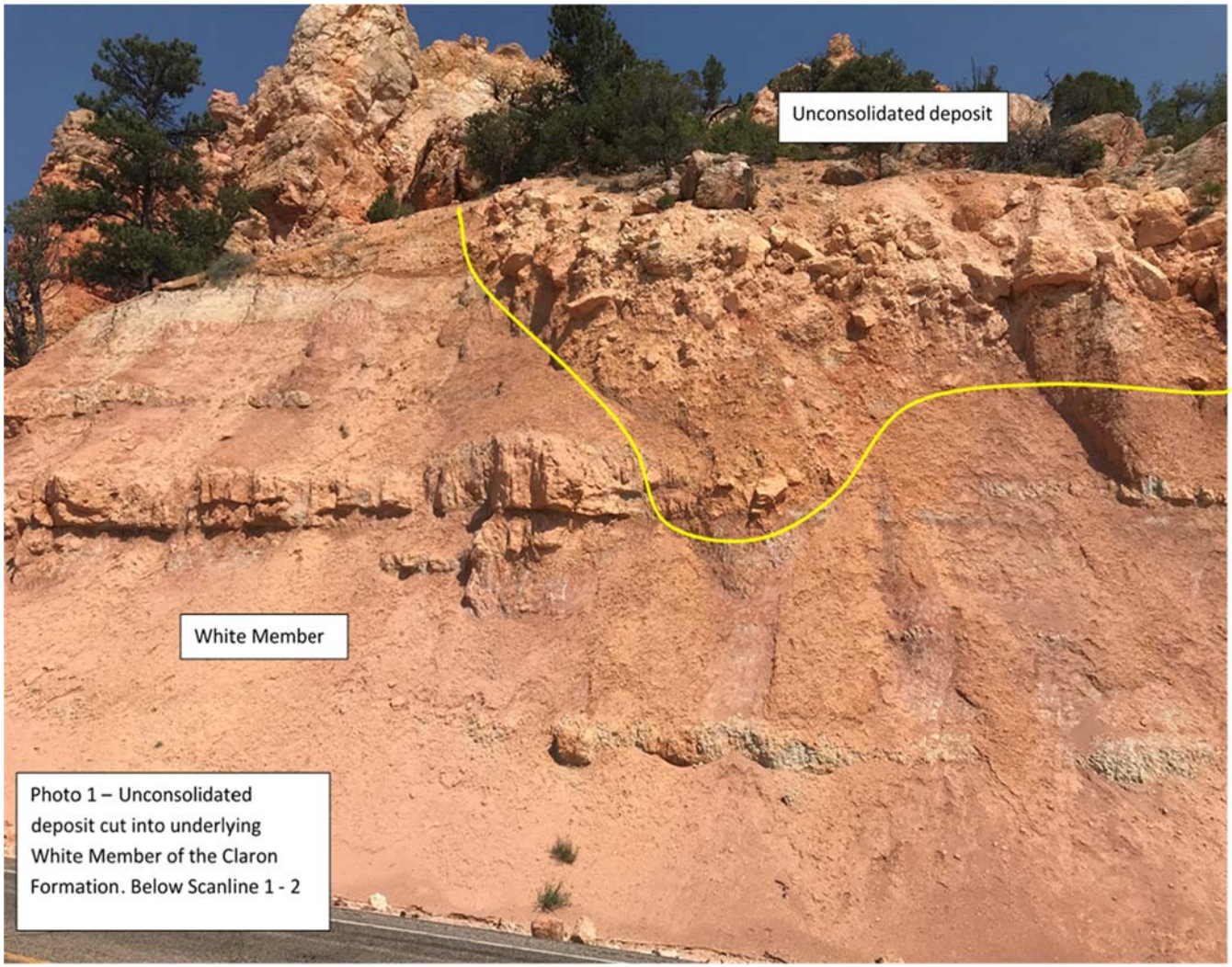

Figure A-3 – Photograph of unconsolidated deposit in roadway below Scanlines 1 and 2

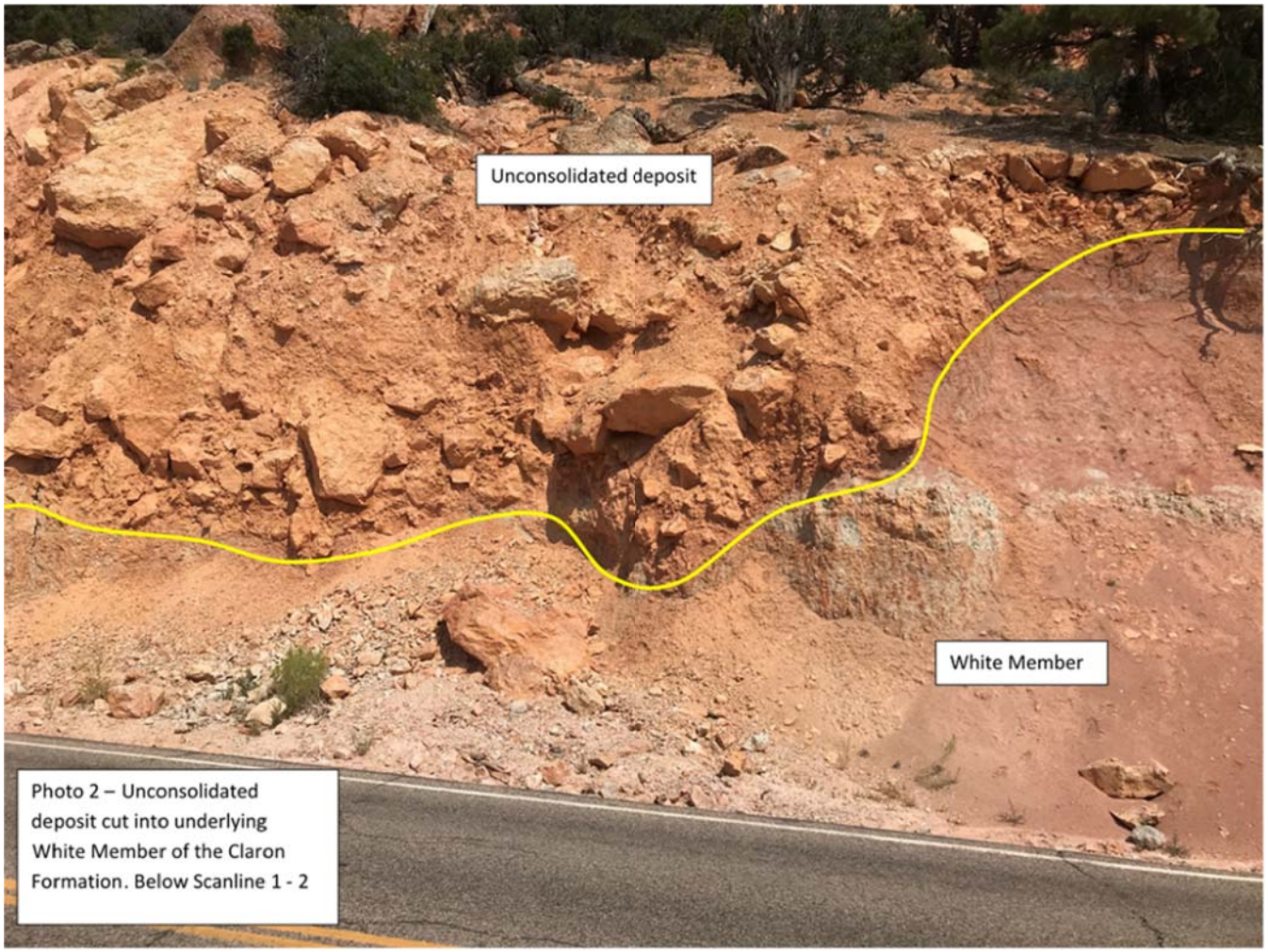

Figure A-4 – Photograph of unconsolidated deposit in roadway below Scanlines 1 and 2

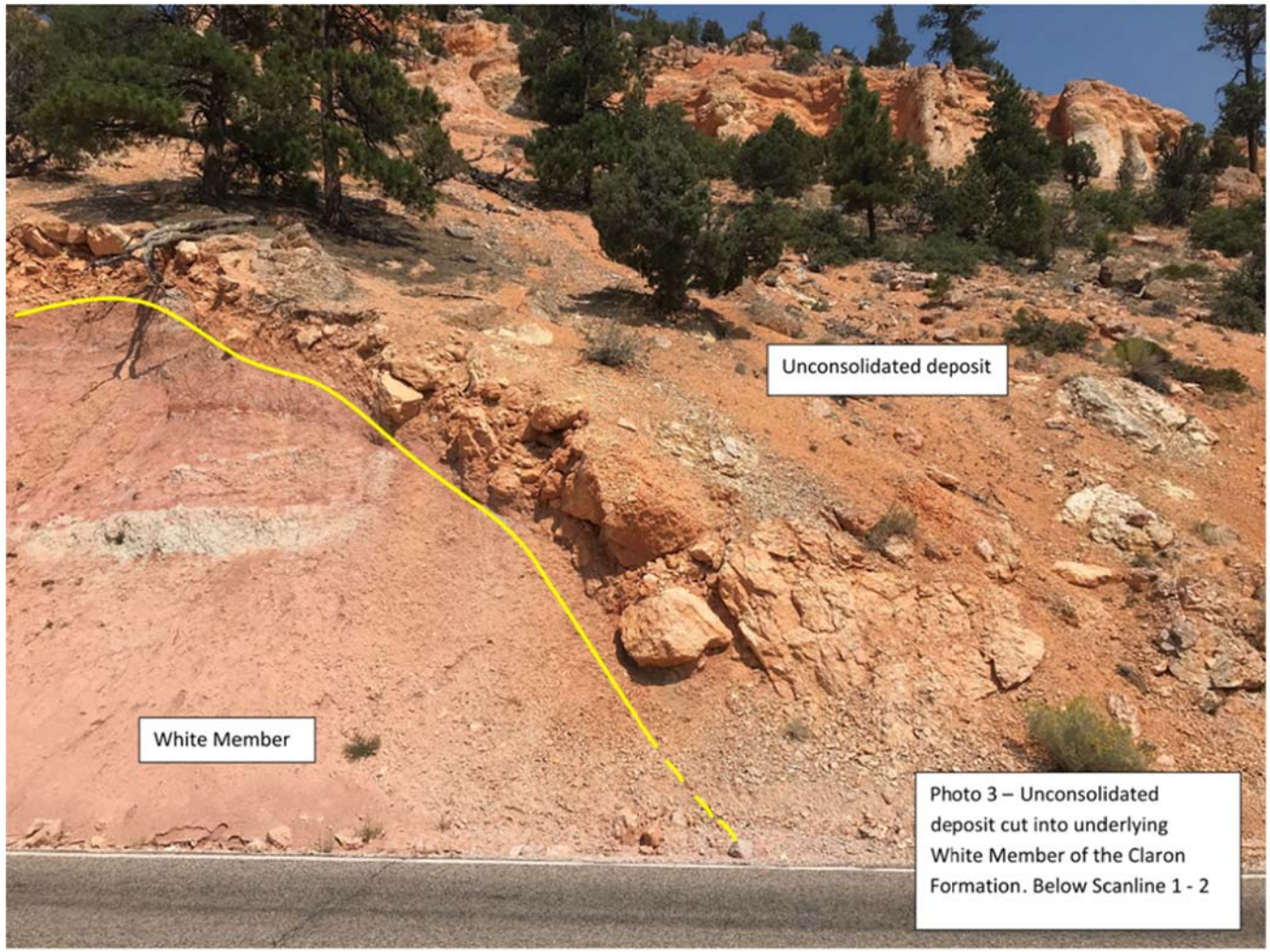

Figure A-5 – Photograph of unconsolidated deposit in roadway below Scanlines 1 and 2

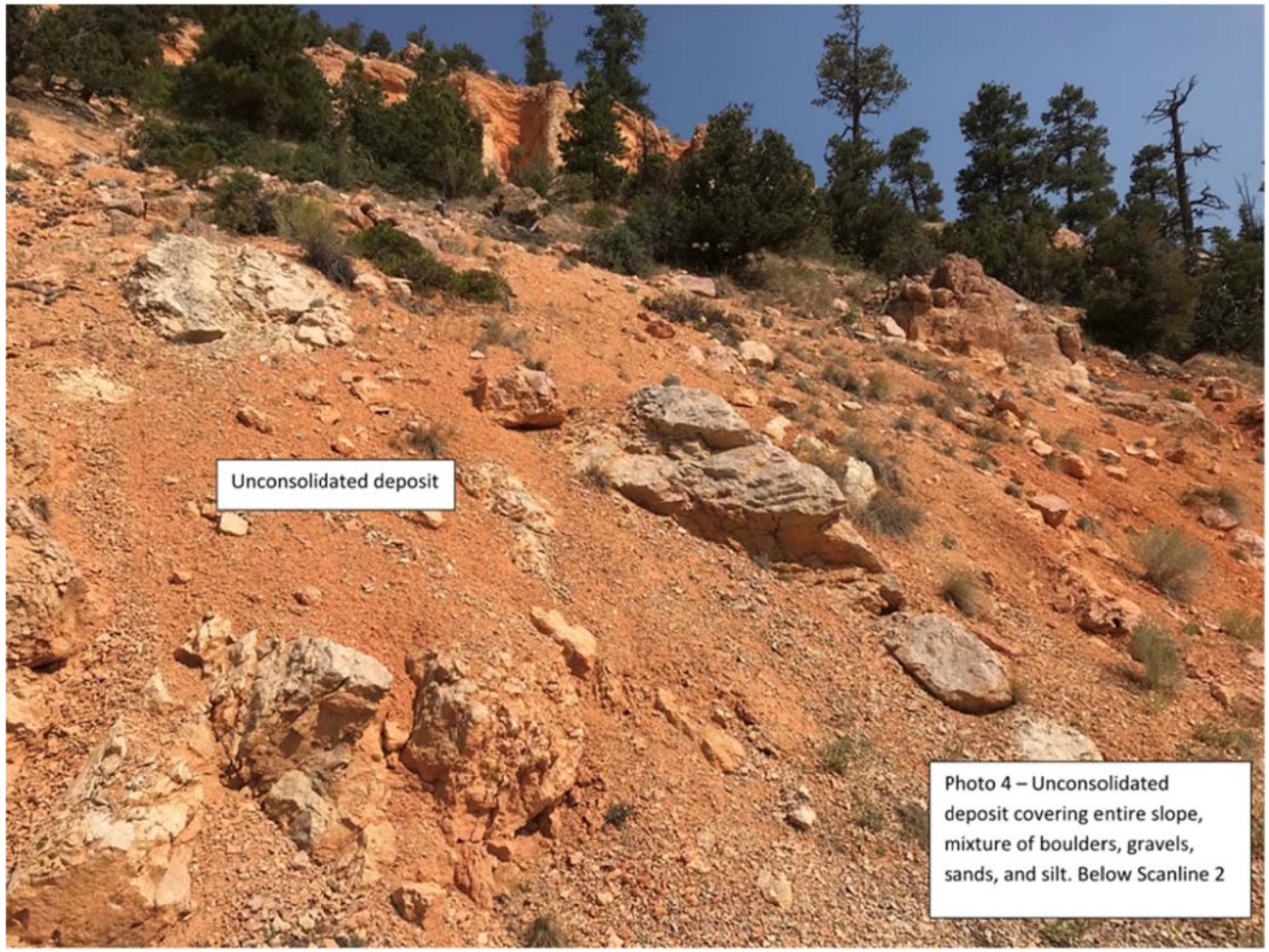

Figure A-6 – Photograph of unconsolidated deposit in roadway below Scanline 2

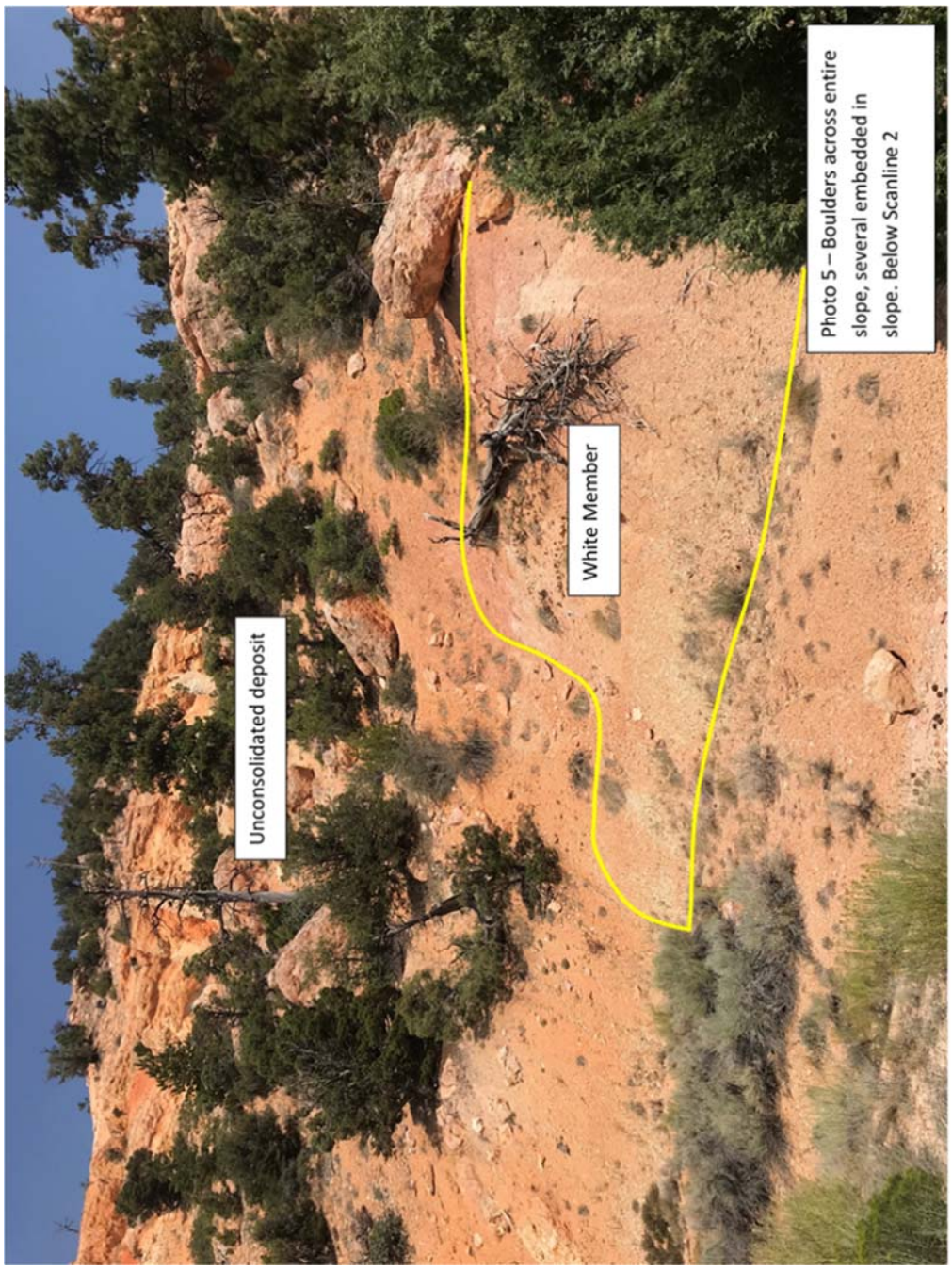

Figure A-7 – Photograph of unconsolidated deposit in roadway below Scanline 2

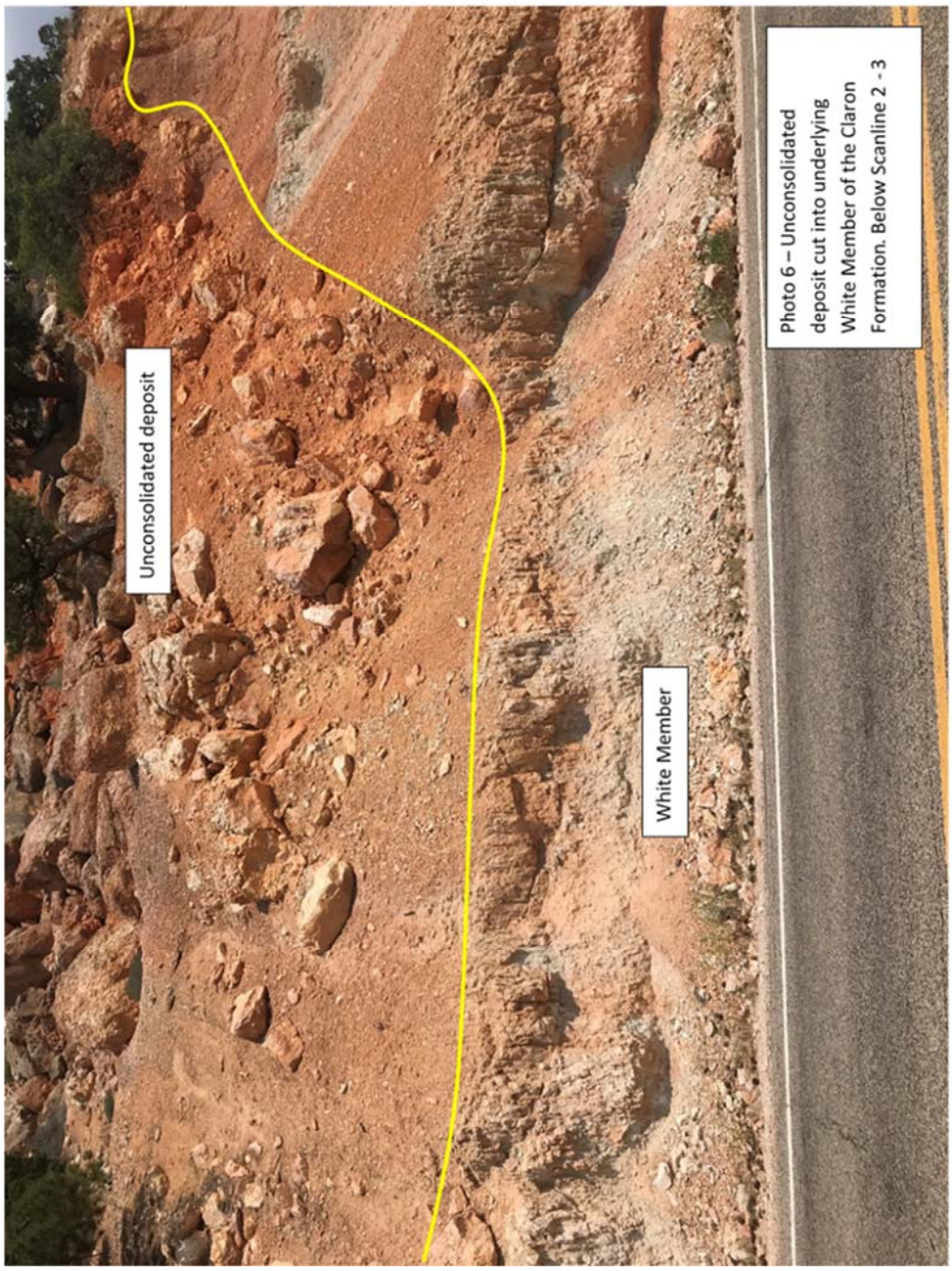

Figure A-8 – Photograph of unconsolidated deposit in roadway below Scanlines 2 and 3

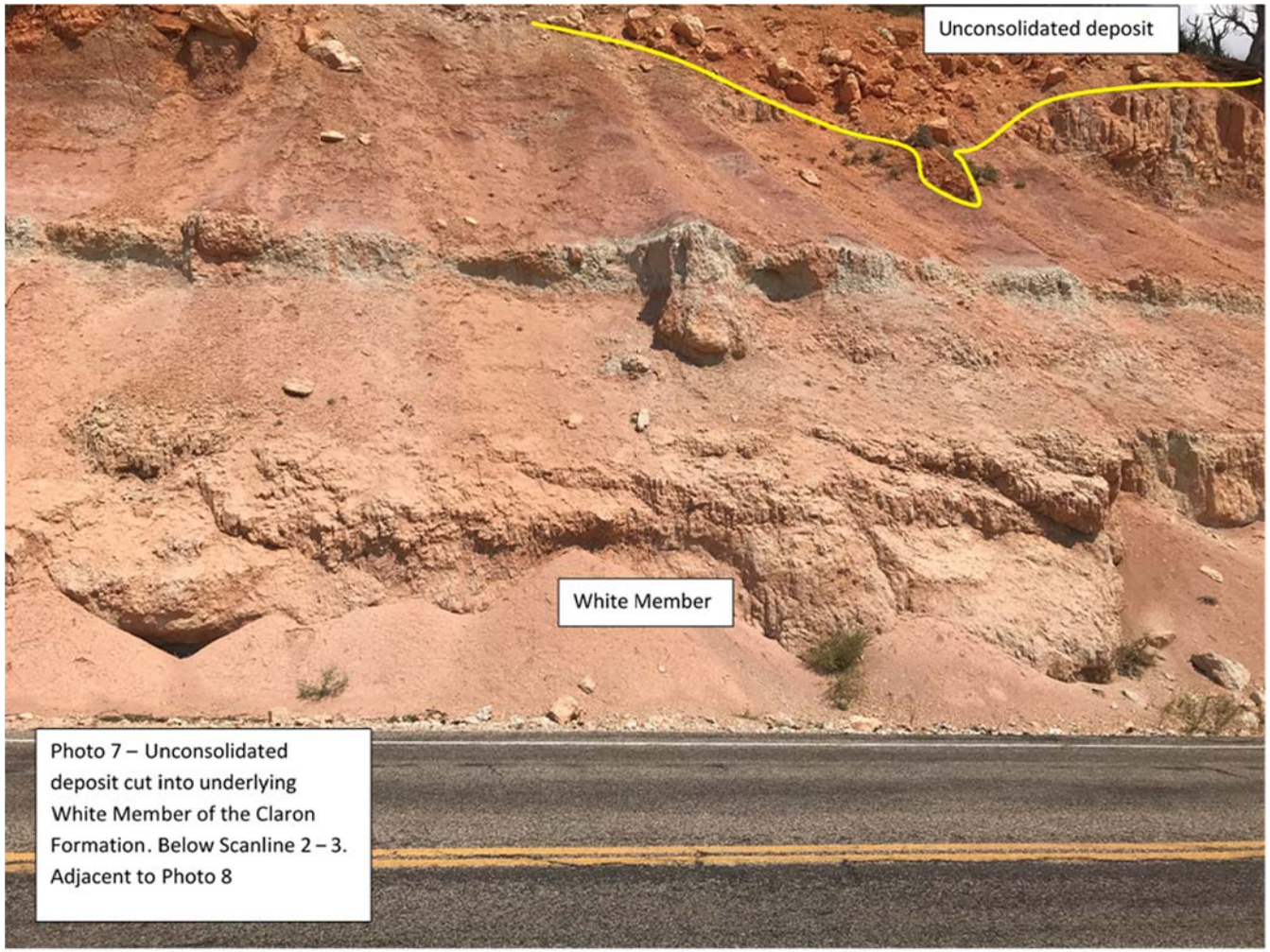

Figure A-9 – Photograph of unconsolidated deposit in roadway below Scanlines 2 and 3

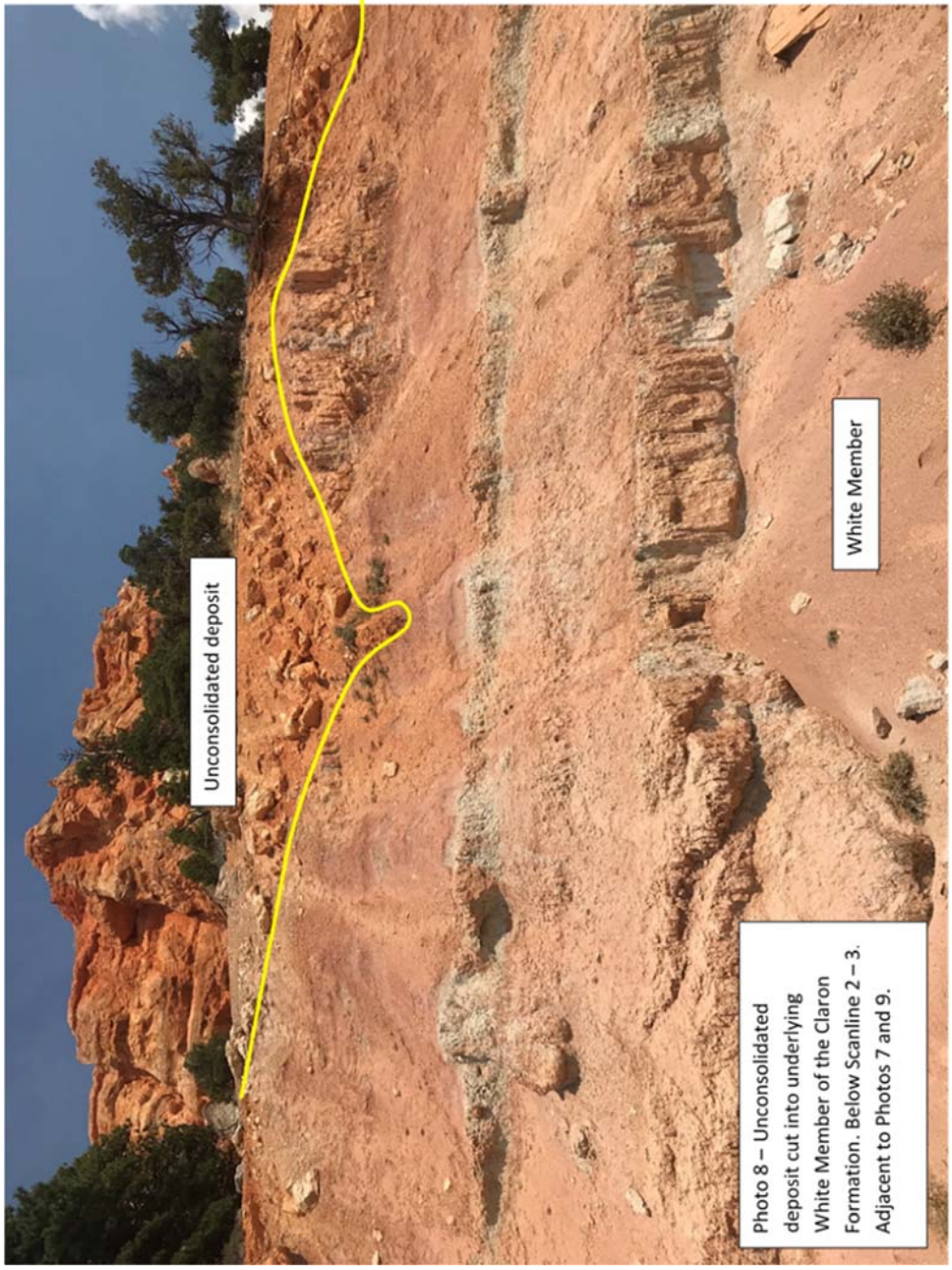

Figure A-10 – Photograph of unconsolidated deposit in roadway below Scanlines 2 and 3

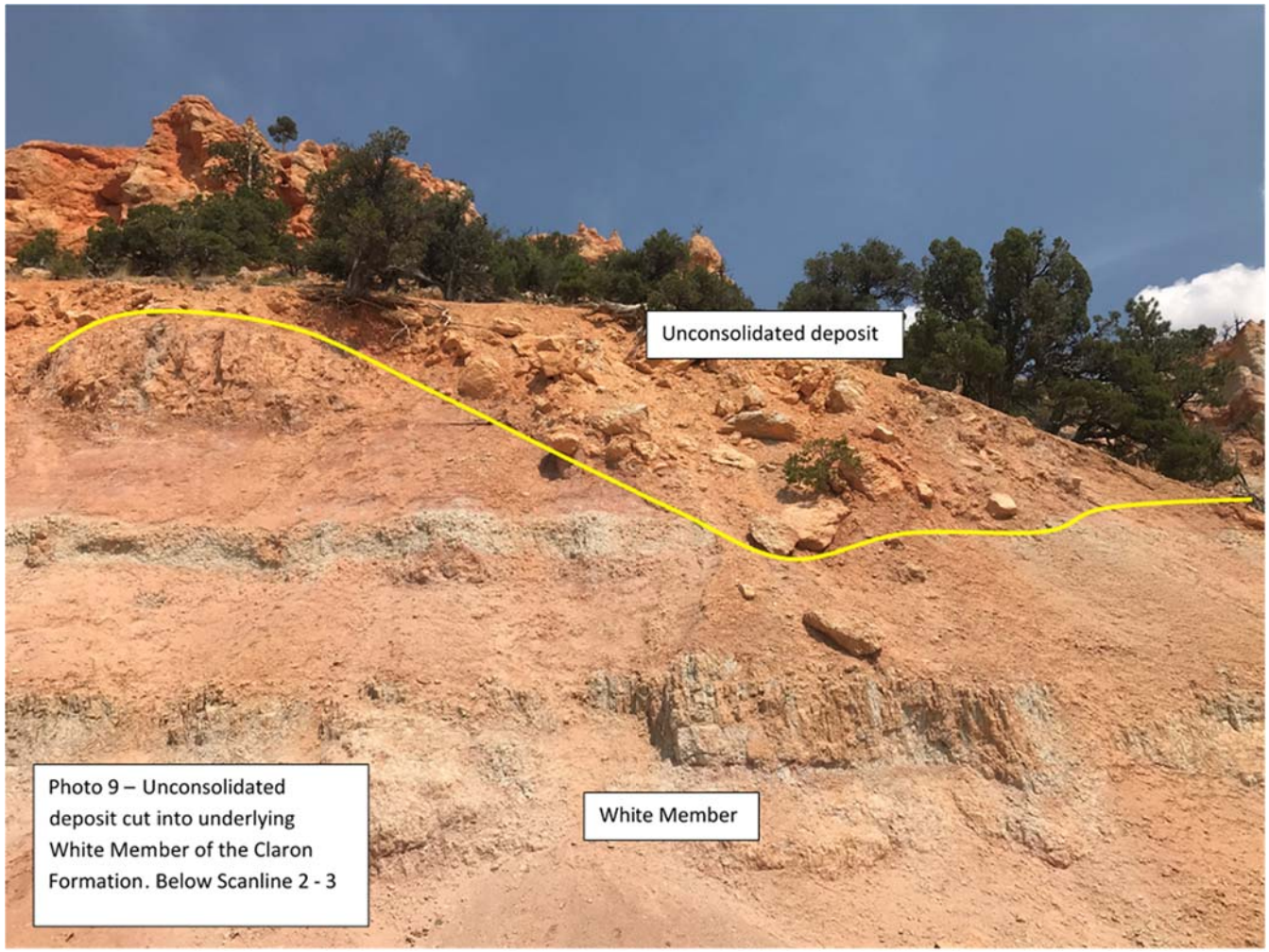

Figure A-11 – Photograph of unconsolidated deposit in roadway below Scanlines 2 and 3

Figure A-12 – Photograph of unconsolidated deposit in roadway below Scanlines 2 and 3

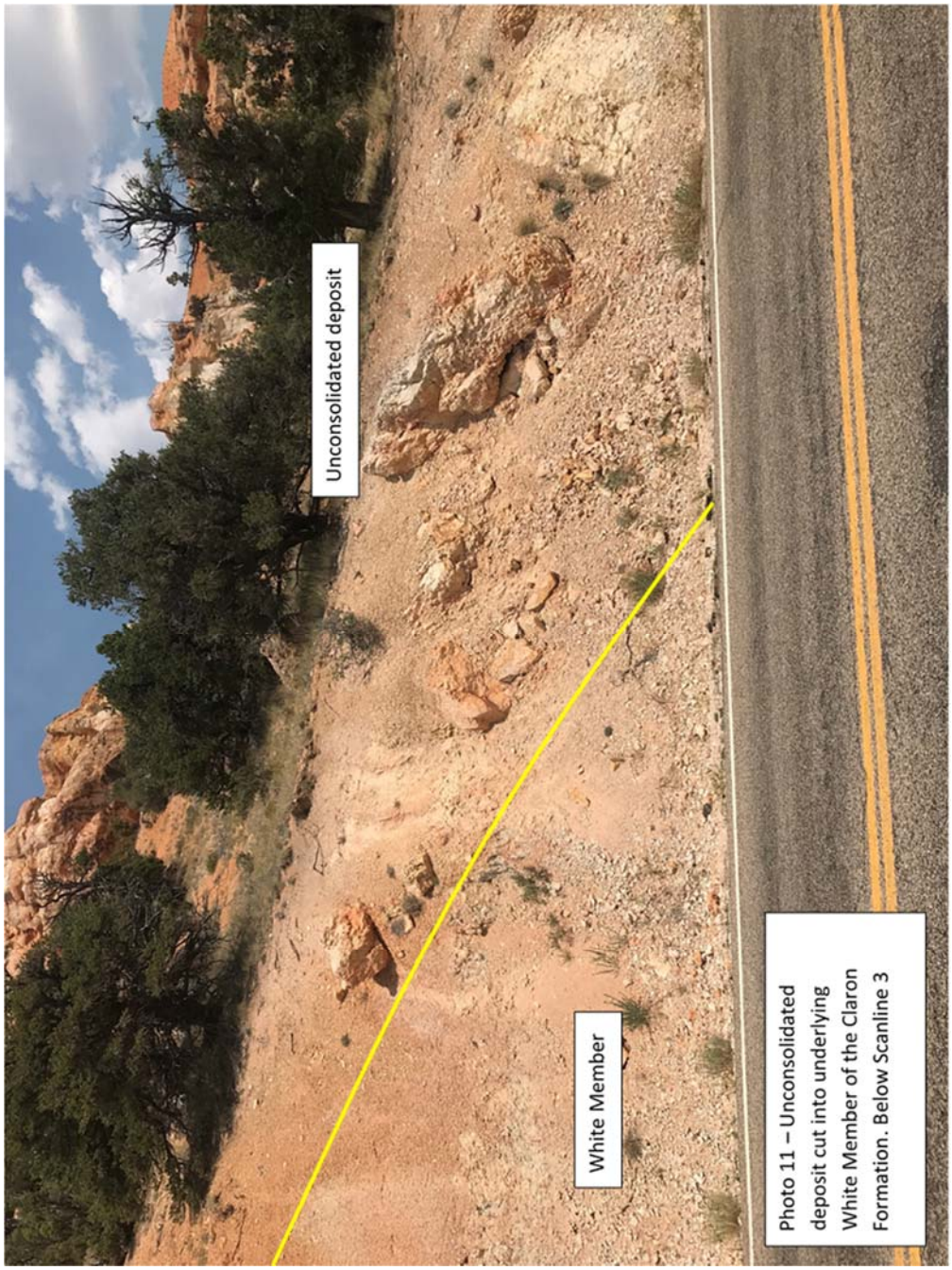

Figure A-13 – Photograph of unconsolidated deposit in roadway below Scanline 3

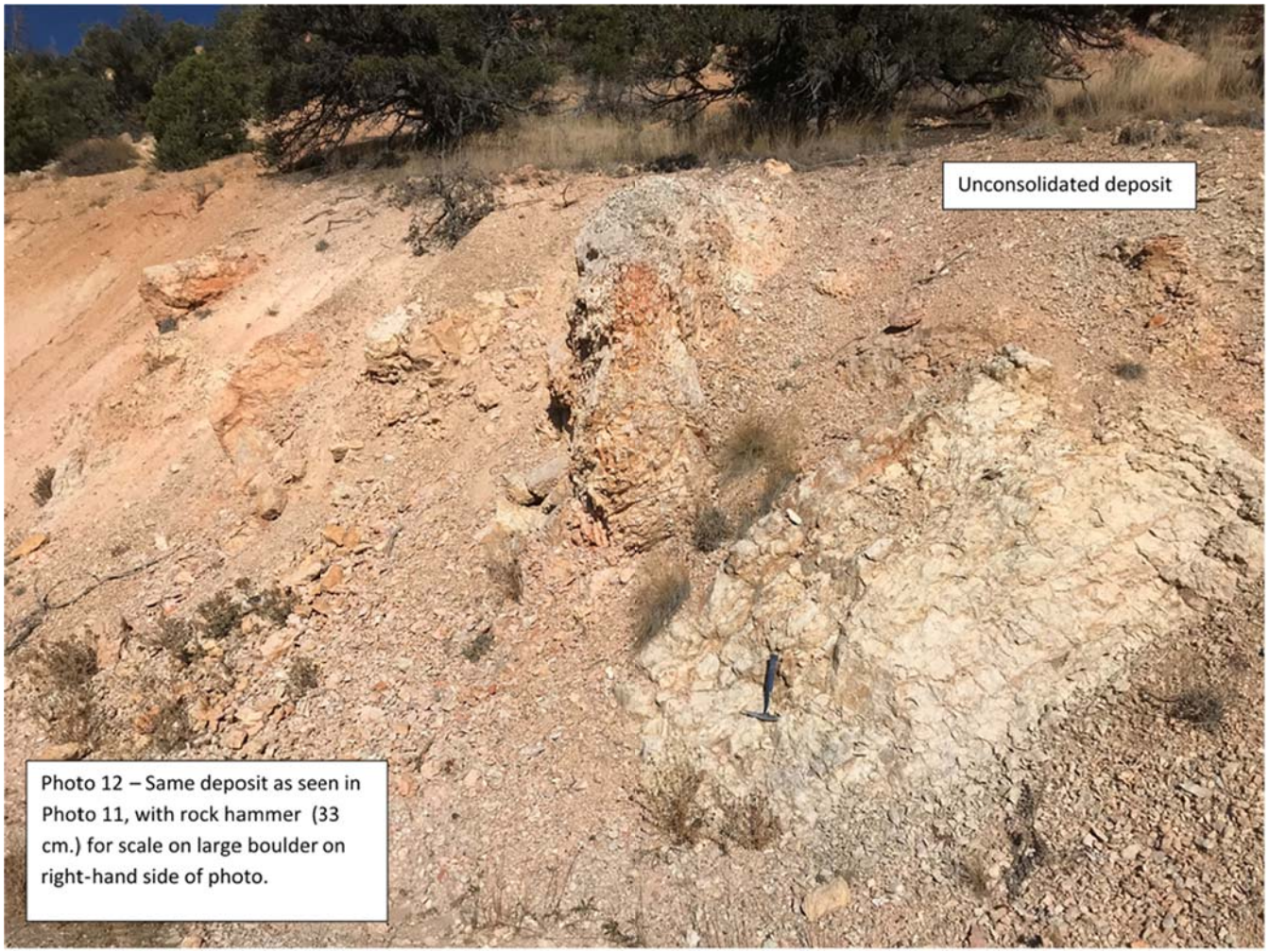

Figure A-14 – Photograph of unconsolidated deposit in roadway below Scanline 3

Figure A-15 – Photograph of unconsolidated deposit in roadway below Scanlines 3 and 4

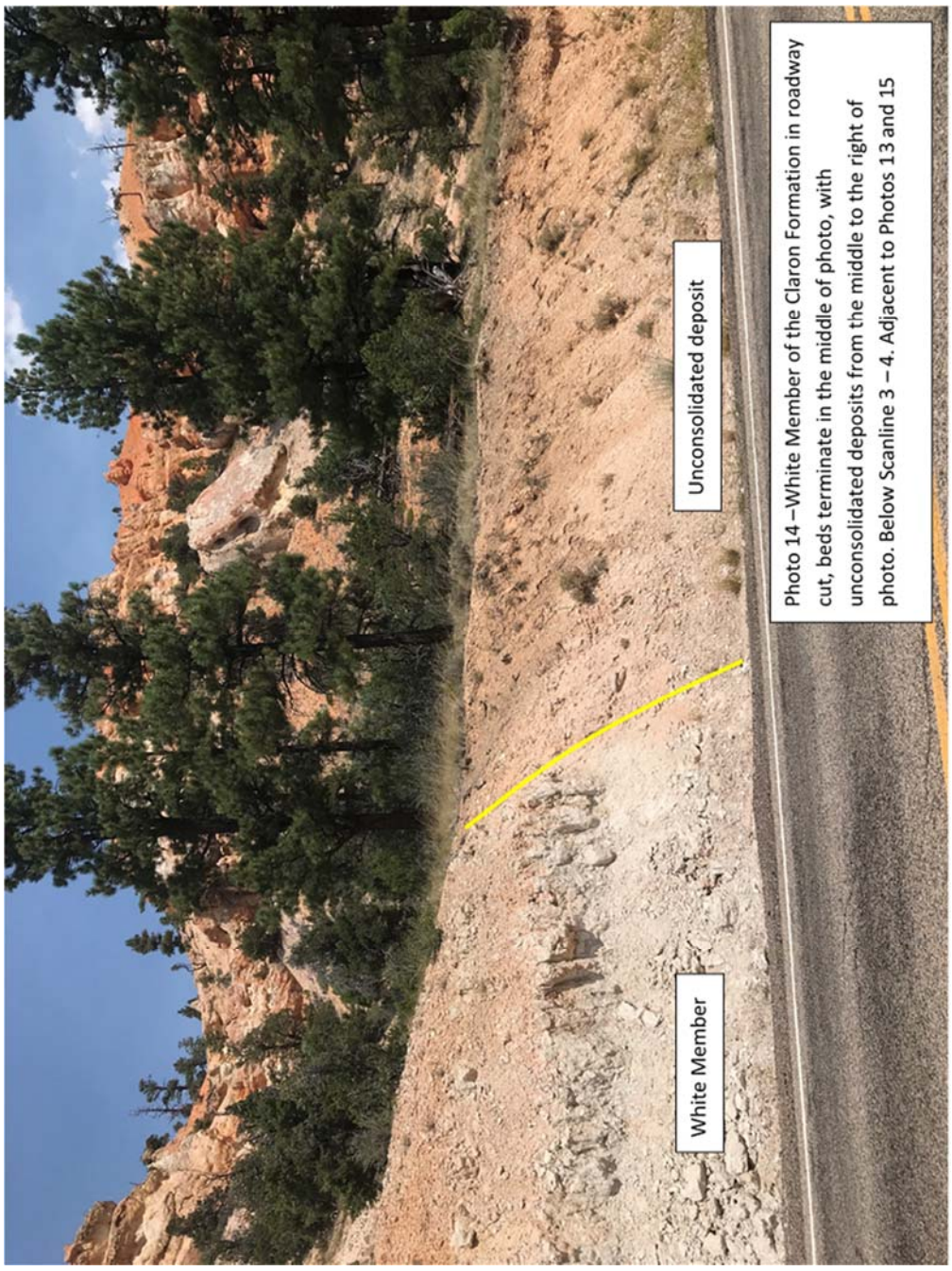

Figure A-16 – Photograph of unconsolidated deposit in roadway below Scanlines 3 and 4

Figure A-17 – Photograph of unconsolidated deposit in roadway below Scanlines 3 and 4

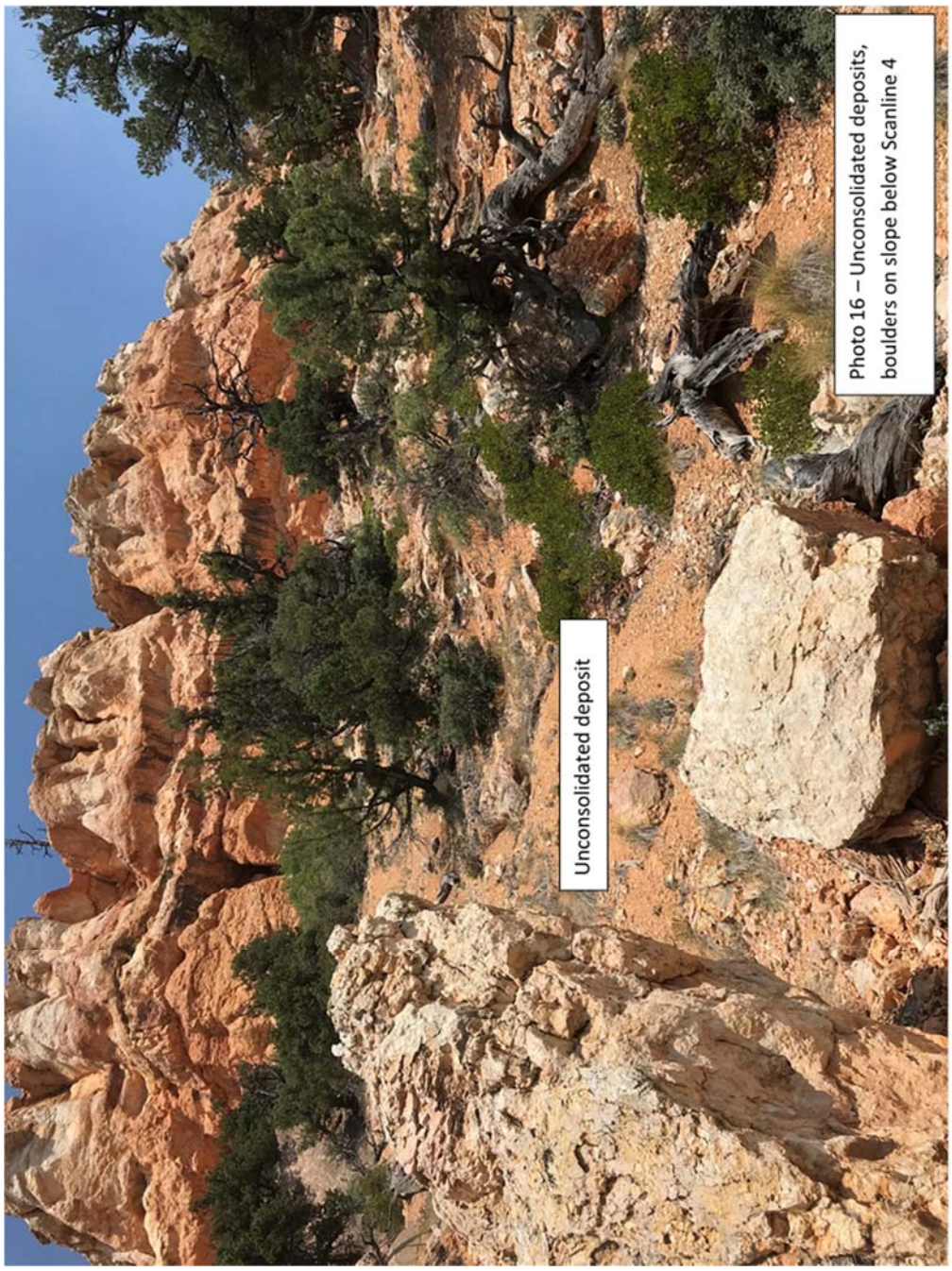

Figure A-18 – Photograph of unconsolidated deposit in roadway below Scanline 4

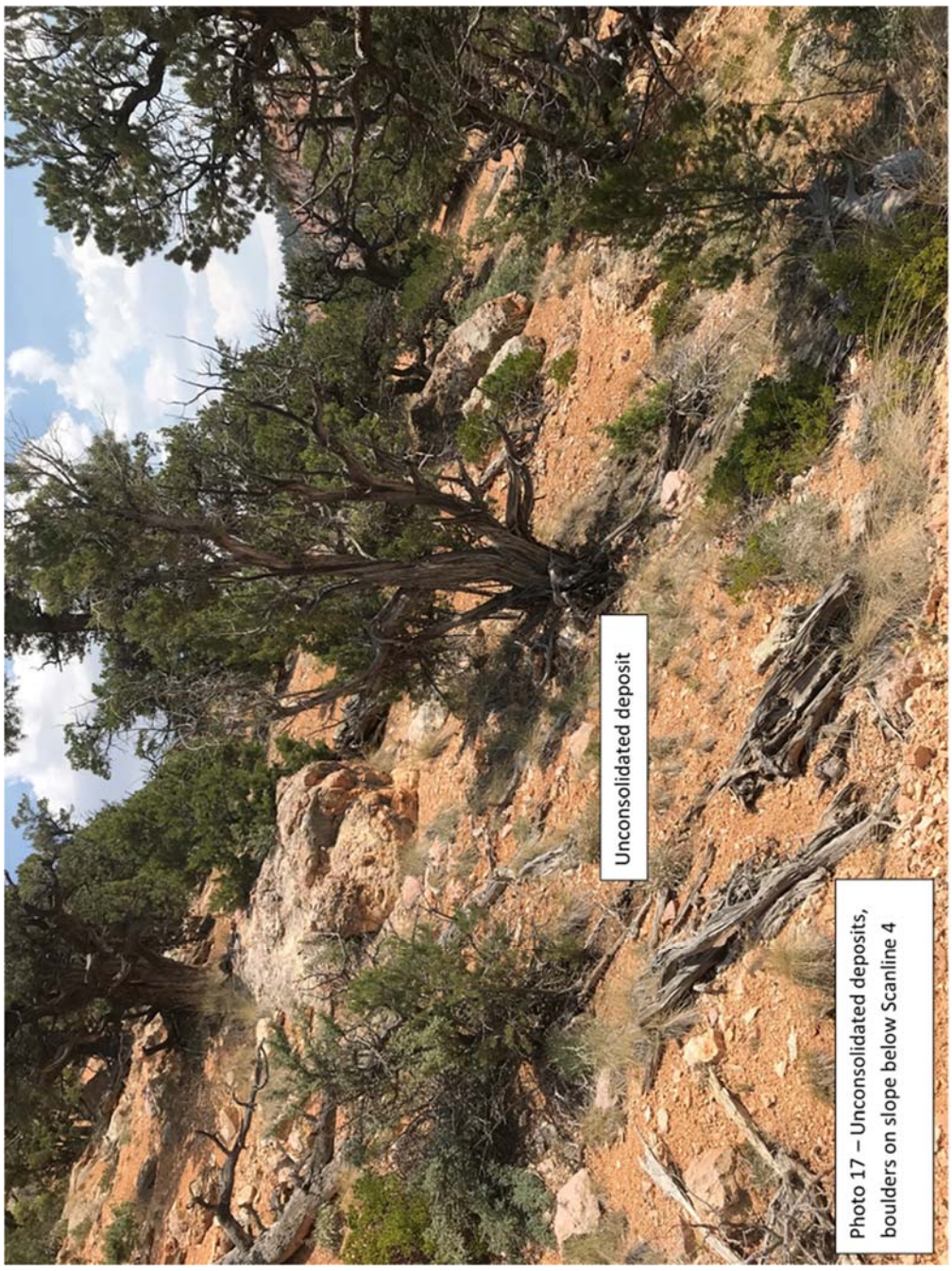

Figure A-19 – Photograph of unconsolidated deposit in roadway below Scanline 4

Figure A-20 – Photograph of unconsolidated deposit in roadway below Scanline 5

Additional outcrop units were described during field work, but were not included in the main text because they were not included in the scanlines. These units were found near scanlines, and are described below.

Scanline Control

Another unit, a marlstone (Figure A-21), was not numbered or sampled. The marlstone was varicolored from light gray to dark yellowish brown to light pinkish red, fissile, massive in terms of bedding, very fine grained, abundant bioturbation in the form of burrows, 65 cm. thick bed, gradational contacts between the marlstone and limestone.

Figure A-21 - Marlstone described near the control scanline. Rock hammer (33 cm. long) for scale, mostly weathered surface

Above a series of limestone/marlstone beds, a conglomerate sits unconformably over limestone bed, with erosional scours cut into the underlying limestone. The

conglomerate is clast supported, mostly pebble with occasional cobbles up to 9 cm., mostly composed of quartzite, limestone, and occasional volcanic and metamorphic clasts. The matrix is a calcareous sandy cement, light orange to light gray, very fine to medium grained, hard (Figure A-22). The unit transitions laterally to the west into a calcareous sandstone. Above the conglomerate there appeared to be a series of interfingering mudstone and sandstone to the top of the outcrop, that could not be described directly due to access. These units were not sampled or numbered.

Figure A-22 – Conglomerate described near the control scanline. Pencil (15 cm. long) for scale

Scanline 1

The unit that was not sampled was visible just below the start of the scanline, but not intersected by the scanline. This unit contained a matrix of yellowish brown sand, with

abundant white, chalky staining. Sand is fine to medium-grained, no sedimentary structure visible. The unit looks significantly altered, and possibly contains clasts of what is interpreted to be the overlying Pink Member (Figure A-23). This unit was not sampled or numbered.

Figure A-23 - Altered unit near Scanline 1, pencil (15 cm. long) for scale. Pencil pointing to a possible fault zone, with what appear to be clasts of Pink Member of the Claron Formation mixed in with the yellowish brown sandy matrix.

Scanline 2

Although the scanline did not cross the footwall material at Scanline 2, the footwall material near Scanline 2 is described here: calcareous mudstone, fissile, breaks up into shaly talus and scree below the cliff, soft to moderately hard, very fine-grained, light pink to light orange, mostly eroded out at Scanline 2, leaving a large overhang (approximately 10 meters measured horizontally) from the hanging wall unit. Interpreted to be part of the

Claron Formation (could be part of the White Member or the Pink Member).

FROM GERHART COLE REPORT, GERHART COLE (2019)

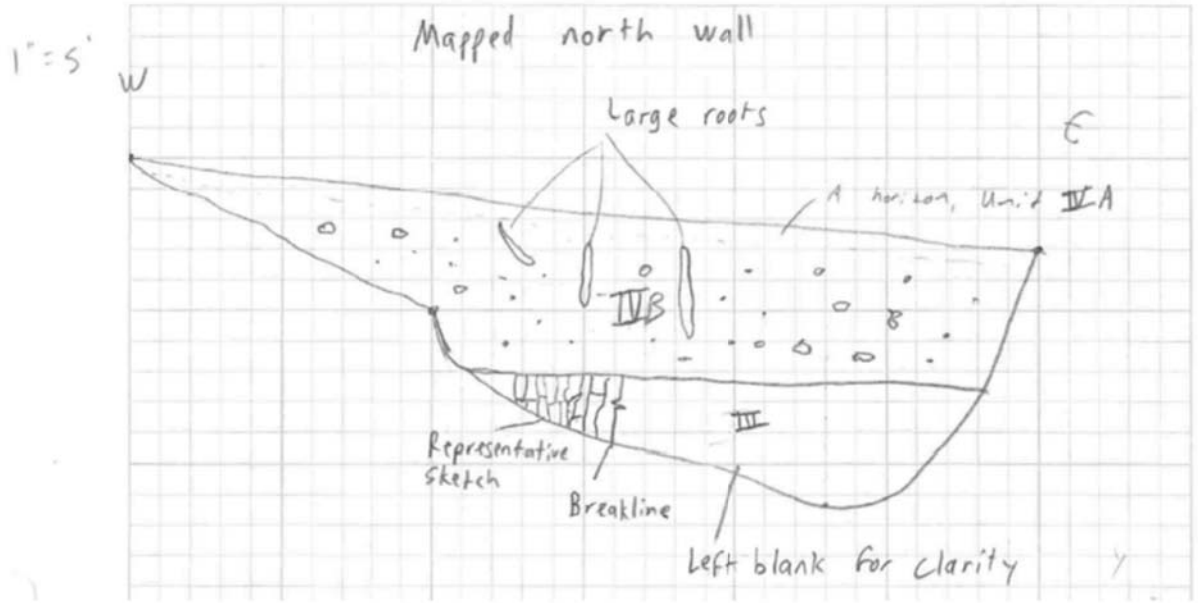

19-TP-11 Unit Descriptions

IVa – Darker soil development on unit Ib, A horizon [TOPSOIL]

IVb – GRAVEL, sandy, some silt. Orange to light tan, angular to subangular, fine to coarse limestone gravels, fine to coarse sand, occasional large (up to 2-in. diameter) roots in upper 3-ft. of layer. [COLLUVIUM]

IIIa – LIMESTONE, very fine grained, orange to light tan, thickly bedded, fresh to slightly weathered, moderately hard. Unable to safely gather discontinuity data inside the test pit, but an analogous outcrop was exposed in the road cut below the test pit, which indicated that the limestone was moderately to intensely fractured, with moderately spaced, discontinuous to slightly continuous horizontal fractures and closely spaced, discontinuous vertical fractures, generally slightly open to open, with very thin to thin fracture filling, not healed, moderately rough undulating, and the fractures were dry and either showed no evidence of previous water flow or showed some iron oxide staining. [CLARON FORMATION, WHITE MEMBER]

Figure A-24 - Test pit log of 19-TP-11 from Gerhart Cole, (2019)

Figure A-24 - Photograph of 19-TP-11 from Gerhart Cole, (2019)

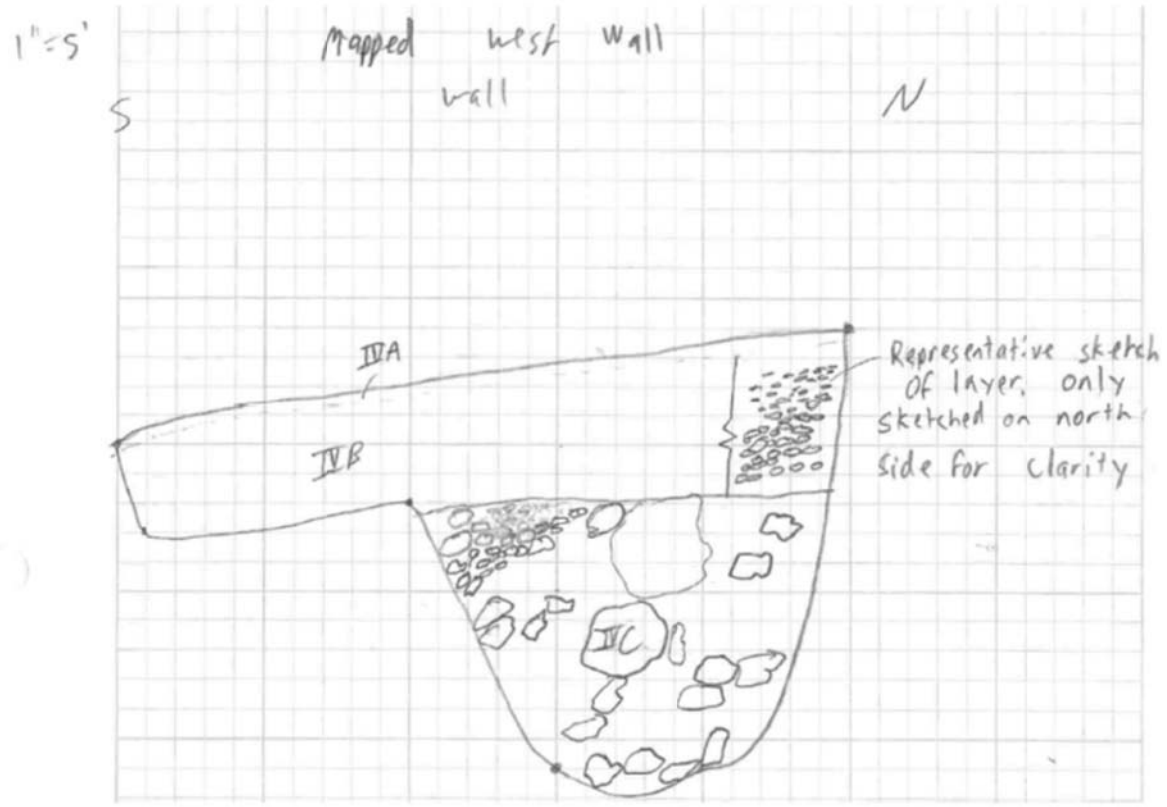

19-TP-12 Unit Descriptions

IVa – Darker soil development on unit Ib, A horizon [TOPSOIL]

IVb – GRAVEL, sandy, some silt. Orange to red, angular to subangular, fine to medium limestone gravels, fine to coarse sand, slight carbonate cementation, occasional fine (up to 1-in. diameter) roots in upper 3-ft. of layer. [COLLUVIUM]

IVc – COBBLES AND BOULDERS, with gravel and sand, some silt. Orange to red, angular to subangular, fine to coarse limestone gravels, cobbles, and boulders, fine to coarse sand, [COLLUVIUM WITH LENSES OF TALUS]

Figure A-26 – Test pit log of 19-TP-12 from Gerhart Cole, (2019)

Figure A-27 - Photograph of 19-TP-12 from Gerhart Cole, (2019)

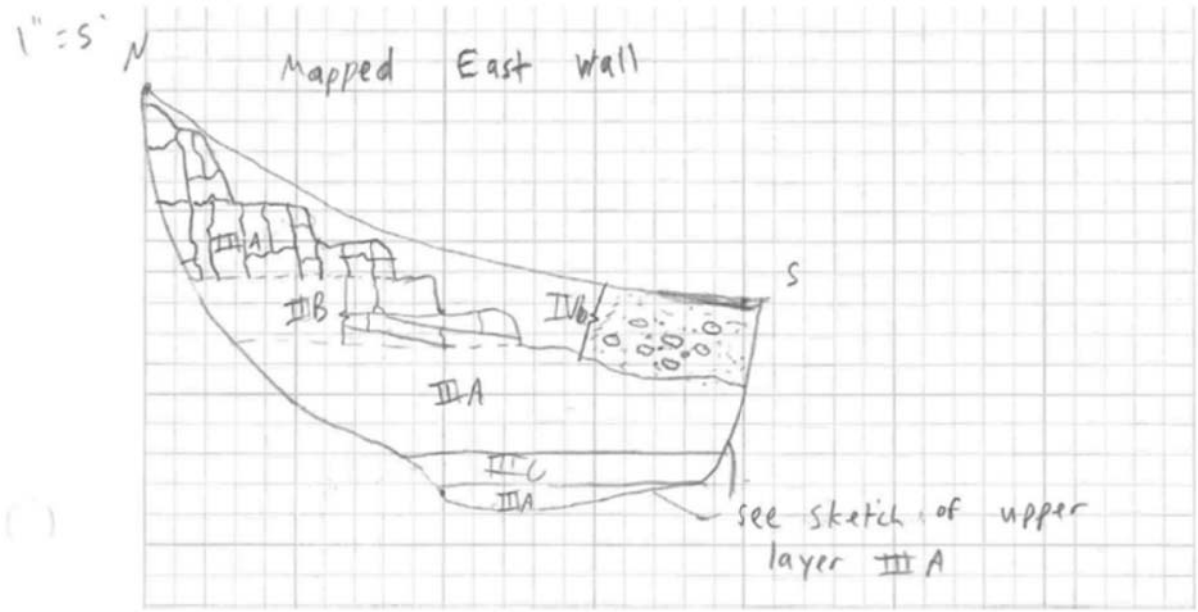

19-TP-13 Unit Descriptions

IVb – GRAVEL, sandy, with clay. Orange to light tan, moist to dry, angular to subangular, fine to medium limestone gravels, fine to coarse sand. [COLLUVIUM]

IIIa – LIMESTONE, very fine grained, light tan to pale olive brown with occasional pink to red staining, thickly to very thickly bedded, fresh to slightly weathered, moderately hard, moderately to intensely fractured, generally closely spaced, discontinuous fractures, slightly open to open fractures with very thin to thin sand and clay fracture filling, not healed, moderately rough undulating, with no evidence of previous water flow, although flow appears possible. [CLARON FORMATION, WHITE MEMBER]

IIIb – LIMESTONE, same as unit IIIa but slightly to moderately fractured. [CLARON FORMATION, WHITE MEMBER]

IIIc – MUDSTONE, olive brown to tan, moist, soft, very fine grained, very thinly bedded to laminated, soft, slightly weathered, difficult to accurately asses fractures due to disturbance in the layer from trackhoe excavation, but appears to be intensely fractured with very closely spaced, discontinuous, tight to slightly open fractures with very thin fracture filling, not healed, smooth planar fractures, with no evidence of previous water flow but flow appears to be possible. [CLARON FORMATION, WHITE MEMBER]

Figure A-28 – Test pit log of 19-TP-13 from Gerhart Cole, (2019)

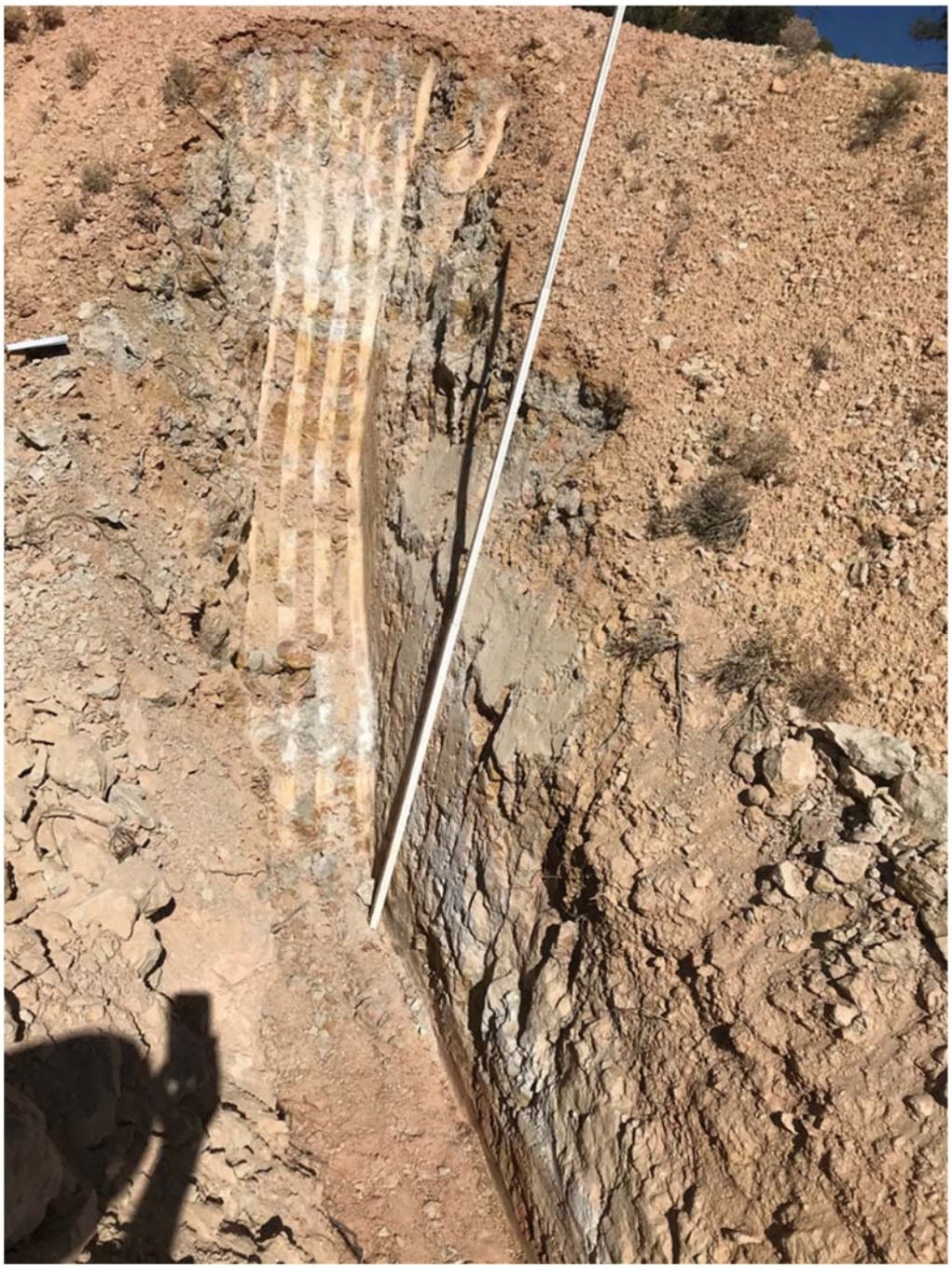

Figure A-29 - Photograph of 19-TP-13 from Gerhart Cole, (2019)

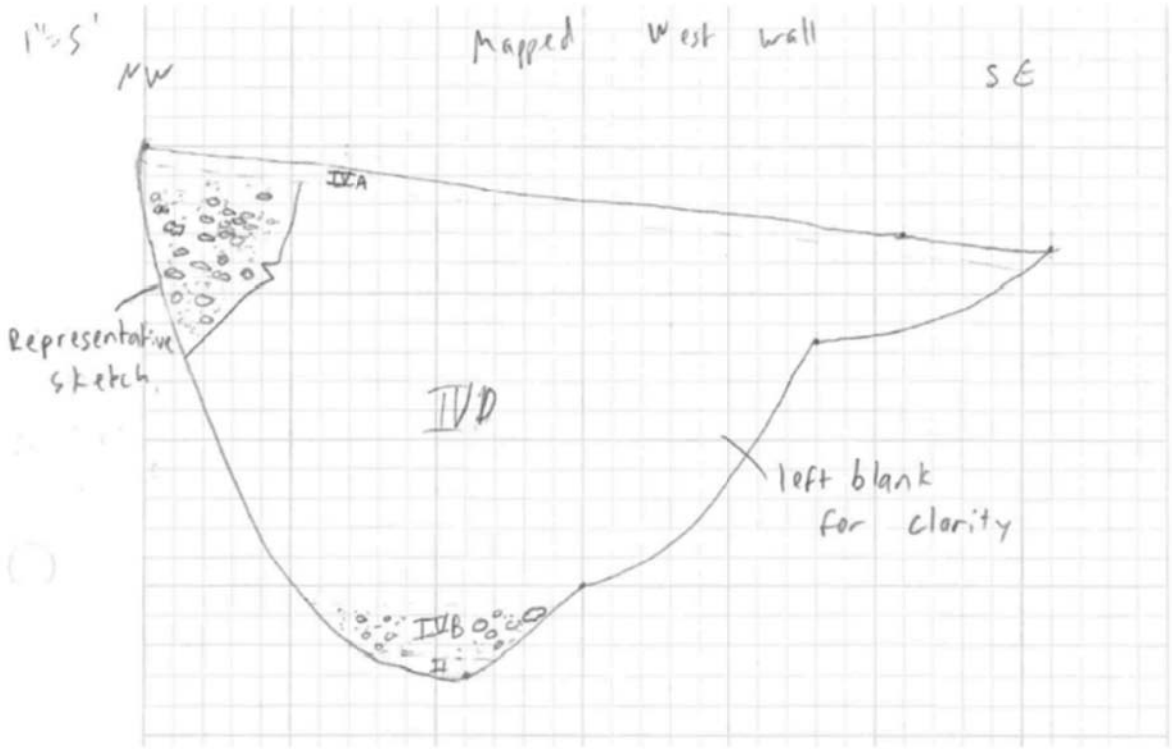

19-TP-14 Unit Descriptions

IVa – Darker soil development on unit IVb, A horizon [TOPSOIL]

IVd – GRAVEL, sandy, silty. Dark yellowish brown, angular to subangular, fine to medium limestone gravels, fine to coarse sand. [COLLUVIUM]

IVb – GRAVEL, sandy, some clay. Orange to light tan, angular to subangular, fine to medium limestone gravels, fine to coarse sand. [COLLUVIUM]

IIIa – LIMESTONE, very fine grained, orange to light tan, thickly bedded, fresh to slightly weathered, moderately hard. Unit mostly obscured in bottom of test pit, so no observations on fractures or fillings could be made. [CLARON FORMATION, WHITE]

Figure A-30 – Test pit log of 19-TP-14 from Gerhart Cole, (2019)

Figure A-31 - Photograph of 19-TP-14 from Gerhart Cole, (2019)

Project: SR-12 Roadway Widening
Project Location: Tropic, Utah
Project Number: 17-905

LOG OF TEST HOLE 19-TH-06

Sheet 1 of 1

Date(s) Drilled	09/18/2019 to 09/18/2019	Logged By	A. Lawrence	Checked By	B. Peterson
Drilling Method	HSA	Drill Bit Size/Type	4.25" Tricone Bit	Total Depth Drilled (feet)	32.0
Drill Rig Type	CME 75	Drilling Contractor	ConeTec (Dave)	Hammer Weight/ Drop (lbs/in.)	Automatic [Energy Ratio 97.5%]
Apparent Groundwater Depth (feet)	Not found	Latitude / Longitude	37.682556 , -112.129147	Ground Surface Elevation (feet)	7449.4
Station/Offset	522+07 / 14 LT	Test Hole Backfill	Cement Slurry / Cold Patch	Weather, H/L	Clear 75/53

Elevation, feet / Depth, feet	Type	Recovery, inches	Sampling Resistance (Uncorrected) N	(N1)60	Sample Name; Testing	AASHTO Classification	Graphic Log	Material Description	Moisture Content (%)	Fines Content (%)	Field Notes
								ASPHALT - 9 inches			
7445 / 5		8	8-22-44-41 66	160	SPT-01 SV			SAND, clayey, some gravel - very dense, moist, dark yellowish brown to light brown, (SC), [FILL]	6.2	37	
7440 / 10		14	6-5-4-3 9	20	SPT-02 SV			- transitions to with gravel, medium dense	7.3	23	
7435 / 15		18	6-9-8-8 17	39	SPT-03 SV			- transitions to some gravel, dense	7.8	24	
7430 / 20		18	2-2-2-1 4	8	SPT-04 SV	A-4		CLAY, silty, sandy, trace gravel - medium stiff, moist, dark yellowish brown to light brown, (CL-ML)	14.5	56	AL (LL=20, PI=6)
		12	0-1-1-1 2	4	SPT-05 SV	A-6		CLAY, sandy, with gravel - soft, moist, dark yellowish brown to light brown, (CL)	12.8	51	AL (LL=24, PI=13)
7425 / 25		18	2-3-4-5 7	14	SPT-06			- transitions to stiff			AL (LL=28, PI=16)
7420 / 30		2	38-5-2-2 7	14	SPT-07						
								Bottom of Hole at 32 feet			
7415 / 35											
7410 / 40											
7405 / 45											
7400 / 50											

Figure A-32 - Test hole log of 19-TH-06 from Gerhart Cole, (2019).

Project: SR-12 Roadway Widening
Project Location: Tropic, Utah
Project Number: 17-905

LOG OF TEST HOLE 19-TH-07

Sheet 1 of 1

Date(s) Drilled	09/17/2019 to 09/18/2019	Logged By	A. Lawrence
Drilling Method	HSA	Drill Bit Size/Type	4.25" Tricone Bit
Drill Rig Type	CME 75	Drilling Contractor	ConeTec (Dave)
Apparent Groundwater Depth (feet)	Not found	Latitude / Longitude	37.682458 , -112.127754
Station/Offset	526+20 / 4 LT	Test Hole Backfill	Cement Slurry / Cold Patch

Checked By	B. Peterson		
Total Depth Drilled (feet)	20.2		
Hammer Weight/ Drop (lbs/in.)	Automatic [Energy Ratio 97.5%]		
Ground Surface Elevation (feet)	7419.3		
Weather, H/L	Clear 75/53		

Elevation, feet / Depth, feet	FIELD DATA: Type	Recovery, inches	Sampling Resistance (Uncorrected) N	(N1)60	Sample Name; Testing	AASHTO Classification	Graphic Log	Material Description	Moisture Content (%)	Fines Content (%)	Field Notes
7415 / 5								ASPHALT - 8 inches SAND, clayey, some gravel - dense to very dense, moist, tan to dark yellowish brown, (SC), [FILL]			
								CLAY, some sand - hard, moist, tan to dark yellowish brown, oxidation stains, (CL)			
	X	12	7-12-14-10 26	63	SPT-01				11.9		AL (LL=28, PI=16)
7410 / 10	X	8	14-32-50/4" [R]	R	SPT-02 SV	A-6			10.4	92	AL (LL=34, PI=21)
7405 / 15	X	3	50/4" [R]	R	SPT-03			MUDSTONE - Claron Formation - interbedded mudstone and siltstone with oxidation stains throughout siltstone fragments, reacts strongly to HCL			
7400 / 20	X	2	50/2" [R]	R	SPT-04			Bottom of Hole at 20.2 feet			
7395 / 25											
7390 / 30											
7385 / 35											
7380 / 40											
7375 / 45											
7370 / 50											

Figure A-33 – Test hole log of 19-TH-07 from Gerhart Cole, (2019).

Project: SR-12 Roadway Widening
Project Location: Tropic, Utah
Project Number: 17-905

LOG OF TEST HOLE 19-TH-08

Sheet 1 of 1

Date(s) Drilled	09/18/2019 to 09/18/2019	Logged By	A. Lawrence
Drilling Method	HSA	Drill Bit Size/Type	4.25" Tricone Bit
Drill Rig Type	CME 75	Drilling Contractor	ConeTec (Dave)
Apparent Groundwater Depth (feet)	Not found	Latitude / Longitude	37.682810 , -112.126421
Station/Offset	530+28 / 14 LT	Test Hole Backfill	Cement Slurry / Cold Patch

Checked By	B. Peterson		
Total Depth Drilled (feet)	29.2		
Hammer Weight/ Drop (lbs/in.)	Automatic [Energy Ratio 97.5%]		
Ground Surface Elevation (feet)	7388.7		
Weather, H/L	Clear 75/53		

Elevation, feet / Depth, feet	FIELD DATA: Type	Recovery, inches	Sampling Resistance (Uncorrected) N	(N1)60	Sample Name; Testing	AASHTO Classification	Graphic Log	Material Description	Moisture Content (%)	Fines Content (%)	Field Notes
								ASPHALT - 9 inches			
7384 / 5		10	4-4-4-4 8	19	SPT-01 SV	A-6		SAND, clayey, with gravel - medium dense, moist, dark yellowish brown to orange, (SC), [FILL]	10.6	43	AL (LL=29, PI=17)
7379 / 10		3	6-8-8-7 16	36	SPT-02			- transitions to dense	8.0		
7374 / 15		13	6-4-3-3 7	16	SPT-03 SV			SAND, with clay and gravel- medium dense, moist to wet, pale olive brown to dark yellowish brown, (SC)	10.6	22	
7369 / 20		13	1-3-7-10 10	21	SPT-04 SV			SAND, clayey, with gravel - medium dense, moist, light brown to dark yellowish brown, (SC)	17.0	43	
								GRAVEL, sandy, clayey - medium dense, moist, yellowish brown to orange, (GC)	11.0	35	
7364 / 25		4	50/3" [R]	R	SPT-05			MUDSTONE - Claron Formation - interbedded mudstone and siltstone with oxidation stains throughout siltstone fragments, reacts strongly to HCL			
7359 / 30		3	50/2" [R]	R	SPT-06			Bottom of Hole at 29.2 feet			
7354 / 35											
7349 / 40											
7344 / 45											
/ 50											

Figure A-34 - Test hole log of 19-TH-08 from Gerhart Cole, (2019)

Project: SR-12 Roadway Widening
Project Location: Tropic, Utah
Project Number: 17-905

LOG OF TEST HOLE 19-TH-10

Sheet 1 of 2

Date(s) Drilled: 09/14/2019 to 09/15/2019	Logged By: A. Lawrence	Checked By: B. Peterson	
Drilling Method: HSA / HQ Coring	Drill Bit Size/Type: 4.25" Tricone Bit / HQ Core	Total Depth Drilled (feet): 60.3	
Drill Rig Type: CME 75	Drilling Contractor: ConeTec (Dave)	Hammer Weight/ Drop (lbs/in.): Automatic [Energy Ratio 97.5%]	
Apparent Groundwater Depth (feet): Not found	Latitude / Longitude: 37.682900 , -112.124835	Ground Surface Elevation (feet): 7357.8	
Station/Offset: 534+85 / 13 RT	Test Hole Backfill: Cement Slurry / Cold Patch	Weather, H/L: Partly Cloudy 87/43	

Elevation, feet / Depth, feet	Type	Recovery, inches	Sampling Resistance (Uncorrected) N	(N1)60	Sample Name; Testing	AASHTO Classification	Graphic Log	Material Description	Moisture Content (%)	Fines Content (%)	Field Notes
								ASPHALT - 5 inches			
								GRAVEL, sandy, with clay - dense, moist, light tan to pink, (GC) [FILL]			
7353 / 5		7	16-18-6-7 24	61	SPT-01 SV				3.9	14	
		11	4-18-11-12 29	70	SPT-02 SV			- transitions to with sand	4.7	20	
		14	6-10-18-39 28	63	SPT-03 SV	A-6		CLAY, with sand - hard, moist, light tan to pink, (CL)	10.2	81	AL (LL=25, PI=13)
7348 / 10		6	42-50/1" [R]	R	SPT-04 SV	A-6		- transitions to trace gravel	7.2	72	AL (LL=23, PI=12)
7343 / 15		1	50/3" [R]	R	SPT-05			MUDSTONE - Claron Formation - interbedded mudstone and siltstone with oxidation stains throughout siltstone fragments, reacts strongly to HCL			
7338 / 20		2	50/3" [R]	R	SPT-06						
		26			RC-01						
7333 / 25		34			RC-02						AL (LL=31, PI=13) AL (LL=37, PI=22)
7328 / 30		60			RC-03						
		12			RC-04						
7323 / 35		49			RC-05						
7318 / 40		60			RC-06						
7313 / 45		62			RC-07						
50											

Figure A-35 - Test hole log of 19-TH-10 from Gerhart Cole, (2019)

Project: SR-12 Roadway Widening
Project Location: Tropic, Utah
Project Number: 17-905

LOG OF TEST HOLE 19-TH-10

Sheet 2 of 2

Date(s) Drilled	09/14/2019 to 09/15/2019	Logged By	A. Lawrence	Checked By	B. Peterson
Drilling Method	HSA / HQ Coring	Drill Bit Size/Type	4.25" Tricone Bit / HQ Core	Total Depth Drilled (feet)	60.3
Drill Rig Type	CME 75	Drilling Contractor	ConeTec (Dave)	Hammer Weight/ Drop (lbs/in.)	Automatic [Energy Ratio 97.5%]
Apparent Groundwater Depth (feet)	Not found	Latitude / Longitude	37.682900 , -112.124835	Ground Surface Elevation (feet)	7357.8
Station/Offset	534+85 / 13 RT	Test Hole Backfill	Cement Slurry / Cold Patch	Weather, H/L	Partly Cloudy 87/43

Elevation, feet / Depth, feet	FIELD DATA: Type	Recovery, inches	Sampling Resistance (Uncorrected) N	(N1)60	Sample Name; Testing	AASHTO Classification	Graphic Log	Material Description	Moisture Content (%)	Fines Content (%)	Field Notes
7303 / 55		64			RC-08			MUDSTONE - Claron Formation - Interbedded mudstone and siltstone with oxidation stains throughout siltstone fragments, reacts strongly to HCL			AL (LL=39, PI=24)
7298 / 60		62			RC-09			Bottom of Hole at 60.3 feet			
7293 / 65											
7288 / 70											
7283 / 75											
7278 / 80											
7273 / 85											
7268 / 90											
7263 / 95											
100											

Figure A-36 - Test hole log of 19-TH-10 (cont'd.) from Gerhart Cole, (2019)

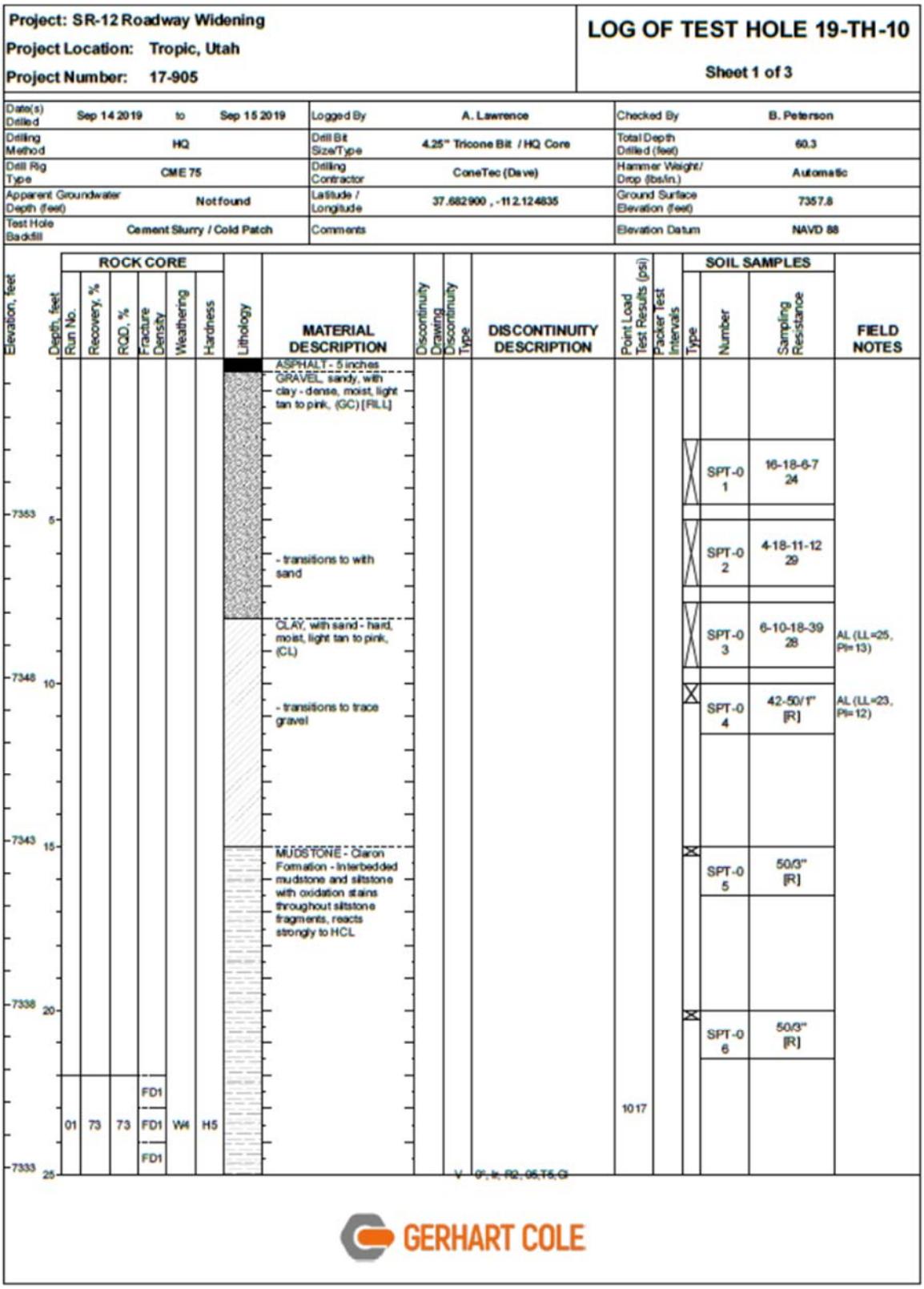

Figure A-37 - Test hole log of 19-TH-10 (cont'd) from Gerhart Cole, (2019)

Project: SR-12 Roadway Widening
Project Location: Tropic, Utah
Project Number: 17-905

LOG OF TEST HOLE 19-TH-10

Sheet 2 of 3

Date(s) Drilled	Sep 14 2019 to Sep 15 2019	Logged By	A. Lawrence
Drilling Method	HQ	Drill Bit Size/Type	4.25" Tricone Bit / HQ Core
Drill Rig Type	CME 75	Drilling Contractor	ConeTec (Dave)
Apparent Groundwater Depth (feet)	Not found	Latitude / Longitude	37.682900 , -112.124835
Test Hole Backfill	Cement Slurry / Cold Patch	Comments	

Checked By	B. Peterson		
Total Depth Drilled (feet)	60.3		
Hammer Weight/ Drop (lbs/in.)	Automatic		
Ground Surface Elevation (feet)	7357.8		
Elevation Datum	NAVD 88		

Elevation, feet	Depth, feet	ROCK CORE: Run No.	Recovery, %	RQD, %	Fracture Density	Weathering	Hardness	Lithology	MATERIAL DESCRIPTION	Discontinuity Drawing	Discontinuity Type	DISCONTINUITY DESCRIPTION	Point Load Test Results (psi)	Packer Test Intervals	SOIL SAMPLES: Type	Number	Sampling Resistance	FIELD NOTES
					FD1		H6		MUDSTONE - Claron Formation - Interbedded mudstone and siltstone with oxidation stains throughout siltstone fragments, reacts strongly to HCL		Me							
					FD1	W5					Jo	0°, Ir, R2, 02,T0						
		02	80	63							Me		1575					
					FD1		H5				Me							
											Me							
													3121					
					FD4	W6	H7											AL (LL=31, PI=13)
7328	30										Me		351					
					FD4													AL (LL=37, PI=22)
		03	100	38	FD4		H5											
					FD4	W5							7910					
					FD4		H6											
		04	100	90	FD3	W4	H4				Me							
7323	35				FD1								3451					
					FD1	W3	H5											
											Jo	0°, Ir, R2, 02, T0						
		05	82	82	FD1								4732					
					FD1						Me							
					FD1	W1	H4				Me							
					FD1						Me							
7318	40										Me		4259					
					FD3													
					FD3						Jo	0°, Ir, R2, 04, T4, Cl, Fe (some clasts 0.5"-1")	1246					
											Jo	0°, Ir, R1, 03, T3, Cl, Fe (was leached away except center)						
		06	100	92	FD3	W2	H5				Jo	0°, Ir, R1, 00, T0	4796					
					FD3							0° to 40°, Ir, R2, 03,T3, Cl, Fe						
					FD3													
											Me							
7313	45										Me							
					FD4						Me							
					FD4	W6	H5				Be	35°, Pl, R2, 00, T0 (intact in original core)						
					FD4	W7					Jo		1933					
						W6												
		07	99	83	FD4						Me							
					FD4								6250					
						W5	H4				Me							
					FD4						Me							
											Me							
											Me							
7308	50										Me							

GERHART COLE

Figure A-38 - Test hole log of 19-TH-10 (cont'd) from Gerhart Cole, (2019)

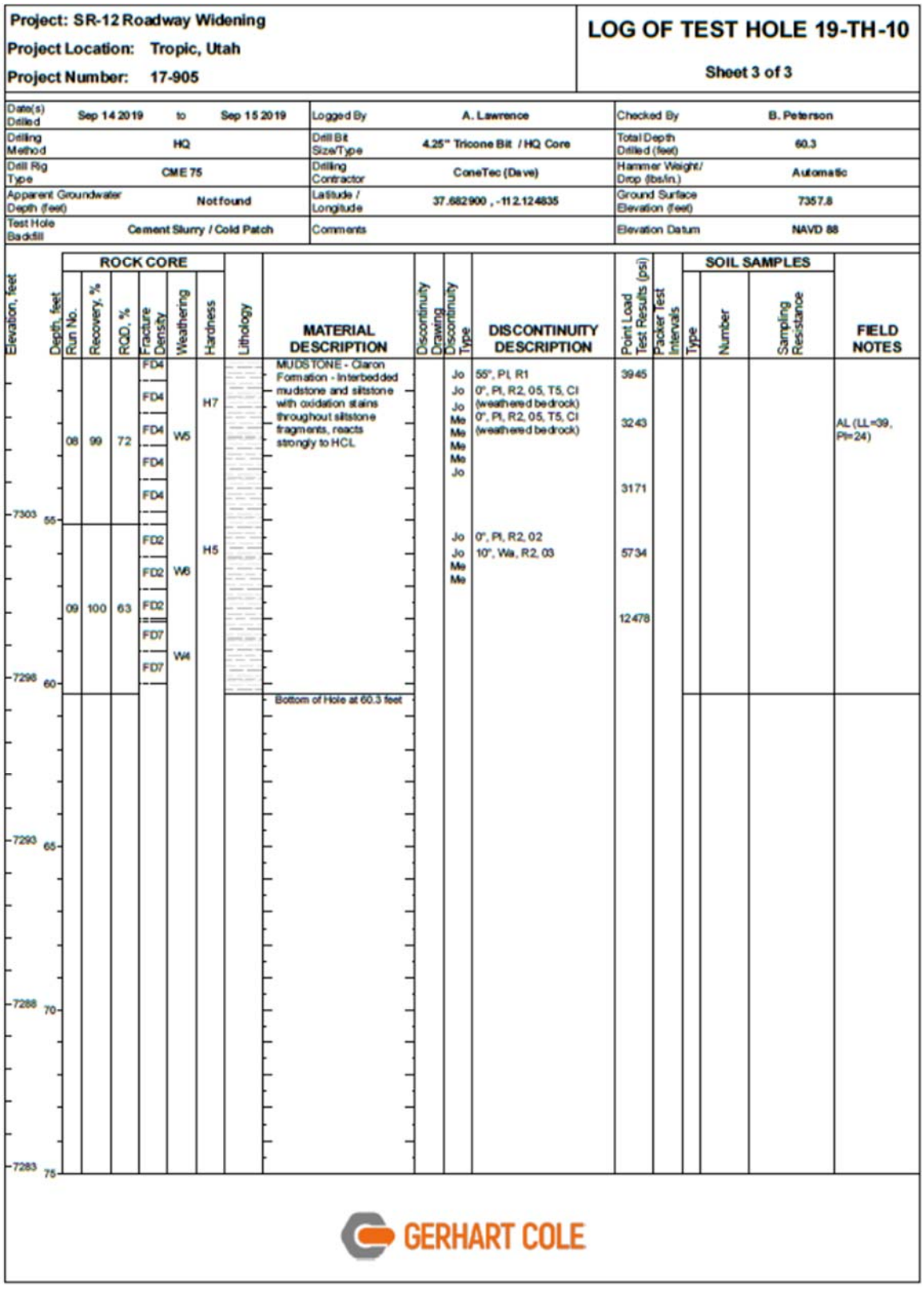

Figure A-39 - Test hole log of 19-TH-10 (cont'd) from Gerhart Cole, (2019)

Figure A-40 – Rock core photographs from 19-TH-10, from Gerhart Cole, (2019)

Figure A-41 – Rock core photographs from 19-TH-10, from Gerhart Cole, (2019)

Figure A-42 – Rock core photographs from 19-TH-10, from Gerhart Cole, (2019)

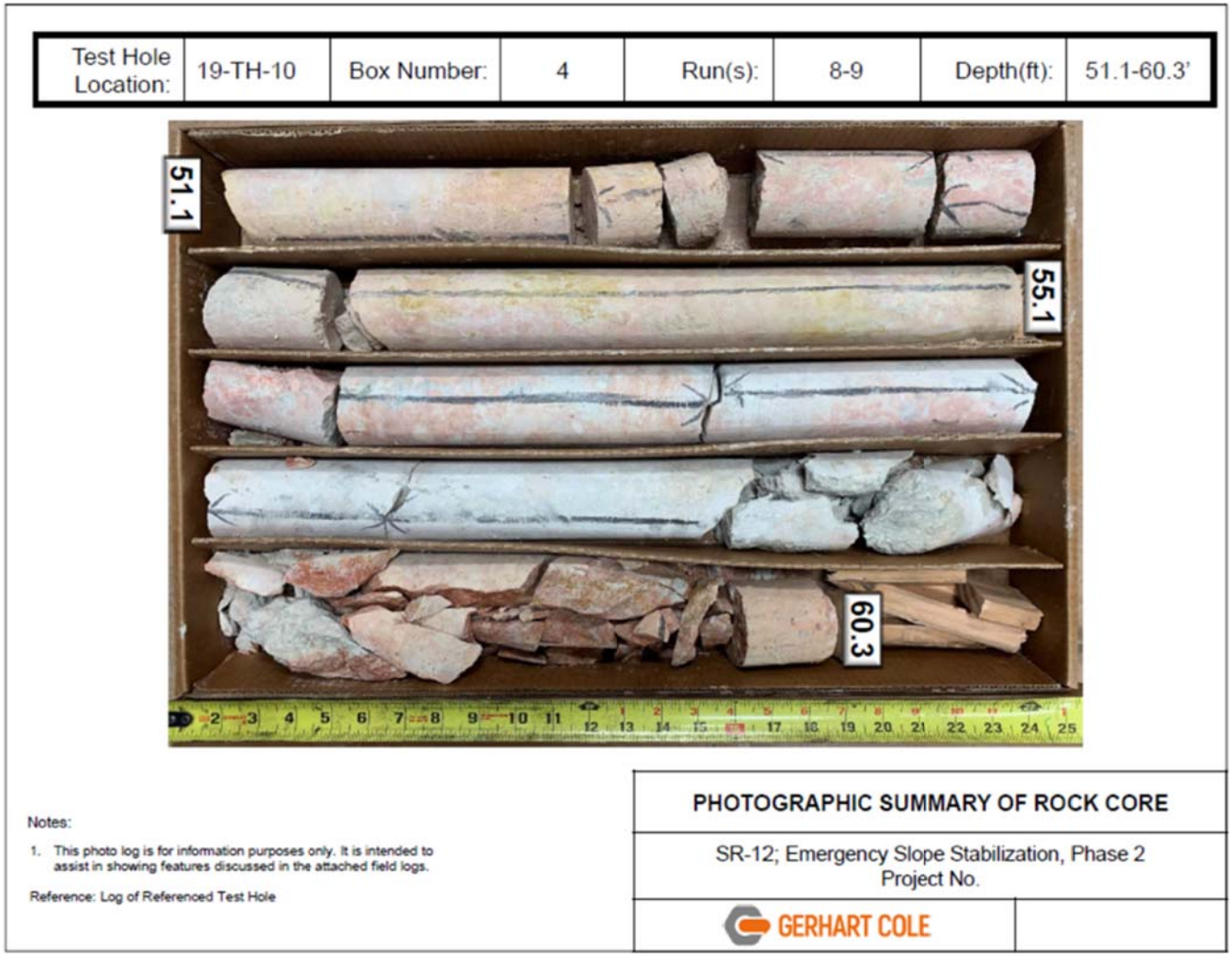

Figure A-43 – Rock core photographs from 19-TH-10, from Gerhart Cole, (2019)

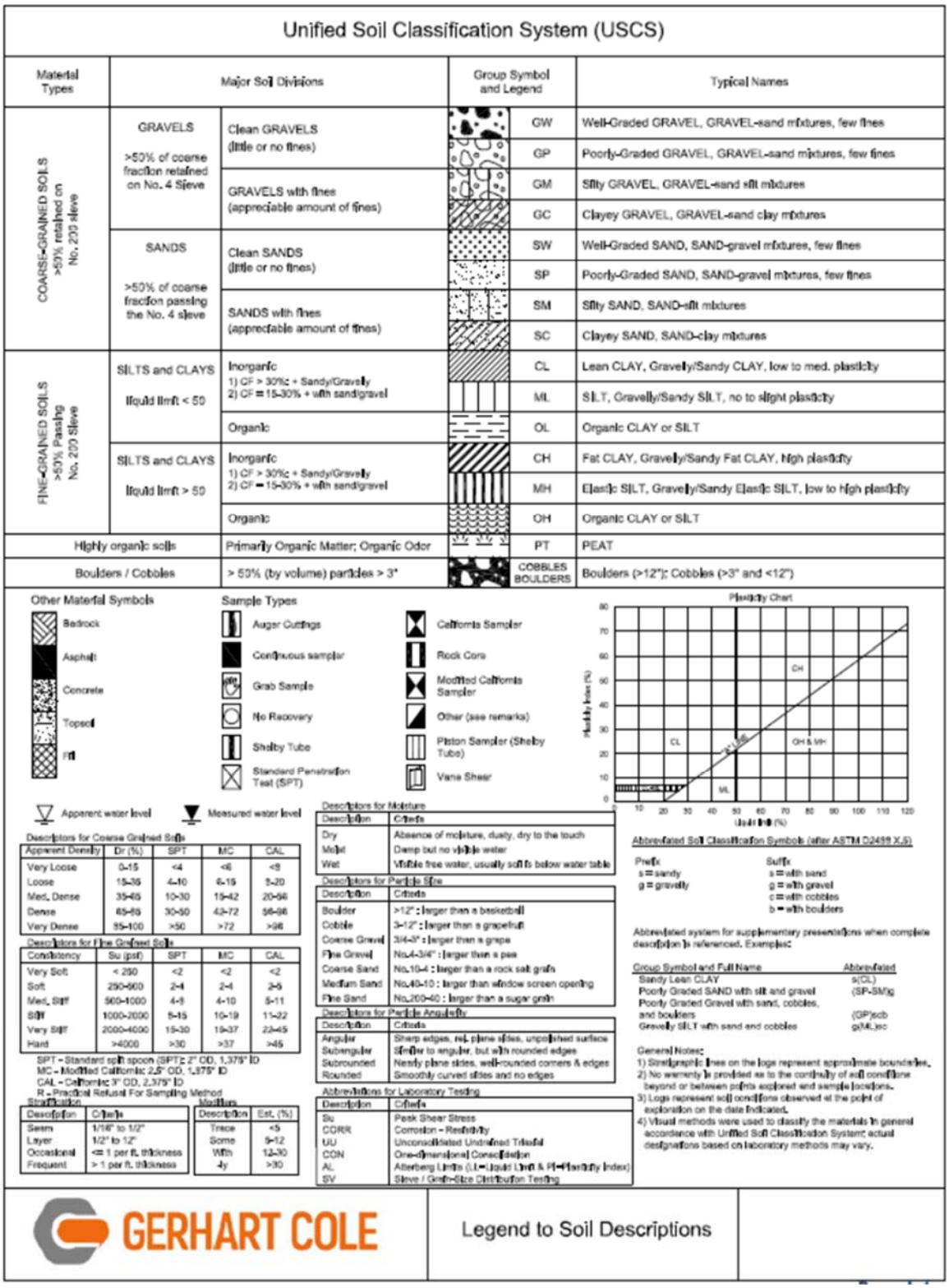

Figure A-44 – Legend to Soil Descriptions, from Gerhart Cole (2019)

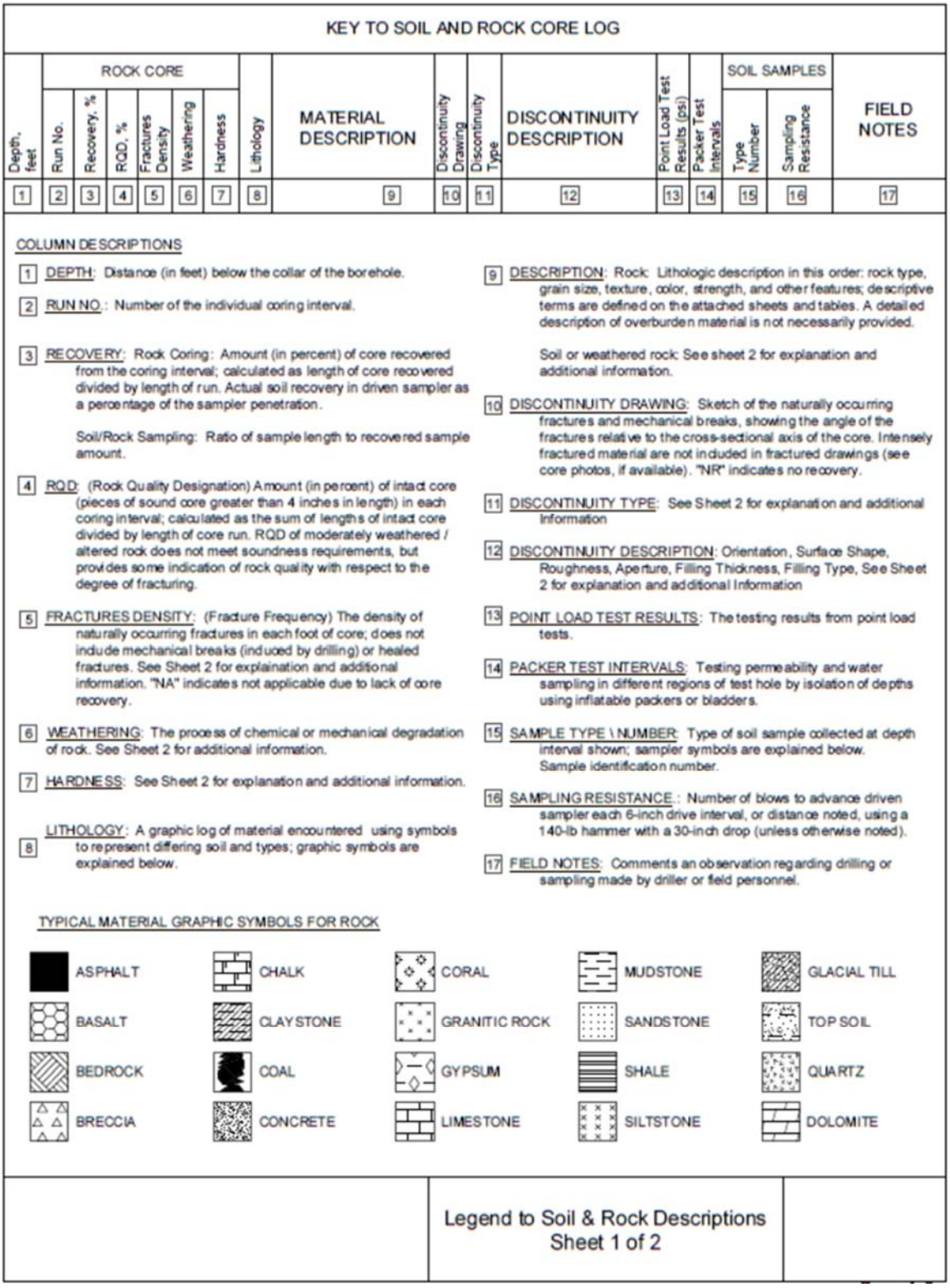

Figure A-45 – Legend to Soil and Rock Descriptions, from Gerhart Cole (2019)

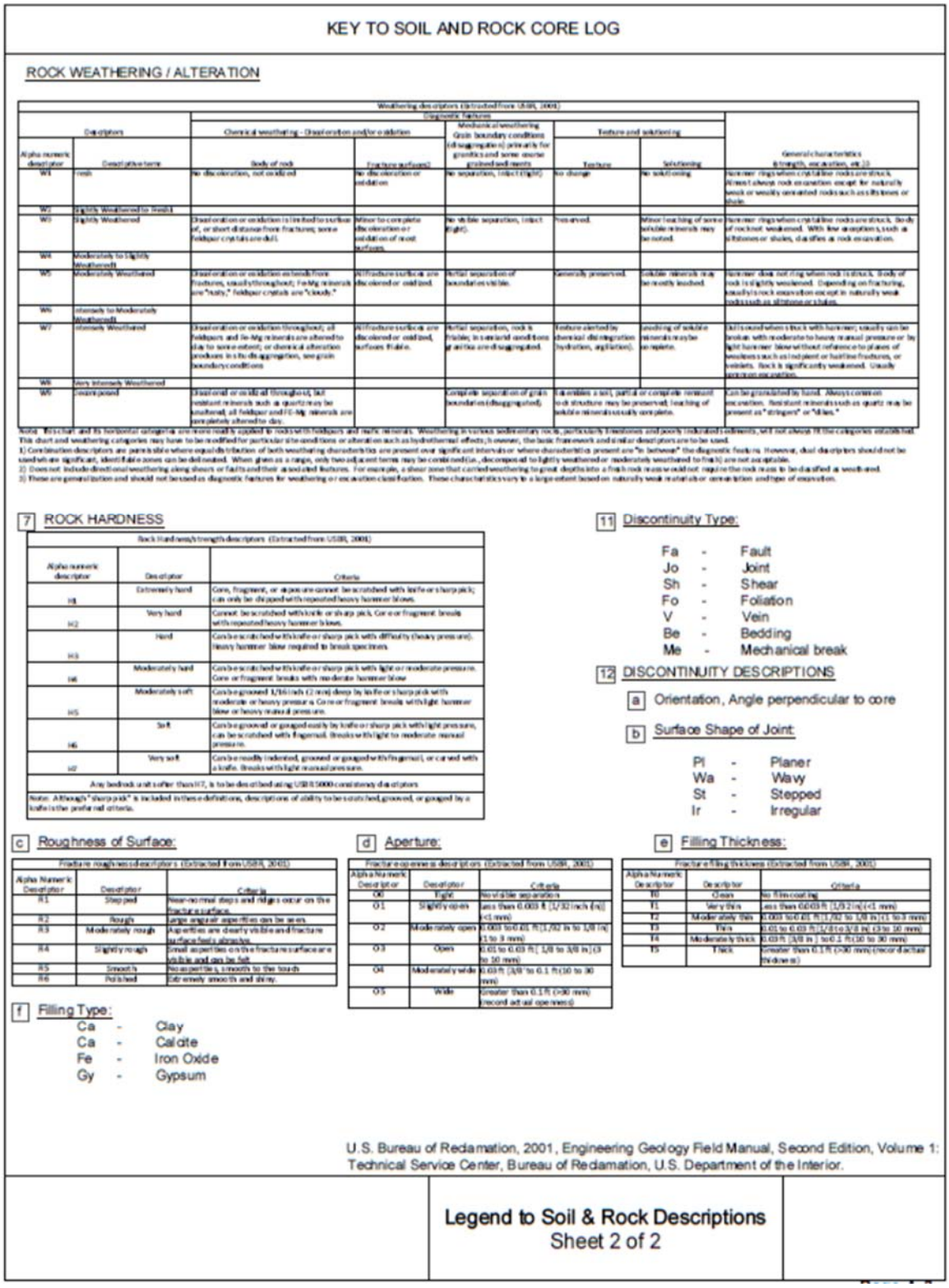

KEY TO SOIL AND ROCK CORE LOG

ROCK WEATHERING / ALTERATION

Weathering descriptors (extracted from USBR, 2001)

Descriptors		Diagnostic features: Chemical weathering - Discoloration and/or oxidation		Mechanical weathering (grain boundary conditions (disaggregation) primarily for granitics and some coarse grained sediments	Texture and solutioning		General characteristics (strength, excavation, etc.))
Alpha numeric descriptor	Descriptive term	Body of rock	Fracture surfaces		Texture	Solutioning	
W1	Fresh	No discoloration, not oxidized	No discoloration or oxidation	No separation, intact (tight)	No change	No solutioning	Hammer rings when crystalline rocks are struck. Almost always rock excavation except for naturally weak or weakly cemented rocks such as siltstones or shale.
W2	Slightly Weathered to Fresh						
W3	Slightly Weathered	Discoloration or oxidation is limited to surface of, or short distance from fractures; some Feldspar crystals are dull.	Minor to complete discoloration or oxidation of most surfaces.	No visible separation, intact (tight).	Preserved.	Minor leaching of some soluble minerals may be noted.	Hammer rings when crystalline rocks are struck. Body of rock not weakened. With few exceptions, such as siltstones or shales, classifies as rock excavation.
W4	Moderately to Slightly Weathered						
W5	Moderately Weathered	Discoloration or oxidation extends from fractures, usually throughout; Fe-Mg minerals are "rusty," feldspar crystals are "cloudy."	All fracture surfaces are discolored or oxidized.	Partial separation of boundaries visible.	Generally preserved.	Soluble minerals may be mostly leached.	Hammer does not ring when rock is struck. Body of rock is slightly weakened. Depending on fracturing, usually is rock excavation except in naturally weak rocks such as siltstone or shales.
W6	Intensely to Moderately Weathered						
W7	Intensely Weathered	Discoloration or oxidation throughout; all feldspars and Fe-Mg minerals are altered to clay to some extent; or chemical alteration produces in situ disaggregation, see grain boundary conditions	All fracture surfaces are discolored or oxidized, surfaces friable.	Partial separation, rock is friable; in semi-arid conditions granites are disaggregated.	Texture altered by chemical disintegration (hydration, argillation).	Leaching of soluble minerals may be complete.	Can be excavated when struck with hammer; usually can be broken with moderate to heavy manual pressure or by light hammer blow without reference to planes of weakness such as incipient or healed fractures, or joints. Rock is significantly weakened. Usually excavation.
W8	Very Intensely Weathered						
W9	Decomposed	Discolored or oxidized throughout; but resistant minerals such as quartz may be unaltered; all feldspar and Fe-Mg minerals are completely altered to clay.		Complete separation of grain boundaries (disaggregated).	Chemical action is complete; a soil, partial or complete remnant rock structure may be preserved; leaching of soluble minerals usually complete.		Can be granulated by hand. Always common excavation. Resistant minerals such as quartz may be present as "stringers" or "dikes."

Note: this chart and its horizontal categories are more readily applied to rocks with feldspars and mafic minerals. Weathering in various sedimentary rocks, particularly limestones and poorly indurated sediments, will not always fit the categories established. This chart and weathering categories may have to be modified for particular site conditions or alteration such as hydrothermal effects; however, the basic framework and similar descriptors are to be used.
1) Combination descriptors are paired to cite where equal distribution of both weathering characteristics are present over significant intervals or where characteristics present are "in between" the diagnostic features. However, dual descriptors should not be used when significant, identifiable zones can be delineated. When given as a range, only two adjacent terms may be combined (i.e., decomposed to lightly weathered or moderately weathered to fresh) are not acceptable.
2) Does not include directional weathering along sheets or faults and their associated features. For example, a shear zone that carried weathering to great depths into a fresh rock mass would not require the rock mass to be classified as weathered.
3) These are generalizations and should not be used as diagnostic features for weathering or excavation classification. These characteristics vary to a large extent based on naturally weak material or cementation and type of excavation.

7 ROCK HARDNESS

Rock Hardness/strength descriptors (Extracted from USBR, 2001)

Alpha numeric descriptor	Descriptor	Criteria
H8	Extremely hard	Core, fragment, or exposure cannot be scratched with knife or sharp pick; can only be chipped with repeated heavy hammer blows.
H2	Very hard	Cannot be scratched with knife or sharp pick. Core or fragment breaks with repeated heavy hammer blows.
H3	Hard	Can be scratched with knife or sharp pick with difficulty (heavy pressure). Heavy hammer blow required to break specimen.
H4	Moderately hard	Can be scratched with knife or sharp pick with light or moderate pressure. Core or fragment breaks with moderate hammer blow
H5	Moderately soft	Can be grooved 1/16 inch (2 mm) deep by knife or sharp pick with moderate or heavy pressure. Core or fragment breaks with light hammer blow or heavy manual pressure.
H6	Soft	Can be grooved or gouged easily by knife or sharp pick with light pressure, can be scratched with fingernail. Breaks with light to moderate manual pressure.
H7	Very soft	Can be readily indented, grooved or gouged with fingernail, or carved with a knife. Breaks with light manual pressure.
Any bedrock unit softer than H7, is to be described using USBR 5000 consistency descriptors		
Note: Although "sharp pick" is included in these definitions, descriptions of ability to be scratched, grooved, or gouged by a knife is the preferred criteria.		

11 Discontinuity Type:

Fa - Fault
Jo - Joint
Sh - Shear
Fo - Foliation
V - Vein
Be - Bedding
Me - Mechanical break

12 DISCONTINUITY DESCRIPTIONS

a Orientation, Angle perpendicular to core

b Surface Shape of Joint:

Pl - Planer
Wa - Wavy
St - Stepped
Ir - Irregular

c Roughness of Surface:

Fracture roughness descriptors (Extracted from USBR, 2001)

Alpha Numeric Descriptor	Descriptor	Criteria
R1	Stepped	Near-normal steps and ridges occur on the fracture surface.
R2	Rough	Large angular asperities can be seen.
R3	Moderately rough	Asperities are clearly visible and fracture surface feels abrasive.
R4	Slightly rough	Small asperities on the fracture surface are visible and can be felt.
R5	Smooth	No asperities, smooth to the touch.
R6	Polished	Extremely smooth and shiny.

d Aperture:

Fracture openness descriptors (Extracted from USBR, 2001)

Alpha Numeric Descriptor	Descriptor	Criteria
O0	Tight	No visible separation
O1	Slightly open	Less than 0.003 ft (1/32 inch (<1 mm)
O2	Moderately open	0.003 to 0.01 ft (1/32 in to 1/8 in) (1 to 3 mm)
O3	Open	0.01 to 0.03 ft (1/8 to 3/8 in) (3 to 10 mm)
O4	Moderately wide	0.03 ft (3/8 in to 0.1 ft (10 to 30 mm)
O5	Wide	Greater than 0.1 ft (>30 mm) (record actual openness)

e Filling Thickness:

Fracture filling thickness (Extracted from USBR, 2001)

Alpha Numeric Descriptor	Descriptor	Criteria
T0	Clean	No film coating
T1	Very thin	Less than 0.003 ft (1/32 in) (<1 mm)
T2	Moderately thin	0.003 to 0.01 ft (1/32 to 1/8 in) (1 to 3 mm)
T3	Thin	0.01 to 0.03 ft (1/8 to 3/8 in) (3 to 10 mm)
T4	Moderately thick	0.03 ft (3/8 in) to 0.1 ft (10 to 30 mm)
T5	Thick	Greater than 0.1 ft (>30 mm) (record actual thickness)

f Filling Type:

Ca - Clay
Ca - Calcite
Fe - Iron Oxide
Gy - Gypsum

U.S. Bureau of Reclamation, 2001, Engineering Geology Field Manual, Second Edition, Volume 1: Technical Service Center, Bureau of Reclamation, U.S. Department of the Interior.

Legend to Soil & Rock Descriptions
Sheet 2 of 2

Figure A-46 – Legend to Soil and Rock Descriptions (cont'd.), from Gerhart Cole (2019)

APPENDIX B

Appendix B includes maps showing the scanline locations and the locations of samples taken from outcrops and toeslopes, as well as the raw data sheets from scanline data collection.

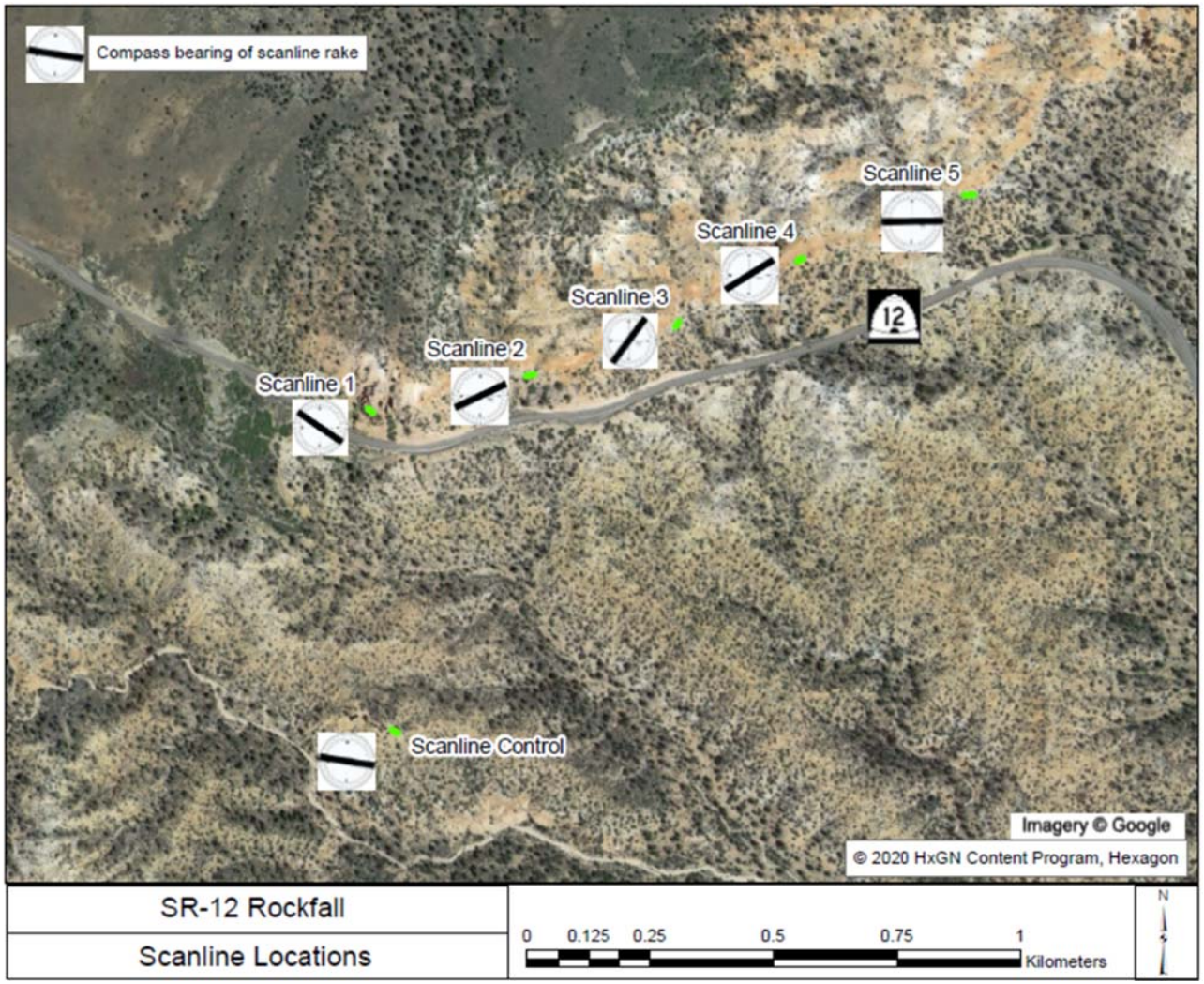

Figure B-1 – Scanline Locations

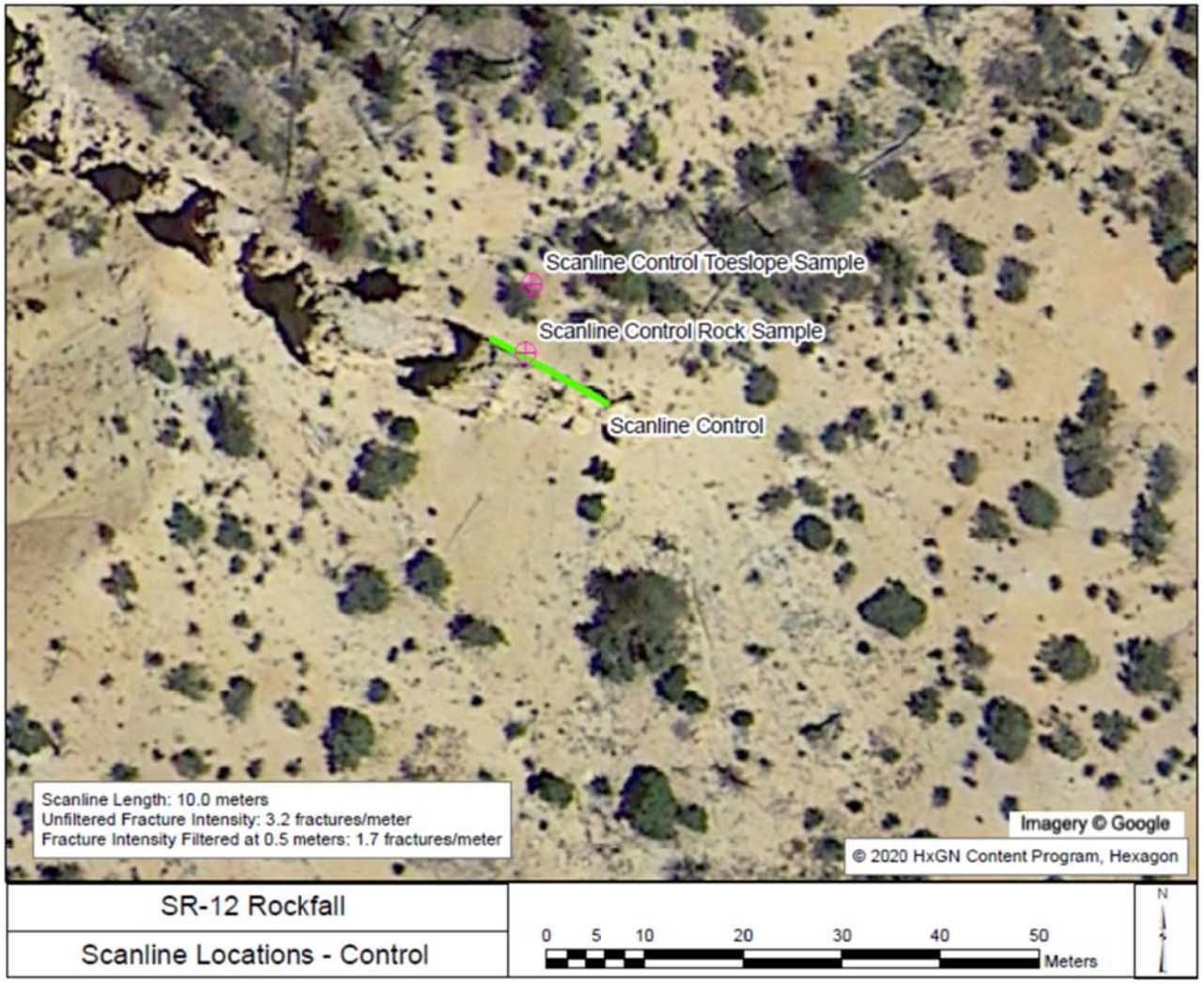

Figure B-2 – Scanline and sample locations for the control scanline

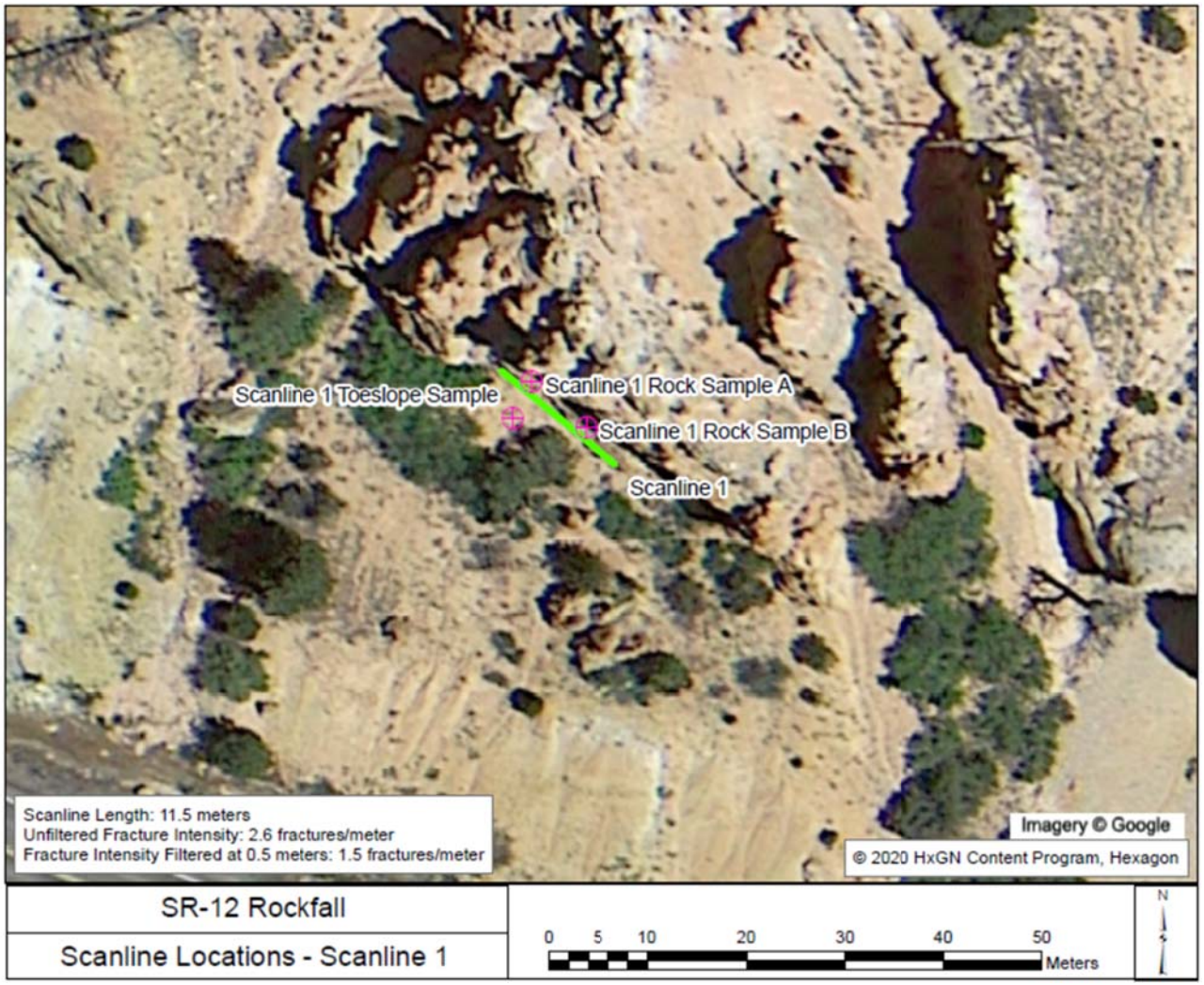

Figure B-3 – Scanline and sample locations for Scanline 1

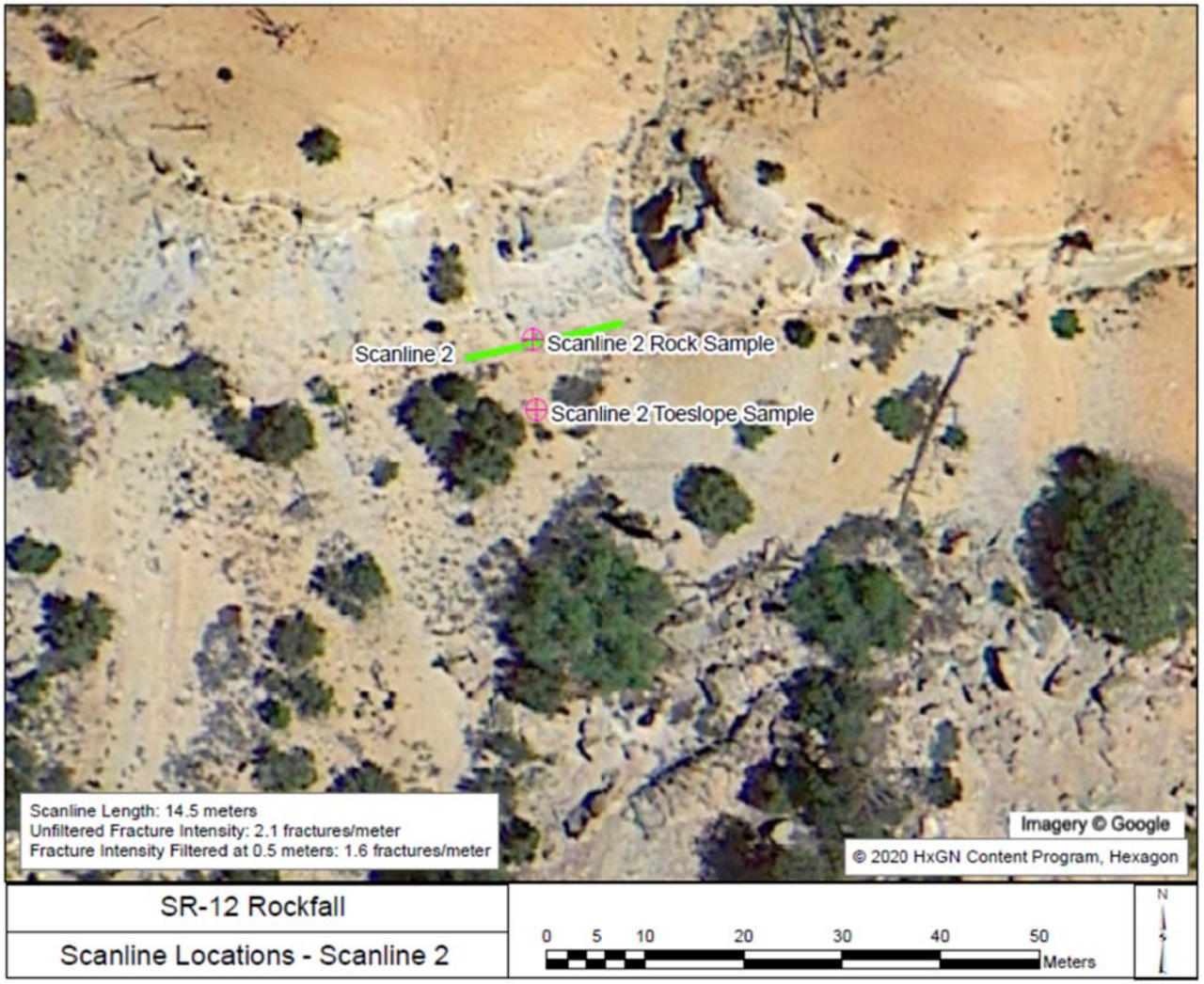

Figure B-4 – Scanline and sample locations for Scanline 2

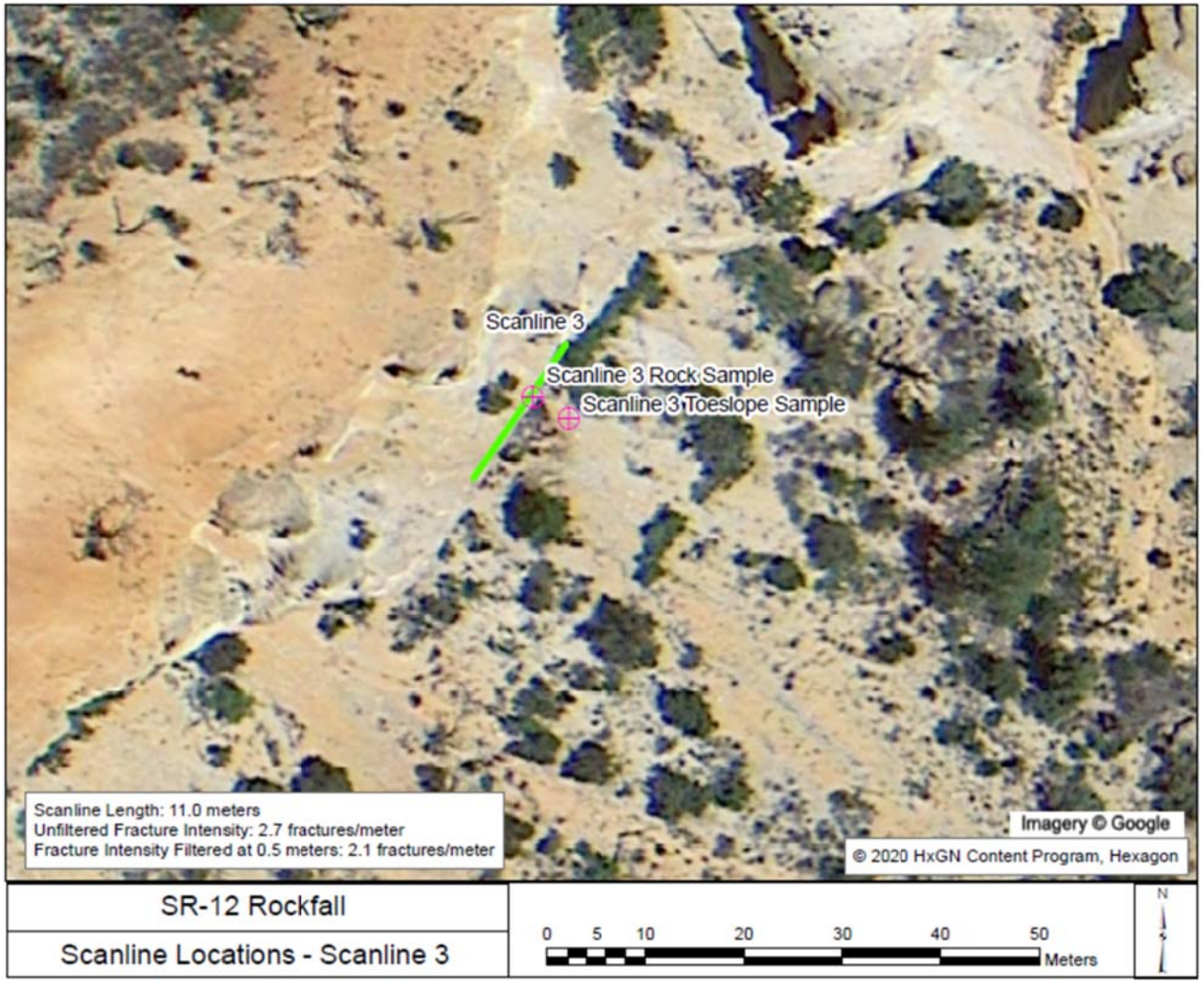

Figure B-5 – Scanline and sample locations for Scanline 3

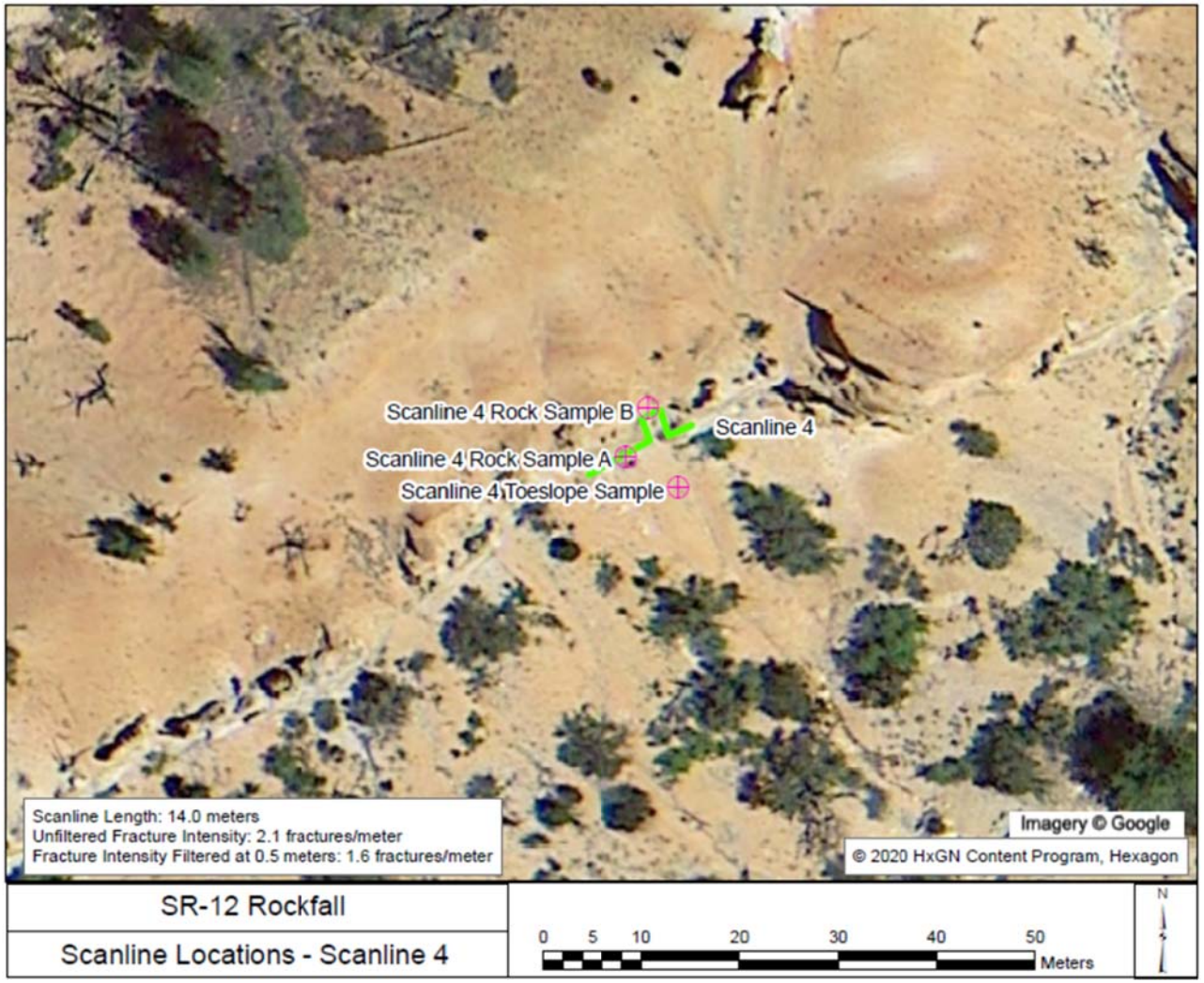

Figure B-6 – Scanline and sample locations for Scanline 4

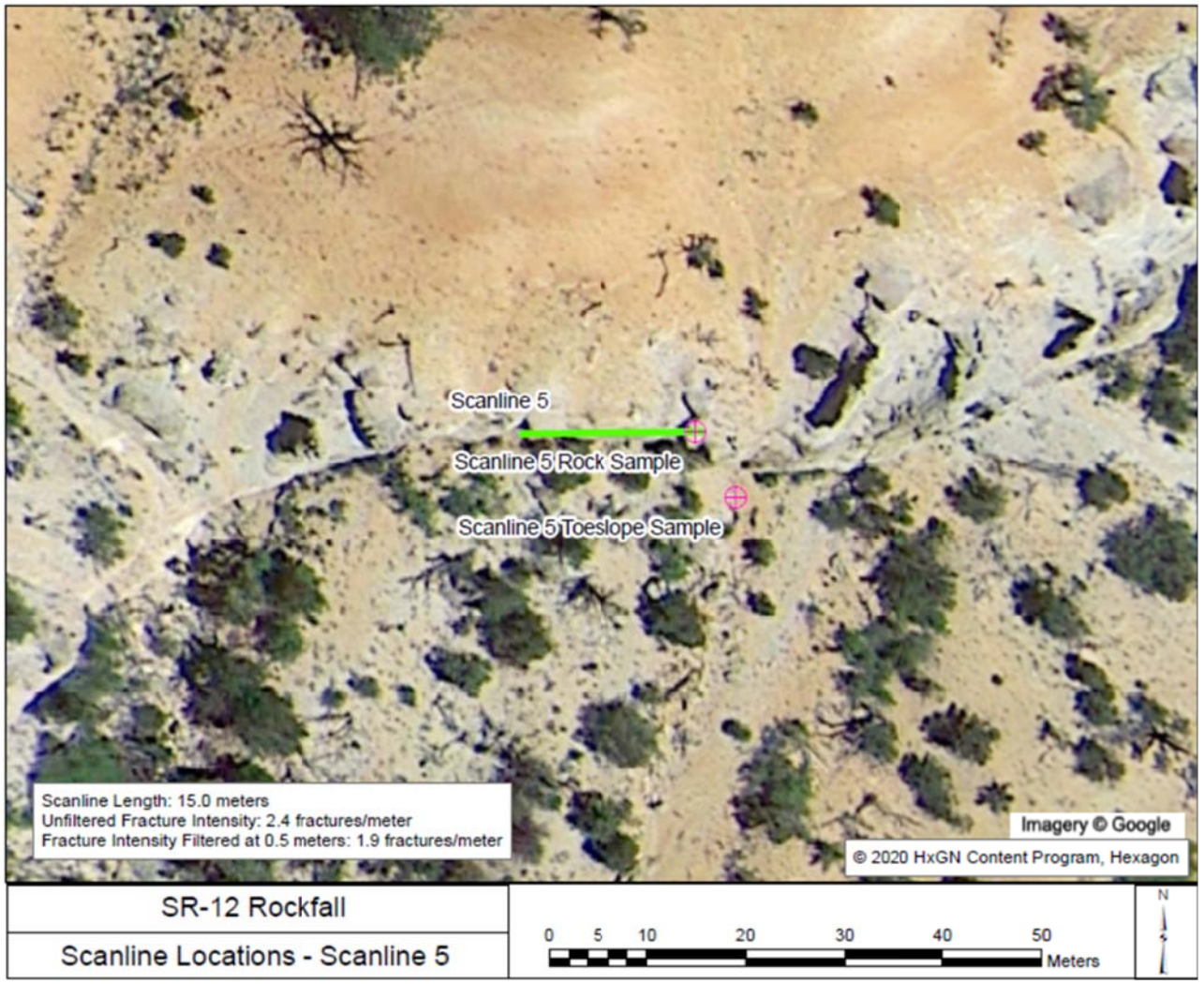

Figure B-7 – Scanline and sample locations for Scanline 5

Linear Scanline Control | Location (GPS): | Weather: | Start: 37.678319, -112.128520. End: 37.678353, -112.128585 | Scientist: T. Reed | Orientation of Tape: | Date: 5/20/2020 | 279° (W-NW), horizontal

Station (cm)	Rock Type	Bd., Flt., or Fr.	Dip/Dip Direction (degrees)	Trace Length	Roughness (JRC)	Coating/Filling Thickness (mm)	Coating/Filling Type	Spacing (cm)	Aperture (mm)	Weathering	Moisture	Notes
0	Dolomite	Fr.	25/300	Infinite	4-6	0	-	-	1-2	Fr.	Dry	
4	Dolomite	Fr.	85/252	64	8-10	1	Cl, S	4	2	Fr. to Sl.	Dry	
14	Dolomite	Fr.	77/294	37	6-8	4	Cl, S	10	8	Fr. to Sl.	Dry	
36	Dolomite	Fr.	88/281	Infinite	NA	50	Cl	22	50	Sl. to Mod.	Dry	Fracture zone, 5 cm. wide
63	Dolomite	Fr.	87/300	156	6-8	0	-	27	1	Fr. to Sl.	Dry	Possible edge of vertical burrow
84	Dolomite	Fr.	88/272	181	6-8	1	Cl, S	21	1	Fr. to Sl.	Dry	
99	Dolomite	Fr.	87/84	61	10-12	0	-	15	1	Fr. to Sl.	Dry	
103		See notes										Vug, 55mm wide and deep
110	Dolomite	Fr.	88/283	425	4-6	2-5	Cl, S	11	2-7	Fr. to Sl.	Dry	
126	Dolomite	Fr.	75/93	185	4-6	1-2	Cl, S	16	3	Fr. to Sl.	Dry	Terminates in large vug
143	Dolomite	Fr.	56/78	105	6-8	0	-	17	1	Fr. to Sl.	Dry	
156		See notes										Vug
197	Dolomite	Fr.	68/259	1350	6-8	0	-	54	1	Fr. to Sl.	Dry	
207	Dolomite	Fr.	23/283	75	8-10	0	-	10	1	Fr. to Sl.	Dry	
230	Dolomite	Fr.	84/116	441	6-8	2-4	Cl, S	23	2-8	Fr. to Mod.	Dry	
250	Dolomite	Fr.	78/331	990	8-10	0	-	20	1	Fr. to Sl.	Dry	
267	Dolomite	Fr.	89/297	630	6-8	1-5	Cl, S	17	2-6	Fr. to Sl.	Dry	
310	Dolomite	Fr.	84/154	>1640	10-12	0-1	Cl, S	43	1-2	Fr. to Sl.	Dry	
326	Dolomite	Fr.	87/144	Infinite	NA	35-60	Cl	16	35-60	Sl. to Mod.	Dry	Clayey infilling with limestone
376	Dolomite	Fr.	82/296	358	8-10	0	-	50	1	Fr. to Sl.	Dry	
390	Dolomite	Fr.	86/277	1055	8-10	0-1	Cl, S	14	2-4	Sl.	Dry	
492	Dolomite	Fr.	83/273	372	4-6	0	-	102	1	Fr. to Sl.	Dry	
510	Dolomite	Fr.	84/120	295	6-8	0	-	18	1	Fr. to Sl.	Dry	
515	Dolomite	Fr.	88/120	>1800	8-10	0-1	Cl, S	5	2	Fr. to Sl.	Dry	
539	Dolomite	Fr.	88/291	912	6-8	0	-	24	1	Fr. to Sl.	Dry	
680	Dolomite	Fr.	28/134	590	8-10	0	-	141	1	Fr. to Sl.	Dry	
700	Dolomite	Fr.	85/101	Infinite	NA	32-40	Cl	20	32-40	Sl. to Mod.	Dry	
720	Dolomite	Fr.	89/329	>2000	NA	10-20	Cl	20	10-20	Sl. to Mod.	Dry	
739	Dolomite	Fr.	86/315	370	6-8	0	-	19	1	Fr. to Sl.	Dry	
768	Dolomite	Fr.	77/290	510	2-4	0	-	29	1	Fr. to Sl.	Dry	
864	Dolomite	Fr.	89/185	1190	6-8	2-4	Cl, S	96	2-10	Fr. to Sl.	Dry	
917	Dolomite	Fr.	87/144	Infinite	6-8	5-14	Cl	53	5-20	Sl. to Mod.	Dry	
930	Dolomite	Fr.	89/265	348	10-12	2-11	Cl, S	13	2-26	Fr. to Sl.	Dry	
955	Dolomite	Fr.	20/150	1390	6-8	0	-	25	1	Fr. to Sl.	Dry	
1000	End of scanline											

Notes:
1) Spacing measured is apparent spacing between previously measured fracture, not necessarily the previous joint from same joint set.
2) Bd. = Bedding, Flt. = Fault, Fr. = Fracture.
3) Coating/fillings explanations: Cl. = Clay, S. = Sand, Ca. = Calcite, MnO = Manganese Oxide
4) Weathering explanations: Fr. = Fresh, Sl. = Slightly weathered, Mod. = Moderately weathered
5) When taking measurements, tape measure was kept taut. Station locations were collected either by holding the tape directly against the rock, or holding an instrument perpendicular to the tape and touching the fractures, if the tape measure did not rest against the rock.

Figure B-8 – Raw scanline data from control scanline

Linear Scanline 1 | Location (GPS): Weather: Sunny, 40s | Start: 37.682858, -112.129233. End: 37.682892, -112.12893[illegible] Scientist: T. Reed Orientation of Tape: | Date: 5/21/2020 124° (SE), dipping at 19°

Station (cm)	Rock Type	Bd., Flt., or Fr.	Dip/Dip Direction (degrees)	Trace Length (mm)	Roughness (JRC)	Coating/Filling Thickness (mm)	Coating/Filling Type	Spacing (cm)	Aperture (mm)	Weathering	Moisture	Notes
0	Dolomite	Fr.	52/285	Infinte	8-10	1	Ca	-	1-12	Sl.	dry	CaCO3 crystals in voids
11	Dolomite	Fr.	81/285	131	6-8	1	Ca	11	1	Fr.	dry	
45	Dolomite	Fr.	65/279	Infinite	8-10	1-2	Ca	34	1-18	Sl.	dry	CaCO3 crystals
47	Dolomite	Fr.	30/258	311	12-14	1	Ca	2	1-5	Sl.	dry	
59	Dolomite	Fr.	84/289	556	8-10	1-2	Ca	12	1-6	Sl.	dry	CaCO3 crystals
61	Dolomite	Fr.	44/218	374	6-8	1	Ca	2	1	Sl.	dry	
80	Dolomite	Fr.	58/227	371	10-12	1	Ca	19	1	Fr.	dry	
90	Dolomite	Fr.	61/292	735	10-12	1	Ca	10	1-21	Sl.	dry	CaCO3 crystals
99	Dolomite	Flt.	77/240	Infinte	6-8	1	Ca	9	1-10	Sl.	dry	Displacement at bottom of outcrop, separation not measurable because it ends below outcrop face
220												Very vuggy between 220-293
293	Dolomite	Fr.	45/275	Infinite	12-14	1-2	Ca, Cl	194	1-24	Sl. to mod.	dry	CaCO3 crystals
344	Dolomite	Fr.	72/246	596	8-10	1-2	Ca, Cl	51	1-2	Sl.	dry	
402	Dolomite	Fr.	59/172	1190	6-8	2-4	Ca, Cl, S	58	2-6	Sl.	dry	Disappears behind rocks, could be infinite
419	Dolomite	Fr.	74/249	770	4-6	1	Ca	17	1	Fr. to sl.	dry	
438	Dolomite	Fr.	87/189	1760	6-8	1	Ca	19	1-15	Sl. to mod.	dry	Fracture accompanied by possible sulphur mineralization or yellow cretaceous sediments
479	Limestone	Fr.	48/25	1630	4-6	1	Ca, Cl	41	1-2	Sl.	dry	Poss. conjugate fracture paired with
511	Limestone	Fr.	62/292	721	4-6	1	Ca, Cl	32	1	Sl.	dry	fracture at sta. 511
582	Limestone	Fr.	35/125	1081	6-8	1-2	Ca, Cl	71	1-5	Sl.	dry	
612	Limestone	Fr.	43/288	979	12-14	2-4	Ca, Cl	30	2-17	Sl.	dry	
697	Limestone	Fr.	79/234	545	6-8	1-3	Cl, S	85	2-4	Sl. to mod.	dry	
714	Limestone	Fr.	51/260	405	6-8	1	Cl, S	17	1	Sl.	dry	
827	Limestone	Fr.	36/153	466	4-6	1	Sa	113	1	Fr. to sl.	dry	
883	Limestone	Fr.	29/162	2050	2-4	0	-	56	1-12	Fr.	dry	
1050	Limestone	Fr.	49/271	693	6-8	0-1	S, Cl	167	1-7	Fr. to sl.	dry	
1082	Limestone	Fr.	56/278	295	6-8	0	-	32	1-2	Fr. to sl.	dry	
1086	Limestone	Fr.	61/284	457	8-10	1	S	4	1-4	Fr. to sl.	dry	
1118	Limestone	Fr.	77/290	193	4-6	0	-	32	1	Fr.	dry	
1120	Limestone	Fr.	7/98	165	2-4	0	-	2	1	Sl.	dry	
1132	Limestone	Fr.	79/298	96	6-8	1	Cl, S	12	1	Fr. to sl.	dry	
1134	Limestone	Fr.	67/292	109	6-8	1	Cl, S	2	2	Fr. to sl.	dry	
1137	Limestone	Fr.	63/263	87	4-6	2	Cl, S	3	2	Fr. to sl.	dry	
1150	End of scanline											

Notes:
1) Spacing measured is apparent spacing between previously measured fracture, not necessarily the previous joint from same joint set.
2) Bd. = Bedding, Flt. = Fault, Fr. = Fracture.
3) Coating/fillings explanations: Cl. = Clay, S. = Sand, Ca. = Calcite, MnO = Manganese Oxide
4) Weathering explanations: Fr. = Fresh, Sl. = Slightly weathered, Mod. = Moderately weathered
5) When taking measurements, tape measure was kept taut. Station locations were collected either by holding the tape directly against the rock, or holding an instrument perpendicular to the tape and touching the fractures, if the tape measure did not rest against the rock.

Figure B-9 – Raw scanline data from Scanline 1

Linear Scanline 2 | Location (GPS): Start: 37.683216, -112.126505. End: 37.683260, -112.12630[illegible] | Date: 5/21/2020
Weather: Sunny, 60s | Scientist: T. Reed | Orientation of Tape: 65° (E-NE), horizontal

Station (cm)	Rock Type	Bd., Flt., or Fr.	Dip/Dip Direction (degrees)	Trace Length (mm)	Roughness (JRC)	Coating/Filling		Spacing (cm)	Aperture (mm)	Weathering	Moisture	Notes
						Thickness (mm)	Type					
49	Limestone	Fr.	23/20	Infinite	4-6	0	-	-	1	Fr. to sl.	dry	
53	Limestone	Fr.	57/6	921	2-4	0	-	4	1	Fr. to sl.	dry	
70	Limestone	Fr.	58/5	490	4-6	0	-	17	1	Fr. to sl.	dry	
165	Limestone	Fr.	81/323	>430	8-10	<1	MnO	95	1	Sl. to mod.	Possibly before	
185	Limestone	Fr.	84/271	Infinite	8-10	<1	MnO	20	2-4	Sl. to mod.	Possibly before	
283	Limestone	Fr.	73/87	Infinite	8-10	<1	MnO	98	1-5	Sl. to mod.	Possibly before	
287	Limestone	Fr.	23/20	Infinite	4-6	0	-	4	1	Fr. to sl.	dry	
377	Limestone	Fr.	81/263	>260	4-6	0	-	90	1	Fr. to sl.	dry	
478	Limestone	Fr.	36/17	710	6-8	0	-	101	1	Fr. to sl.	dry	
500	Limestone	Fr.	36/35	281	4-6	0	-	22	1	Fr. to sl.	dry	
583	Limestone	Fr.	89/56	323	8-10	<1	MnO	83	1	Sl. to mod.	Possibly before	
600	Limestone	Fr.	87/50	Infinite	6-8	<1	MnO, Ca	17	1	Sl. to mod.	Possibly b	CaCO3 crystals
770	Limestone	Fr.	83/269	>870	6-8	<1	MnO	170	1	Sl.	Possibly before	
779	Limestone	Fr.	73/269	>890	4-6	<1	MnO	9	1	Sl.	Possibly before	
820	Limestone	Fr.	43/284	390	4-6	0	-	41	1	Sl.	dry	
821	Limestone	Fr.	74/87	Infinte	10-12	<1-2	MnO, Ca	1	1-12	Sl. to mod.	Possibly b	CaCO3 crystals
845	Limestone	Fr.	70/83	632	6-8	<1	MnO, Ca	24	1	Sl. to mod.	Likely, moss in fracture	
855	Limestone	Fr.	62/49	481	4-6	0	-	10	1	Sl.		
897	Limestone	Fr.	43/93	89	4-6	0	-	42	1	Sl.		
1000	Limestone	Fr.	83/280	211	8-10	<1	MnO	103	1	Sl. to mod.	Possibly before	
1035	Limestone	Fr.	88/71	Infinite	10-12	<1	MnO	35	1-15	Sl. to mod.	likely, pine sprout in fracture	
1054	Limestone	Fr.	84/244	Infinite	10-12	<1	MnO	19	1-26	Sl. to mod.	Likely, moss in fracture	
1140	Limestone	Fr.	18/70	>810	4-6	0	-	86	1	Fr. to sl.	dry	
1152	Limestone	Fr.	50/3	>340	6-8	0	-	12	1	Fr. to sl.	dry	
1180	Limestone	Fr.	13/38	375	6-8	1	Ca	28	1-4	Sl.	dry	
1245	Limestone	Fr.	84/269	>320	6-8	<1	MnO	65	1	Sl.	Possibly before	
1278	Limestone	Fr.	89/86	Infinite	8-10	<1	MnO, Ca	33	1-12	Sl. to mod.	Possibly b	CaCO3 crystals
1294	Limestone	Fr.	56/11	>380	6-8	0	-	16	1	Sl.	dry	
1424	Limestone	Fr.	59/256	>491	8-10	0	-	130	1	Sl.	dry	
1438	Limestone	Fr.	86/272	>270	6-8	0	-	14	1	Sl.	dry	
1443	Limestone	Fr.	89/93	>260	6-8	0	-	5	1	Sl.	dry	
1450	End of scanline											

Notes:
1) Spacing measured is apparent spacing between previously measured fracture, not necessarily the previous joint from same joint set.
2) Bd. = Bedding, Flt. = Fault, Fr. = Fracture.
3) Coating/fillings explanations: Cl. = Clay, S. = Sand, Ca. = Calcite, MnO = Manganese Oxide
4) Weathering explanations: Fr. = Fresh, Sl. = Slightly weathered, Mod. = Moderately weathered
5) When taking measurements, tape measure was kept taut. Station locations were collected either by holding the tape directly against the rock, or holding an instrument perpendicular to the tape and touching the fractures, if the tape measure did not rest against the rock.

Figure B-10 – Raw scanline data from Scanline 2

Linear Scanline 3 | Location (GPS): Start: 37.684161, -112.123391. End: 37.684300, -112.12333(| Weather: Windy, 60s | Scientist: T. Reed | Orientation of Tape: | Date: 5/22/2020 | 37° (NE), dipping at 6°

Station (cm)	Rock Type	Bd., Flt., or Fr.	Dip/Dip Direction (degrees)	Trace Length (mm)	Roughness (JRC)	Coating/Filling Thickness (mm)	Coating/Filling Type	Spacing (cm)	Aperture (mm)	Weathering	Moisture	Notes
29	Dolomite	Fr.	75/51	874	12-14	0	-	-	<1	Fr. to sl.	dry	Almost completely healed at surface
50	Dolomite	Fr.	89/72	363	6-8	0	-	21	<1	Fr. to sl.	dry	Cleavage zone between 35-50 cm
59	Dolomite	Fr.	61/236	208	6-8	0	-	9	<1	Fr. to sl.	dry	
65	Dolomite	Fr.	72/254	311	8-10	1-2	Ca, MnO	6	1-2	Fr. to sl.	dry	
69	Dolomite	Fr.	70/19	Infinite	10-12	0	-	4	<1	Fr. to sl.	dry	
72	Dolomite	Fr.	84/263	1757	6-8	0-4	Cl, S	3	1-5	Sl. to mod.	Possibly before, moss in fracture	
146	Dolomite	Fr.	85/157	836	8-10	0	-	74	1-8	Fr. to sl.	dry	
210	Dolomite	Fr.	73/255	>800	12-14	0	-	64	1	Sl. to mod.	dry	
229	Dolomite	Fr.	79/18	622	8-10	0	-	19	<1	Fr.	dry	
245	Dolomite	Fr.	82/340	>900	14-16	0	-	16	1	Sl. to mod.	dry	
255	Dolomite	Fr.	86/94	Infinite	8-10	1-10	S	10	1-12	Sl. to mod.	Possibly before, moss in fracture	
304	Dolomite	Fr.	84/132	Infinite	10-12	0	-	49	1-3	Sl. to mod.	dry	
310	Dolomite	Flt.	89/308	>760	10-12	0	-	6	Open face	Fr. to sl.	dry	Slickensides/steps at 19/211, 20/220
330	Dolomite	Fr.	80/101	>1100	10-12	<1	MnO	20	1-4	Fr. to sl.	dry	
379	Dolomite	Fr.	74/193	>1400	6-8	<1	MnO	49	1	Fr. to sl.	dry	
446	Dolomite	Fr.	85/194	241	6-8	<1	MnO	67	<1	Fr. to sl.	dry	
455	Dolomite	Fr.	71/154	>640	6-8	0	-	9	<1	Fr.	dry	
544	Dolomite	Fr.	84/246	Infinite	8-10	0-4	MnO	89	1-9	Fr. to sl.	Possibly before, moss in fracture	
570	Dolomite	Fr.	83/274	>1110	10-12	0	-	26	<1	Fr.	dry	
599	Dolomite	Fr.	80/220	Infinite	8-10	<1	MnO	29	1-4	Fr. to sl.	dry	
628	Dolomite	Fr.	81/226	791	4-6	<1	MnO	29	<1	Fr. to sl.	dry	Almost completely healed
674	Dolomite	Fr.	29/332	773	4-6	<1	MnO	46	<1	Fr. to sl.	dry	
713	Dolomite	Fr.	52/202	187	8-10	0	-	39	<1	Fr.	dry	
726	Dolomite	Fr.	38/201	267	6-8	<1	MnO	13	<1	Fr.	dry	
730	Dolomite	Fr.	50/212	198	6-8	<1	MnO	4	<1	Fr.	dry	
779	Dolomite	Fr.	45/34	678	8-10	0	-	49	<1	Fr.	dry	
786	Dolomite	Fr.	83/228	Infinite	8-10	<1	S, MnO	7	1-4	Fr. to sl.	dry	
819	Dolomite	Fr.	62/275	634	6-8	<1	MnO	33	1-3	Fr. to sl.	dry	
1011	Dolomite	Fr.	86/225	Infinite	8-10	0	-	192	<1	Fr.	dry	
1077	Dolomite	Fr.	54/210	>1100	8-10	0	-	66	<1	Fr.	dry	
1100	End of scanline											

Notes:
1) Spacing measured is apparent spacing between previously measured fracture, not necessarily the previous joint from same joint set.
2) Bd. = Bedding, Flt. = Fault, Fr. = Fracture.
3) Coating/fillings explanations: Cl. = Clay, S. = Sand, Ca. = Calcite, MnO = Manganese Oxide
4) Weathering explanations: Fr. = Fresh, Sl. = Slightly weathered, Mod. = Moderately weathered
5) When taking measurements, tape measure was kept taut. Station locations were collected either by holding the tape directly against the rock, or holding an instrument perpendicular to the tape and touching the fractures, if the tape measure did not rest against the rock.
6) Cleavage distinguished from fractures by continuity, planarity, and depth.

Figure B-11 – Raw scanline data from Scanline 3

Linear Scanline 4 | Location (GPS): Start: 37.685093, -112.121216. End: 37.685187, -112.12113? | Date: 5/22/2020

Weather: Windy, 70s | Scientist: T. Reed | Orientation of Tape: 57° (NE), horizontal until sta. 600, when the scanline makes a bend to strike at 354° (N), then bends again at sta. 920 to strike at 57°, then bends again at sta. 1030 to strike at 354°, then bends one last time at sta. 1300 to strike at 57°

Station (cm)	Rock Type	Bd., Flt., or Fr.	Dip/Dip Direction (degrees)	Trace Length (mm)	Roughness (JRC)	Coating/Filling		Spacing (cm)	Aperture (mm)	Weathering	Moisture	Notes
						Thickness (mm)	Type					
66	Limestone	Fr.	89/266	Infinite	6-8	1-4	Cl, S	-	1-11	Sl.	dry	Filling likely washed down from above
185	Limestone	Fr.	38/214	584	6-8	0	-	119	<1	Fr.	dry	
206	Limestone	Fr.	41/242	749	4-6	0	-	21	<1	Fr.	dry	
210	Limestone	Fr.	86/235	Infinite	8-10	0	-	4	<1	Fr.	dry	
304	Limestone	Fr.	88/63	Infinite	4-6	<1	MnO	94	1	Fr. to sl.	dry	
310	Limestone	Fr.	32/313	Infinite	8-10	-	-	6	1	Fr.	dry	
345	Limestone	Fr.	58/77	811	6-8	0	-	35	<1	Fr. to sl.	dry	
391	Limestone	Fr.	38/265	609	4-6	0	-	46	<1	Fr.	dry	
435	Limestone	Fr.	47/216	>3000	8-10	>1	Ca, MnO	44	1	Sl. to mod.	Possibly before, moss in fracture	
486	Limestone	Fr.	52/227	278	6-8	0	-	51	1	Fr. to sl.	dry	
519	Limestone	Fr.	64/259	355	6-8	0	-	33	1-2	Fr. to sl.	dry	
520	Limestone	Fr.	85/95	190	8-10	0	-	1	1	Fr. to sl.	dry	
562	Limestone	Flt.	76/73	Infinite	14-16	1-2	Ca	42	1-23	Sl. to mod.	dry	No slickenlines, but slight offset
696	Limestone	Fr.	20/293	Infinite	6-8	0	-	134	1	Sl.	dry	visible on a cross-cutting crack (~20 mm.)
701	Limestone	Fr.	82/123	249	4-6	0	-	5	1	Fr. to sl.	dry	
775	Limestone	Fr.	53/230	354	4-6	0	-	74	<1	Fr.	dry	
807	Limestone	Fr.	70/245	401	6-8	0	-	32	<1	Fr.	dry	
830	Limestone	Fr.	83/238	Infinite	2-4	1	Ca	23	1	Sl.	dry	Fully healed in places
920	Limestone	Fr.	86/246	Infinite	8-10	1-4	Ca	90	1-20	Sl. to mod.	dry	
959	Limestone	Fr.	84/251	Infinite	8-10	1	Ca	39	1-25	Sl. to mod.	dry	
1029	Limestone	Fr.	67/151	>1000	6-8	1-2	Ca	70	1-2	Sl.	dry	Fully healed in places
1032	Limestone	Fr.	76/39	>490	10-12	0	-	3	1	Sl.	dry	
1036	Limestone	Fr.	48/322	>600	6-8	0	-	4	<1	Fr. to sl.	dry	
1057	Limestone	Fr.	36/339	205	6-8	0	-	21	<1	Fr. to sl.	dry	
1086	Limestone	Fr.	41/352	>560	6-8	0	-	29	<1	Fr. to sl.	dry	
1140	Limestone	Fr.	80/298	Infinite	2-4	1-2	Ca	54	1-2	Fr. to sl.	dry	
1150	Limestone	Fr.	45/250	Infinite	8-10	0	-	10	1	Fr. to sl.	dry	
1331	Limestone	Fr.	80/85	Infinite	8-10	0	-	181	1-2	Fr. to sl.	dry	
1355	Limestone	Fr.	67/60	664	6-8	1-3	Ca	24	1-5	Fr. to sl.	dry	
1385	Limestone	Fr.	68/41	1670	8-10	1-4	Ca	30	1-9	Fr. to sl.	dry	
1400	End of scanline											

Notes:
1) Spacing measured is apparent spacing between previously measured fracture, not necessarily the previous joint from same joint set.
2) Bd. = Bedding, Flt. = Fault, Fr. = Fracture.
3) Coating/fillings explanations: Cl. = Clay, S. = Sand, Ca. = Calcite, MnO = Manganese Oxide
4) Weathering explanations: Fr. = Fresh, Sl. = Slightly weathered, Mod. = Moderately weathered
5) When taking measurements, tape measure was kept taut. Station locations were collected either by holding the tape directly against the rock, or holding an instrument perpendicular to the tape and touching the fractures, if the tape measure did not rest against the rock.
6) Cleavage distinguished from fractures by continuity, planarity, and depth.

Figure B-12 – Raw scanline data from Scanline 4

Linear Scanline	Location (GPS):	Start: 37.686107, -112.118195. End: 37.686052, -112.11803			Date:	5/22/2020						
5	Weather:	Sunny, 40s	Scientist:	T. Reed	Orientation of Tape:		89° (E), horizontal					

Station (cm)	Rock Type	Bd., Flt., or Fr.	Dip/Dip Direction (degrees)	Trace Length (mm)	Roughness (JRC)	Coating/Filling		Spacing (cm)	Aperture (mm)	Weathering	Moisture	Notes
						Thickness (mm)	Type					
33	Limestone	Flt.	82/225	Infinite	6-8	0	-	-	1-2	Fr. to sl.	dry	Fracture ends before bottom
35	Limestone	Cleavage	86/223	158	8-10	0	-	2	<1	Fr.	dry	of outcrop, but cannot see
37	Limestone	Cleavage	82/210	91	8-10	0	-	2	<1	Fr.	dry	terminus at top
40	Limestone	Cleavage	82/215	266	8-10	<1	Ca	3	<1	Fr.	dry	CaCO3 vein
45	Limestone	Cleavage	85/226	145	8-10	0	-	5	<1	Fr.	dry	
47	Limestone	Cleavage	89/224	141	8-10	0	-	2	<1	Fr.	dry	
64	Limestone	Fr.	57/64	712	10-12	0	-	17	<1	Fr.	dry	
70	Limestone	Fr.	43/1	608	10-12	0	-	6	<1	Fr.	dry	
74	Limestone	Flt.	83/239	>2400	6-8	0	-	4	1-2	Fr. to sl.	dry	Smooth surface, pitting, no
84	Limestone	Cleavage	41/62	380	8-10	0	-	10	<1	Fr.	dry	visible slickenlines or evident
95	Limestone	Cleavage	80/82	168	6-8	0	-	11	<1	Fr.	dry	separation because materials
98	Limestone	Cleavage	78/80	79	8-10	0	-	3	<1	Fr.	dry	are the same on either side
104	Limestone	Cleavage	76/70	329	8-10	0	-	6	<1	Fr.	dry	
112	Limestone	Cleavage	60/66	115	8-10	0	-	8	<1	Fr.	dry	
115	Limestone	Fr.	70/249	695	6-8	0	-	3	1	Fr.	dry	
120	Limestone	Cleavage	74/156	133	6-8	0	-	5	<1	Fr.	dry	
131	Limestone	Fr.	72/82	643	6-8	0	-	11	1	Fr.	dry	
160	Limestone	Fr.	87/170	>990	8-10	2-4	S	29	2-17	Sl. to mod.	Possibly before, moss in fracture	
205	Limestone	Fr.	78/258	708	6-8	1-2	MnO	45	1-2	Sl. to mod.	Possibly before, lichen in fracture	
250	Limestone	Fr.	-	-	-	-	-	-	-	-	-	Same fracture as at sta. 160
253	Limestone	Fr.	74/105	>1480	4-6	0	-	3	<1	Fr.	dry	
257	Limestone	Fr.	-	-	-	-	-	-	-	-	-	Same fracture as at sta. 160
274	Limestone	Fr.	70/150	541	8-10	0	-	17	<1	Fr.	dry	Sta. 260-375 - cleavage zone
460	Limestone	Fr.	80/260	Infinite	8-10	0-2	S	186	1-5	Sl. to mod.	Possibly before, moss in fracture	
507	Limestone	Fr.	73/246	Infinite	6-8	0	-	47	<1	Fr.	dry	
680	Limestone	Fr.	76/245	1071	4-6	0	-	173	<1	Fr.	dry	
744	Limestone	Fr.	82/172	>280	6-8	0	-	64	<1	Fr.	dry	
751	Limestone	Fr.	89/280	>310	6-8	0	-	7	<1	Fr.	dry	
771	Limestone	Fr.	84/221	>1120	6-8	0	-	20	<1	Fr.	dry	
807	Limestone	Fr.	61/145	211	4-6	0	-	36	1-3	Fr.	dry	
817	Limestone	Fr.	74/175	144	4-6	0	-	10	1	Fr.	dry	
826	Limestone	Fr.	85/75	498	4-6	0	-	9	<1	Fr.	dry	
866	Limestone	Fr.	73/279	611	4-6	0	-	40	<1	Fr.	dry	
896	Limestone	Fr.	87/174	Infinite	6-8	0	-	30	<1	Fr.	dry	Obscured into wall
929	Limestone	Fr.	86/229	270	8-10	0	-	33	Open face	Fr.	dry	
946	Limestone	Fr.	43/267	521	4-6	0	-	17	<1	Fr.	dry	
1039	Limestone	Fr.	87/256	Infinite	6-8	1-4	Ca	93	2-16	Fr.	Possibly before, moss in fracture	
1052	Limestone	Fr.	34/311	426	4-6	0	-	13	<1	Fr.	dry	
1076	Limestone	Fr.	39/315	Infinite	4-6	0	-	24	<1	Fr.	dry	
1099	Limestone	Fr.	33/296	1561	4-6	0	-	23	<1	Fr.	dry	
1120	Limestone	Fr.	34/305	666	4-6	0	-	21	<1	Fr.	dry	
1140	Limestone	Fr.	81/174	>1320	6-8	1		20	1-2	Fr.	Possibly before, lichen in fracture	
1215	Limestone	Fr.	82/146	Infinite	8-10	0	-	75	Open face	Fr.	dry	Sta. 1140-1210 - cleavage zone
1320	Limestone	Fr.	83/236	Infinite	8-10	0	-	105	Open face	Fr.	dry	
1346	Limestone	Fr.	89/145	>4000	4-6	0	-	26	Open face	Fr.	dry	

Figure B-13 – Raw scanline data from Scanline 5

1425	Limestone	Fr.	78/167	596	4-6	0	-	79	<1	Fr.	dry	Calcite vein, almost fully healed
1460	Limestone	Flt.	89/203	>3000	8-10	1		35	1-4	Fr. to sl.	dry	Either slickenlines or CaCO3 crystals
1500	End of scanline											

Notes: 1) Spacing measured is apparent spacing between previously measured fracture, not necessarily the previous joint from same joint set.
2) Bd. = Bedding, Flt. = Fault, Fr. = Fracture.
3) Coating/fillings explanations: Cl. = Clay, S. = Sand, Ca. = Calcite, MnO = Manganese Oxide
4) Weathering explanations: Fr. = Fresh, Sl. = Slightly weathered, Mod. = Moderately weathered
5) When taking measurements, tape measure was kept taut. Station locations were collected either by holding the tape directly against the rock, or holding an instrument perpendicular to the tape and touching the fractures, if the tape measure did not rest against the rock.
6) Cleavage distinguished from fractures by continuity, planarity, and depth.

Figure B-14 – Raw scanline data from Scanline 5 (cont'd.)

APPENDIX C

Appendix C includes historic rockfall information from UDOT maintenance personnel, along with photographs of boulders that have become dislodged from the slope, and are representative of sizes of rocks that could be expected in potential future rockfall events.

Rockfall Historical Information

Question (from Tomsen Reed, Gerhart Cole) / Answer (from Gary Spencer, UDOT)

1) Q: How often have rockfalls needed to be cleaned off the road through our proposed project boundaries?
A: Rockfalls usually only occur during storm events or springtime thaw. We are called out for rocks on roadway usually between 6 to 8 times annually but some are cleaned off with snow plow operations.

2) Q: How large have the largest rockfalls been (or if they just have some qualitative records on rockfalls cleanup, could we have access to those records just to get an idea for ourselves what the rock sizes have been like)?
A: Rockfalls are usually small with just a few individual rocks, less than ten and usually less than 12" diameter but occasionally larger rocks have fallen but are usually contained in the cut ditch.

3) Q: Have any rockfalls traveled into the far lane of traffic?
A: Seldom, maybe once or twice annually

4) Q: Where along the project alignment have the most frequent rockfalls happened?
A: Most rockfalls occur between MP 15.2 and MP 15.4 but have occurred almost the entire length of the project.

5) Q: Have any rockfalls damaged the pavement?
A: I have not seen any pavement damage due to rockfalls in this section,26 years.

Figure C-1 – Historical rockfall information, from Gary Spencer, UDOT Region 4 Maintenance

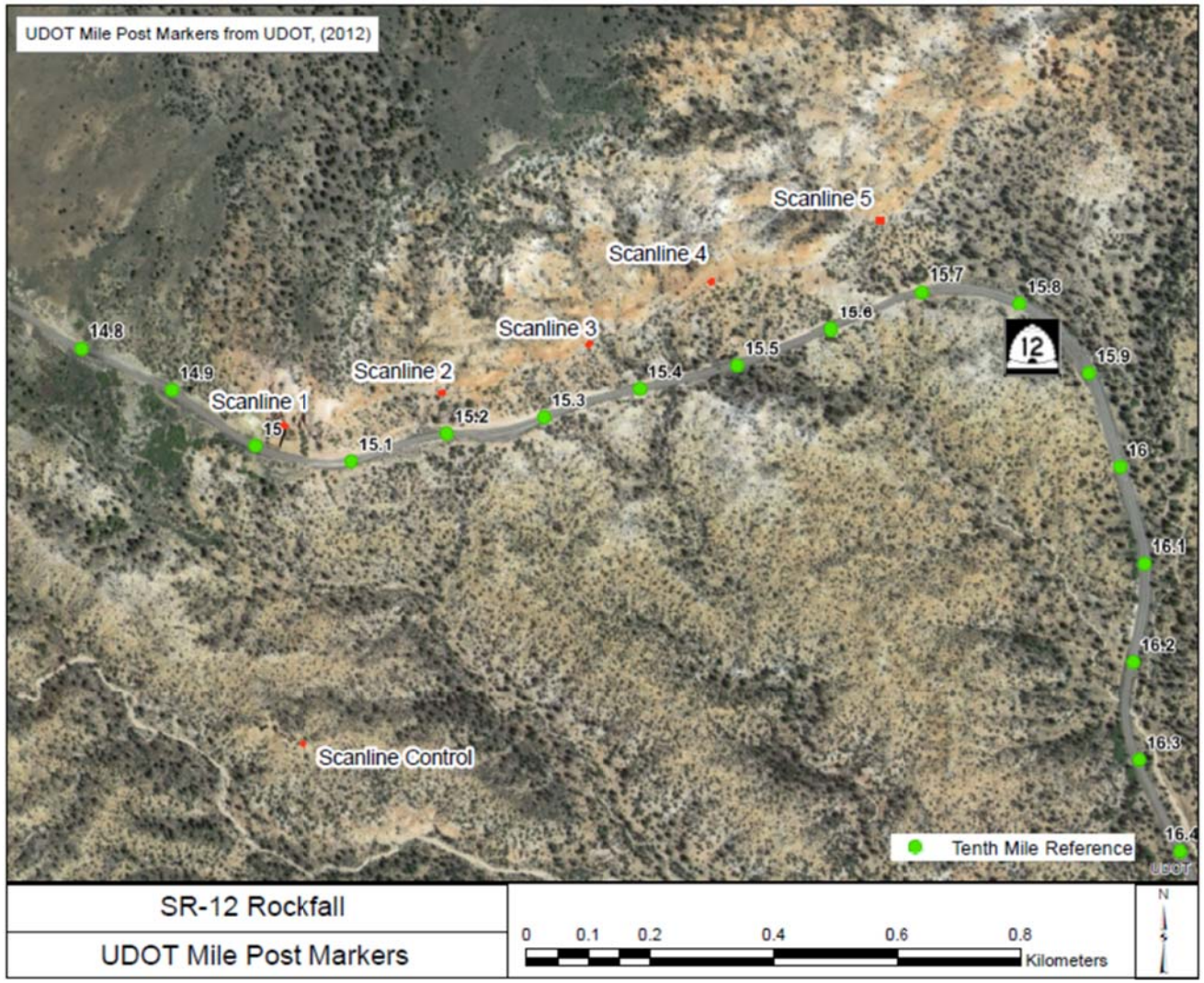

Figure C-2 – UDOT Mile post marker locations with respect to the project alignment

Figure C-3 – Photo of boulder found during field studies, indicating both the size of potential rockfall blocks and the potential for blocks with dissolution cleavage to still release in a larger mass

Figure C-4 – Large boulders partially embedded in the slope near Scanline 4

Figure C-5 – Very large boulder partially embedded in slope

Figure C-6 – Large boulder sitting on top of slope

Figure C-7 – Large boulder at roadway level between Scanlines 2 and 3, new as of Spring 2020, appears to have been pushed off the road or shoulder

Figure C-8 – Additional photograph of the new boulder shown in C-7

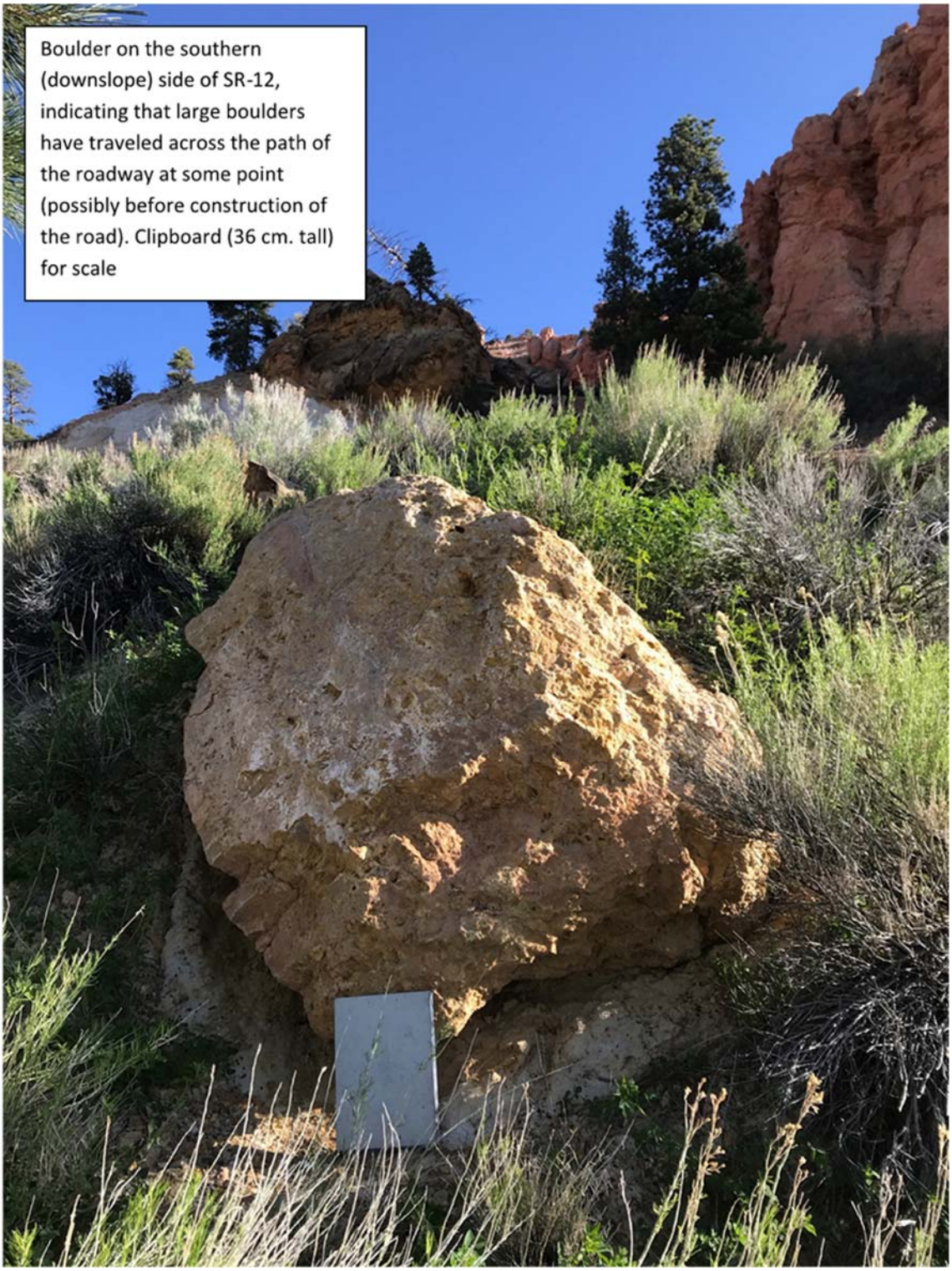

Figure C-9 – Photograph of boulder below highway level

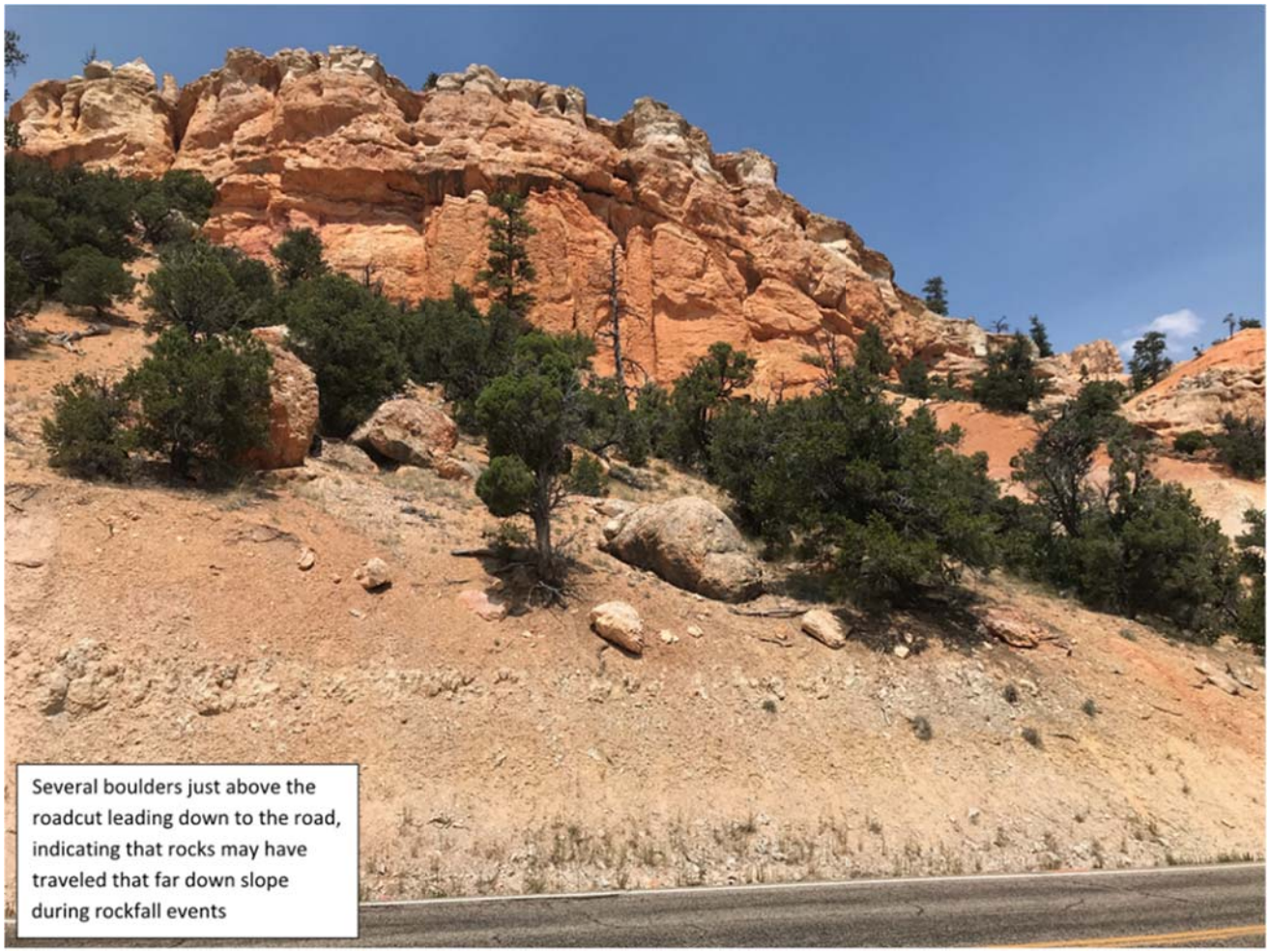

Figure C-10 – Photograph of boulders sitting just above the roadway cut, between Scanlines 4 and 5

Figure C-11 – Photograph of large (up to 15-meter diameter) blocks that have detached from the main cliff band

APPENDIX D

Appendix D presents the inputs and results for the kinematic analysis at each scanline. Critical intersections are plotted on the printouts, but the remaining intersections are not plotted, for clarity. However, the number of total intersections is displayed on the legend of the printouts (Appendix D).

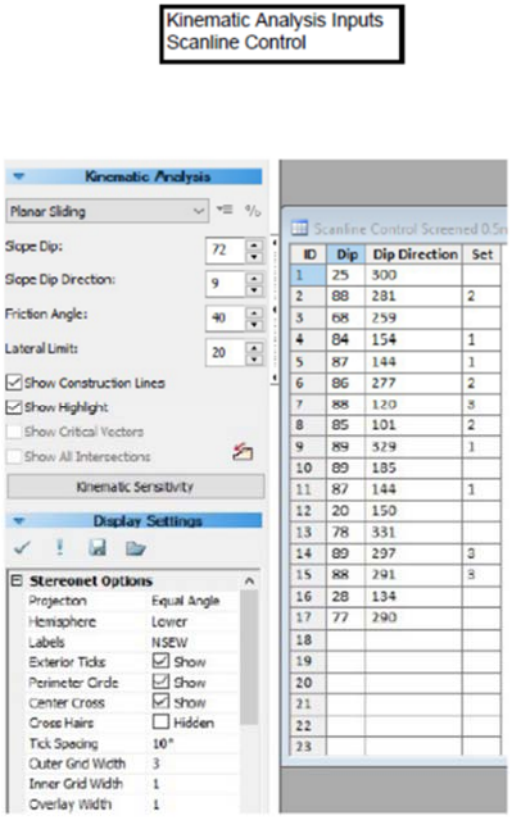

Figure D-1 – Inputs for the kinematic analysis performed at the control scanline

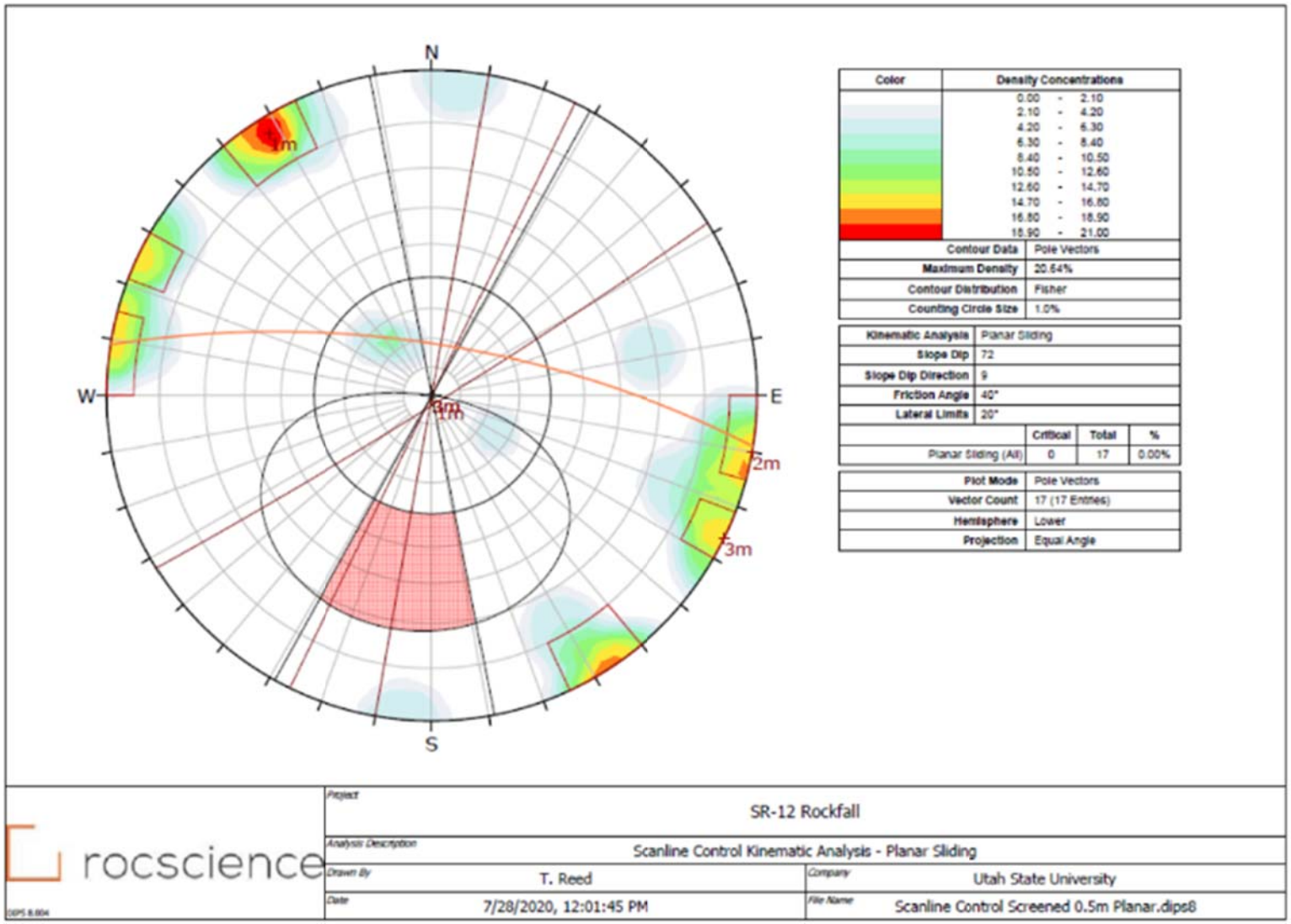

Figure D-2 – Planar sliding kinematic analysis at the control scanline

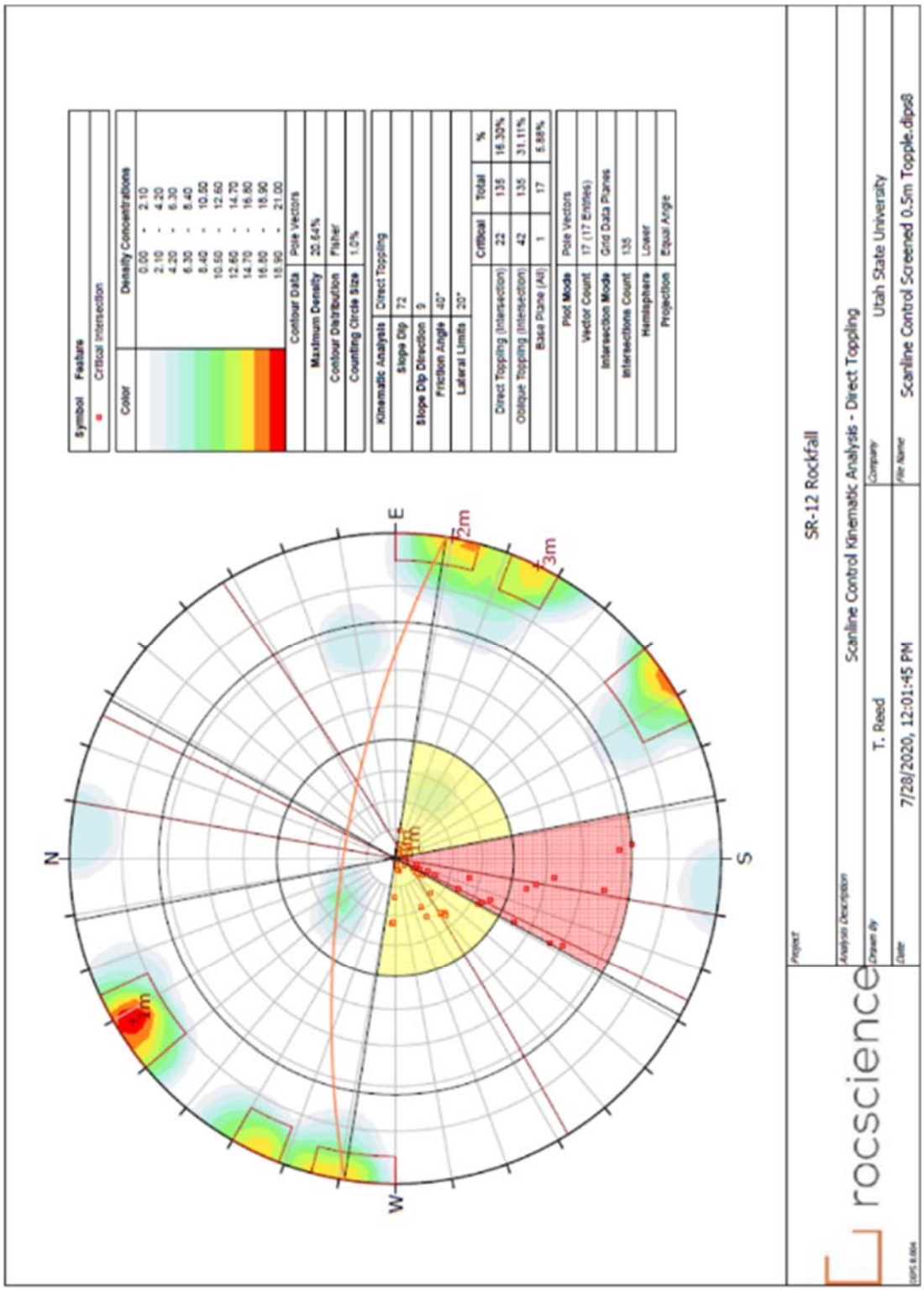

Figure D-3 – Direct toppling kinematic analysis at the control scanline

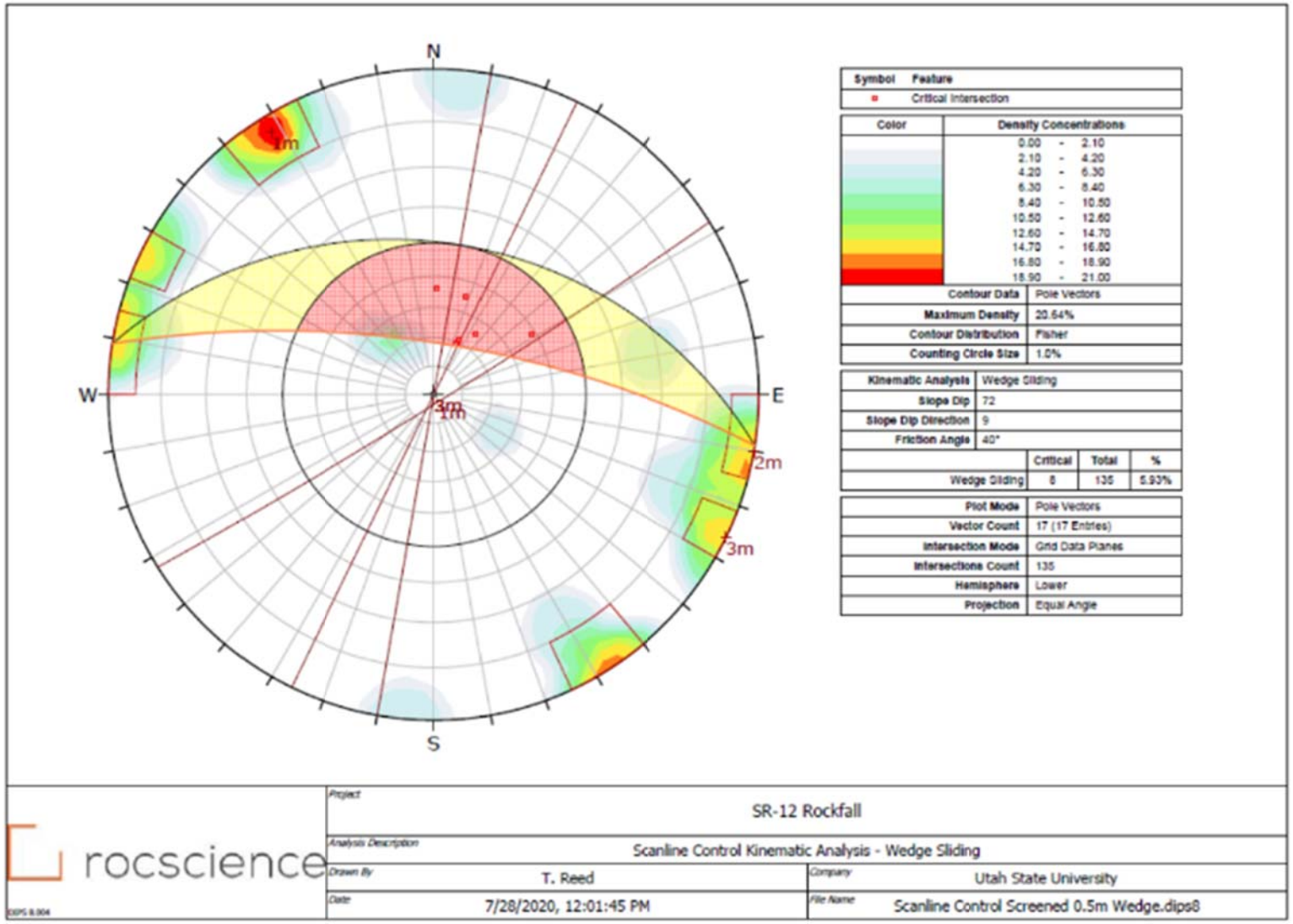

Figure D-4 – Wedge sliding kinematic analysis at the control scanline

Kinematic Analysis Inputs
Scanline 1

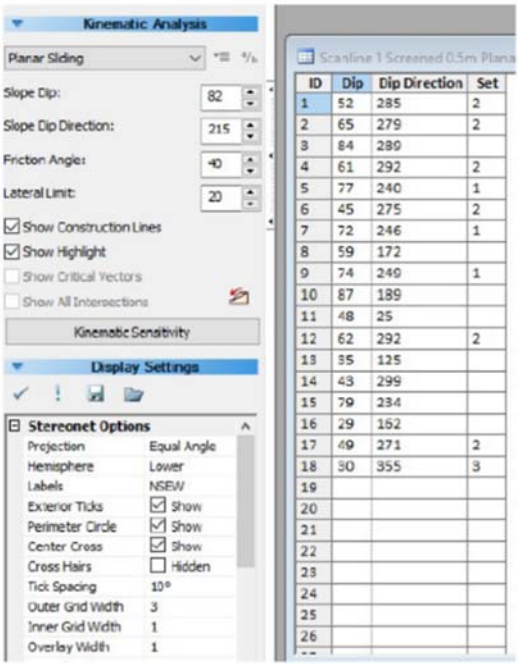

ID	Dip	Dip Direction	Set
1	52	285	2
2	65	279	2
3	84	289	
4	61	292	2
5	77	240	1
6	45	275	2
7	72	246	1
8	59	172	
9	74	249	1
10	87	189	
11	48	25	
12	62	292	2
13	35	125	
14	43	299	
15	79	234	
16	29	162	
17	49	271	2
18	30	355	3
19			
20			
21			
22			
23			
24			
25			
26			

Figure D-5 – Inputs for the kinematic analysis performed at Scanline 1

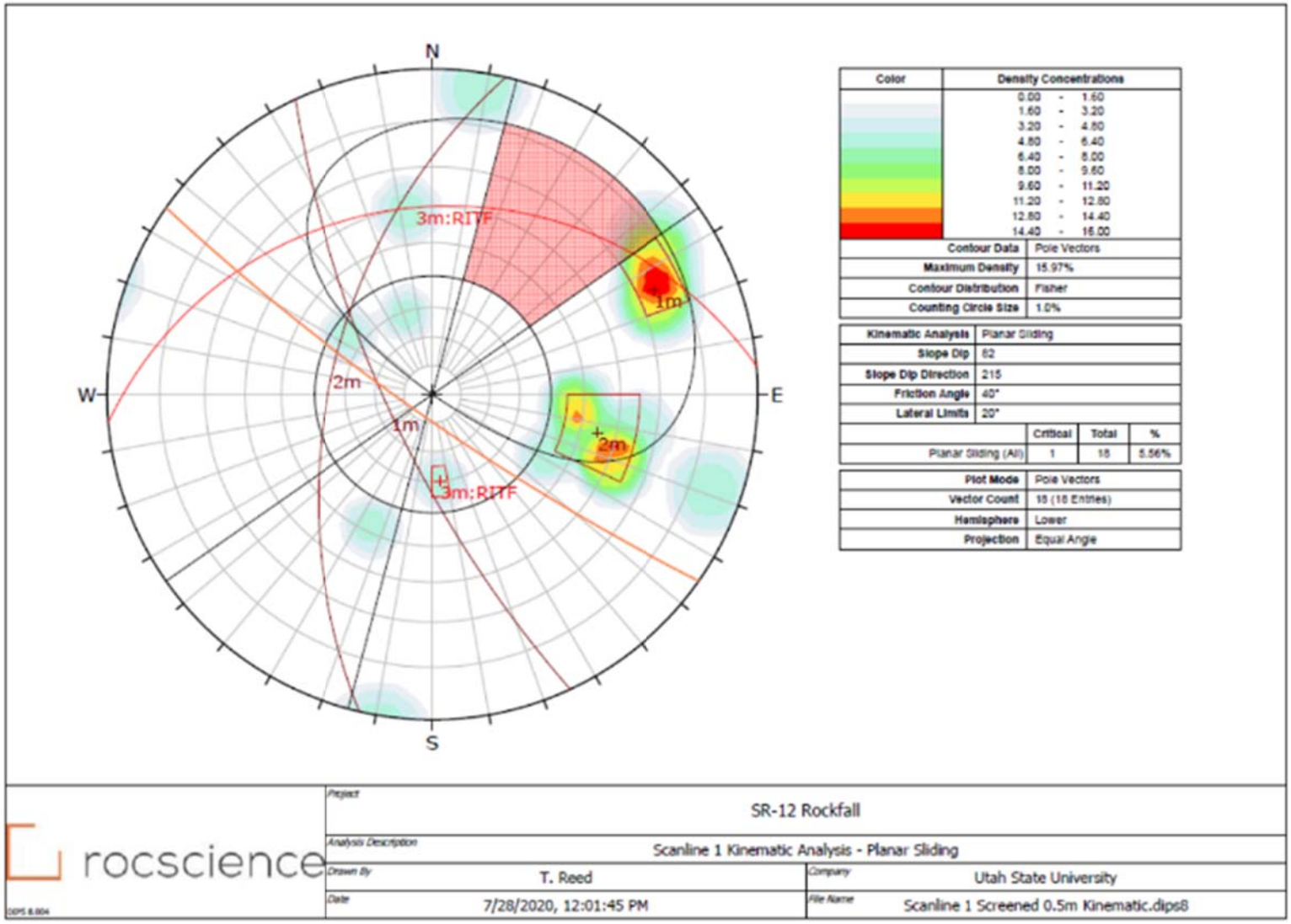

Figure D-6 – Planar sliding kinematic analysis at Scanline 1

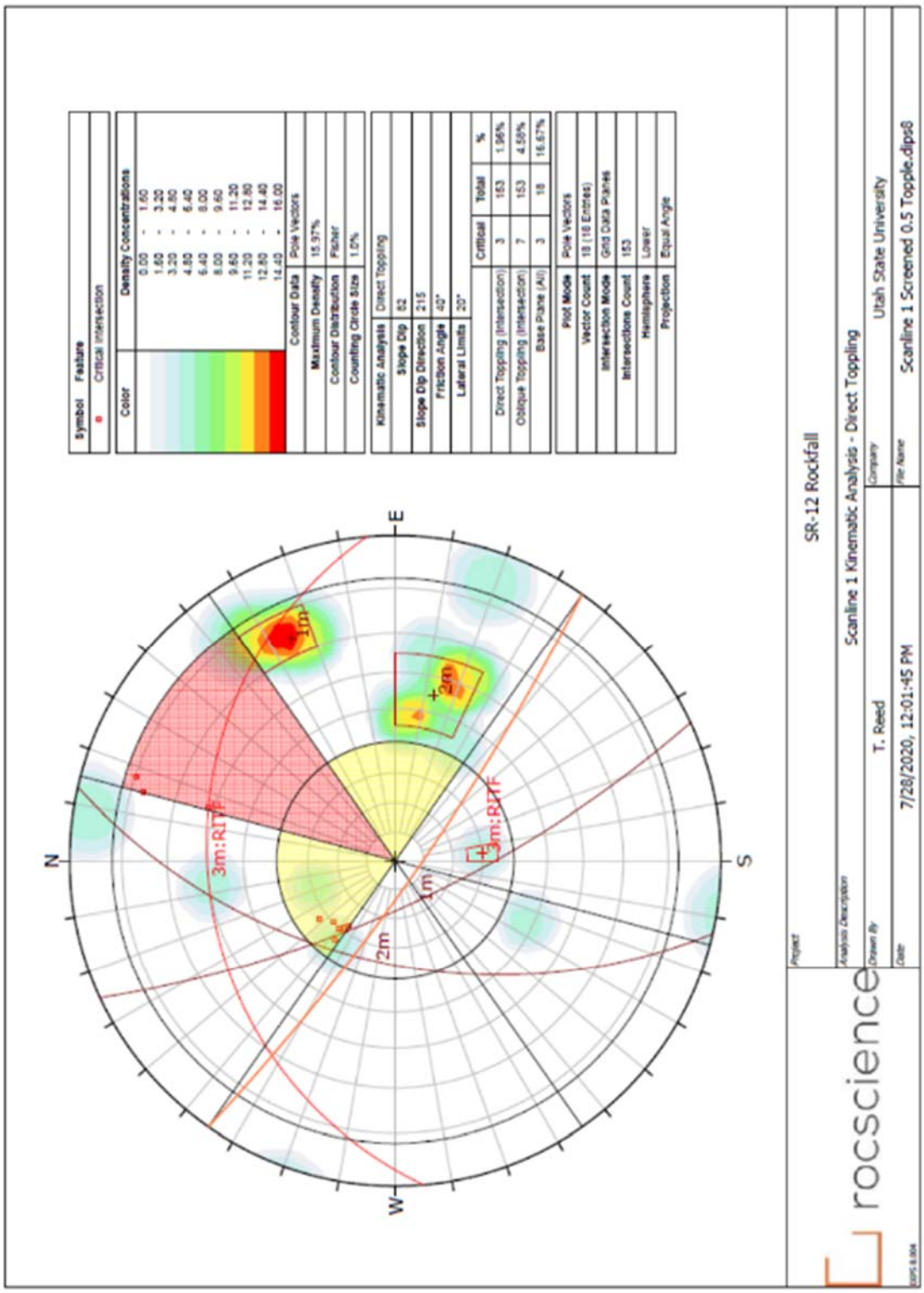

Figure D-7 – Direct toppling kinematic analysis at Scanline 1

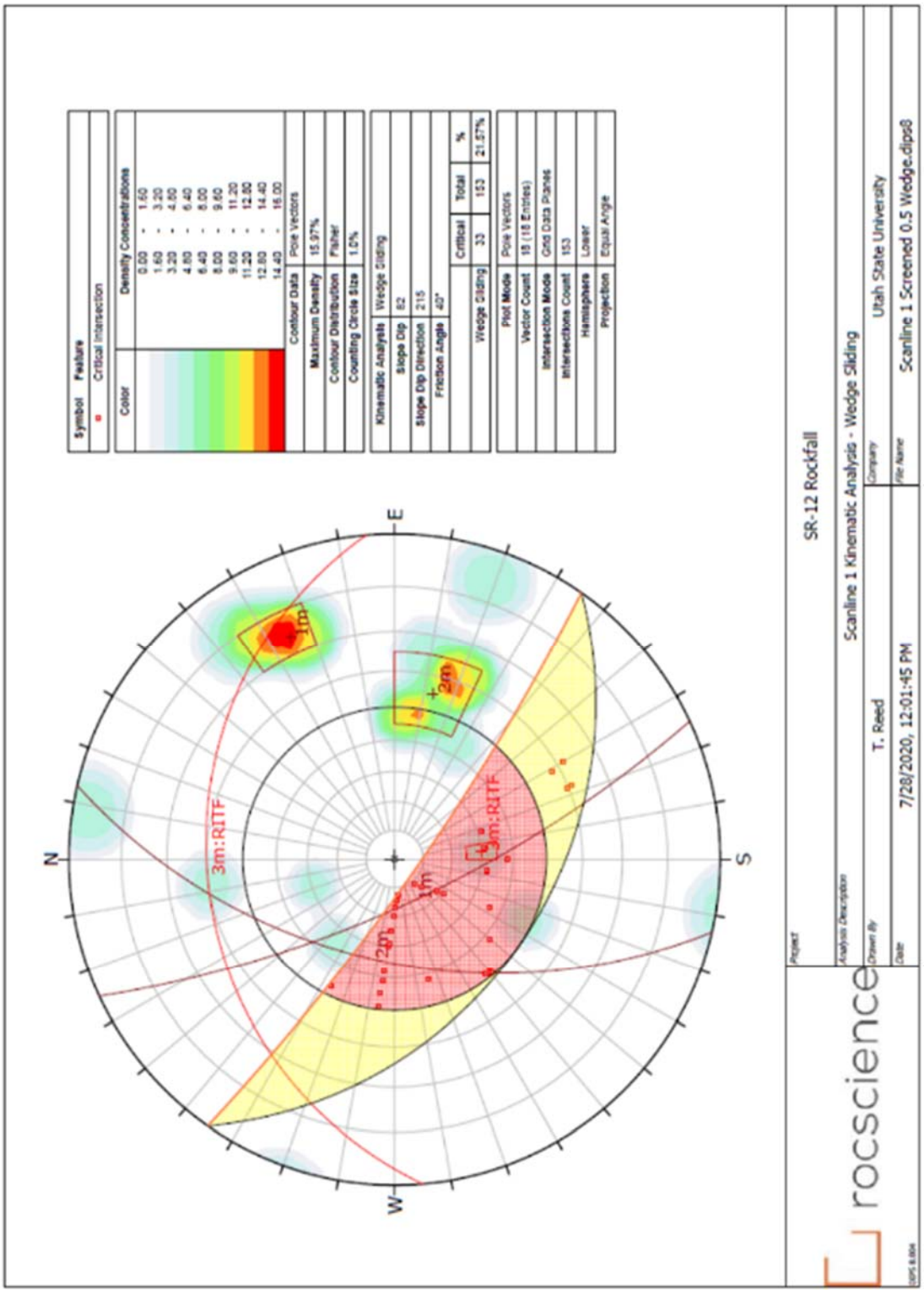

Figure D-8 – Wedge sliding kinematic analysis at Scanline 1

Kinematic Analysis Inputs
Scanline 2

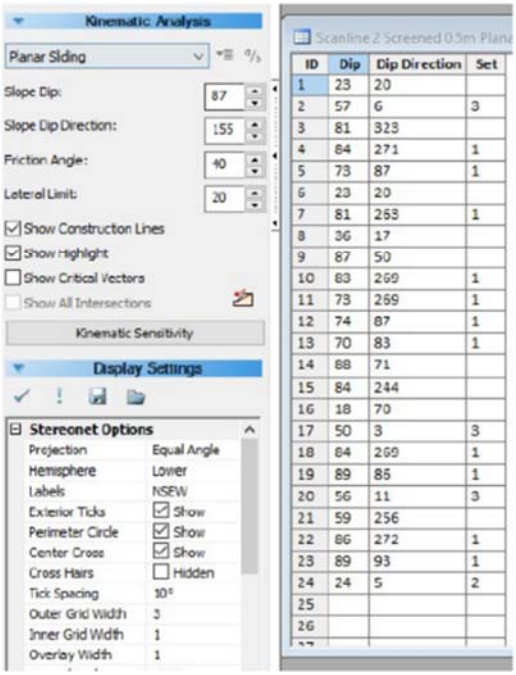

ID	Dip	Dip Direction	Set
1	23	20	
2	57	6	3
3	81	323	
4	84	271	1
5	73	87	1
6	23	20	
7	81	253	1
8	36	17	
9	87	50	
10	83	269	1
11	73	269	1
12	74	87	1
13	70	83	1
14	88	71	
15	84	244	
16	18	70	
17	50	3	3
18	84	269	1
19	89	85	1
20	56	11	3
21	59	256	
22	86	272	1
23	89	93	1
24	24	5	2
25			
26			

Figure D-9 – Inputs for the kinematic analysis performed at Scanline 2

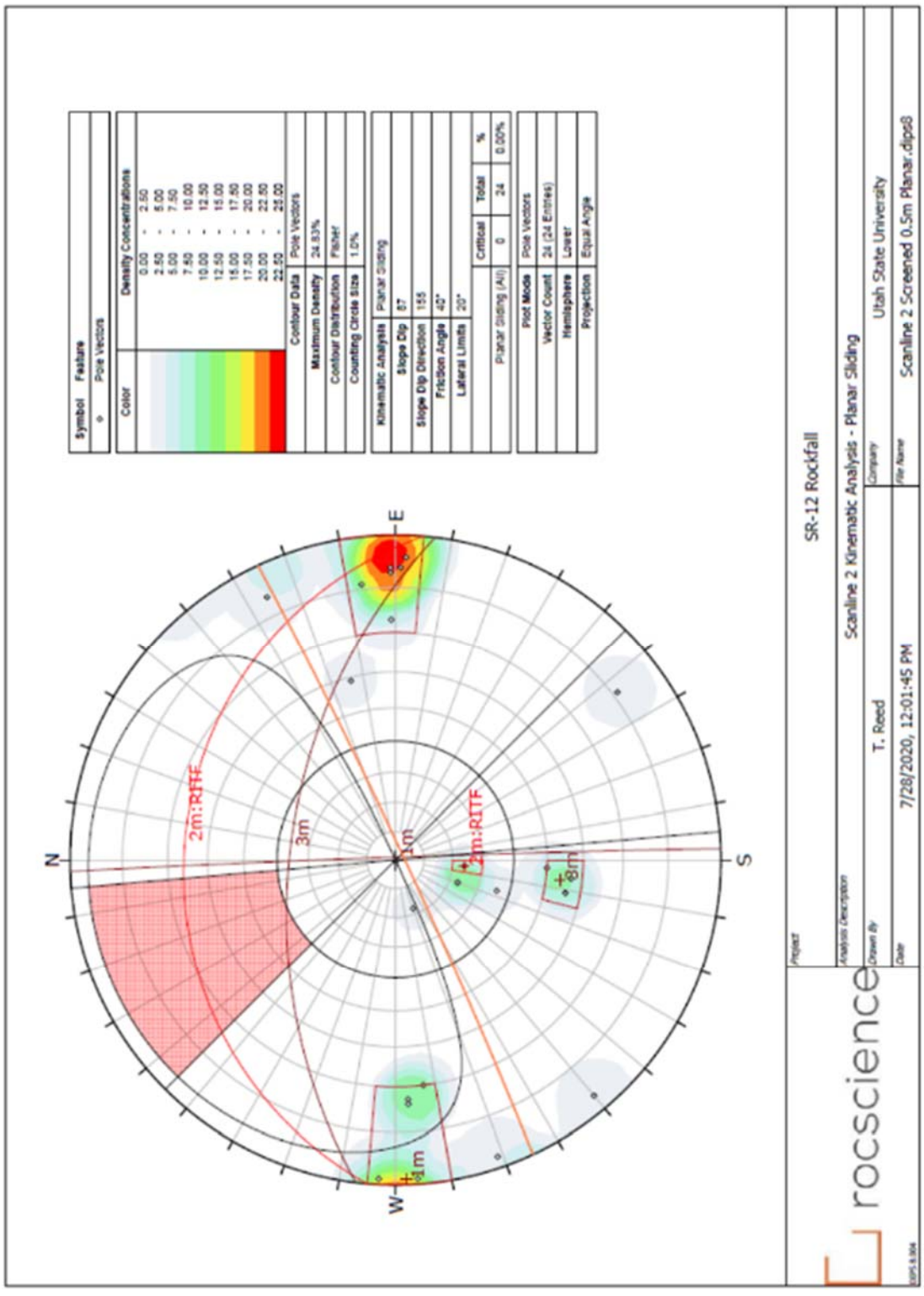

Figure D-10 – Planar sliding kinematic analysis at Scanline 2

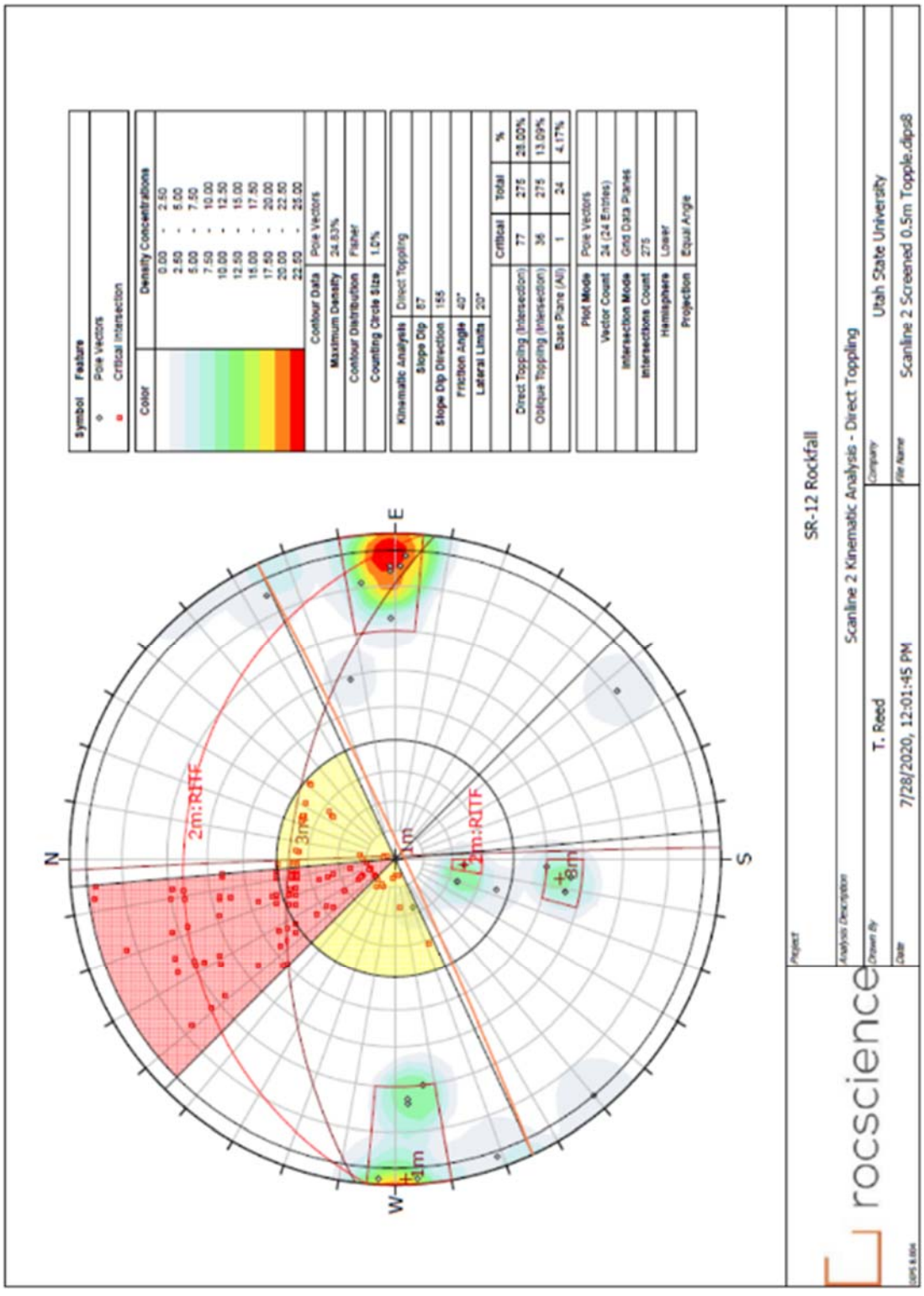

Figure D-11 – Direct toppling kinematic analysis at Scanline 2

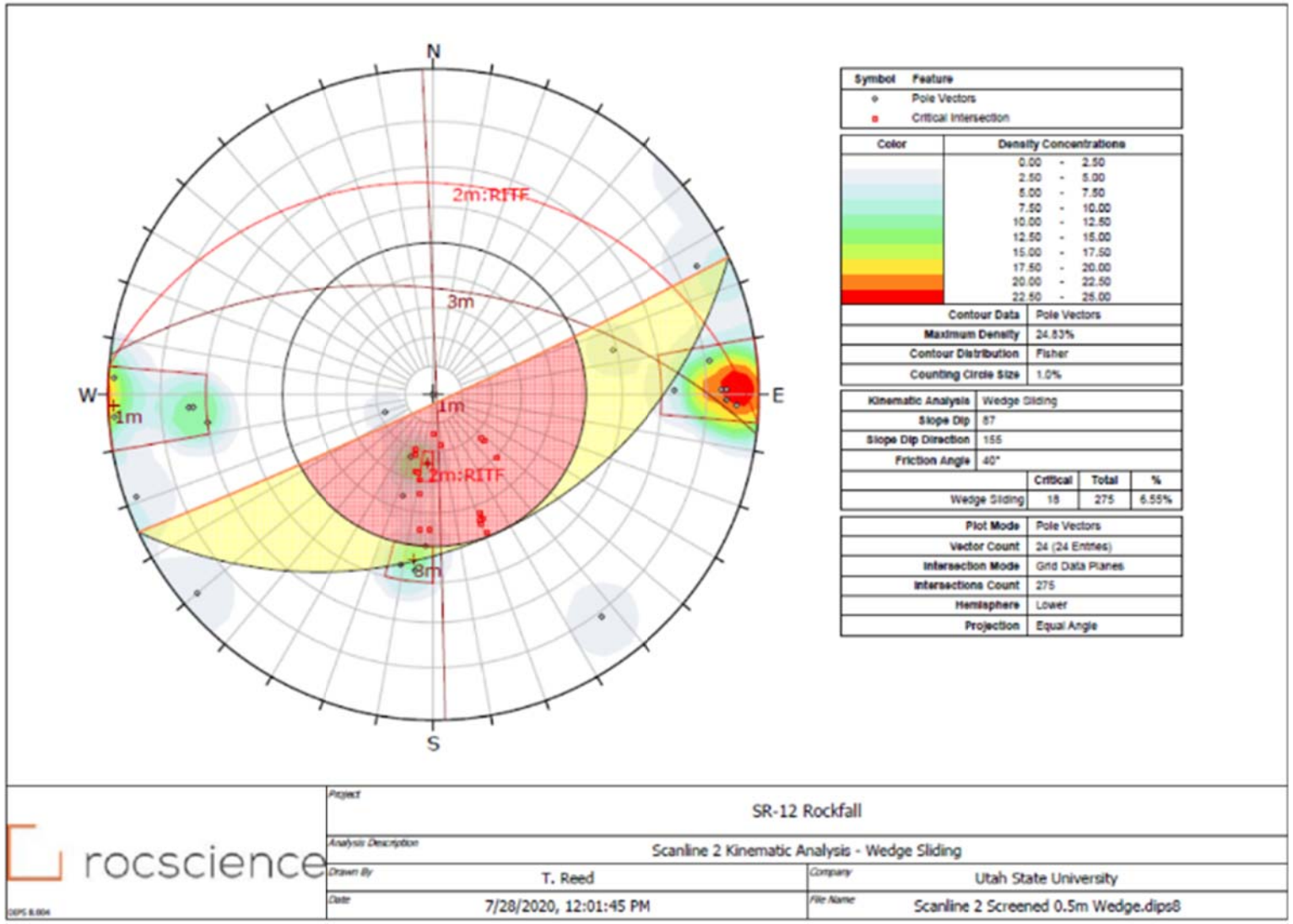

Figure D-12 – Wedge sliding kinematic analysis at Scanline 2

Kinematic Analysis Inputs
Scanline 3

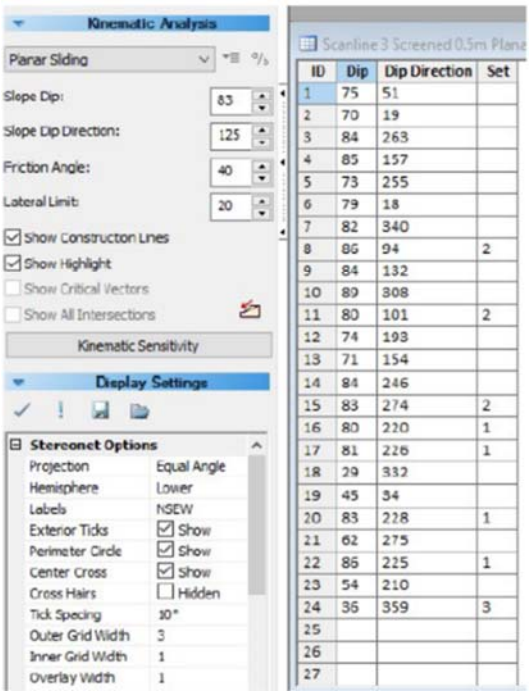

ID	Dip	Dip Direction	Set
1	75	51	
2	70	19	
3	84	263	
4	85	157	
5	73	255	
6	79	18	
7	82	340	
8	86	94	2
9	84	132	
10	89	308	
11	80	101	2
12	74	193	
13	71	154	
14	84	246	
15	83	274	2
16	80	220	1
17	81	226	1
18	29	332	
19	45	54	
20	83	228	1
21	62	275	
22	86	225	1
23	54	210	
24	36	359	3
25			
26			
27			

Figure D-13 – Inputs for the kinematic analysis performed at Scanline 3

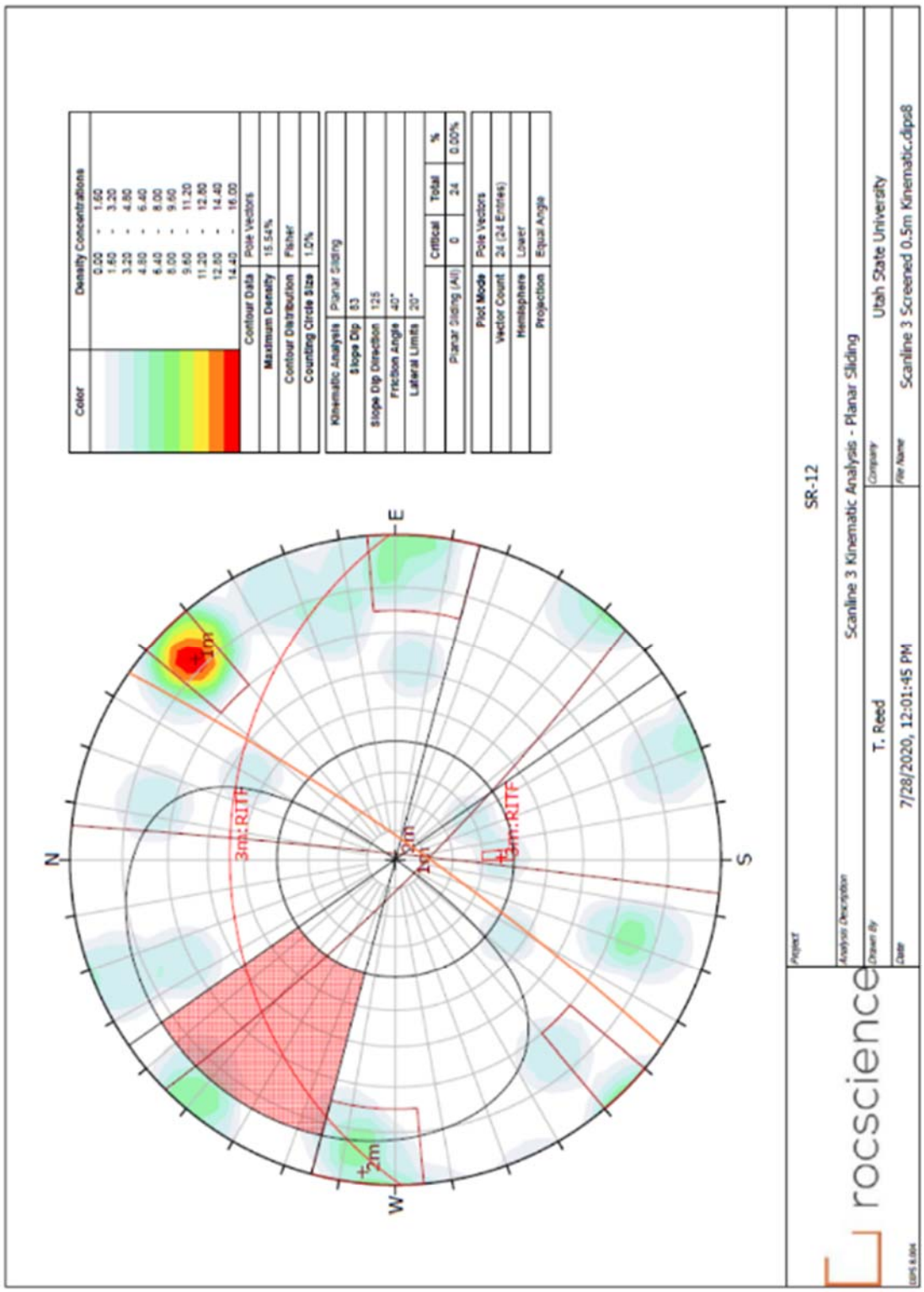

Figure D-14 – Planar sliding kinematic analysis at Scanline 3

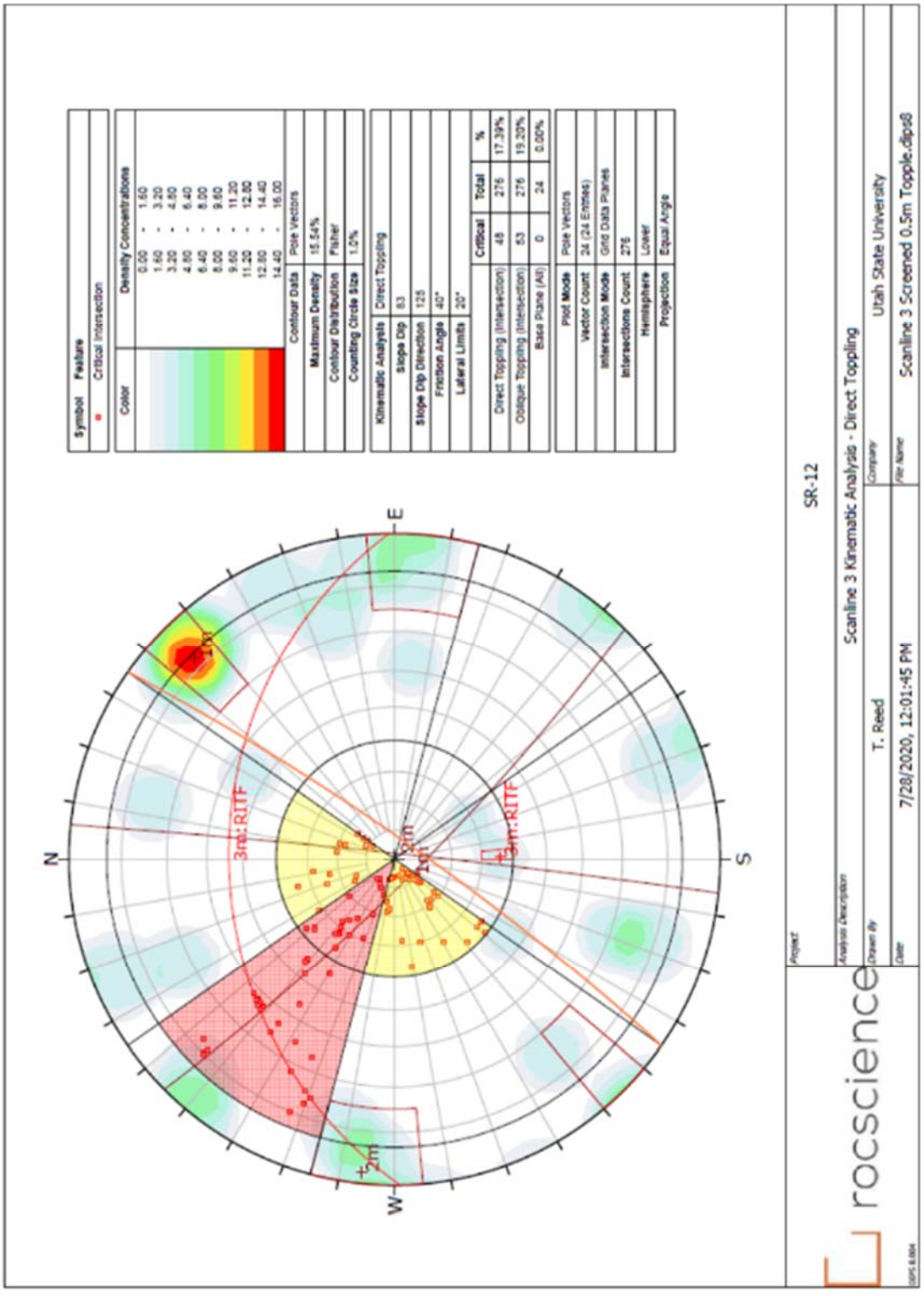

Figure D-15 – Direct toppling kinematic analysis at Scanline 3

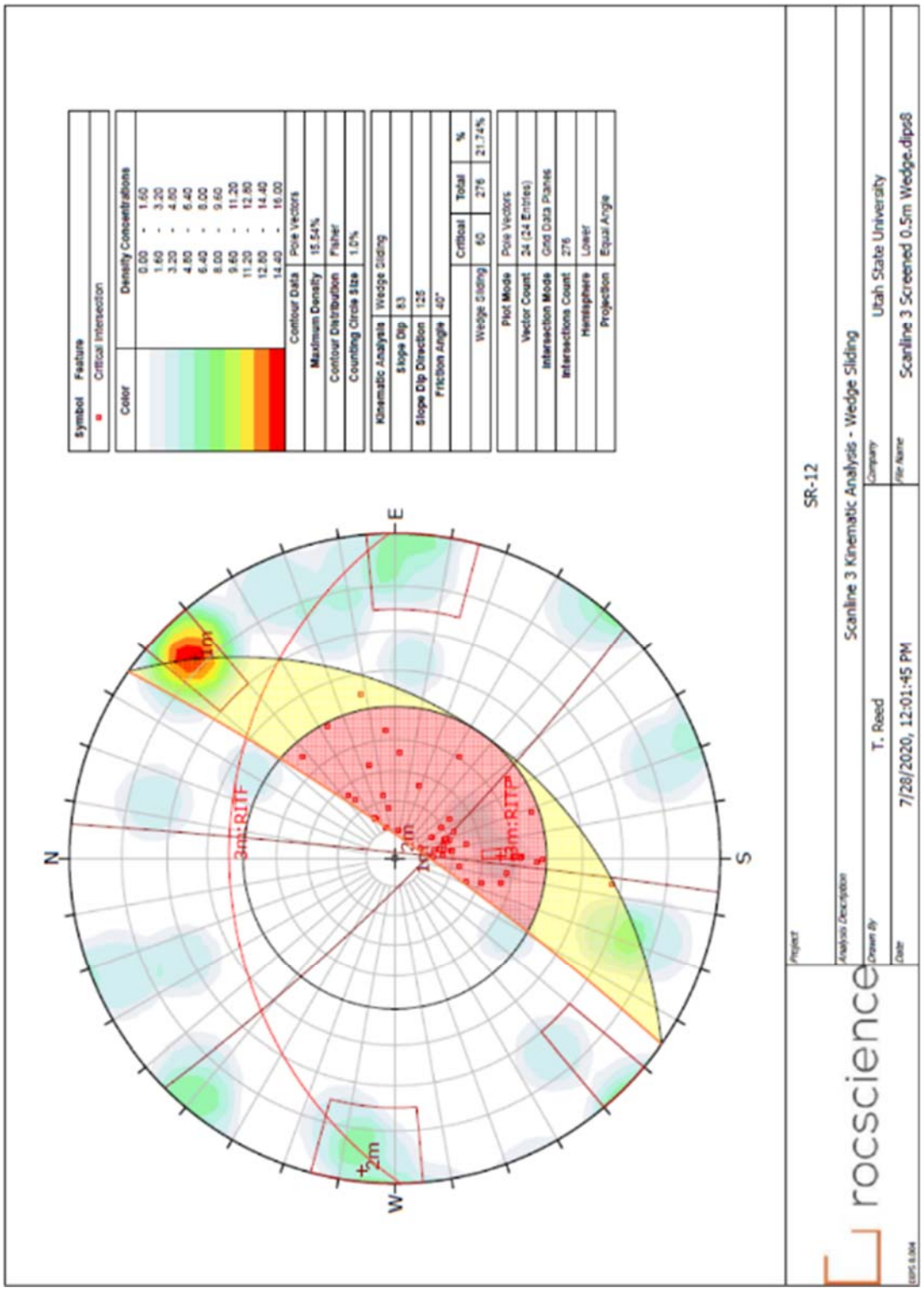

Figure D-16 – Wedge sliding kinematic analysis at Scanline 3

Kinematic Analysis Inputs
Scanline 4

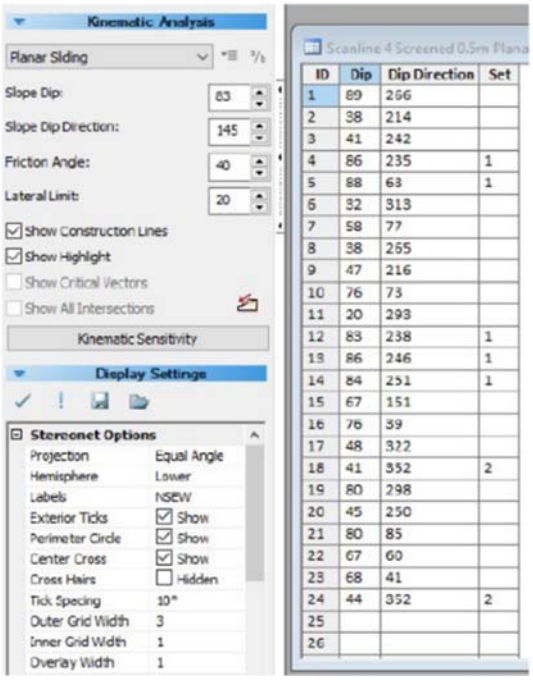

ID	Dip	Dip Direction	Set
1	89	266	
2	38	214	
3	41	242	
4	86	235	1
5	88	63	1
6	32	313	
7	58	77	
8	38	255	
9	47	216	
10	76	73	
11	20	293	
12	83	238	1
13	86	246	1
14	84	251	1
15	67	151	
16	76	39	
17	48	322	
18	41	352	2
19	80	298	
20	45	250	
21	80	85	
22	67	60	
23	68	41	
24	44	352	2
25			
26			

Figure D-17 – Inputs for the kinematic analysis performed at Scanline 4

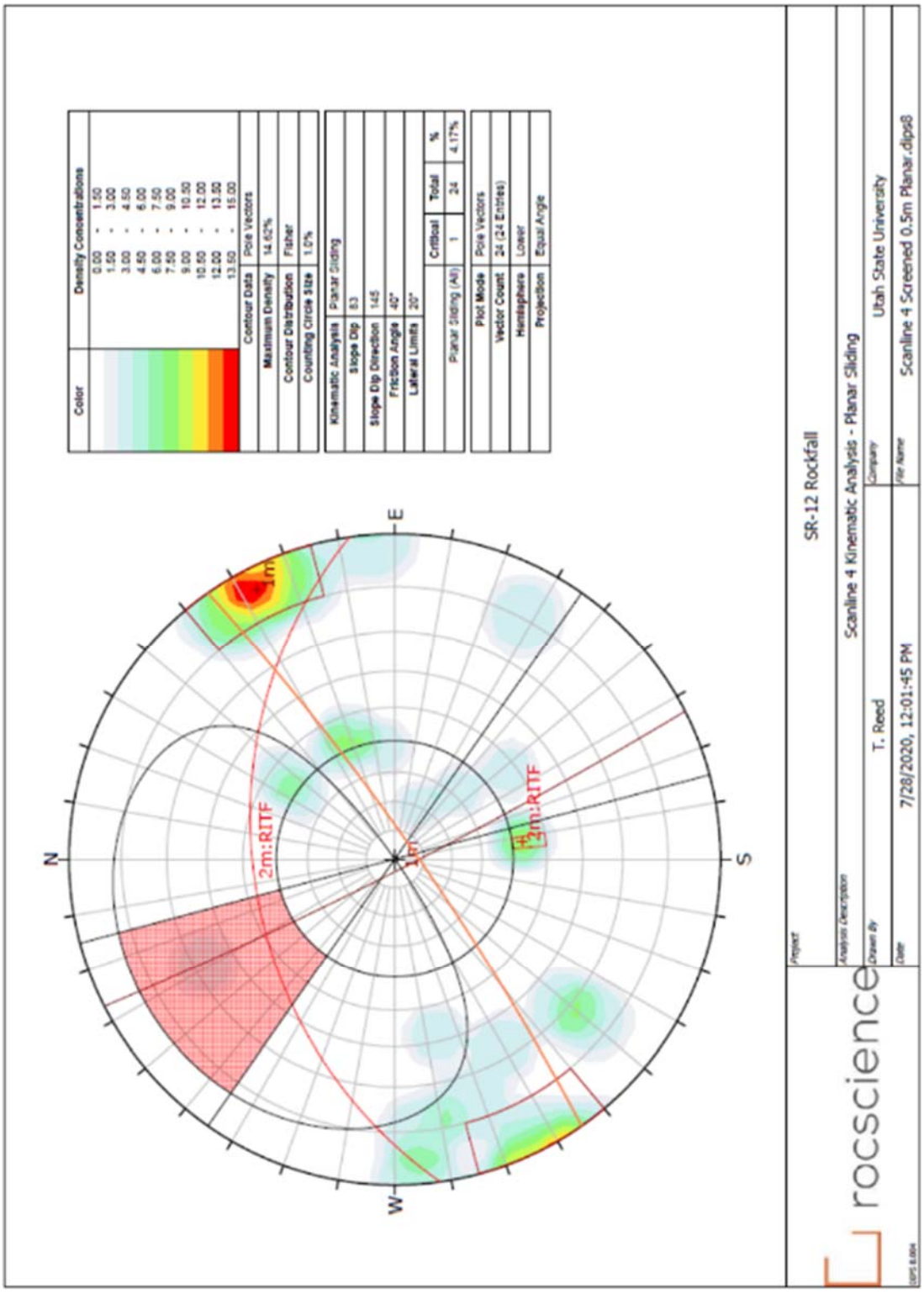

Figure D-18 – Planar sliding kinematic analysis at Scanline 4

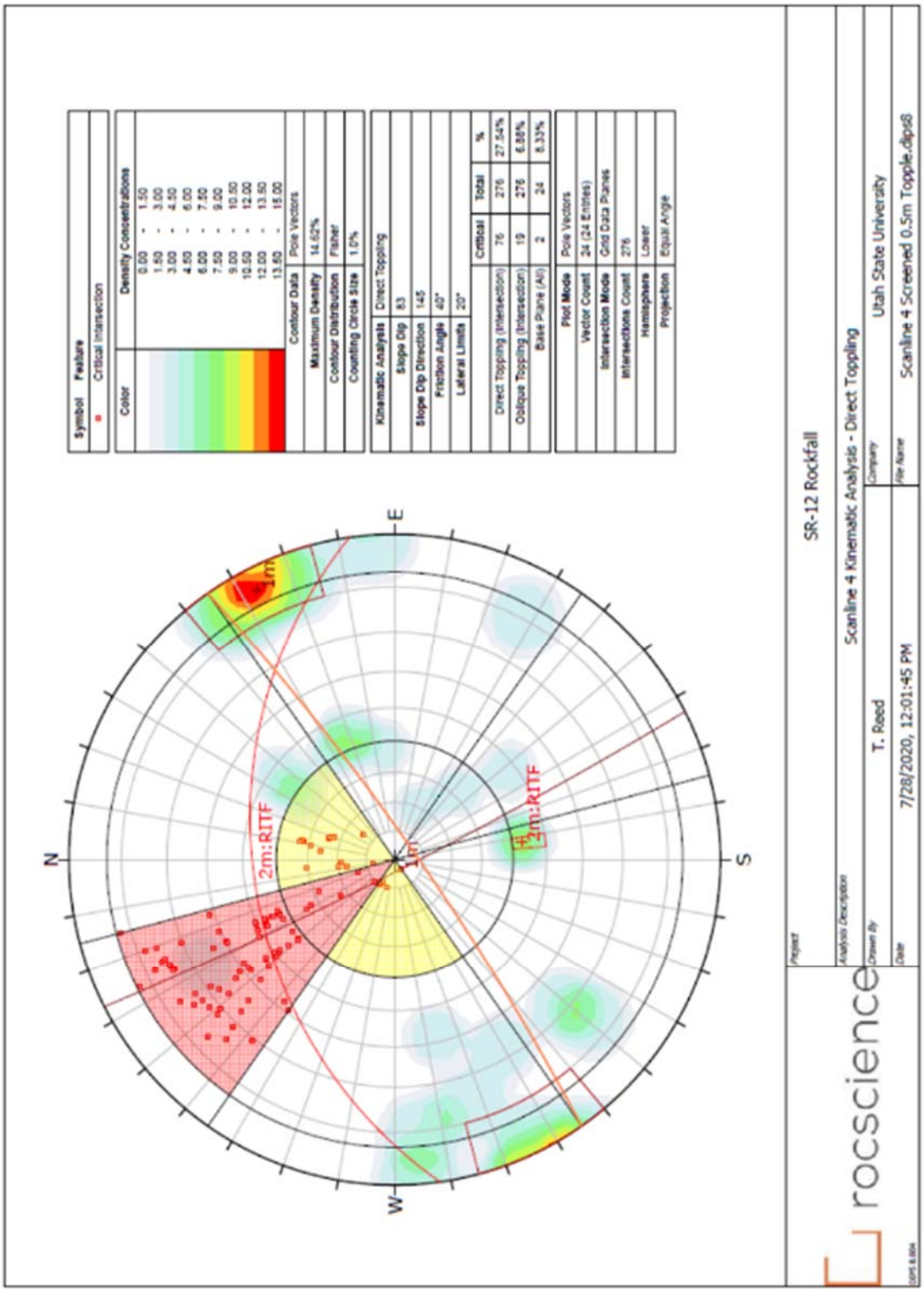

Figure D-19 – Direct toppling kinematic analysis at Scanline 4

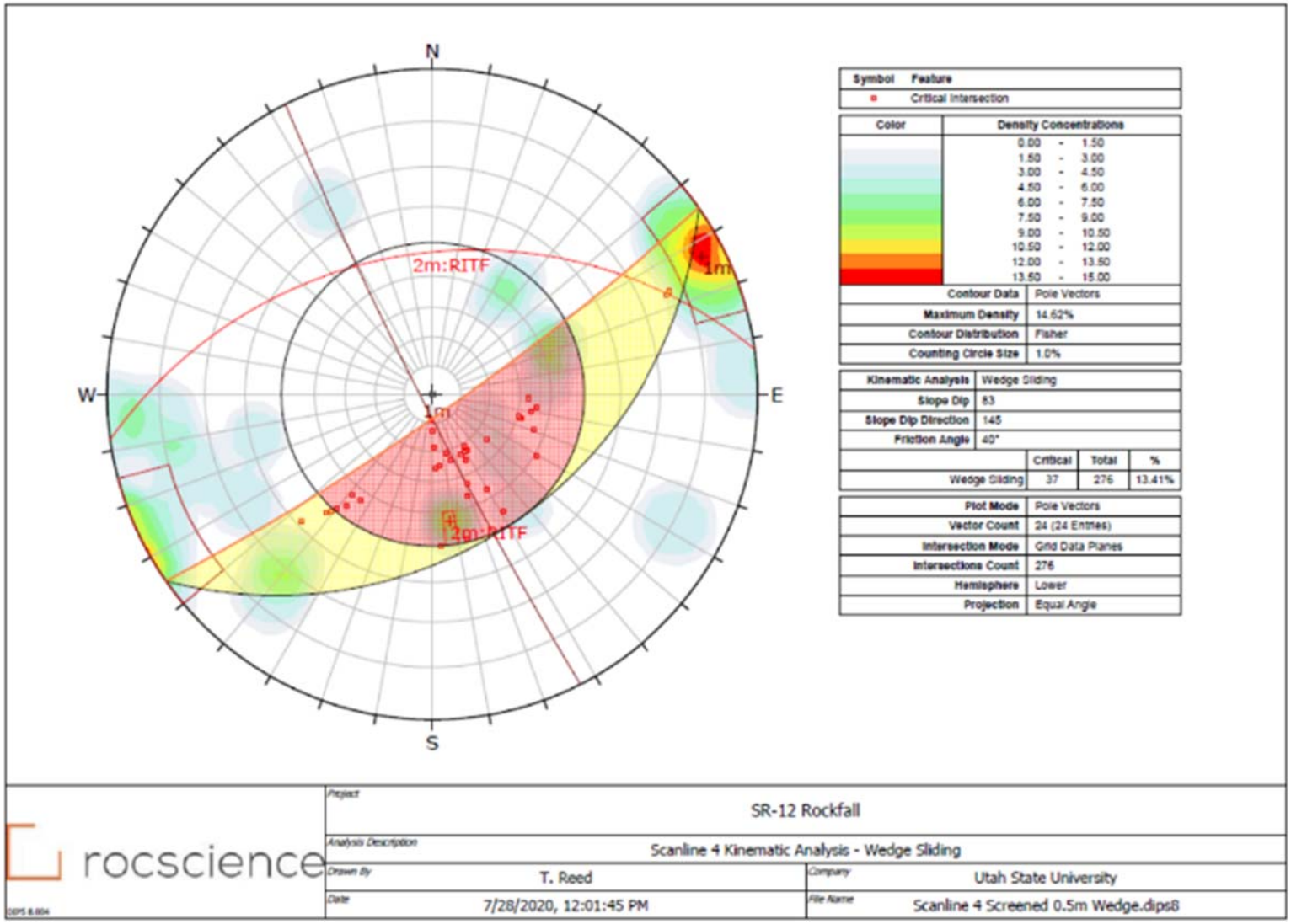

Figure D-20 – Wedge sliding kinematic analysis at Scanline 4

Kinematic Analysis Inputs
Scanline 5

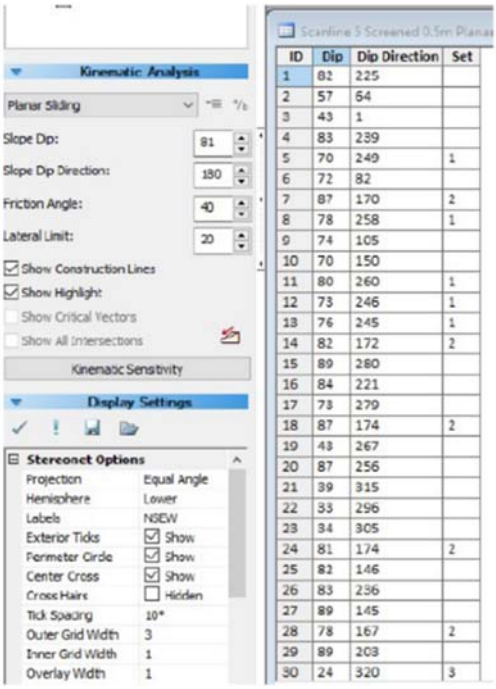

Scanline 5 Screened 0.5m Planar

ID	Dip	Dip Direction	Set
1	82	225	
2	57	64	
3	43	1	
4	83	239	
5	70	249	1
6	72	82	
7	87	170	2
8	78	258	1
9	74	105	
10	70	150	
11	80	260	1
12	73	246	1
13	76	245	1
14	82	172	2
15	89	280	
16	84	221	
17	73	279	
18	87	174	2
19	43	267	
20	87	256	
21	39	315	
22	33	296	
23	34	305	
24	81	174	2
25	82	146	
26	83	236	
27	89	145	
28	78	167	2
29	89	203	
30	24	320	3

Figure D-21 – Inputs for the kinematic analysis performed at Scanline 5

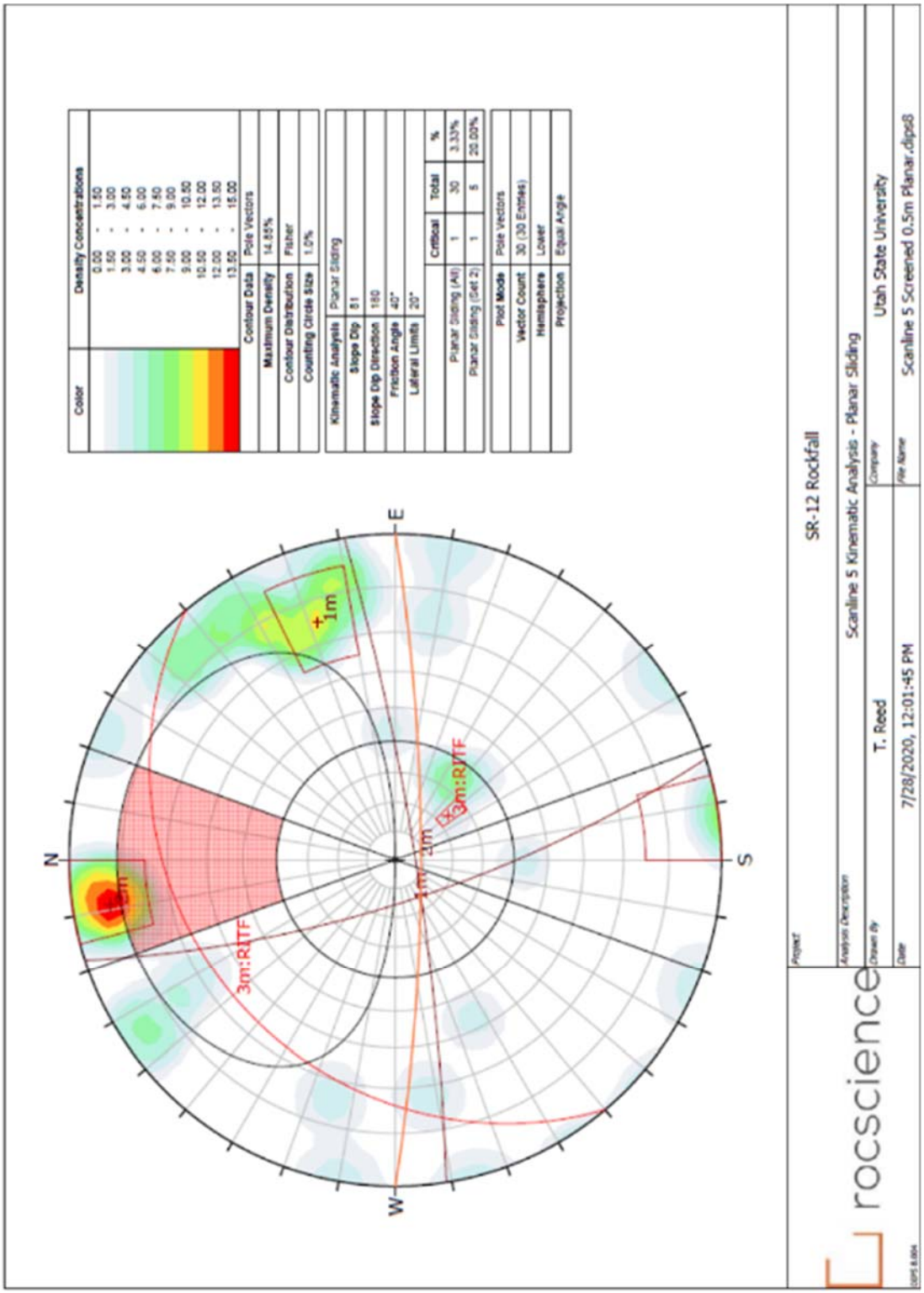

Figure D-22 – Planar sliding kinematic analysis at Scanline 5

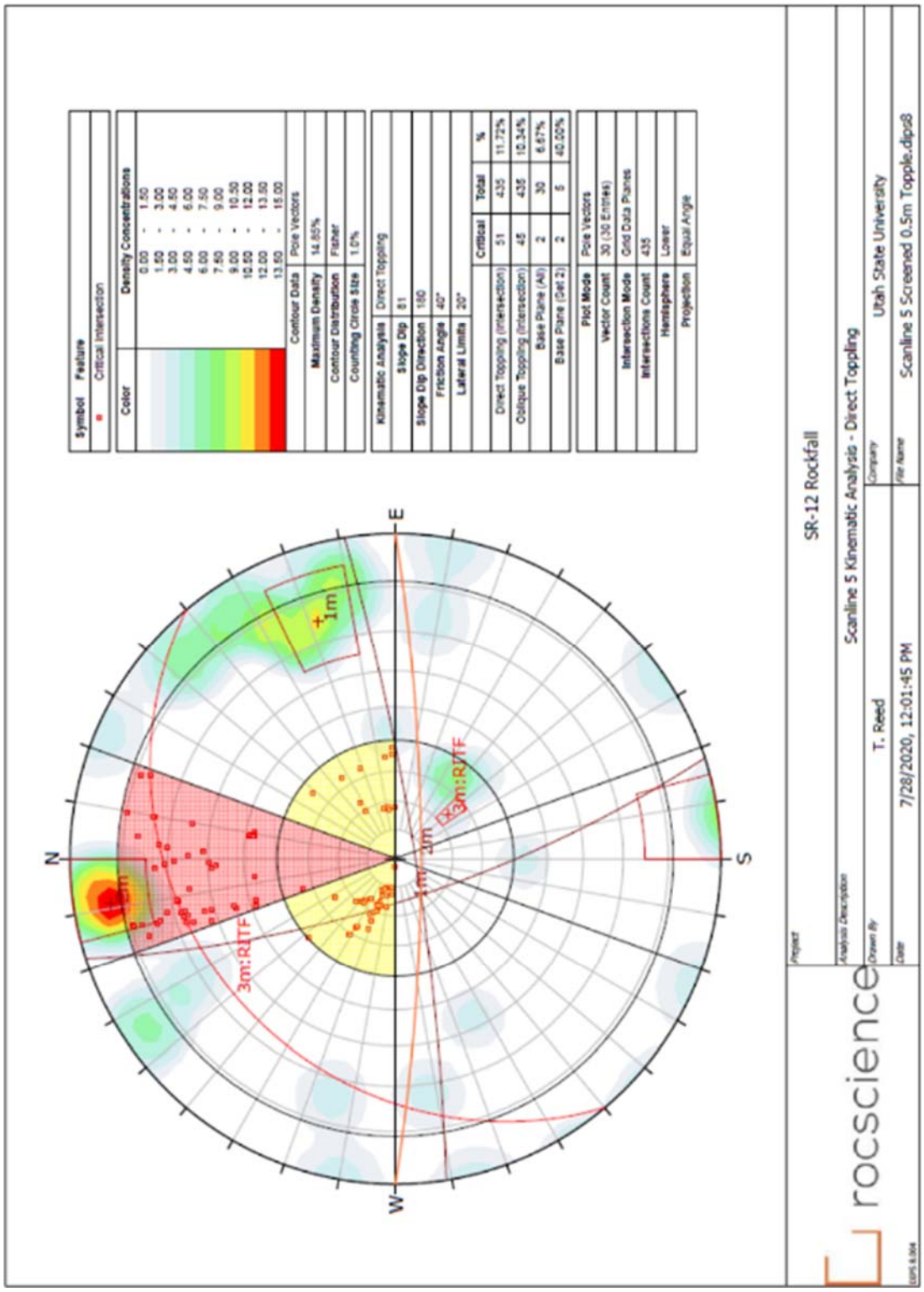

Figure D-23 – Direct toppling kinematic analysis at Scanline 5

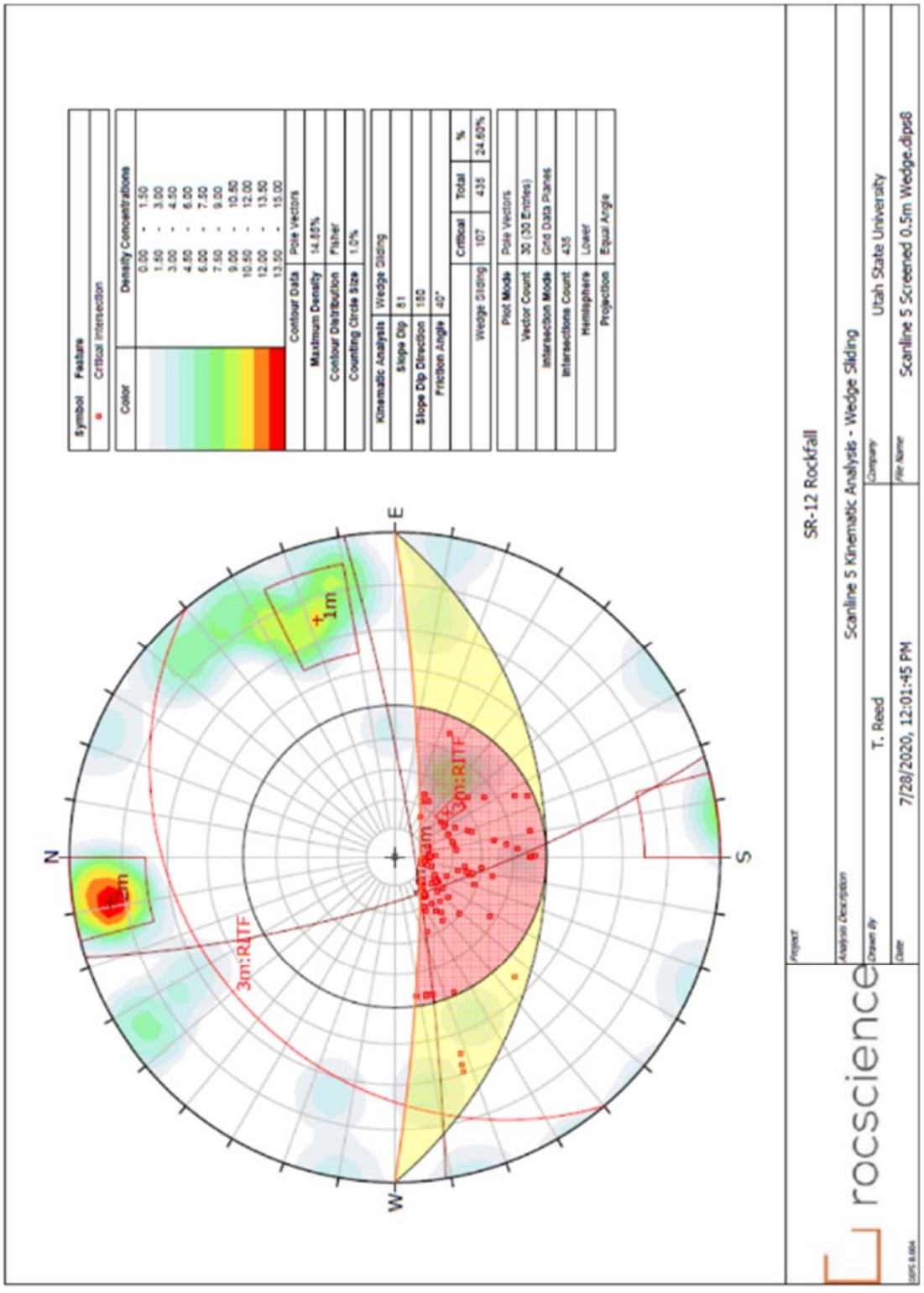

Figure D-24 – Wedge sliding kinematic analysis at Scanline 5

APPENDIX E

Appendix E presents the inputs and results from the rockfall modeling performed at each scanline location.

Material Name	Color	Normal Restitution	Tangential Restitution	Friction Angle	Slope Roughness (deg)
Bedrock Outcrops		Normal Mean: 0.38 Std Dev: 0.04 Rel. Min: 0.12 Rel. Max: 0.12	Normal Mean: 0.9 Std Dev: 0.04 Rel. Min: 0.1 Rel. Max: 0.1	Normal Mean: 30 Std Dev: 4 Rel. Min: 12 Rel. Max: 12	0
Asphalt		Normal Mean: 0.4 Std Dev: 0.04 Rel. Min: 0.12 Rel. Max: 0.12	Normal Mean: 0.9 Std Dev: 0.03 Rel. Min: 0.09 Rel. Max: 0.09	Normal Mean: 30 Std Dev: 2 Rel. Min: 6 Rel. Max: 6	0
Clean hard bedrock		Normal Mean: 0.53 Std Dev: 0.04 Rel. Min: 0.12 Rel. Max: 0.12	Normal Mean: 0.99 Std Dev: 0.04 Rel. Min: 0.12 Rel. Max: 0.01	Normal Mean: 30 Std Dev: 2 Rel. Min: 6 Rel. Max: 6	0

Rocfall material parameter inputs

Scanline Number	Block Diameter (cm)	Block Volume (m^3)	Block Mass (kg)
Scanline Control	192	3.71	9264.933727
Scanline 1	194	3.82	9557.489306
Scanline 2	232	6.54	16345.66469
Scanline 3	146	1.63	4073.776498
Scanline 4	188	3.48	8697.855309
Scanline 5	250	8.18	20453.07717
Notes:	1) Average block size based on the weighted average spacing for each scanline 2) Block mass calculated as a sphere		

Rocfall mass inputs

Figure E-1 – Rockfall modeling inputs

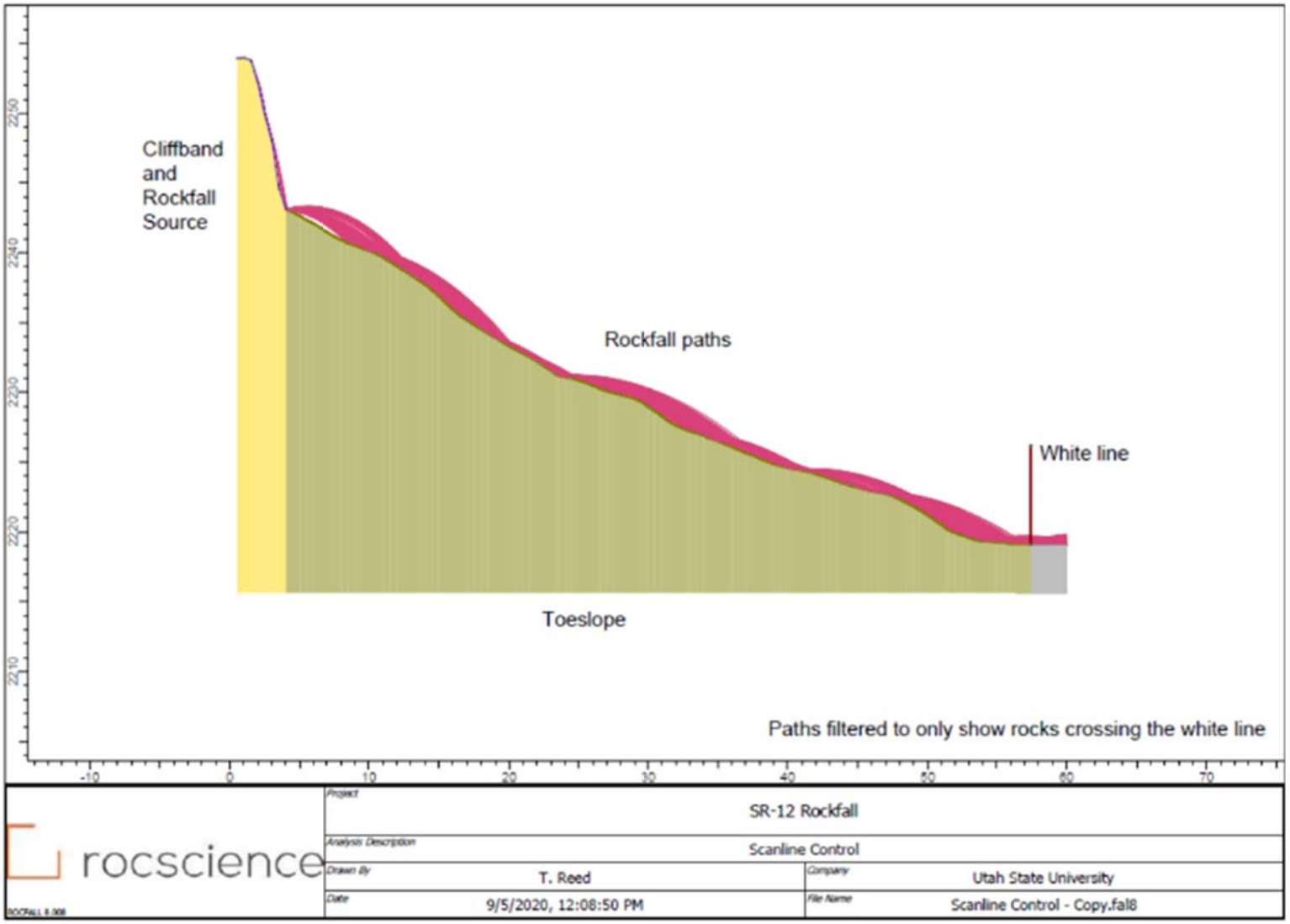

Figure E-2 – Rockfall model setup for the control scanline

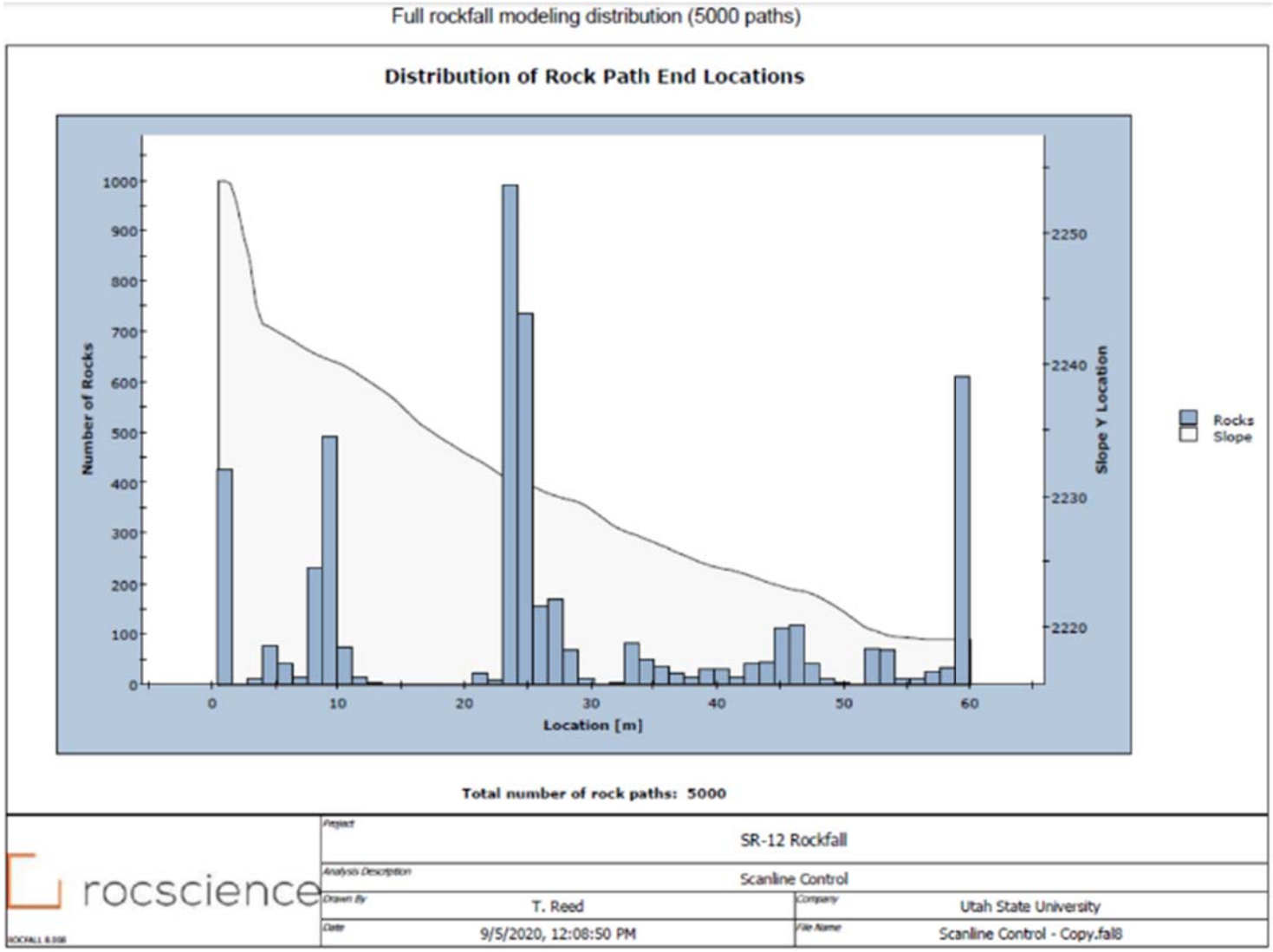

Figure E-3 – Full rockfall modeling results distribution for the control scanline

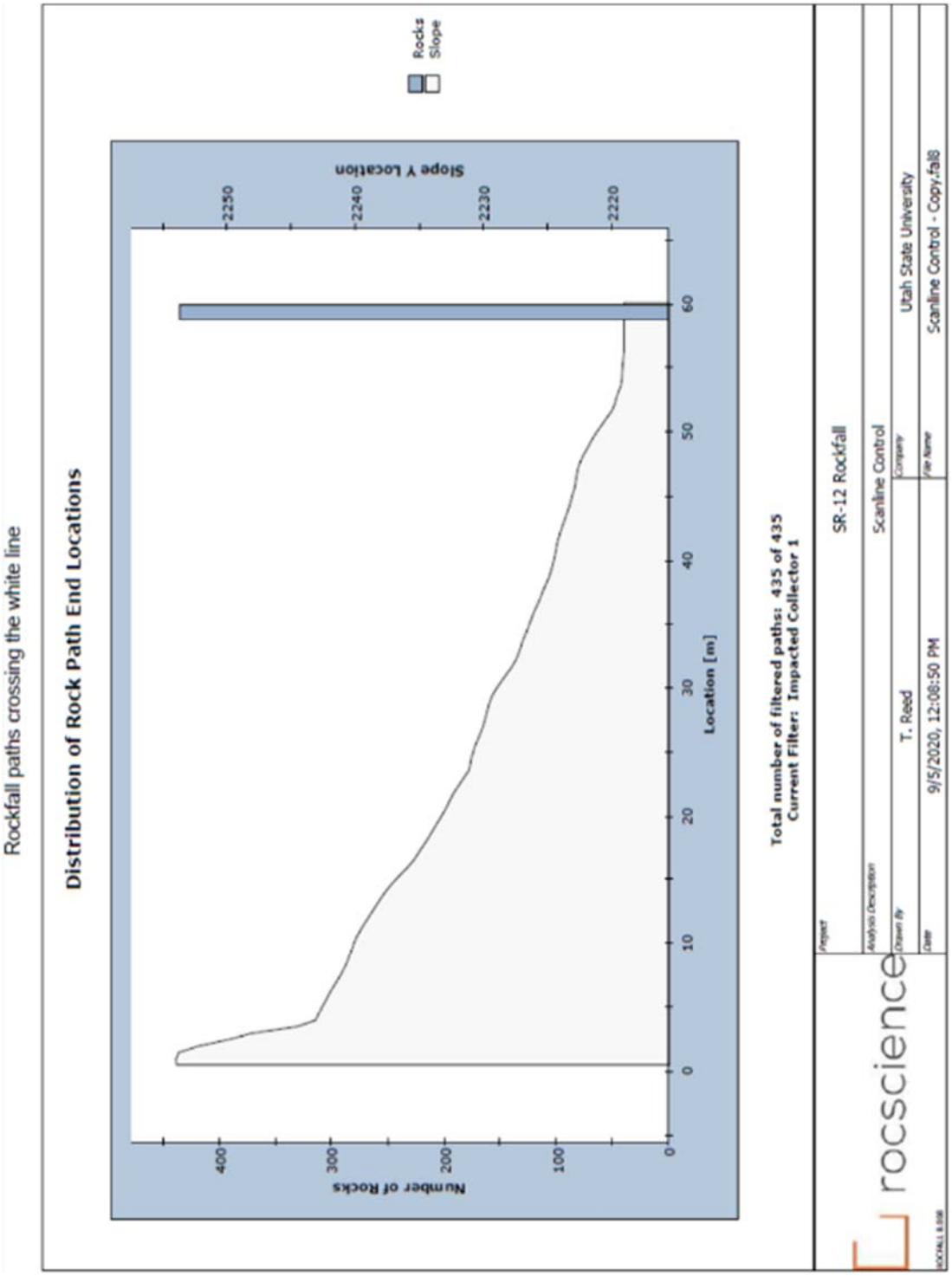

Figure E-4 – Rockfall modeling results crossing the white line for the control scanline

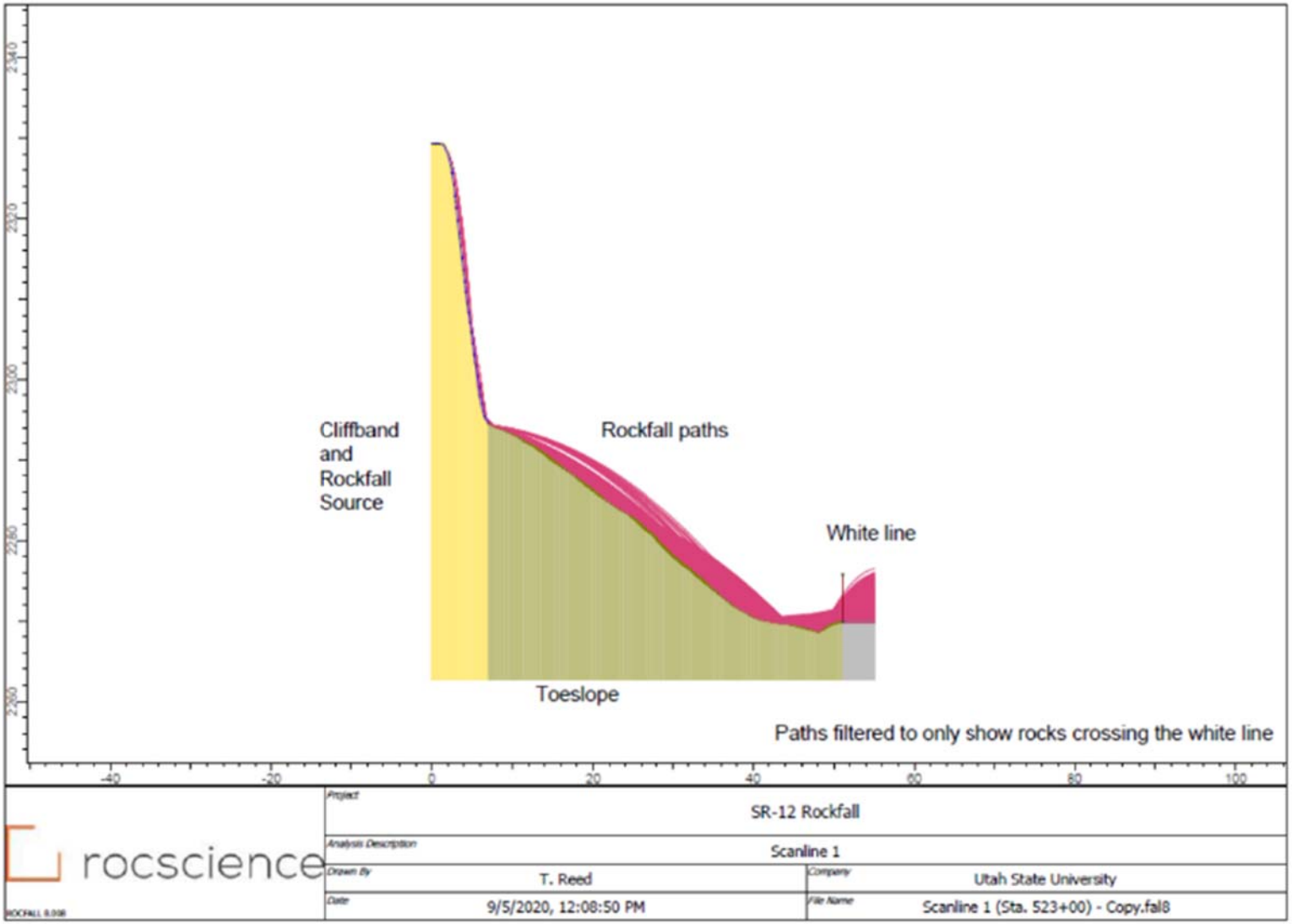

Figure E-5 – Rockfall model setup for Scanline 1

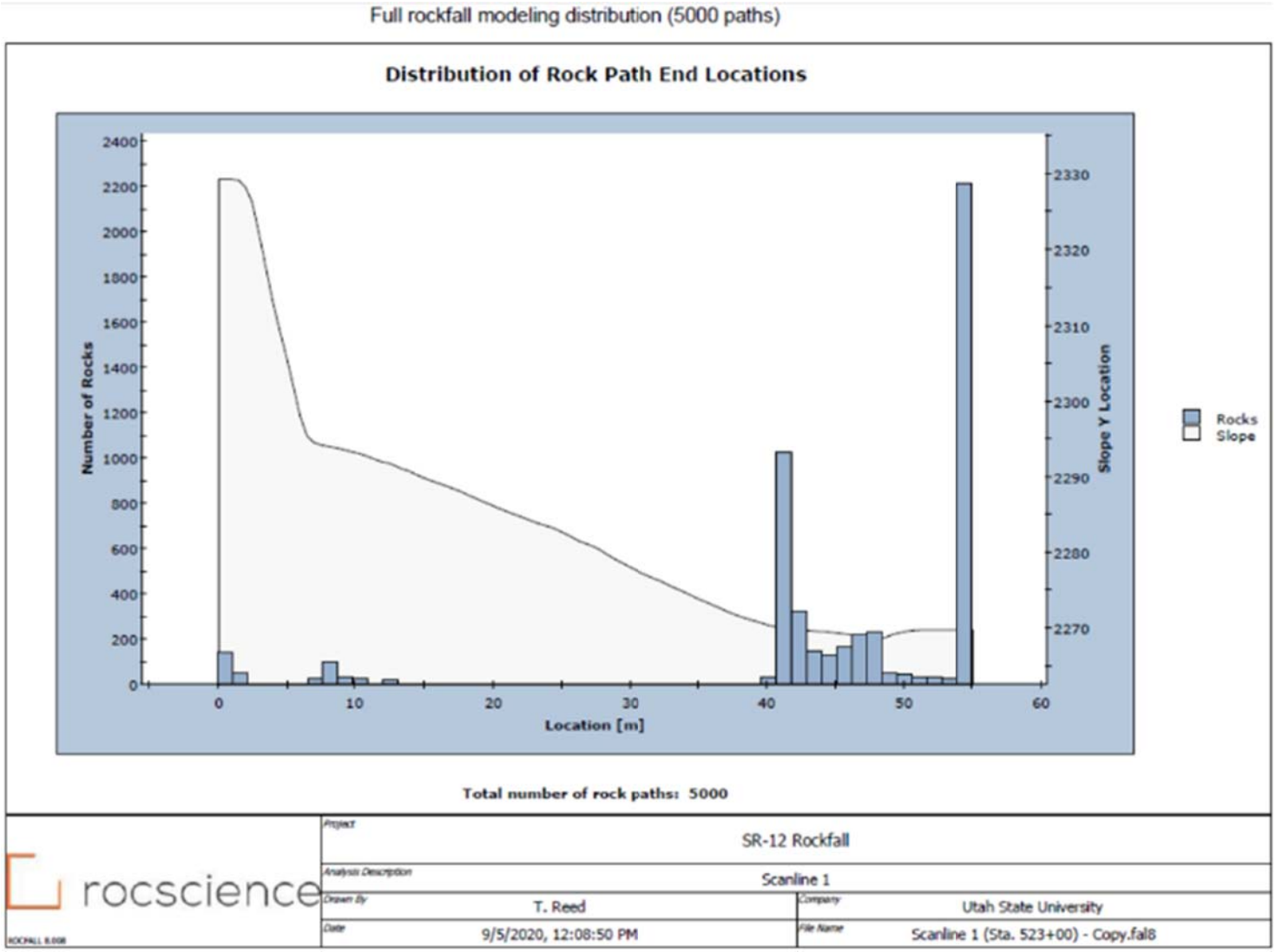

Figure E-6 – Full rockfall modeling results distribution for Scanline 1

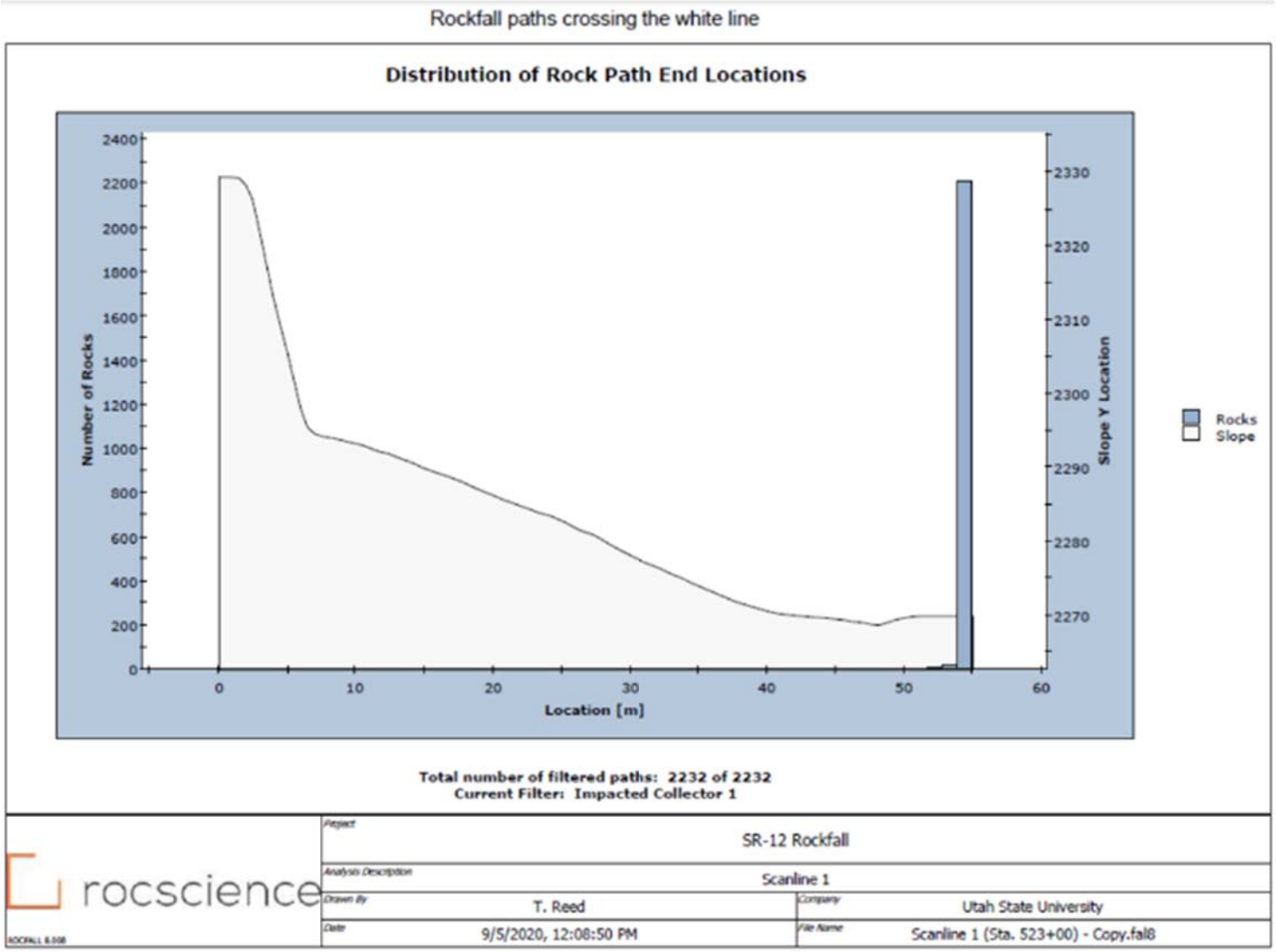

Figure E-7 – Rockfall modeling results crossing the white line for Scanline 1

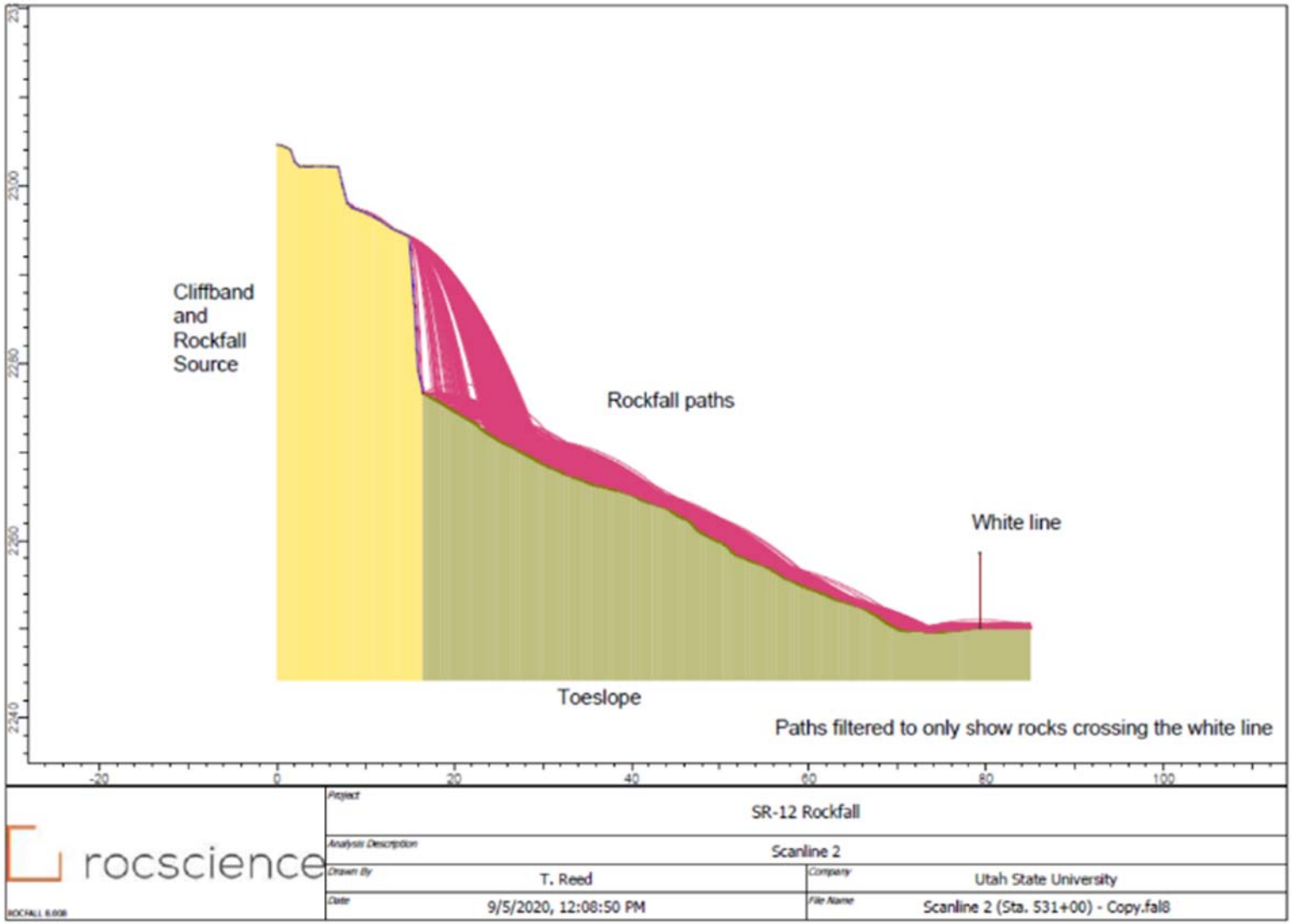

Figure E-8 – Rockfall model setup for Scanline 2

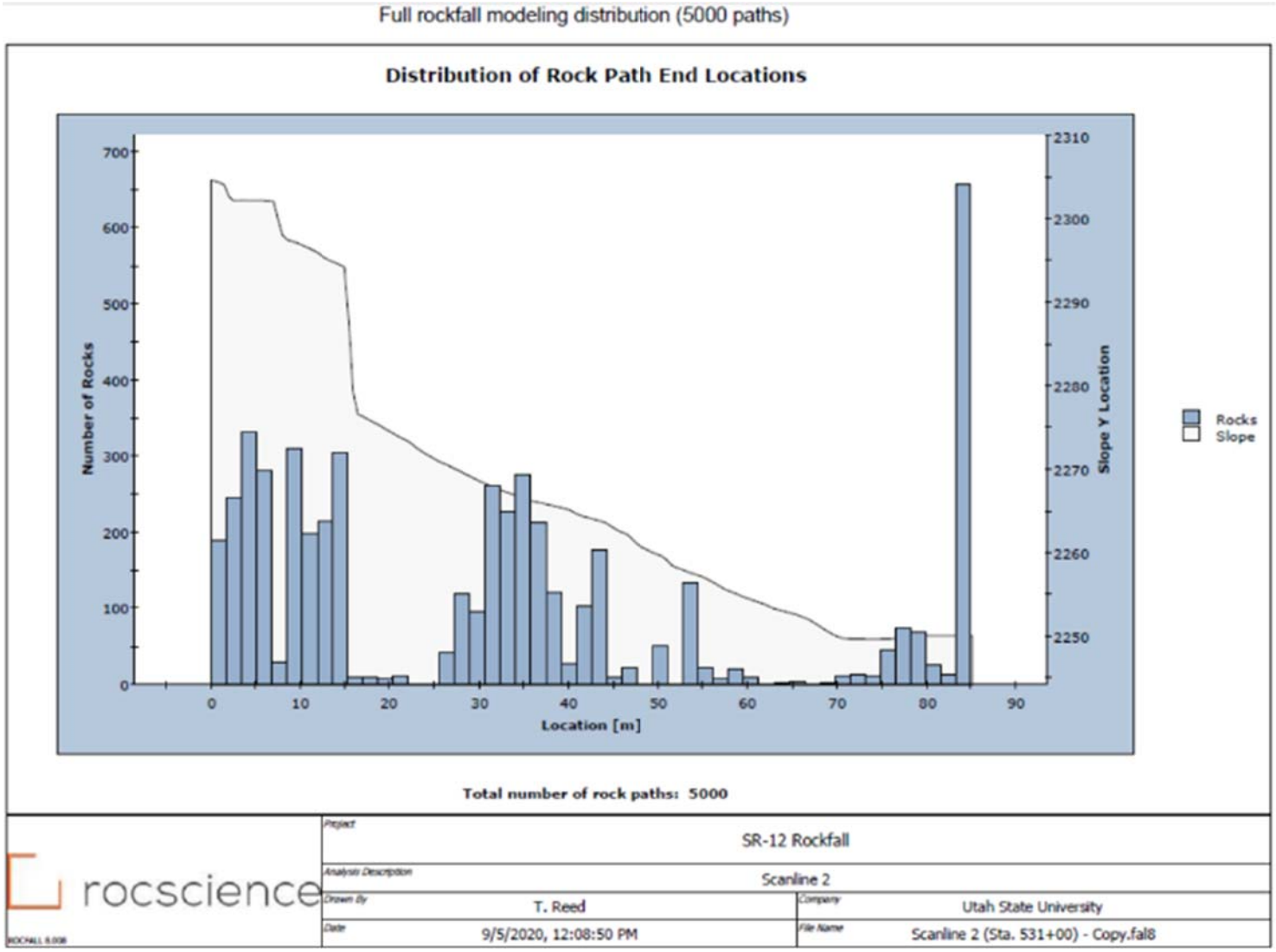

Figure E-9 – Full rockfall modeling results distribution for Scanline 2

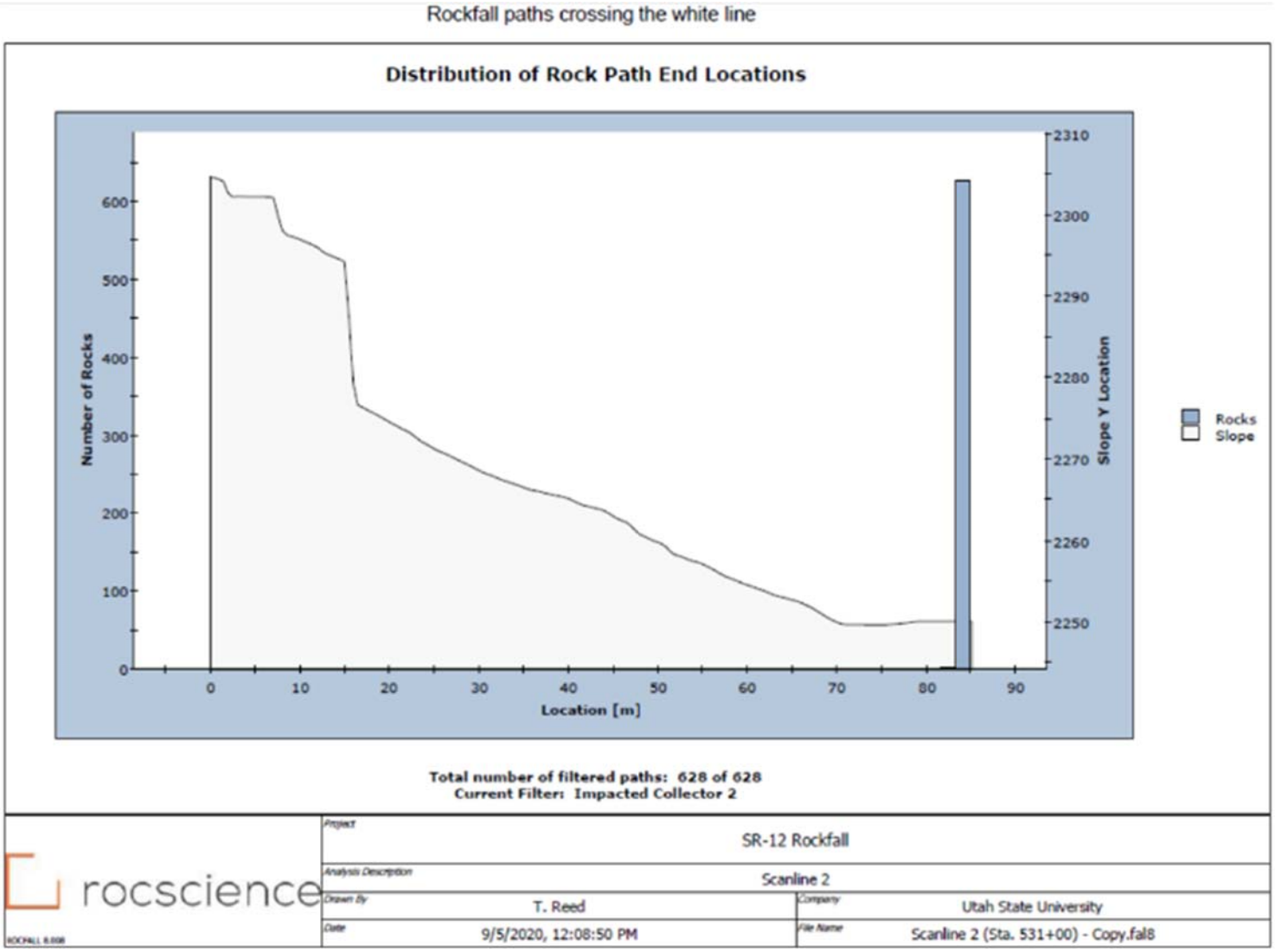

Figure E-10 – Rockfall modeling results crossing the white line for Scanline 2

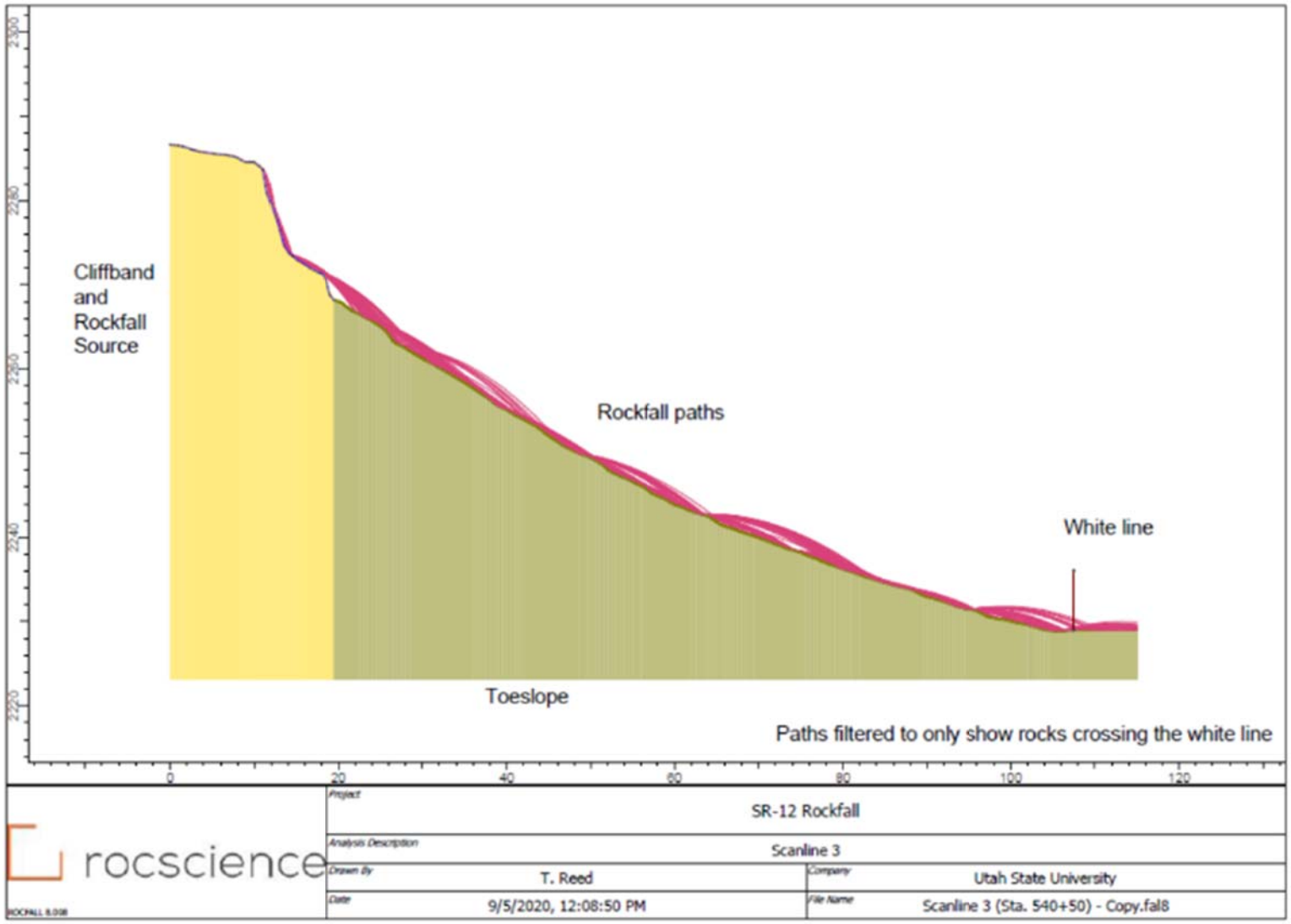

Figure E-11 – Rockfall model setup for Scanline 3

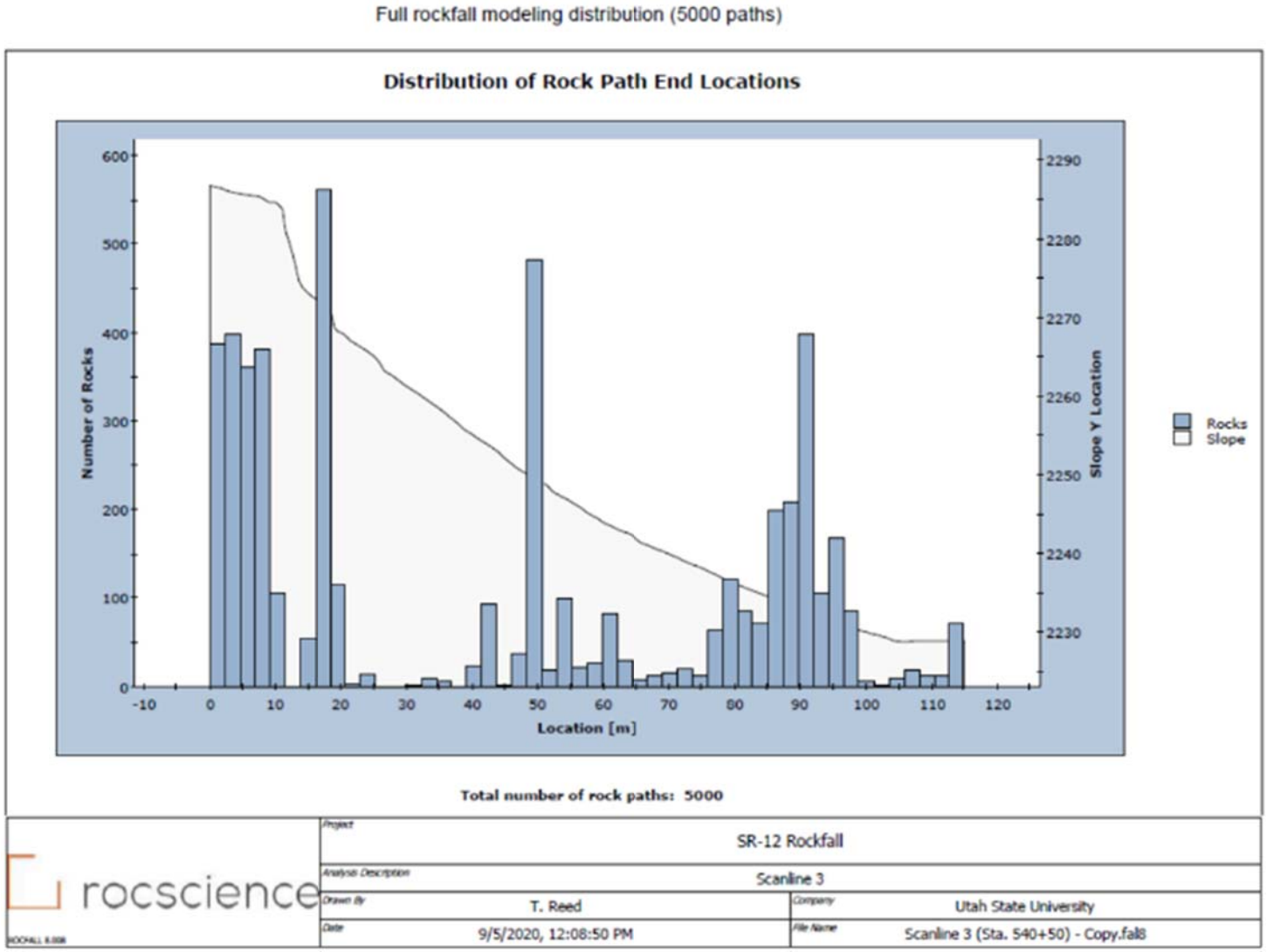

Figure E-12 – Full rockfall modeling results distribution for Scanline 3

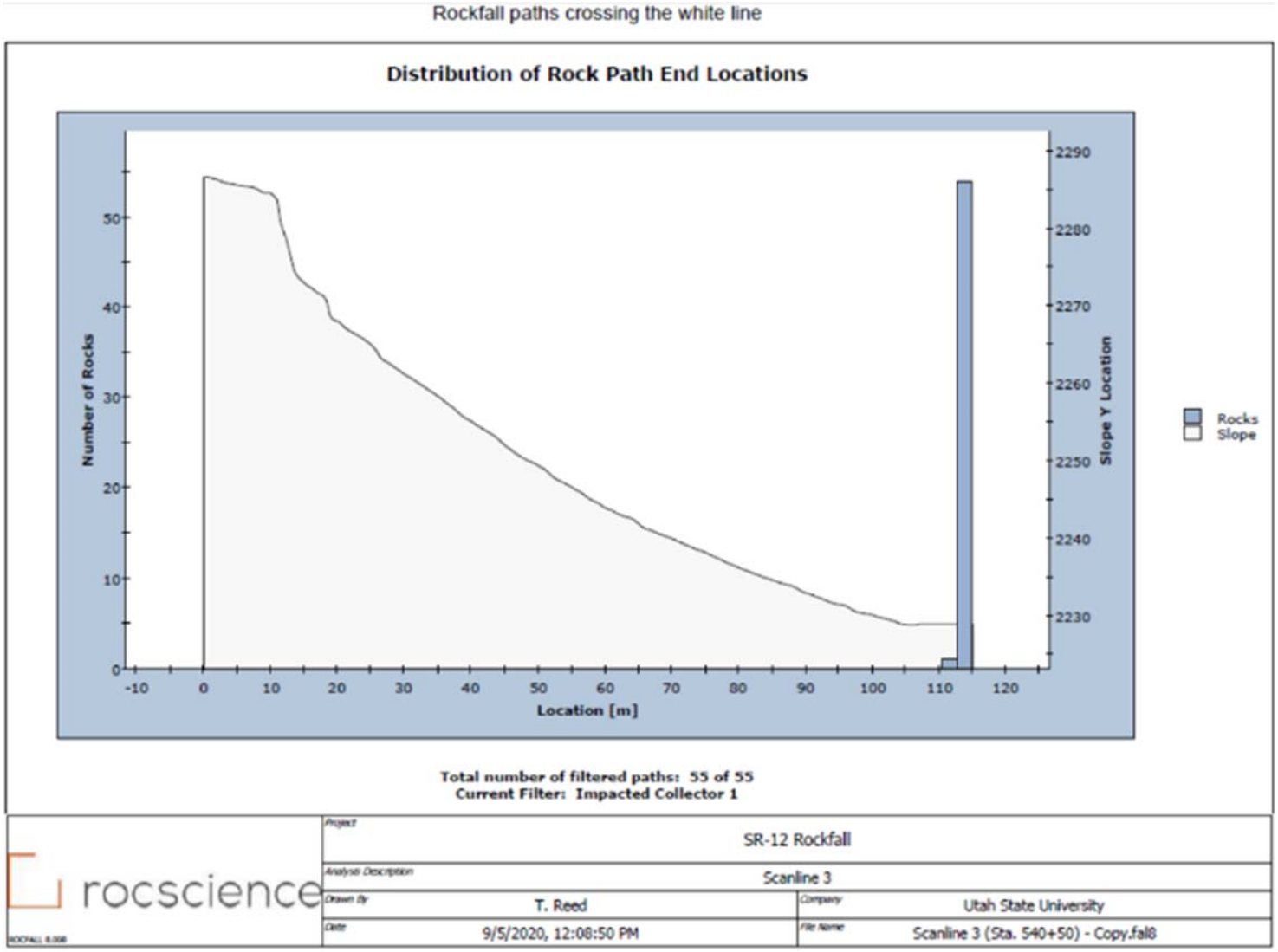

Figure E-13 – Rockfall modeling results crossing the white line for Scanline 3

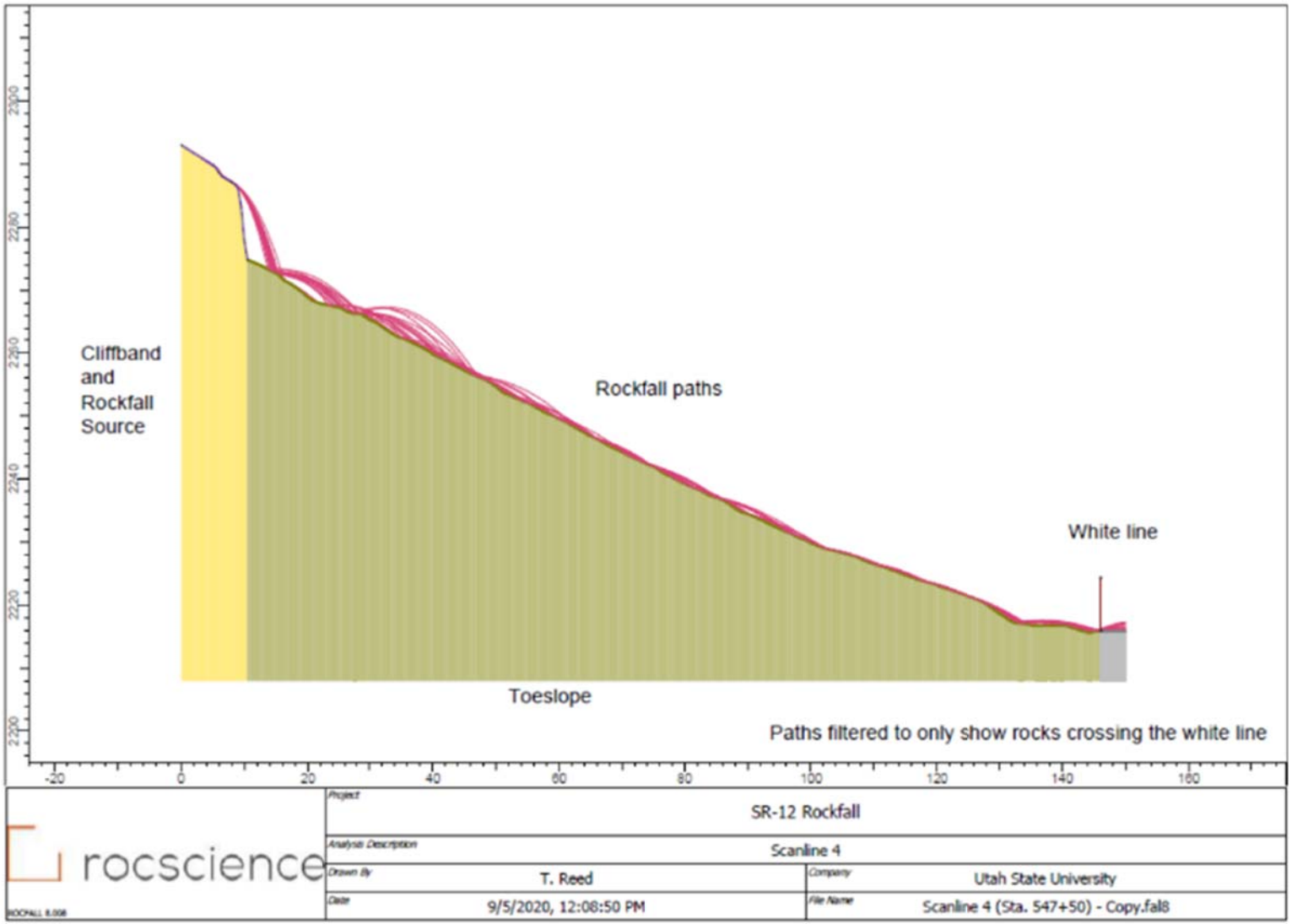

Figure E-14 – Rockfall model setup for Scanline 4

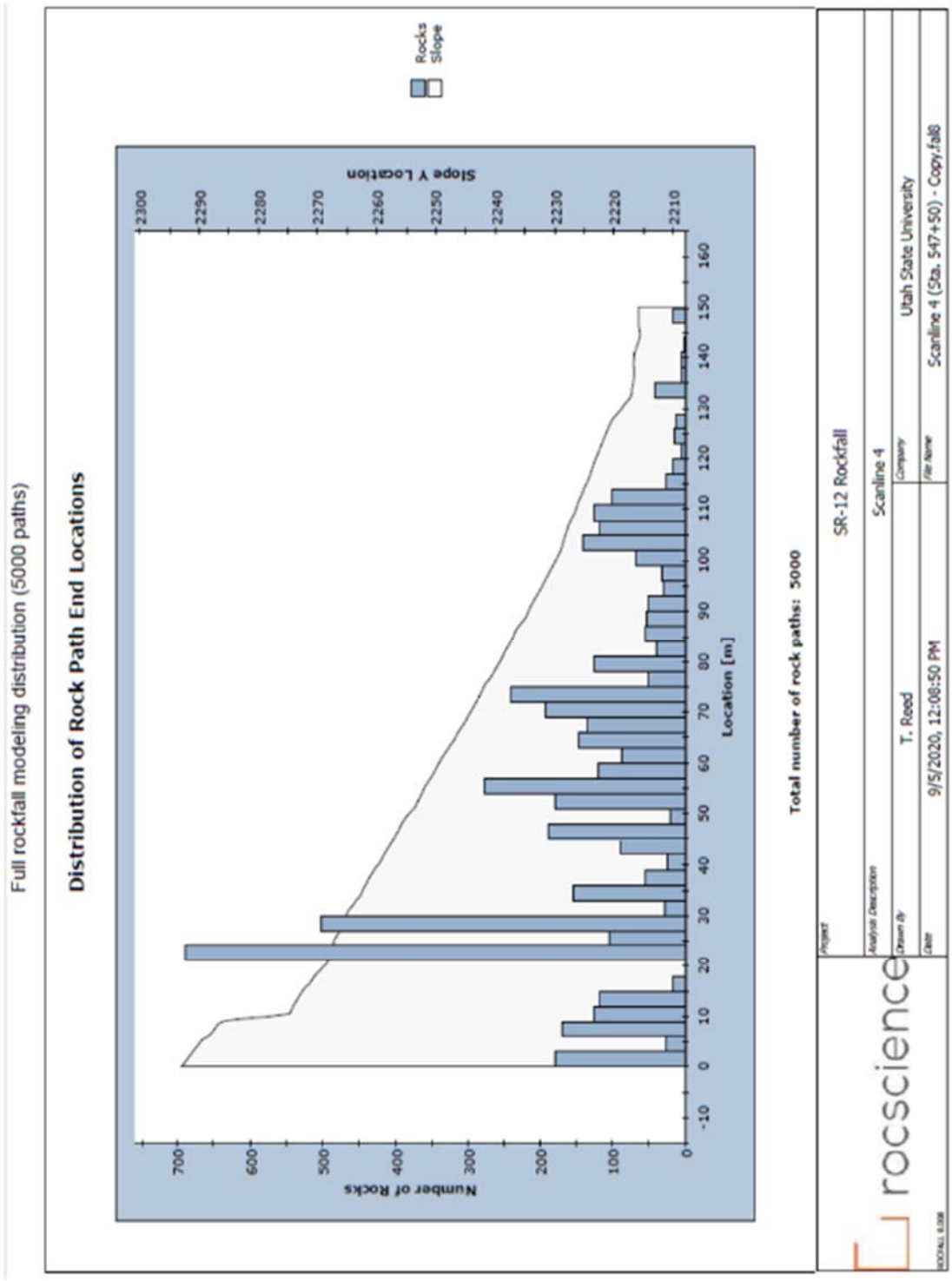

Figure E-15 – Full rockfall modeling results distribution for Scanline 4

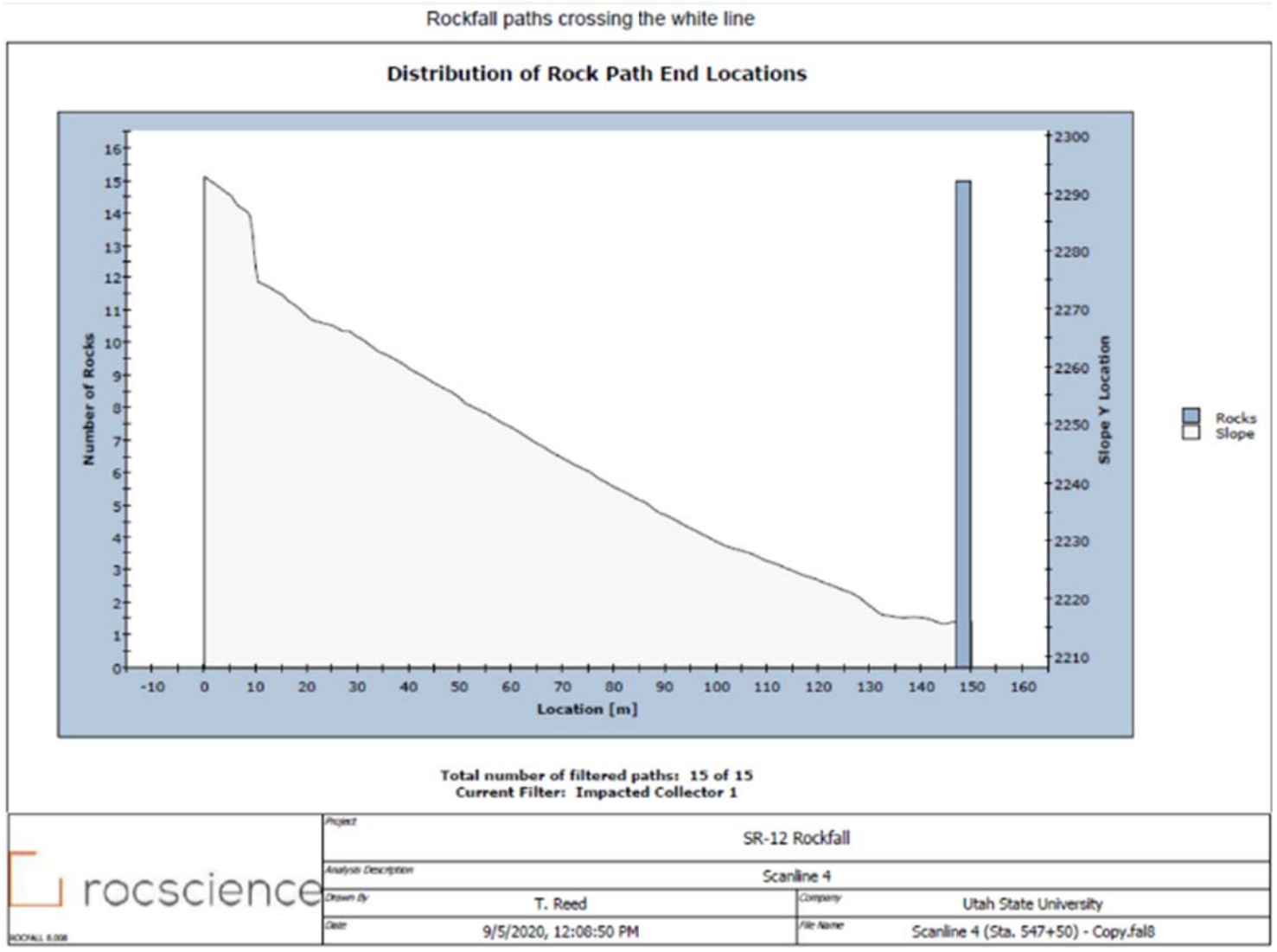

Figure E-16 – Rockfall modeling results crossing the white line for Scanline 4

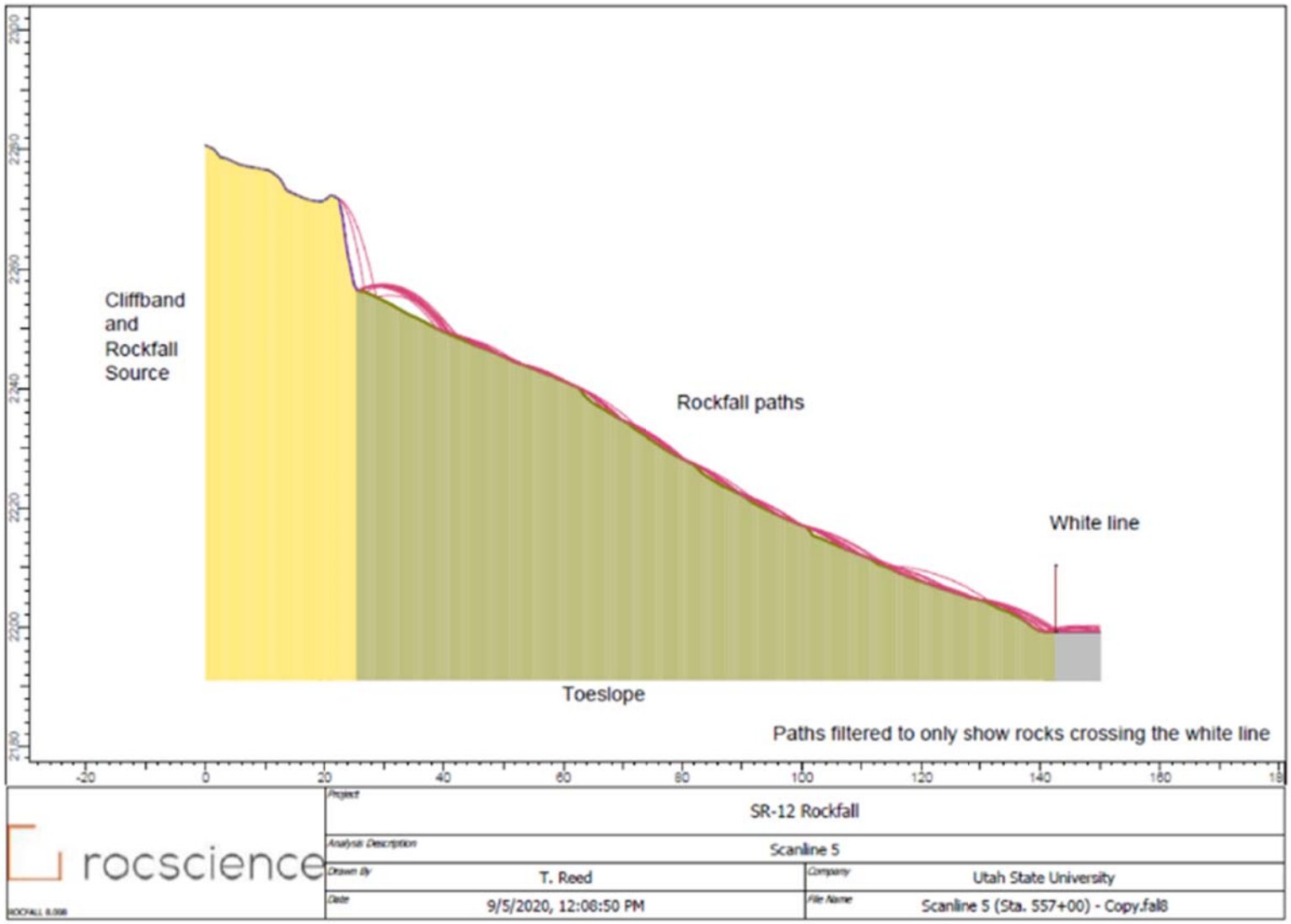

Figure E-17 – Rockfall model setup for Scanline 5

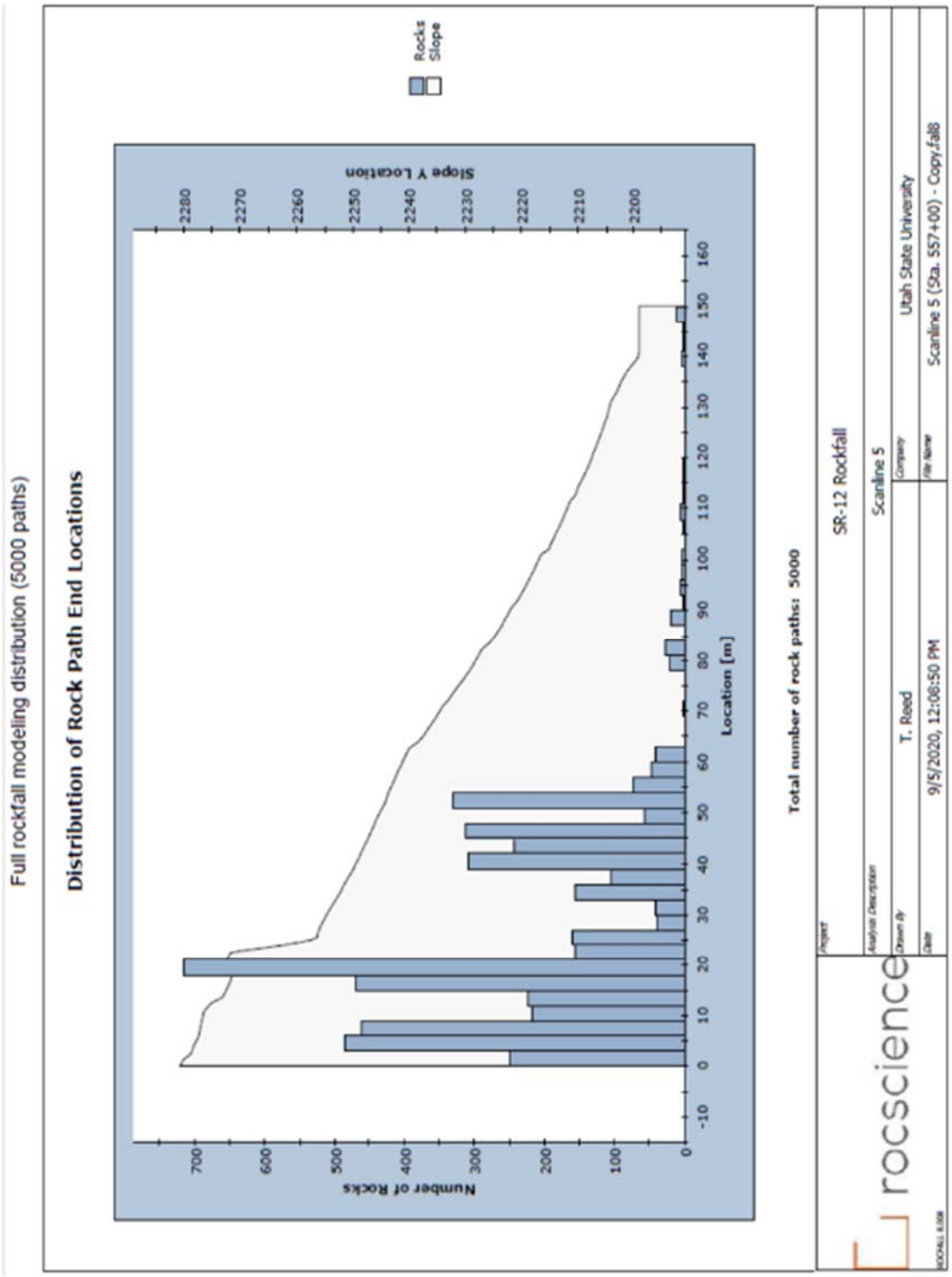

Figure E-18 – Full rockfall modeling results distribution for Scanline 5

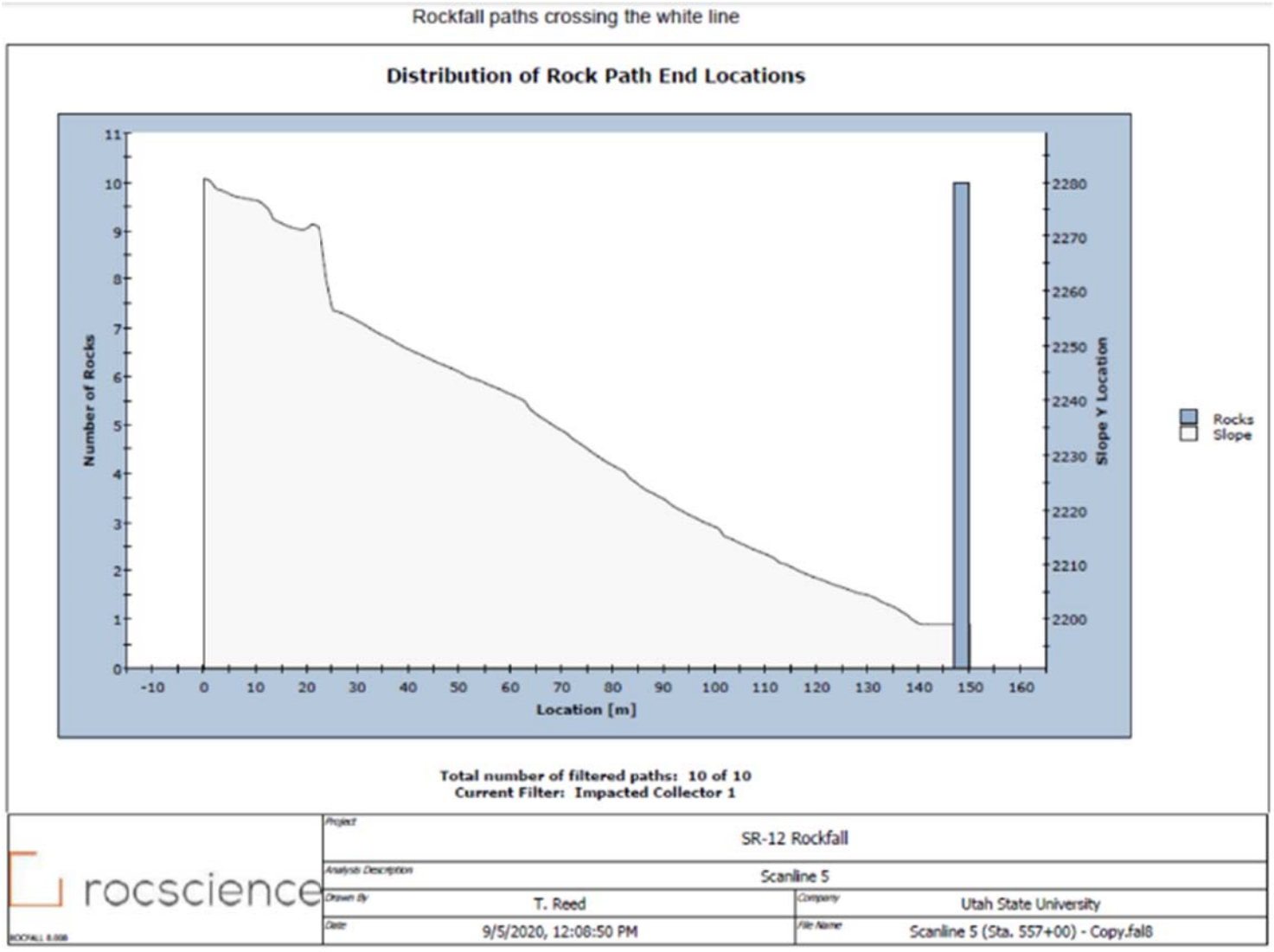

Figure E-19 – Rockfall modeling results crossing the white line for Scanline 5

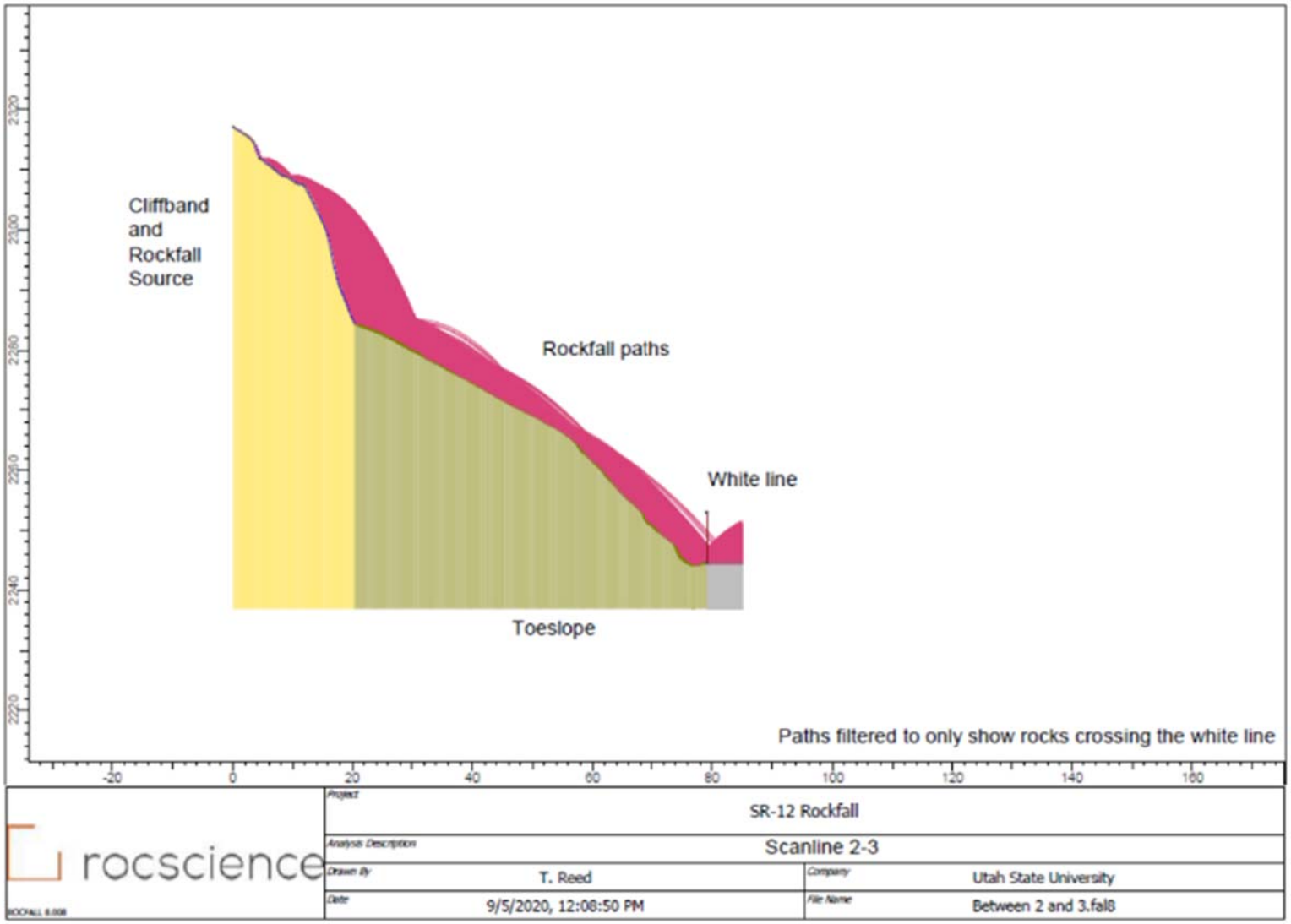

Figure E-20 – Rockfall model setup for between Scanlines 2 and 3

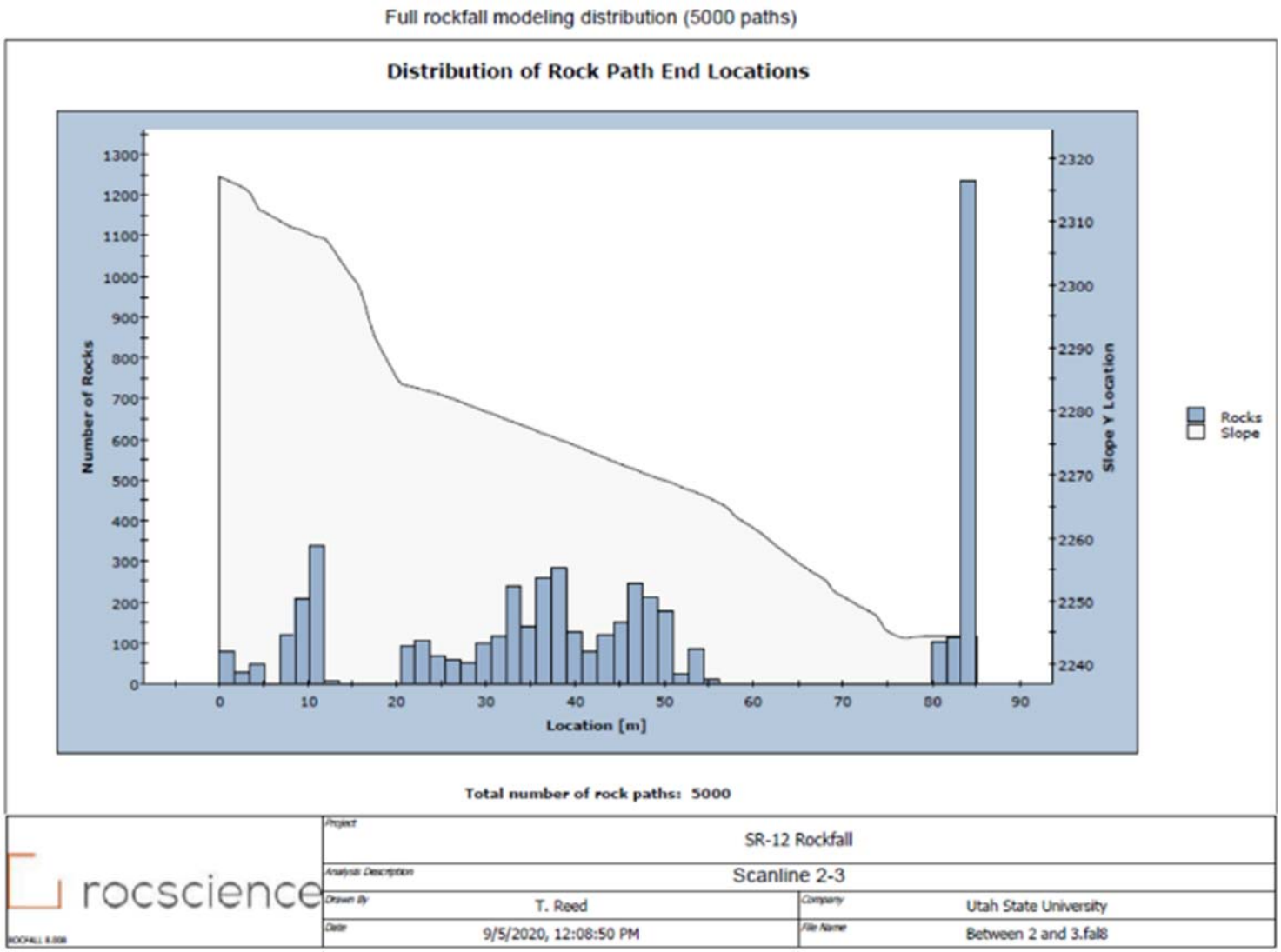

Figure E-21 – Full rockfall modeling results distribution for between Scanlines 2 and 3

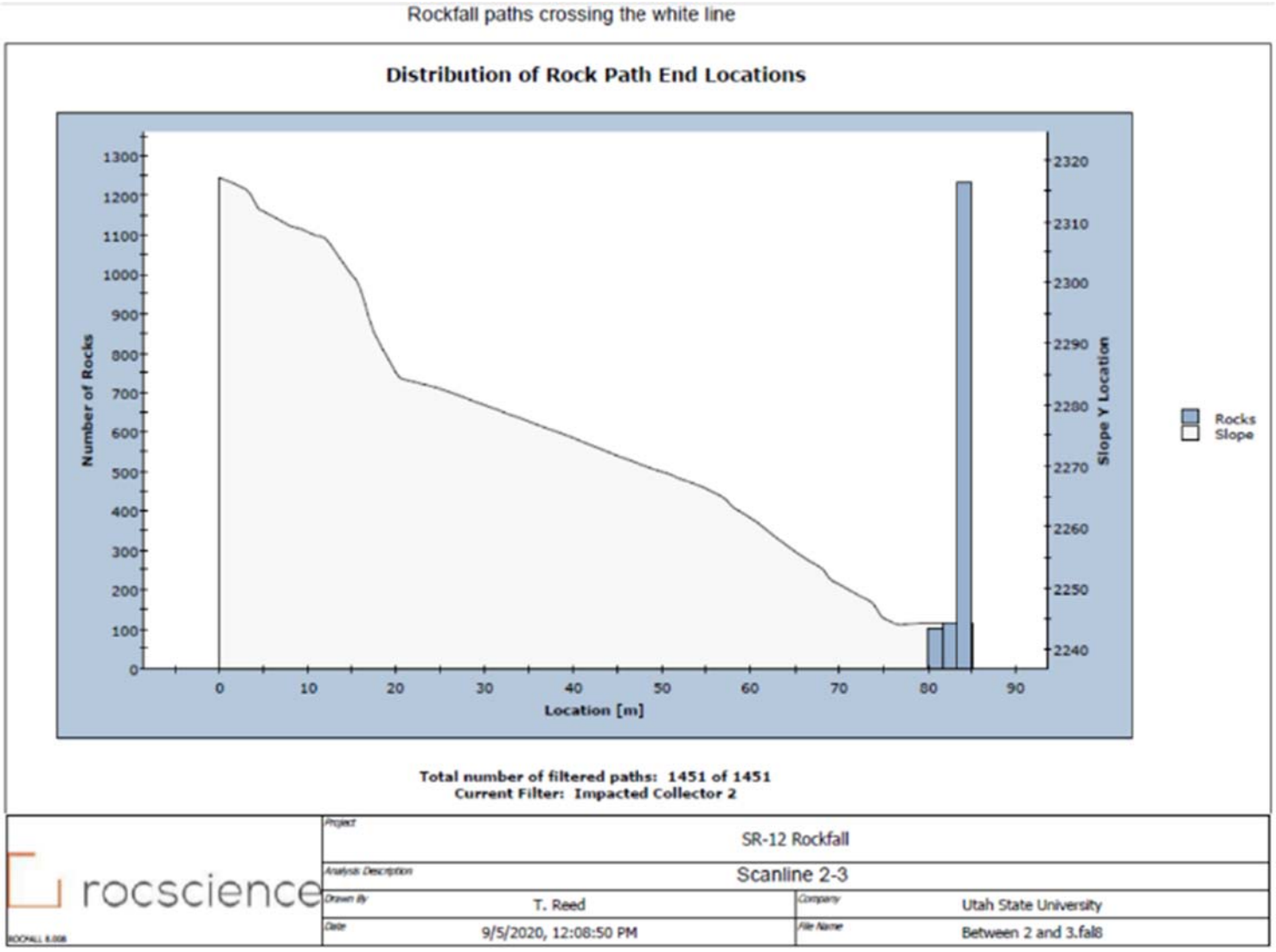

Figure E-22 – Rockfall modeling results crossing the white line for between Scanlines 2 and 3

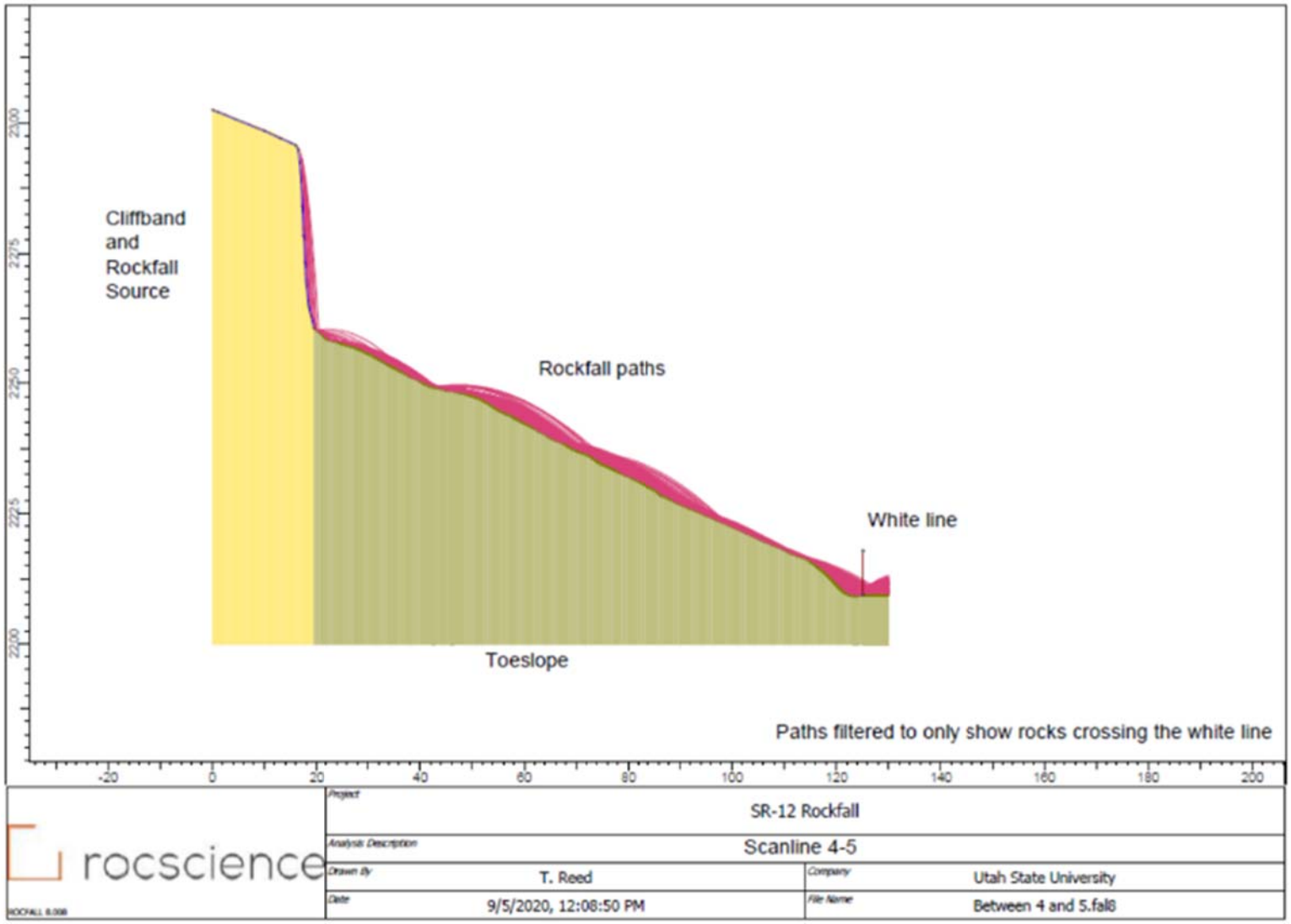

Figure E-23 – Rockfall model setup for between Scanlines 4 and 5

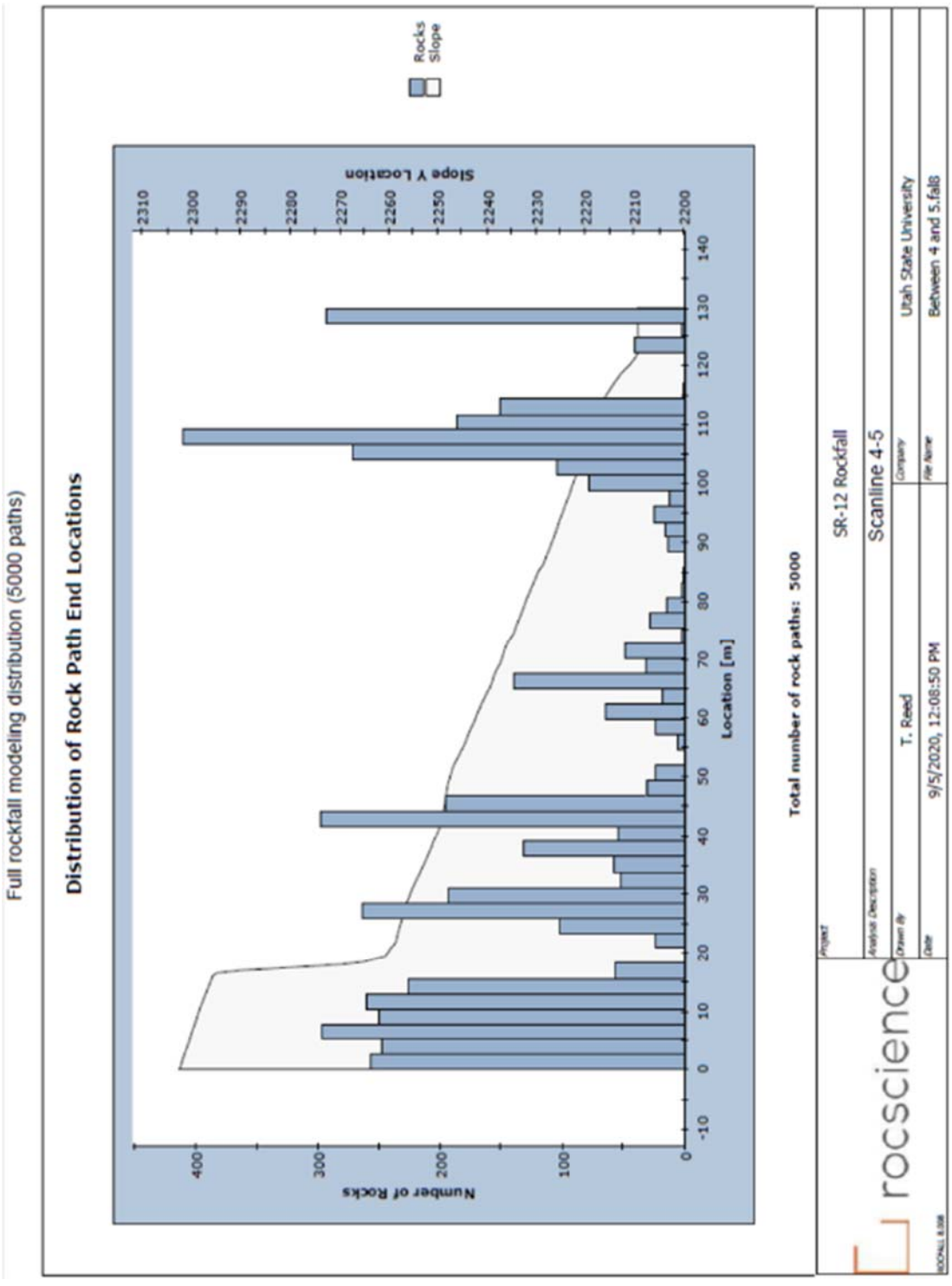

Figure E-24 – Full rockfall modeling results distribution for between Scanlines 4 and 5

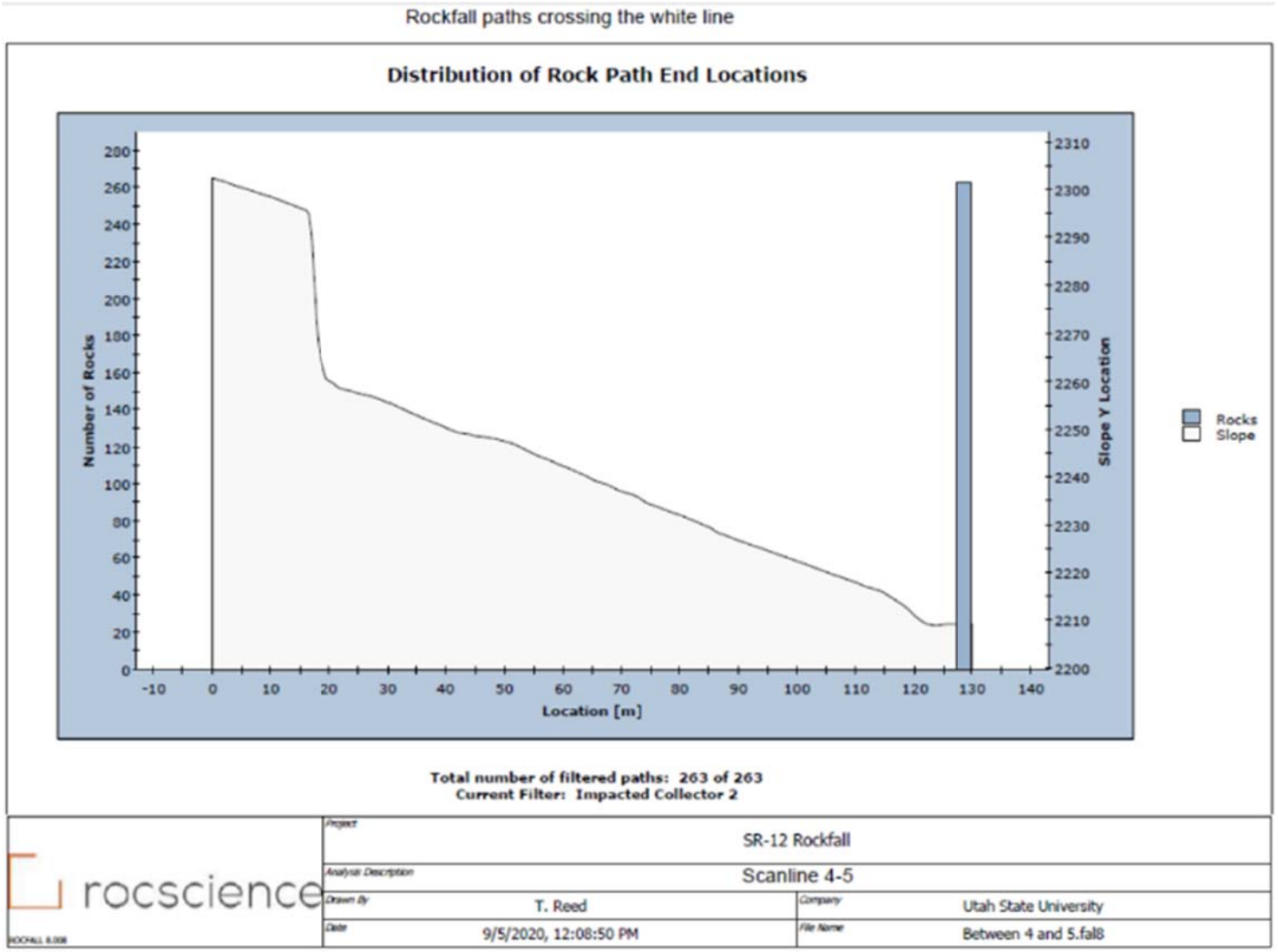

Figure E-25 – Rockfall modeling results crossing the white line for between Scanlines 4 and 5

APPENDIX G

Appendix G contains results from OSL testing performed on a sample from a deposit mapped as piedmont gravel, gathered from the top of the Paunsaugunt Plateau. The deposit consisted of medium-grained sand in between two layers of gravel, exposed in a roadway cut alongside SR-12. The sample was gathered by driving a steel tube into the deposit, approximately 1.1 meters below the surface, at GPS coordinates 37.685456°, -112.135886° (WGS 1984). The sample was tested at the Utah State University Luminescence Lab, and results from the analyses are found below.

Table G-1. Infrared Stimulated Luminescence (IRSL) Age Information

Sample num.	USU num.	Num. of aliquots[1]	Dose rate (Gy/kyr)	Fading Rate g_{2days} (%/decade)	Equivalent Dose[2] ± 2σ (Gy)	IRSL age[3] ± 2σ (ka)
SR12-19-01	USU-3201	13 (19)	1.30 ± 0.06	3.2 ± 1.0	550.1 ± 112.0	**328.1 ± 72.17**

[1] Age analysis using the single-aliquot regenerative-dose procedure of Wallinga et al. (2000) on 1-mm small-aliquots of feldspar sand (150-250 μm) at 50°C IRSL. Number of aliquots used in age calculation and number of aliquots analyzed in parentheses.

[2] Equivalent dose (D_E) and IRSL age calculated using the Central Age Model (CAM) of Galbraith and Roberts (2012).

[3] IRSL age on each aliquot corrected for fading following the method by Auclair et al. (2003) and correction model of Huntley and Lamothe (2001).

Table G-2. Dose Rate Information

Depth (m)	D_R Sample[1]	K (%)[2]	Rb (ppm)[2]	Th (ppm)[2]	U (ppm)[2]	Cosmic (Gy/kyr)
	Upper unit <1.7mm	0.47±0.02	21.2±0.8	5.8±0.5	1.4±0.1	
	Lower unit <1.7mm	0.66±0.03	30.1±1.2	4.9±0.4	1.4±0.1	
	Upper unit 1.7-16mm	0.21±0.01	9.3±0.4	2.3±0.2	1.3±0.1	
1.1	Lower unit 1.7-16mm	0.32±0.01	14.0±0.6	2.4±0.2	1.8±0.1	0.29±0.03
	Upper unit >16mm	0.06±0.001	3.2±0.1	0.6±0.1	1.1±0.1	
	Lower unit >16mm	0.1±0.001	4.8±0.2	0.8±0.1	0.7±0.1	
	OSL sand unit	0.62±0.02	27.1±1.1	3.7±0.3	1.2±0.1	

[1] Dose rate (D_R) subsample is grain size based (in mm). Gamma dose rate uses weighted average of subsamples from poorly-sorted units above and below OSL sand / D_E sample unit: <1.7 mm (35%), 1.7-16 mm (30%) and >16 mm (35%). External beta dose rate calculation includes geochemical concentrations from OSL sand unit only.

[2] Radioelemental concentrations determined using ICP-MS and ICP-AES techniques; dose rate is derived from concentrations by conversion factors from Guérin et al. (2011). Grain-size based internal beta dose rate determined assuming 12.5% K and 400ppm Rb using Mejdahl (1979). Alpha contribution to dose rate determined using an efficiency factor, or 'a-value', of 0.09±0.01 after Rees-Jones (1995). In-situ moisture content was 2.3%, 5±2% was used as moisture content over burial history.